Università degli Studi di Ferrara

DOCTORAL COURSE IN "CHEMICAL SCIENCES"

CYCLE XXXII

DIRECTOR
Prof. Cavazzini Alberto

Synthesis and biological evaluation of small anticancer molecules acting as tubulin polymerization inhibitors

Scientific/Disciplinary Sector (SDS) CHIM/08

Candidate
Dr Oliva Paola

Supervisor
Prof. Romagnoli Romeo

Years 2016/2019

List of papers

This thesis is based on the following papers.

I **Synthesis and Biological Evaluation of 2-Methyl-4,5-Disubstituted Oxazoles as a Novel Class of Highly Potent Antitubulin Agents**, Romagnoli R., Baraldi P.G., Prencipe F., Oliva P.,Baraldi S., Salvador M.K., Lopez-Cara LC., Brancale A., Ferla S., Hamel E., Ronca R., Bortolozzi R., Mariotto E., Porcù E., Basso G., Viola G., Sci Rep. **2017**, 7, 46356.

II **2-Alkoxycarbonyl-3-arylamino-5-substituted thiophenes as a novel class of antimicrotubule agents: Design, synthesis, cell growth and tubulin polymerization inhibition,** Romagnoli R., Kimatrai Salvador M., Schiaffino Ortega S., Baraldi PG., Oliva P., Baraldi S., Lopez-Cara L.C., Brancale A., Ferla S., Hamel E., Balzarini J., Liekens S., Mattiuzzo E., Basso G., Viola G.. Eur J Med Chem. **2018**, 143, 683-698.

III **Design, Synthesis, and Biological Evaluation of 6-Substituted Thieno[3,2-d]pyrimidine Analogues as Dual Epidermal Growth Factor Receptor Kinase and Microtubule Inhibitors**, Romagnoli R., Prencipe F., Oliva P., Baraldi S., Baraldi P. G., Schiaffino Or. Santiago, C. Mariem, K. S. Maria Lopez-Cara, L.C. Brancale, Journal of Medicinal Chemistry (**2019**), 62(3), 1274-1290.

IV **Design, Synthesis, in Vitro and in Vivo Biological Evaluation of 2-Amino-3-Aroyl Benzofuran Derivatives as Highly Potent Tubulin Polymerization Inhibitors**, Oliva P., Romagnoli R., Brancale A., Hamel E., Bortolozzi R, Viola G., in preparation.

Papers not included in this thesis

Design, synthesis and biological evaluation of 3-substituted-2-oxindole hybrid derivatives as novel anticancer agents, Romagnoli R., Baraldi P.G., Prencipe F., Oliva P**.**, Baraldi S., Salvador M.K., Lopez-Cara L.C., Bortolozzi R., Mattiuzzo E., Basso G., Viola G.. *Eur J Med Chem.* **2017**, *134:*258-270.

Arylamidonaphtalene sulfonate compounds as a novel class of heparanase inhibitors, Rondanin R., Fochi S., Baruchello R., Bernardi T., Oliva P., Semeraro F., Simoni D., Giannini G. *Bioorg Med Chem Lett*. **2017**, *27*, 4421-4425.

Synthesis and biological evaluation of alpha-α bromoacryloylamido indolyl pyridinyl propenones as potent apoptotic inducers in human leukemia cells, Romagnoli R., Prencipe F., Lopez-Cara L. C., Oliva P., Baraldi S., Baraldi P.G., Estevez-Sarmiento F., Quintana J. Estevez, *Journal of Enzyme Inhibition and Medicinal Chemistry* (**2018**), 33(1), 727-742.

3-Aryl /Heteroaryl-5-amino-1-(3',4',5'-trimethoxybenzoyl)-1,2,4-triazoles as antimicrotubule agents. Design, synthesis, antiproliferative activity and inhibition of tubulin polymerization, Romagnoli R., Prencipe F., Oliva P., Baraldi S., Baraldi P. G., Brancale A., Ferla S., Hamel E., Bortolozzi R., Viola G., *Bioorganic Chemistry* (**2018**), 80, 361-374.

Design, synthesis and biological evaluation of novel vicinal diaryl-substituted 1H-Pyrazole analogs of combretastatin A-4 as highly potent tubulin polymerization inhibitors, Romagnoli R., Oliva P., Salvador MK., Camacho ME., Padroni C., Brancale A., Ferla S., Hamel E., Ronca R., Grillo E., Bortolozzi R., Rruga F., Mariotto E., Viola G. *Eur J Med Chem*. **2019**; 181:111577.

Contents

1. Introduction

1.1 General remarks

I. General Introduction

Nature is a plentiful source of chemical compounds with a therapeutic potential, that could be useful in the prevention and treatment of diseases such as cancer. Over 60% of chemotherapeutic agents currently used in therapies are derived from natural compounds originating from plants, animals, marine agents and microorganism.[1] Plant material has been exploited as source of relevant medical chemical agents for over 70 years. Some of the earliest reports include vinca alkaloids: vinblastine and vincristine, and the isolation of podophyllotoxin.[2] However, despite the discovery of the therapeutic activities of many natural compounds and our ability to synthesize a broad spectrum of them, the use of natural products has intrinsic problems, that include accessibility of the starting material, limited availability, ecological and legal considerations. Importantly, many of these natural compounds do not exhibit significant pharmacological effects in the treatment of cancer.[3]

In order to discover products useful for the treatment of malignancies, intense research efforts have been undertaken in the last years in field of cancer drug discovery, however, effective drugs against many types of tumours still remain to be discovered. Most important component of the research efforts is to develop compounds that show improved selectivity, only targeting cancer cells, as compared to the classical therapeutic options, such as chemotherapy and radiotherapy, that are indiscriminate.[4]

The holy grail of oncology research is to discover novel therapeutic approaches that exploit differences between tumour and healthy cells.[4] In order to reach this goal, current treatments with small molecule agents are often performed in combination with others therapies. Moreover, small molecules agent side-effects that include toxicity and acquired drug resistance, inspired a new series of studies aimed at the synthesis of more active and effective compounds for cancer therapies.[5]

II. Specific Drugs General Introduction

Amongst diverse cancer therapeutic targets, drugs targeting **microtubules** represent one of the most effective classes of cancer chemotherapeutic compounds available to date.[6] This is in part due to the great body of structural and biophysical knowledge of tubulin protein, which enables scientists to perform structural modelling and drug efficacy studies aimed to continuously develop new and better active compounds.

A large number of chemically distinct compounds, binding to soluble tubulin and/or directly to tubulin in microtubules, have been shown to exhibit significant antimitotic properties, and to inhibit cell proliferation by interfering with microtubule polymerization dynamics.[7] The microtubule system has been selected as preferential target for development of drugs because it is essential in a variety of fundamental cellular processes, including mitosis, formation and maintenance of cell shape, regulation of motility, secretion and intracellular transport.[8]

Moreover, tumour vasculature is an attractive new target for cancer therapy.[9] From an anatomical and functional points of view, the vascular system formed within cancerous tumours is abnormal.[10] Tumour blood vessels are often structurally irregular, chaotic, tortuous, lack of mural cell coverage and have a relatively higher density compared to normal vasculature.[10]

Recently, it has been observed that several drugs, especially microtubule-targeted drugs, can act as **vascular disrupting agents (VDAs)**, targeting the tumour vascular network thus causing an interruption of the supply of nutrients to the tumour, which leads to the death of the surrounding cells.[11] Of most relevance to the work of this thesis is Combretastatin A-4 (CA-4), a natural *cis-stilbene* isolated in 1989 from the South-African tree *Combretum Caffrum*.[12] CA-4 is one of the most potent molecules able to bind a specific site on the tubulin subunit, inhibiting tubulin polymerization and the formation of microtubules.[13] As a result of CA-4 binding, tumour cell proliferation is inhibited that consequently leads to apoptosis, which has been attributed to defects in the mitotic spindle formation.[7] Importantly, CA-4 also showed to have vascular-disrupting properties, acting at the level of tumour vascular system, leading to the interruption of blood flow and consequent necrosis of the tumour tissue.[10]

In addition to CA-4, there have been many other related synthetic compounds synthesized to interfere with tubulin biology by diverse mechanisms. Many of these compounds could be promising candidates for use in cancer therapies, however, further studies are needed to characterize their effectiveness or to derivatize them to improve their efficacy.[14,15]

1.2 Tubulin and microtubules

1.2.1 Composition and organization

Microtubules (MTs) are dynamic cytoskeletal polymers present in all eukaryotic cells. The organization of microtubule network plays crucial structural and functional roles in many fundamental biological processes, including cell division, development and maintenance of cell shape, regulation of motility, cell signaling and intracellular transport.[16]

Structurally, microtubules are comprised of long polymers that are composed of two globular proteins, α- and β-tubulin (TB). α- and β-tubulin bind together to form a dimer in a GTP-dependent manner, which is the basic unit of longer polymer. The tertiary structure of tubulin proteins is comprised of a core of two β-sheets surrounded by α-helices and the protein can be divided into three functional domains: the amino (N)-terminal, intermediate and carboxy (C)-terminal domains.[17] The two tubulin proteins exist in different isotype forms: there are six isotypes of each α- and β tubulins in human cells;[18] they share 40% amino acid sequence homology in the N-terminal domain and both undergo a variety of post translational modifications.[19] When multiple α- and β-tubulin polymers come together, they form hollow tubes of about 250 Å in diameter which are called microtubules.[20] More specifically, the α- and β-subunits heterodimers aggregate in a head to tail-specific manner to form a long protofilament.[19] The protofilaments then associate in a parallel manner to form a pipe-like structure or the microtubule. The polymerization process is very dynamic: a single microtubule can be observed in living cells to grow on one end and disappear on the opposite at the same time.[21] The tubulin filaments can make two different type of contacts: **longitudinal** contacts that run along the length of the protofilament, and the **lateral** contacts between protofilaments which make up the circumference of the microtubule.[22] *In vivo*, typically 13 protofilaments arrange in parallel making up the microtubule (MT)[23] (Figure 1). Each protofilament has intrinsic polarity with α-tubulin exposed at one end (called the "**minus end**") and β-tubulin exposed on the other end (called "**plus end**").[24] The plus end of the microtubule is usually rapidly growing and is kinetically more dynamic as opposed to the minus end, which tends to lose subunits if is not stabilized. Although both ends alternately grow or shorten, net growth occurs at the plus end and net shortening at the minus end.[25]

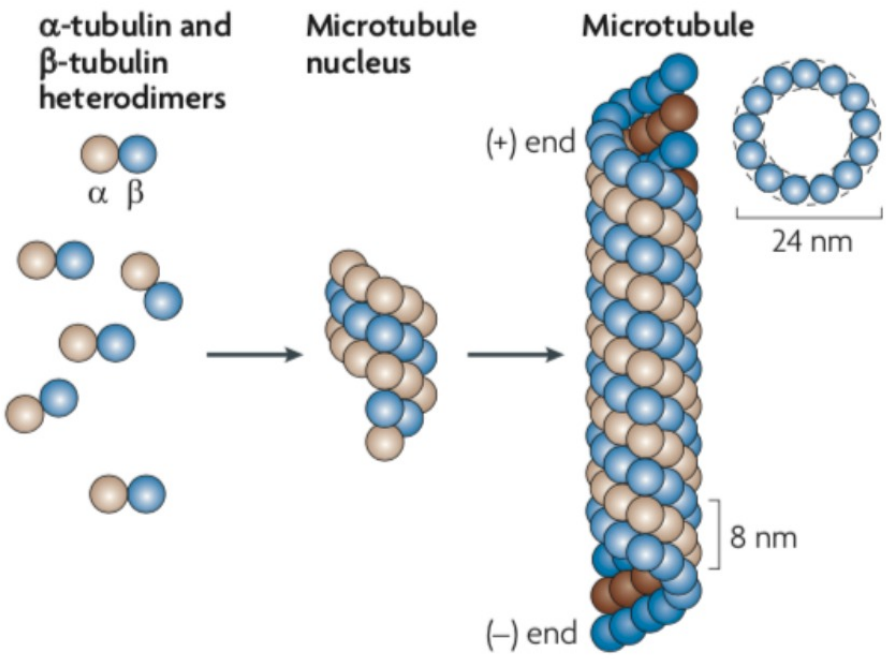

Figure 1. Microtubule components.[25]

Atomic structure

Many structural studies have played a pivotal role in contributing to our understanding of the microtubule organization. The tertiary crystal structure of α- and β-tubulin dimer depicts the orientation of the two subunits in the dimer (Figure 2). This structure highlights, the head tail organization of dimer, tertiary structure similarities, and the association with the two nucleotides.[19,26] As mentioned before, the both tubulins are comprised of three functional domains: the amino (N)-terminal, intermediate, and carboxy (C)-terminal domains.[17]

The **N-terminal domain** contains the nucleotide-binding region for guanosine triphosphate (GTP); GTP binding is very important both for structure of tubulin heterodimers and for the conformation of longitudinal protofilaments (see the section 1.2.2). Both α- and β-tubulin forms bind one molecule of guanine nucleotide with high affinity[24] (Figure 2). The **intermediate domain** mediates longitudinal and lateral interactions. It contains a binding site for the microtubule-stabilizing agent Taxol (discussed later in section 1.3.2.1.), an important therapeutic agent.[19] The last, **carboxy-terminal domain** constitutes the binding surface for several enzymes, motor proteins, and MT-associated proteins (MAPs), all of which are involved in the modulation of MT function and dynamics.[17]

In conclusion, microtubules are an essential component of many important biological processes, including cell division or intracellular transport. Their structural nature and their dynamic features have made them subject of many research studies seeking to develop new and effective anti-cancer drugs. The research strategies and number of compounds will be discussed in the following sections.

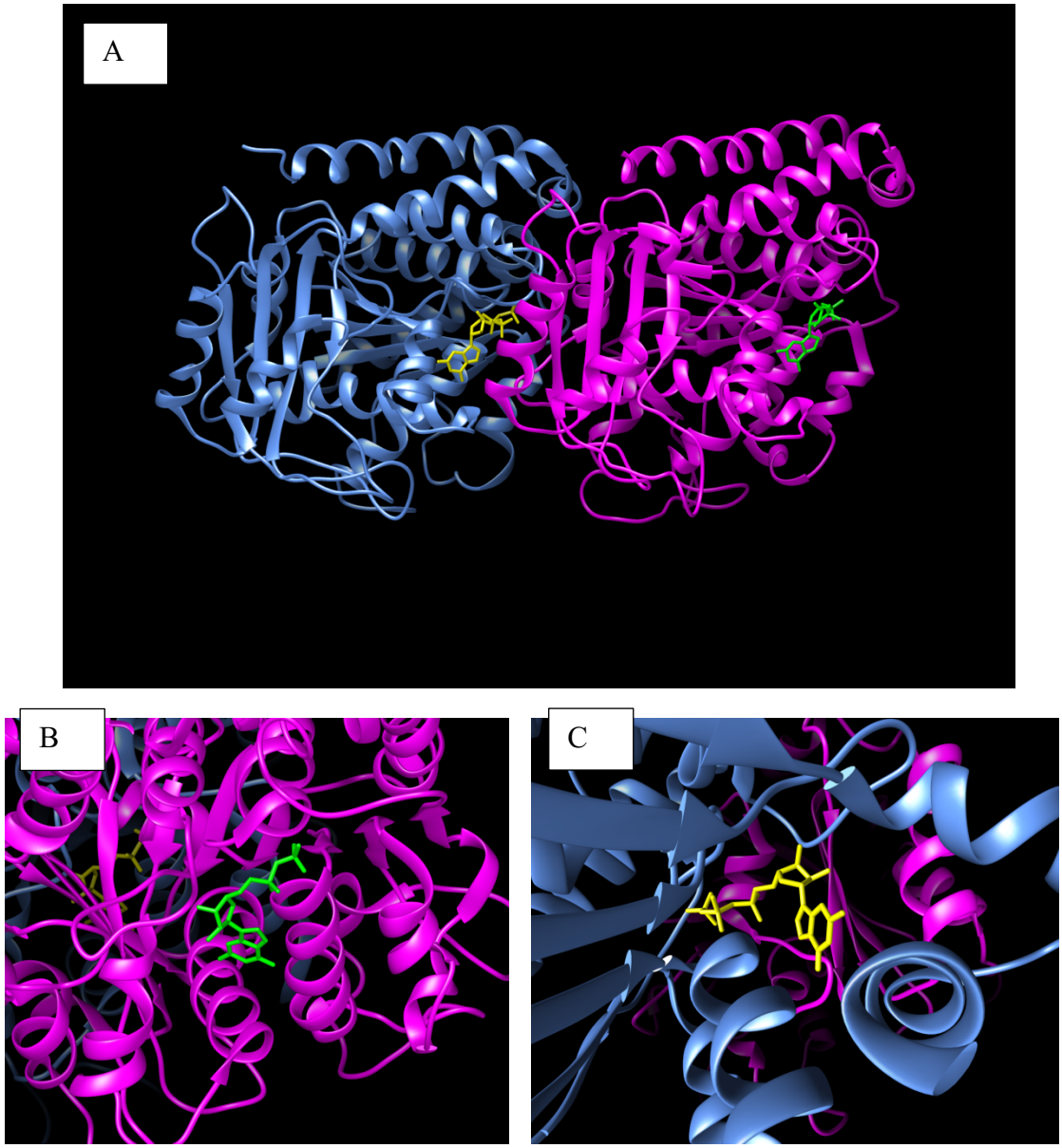

Figure 2. Crystal structure of αβ- tubulin dimer. (A) Ribbon diagram of the zinc-induced αβ-tubulin dimer (**α-tubulin** in blue, **β-tubulin** in magenta, **GDP** in green, **GTP** in yellow; PDB code: 1JFF). The head to tail organization of tubulin proteins, structural similarity, and association with two nucleosides is readily apparent. (B, C) Close up view of the two nucleoside binding sites on each tubulin protein.

1.2.2 Microtubule dynamics: Dynamic Instability and Treadmilling

MTs are highly dynamic structures, that are in a state of permanent turnover.[27] They exhibit rapid and complex polymerization dynamics, which is essential to maintaining morphology of microtubule array and cellular structure, and at the same allow cells to be flexible and quickly adapt to the extracellular environments.[6]

The formation of microtubule polymers occurs through a "**nucleation-elongation mechanism,**" where the slow formation of a short microtubule "nucleus" is followed by rapid elongation of the microtubule at its ends with the addition of tubulin dimers to grow the polymer.[6] The growth and shrinkage of microtubules happen through concurrent addition and release of subunits at the opposing ends of the polymer. This process is called "dynamic instability," and was first described over thirty years ago by Mitchison and Kirschner[28] (Figure 3). The two ends of an MT are not equivalent during the different phases of dynamic instability, and are influenced by the presence of many microtubule-associated protein.[6] The primary factor that determines the rate of microtubule growth/shrinkage is the local concentrations of tubulin subunits, although this alone is not sufficient to completely explain the dynamic properties of MT.[21] The polymerization process happens in a stochastic manner and is also influenced by factors such as the concentration of tubulin or the temperature.[21] The change from microtubule growth to shrinkage is called "catastrophe". The opposing process, when after a while a shrinking MT end "pauses" and/or begins to grow again is referred to as "rescue".[21] Other characteristics commonly used to describe microtubules are: the growth rate and its duration, the shortening rate and its duration, and the frequency of catastrophe and rescue events.[21]

The "treadmilling" (Figure 4) is another dynamic behaviour of microtubules which describes unidirectional movement of tubulin subunits from the plus end to the minus end of the polymer without a significant change in microtubule length. It is governed by differences in the critical subunit concentrations at the opposite MT ends and it is essential during mitosis.[29]

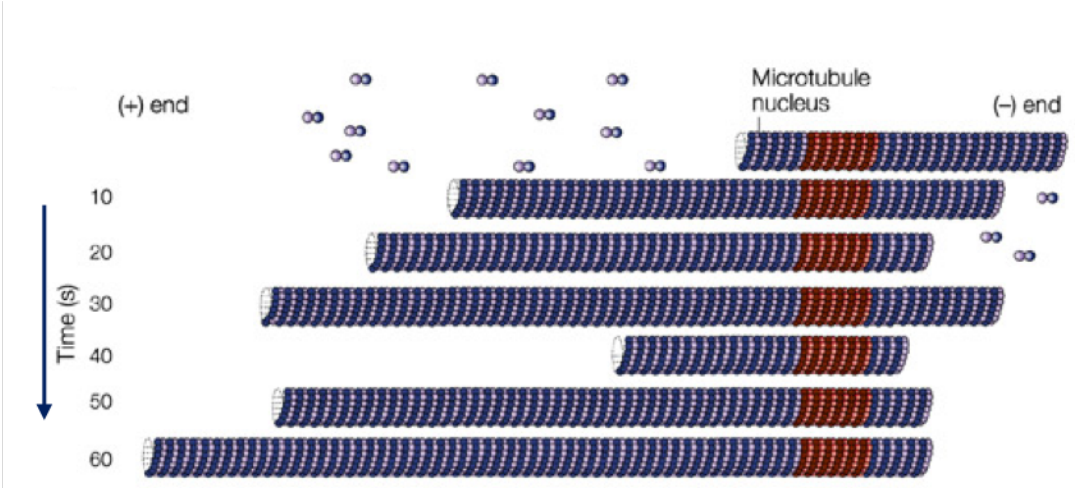

Figure 3. Dynamic instability of MTs. Changes in length of a single MT over time.[6]

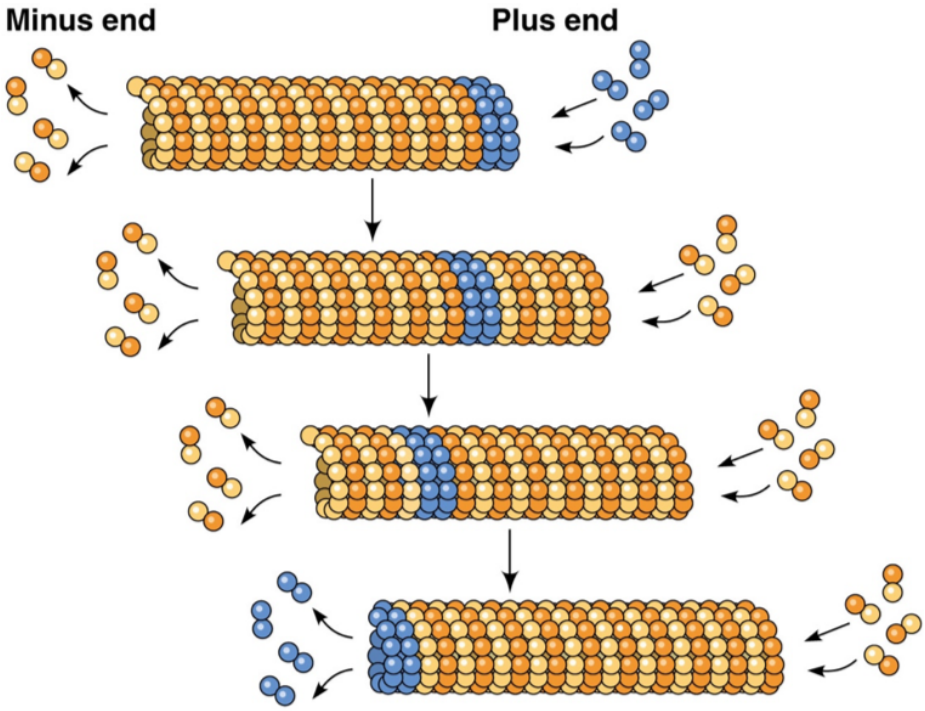

Figure 4. Treadmilling MT. Tubulin heterodimers are added at the plus end of the MT and are lost from the minus end without a significant change in microtubule length (Principles of Cell Biology).

Both "**dynamic instability**" and "**treadmilling**" behaviours are modulated through GTP hydrolysis by tubulin proteins. Both α- and β- tubulin molecules bind one molecule of GTP, but only the GTP bound to the β-tubulin can be exchanged, and it is hydrolysed shortly after being incorporated into the polymer.[21] GTP-tubulin complex forms more stable inter-subunit interactions, while GDP-tubulin complex establishes comparatively much weaker interactions and is prone to depolymerization. In fact, it is generally accepted that the newly formed microtubule tip contains a cap of GTP-tubulin (called the **GTP-cap**), which has stabilizing properties, whereas the microtubule shaft is composed of GDP-tubulin and it is intrinsically unstable.[29] In the presence of the cap, a microtubule continues growing, meanwhile the loss of the cap leads to rapid shrinkage[21] (Figure 5).

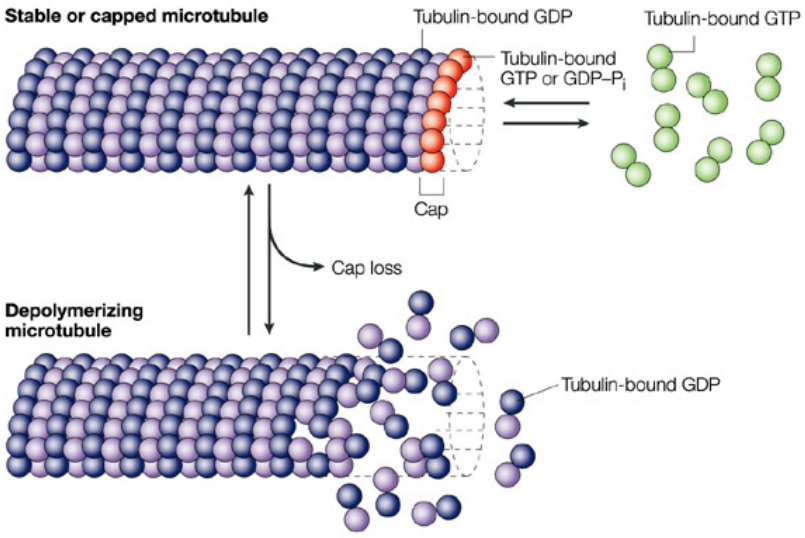

Figure 5. Microtubule stability and GTP. GTP bound to *β*-tubulin is hydrolyzed to GDP and inorganic phosphate (P_i) at the time that tubulin dimer is added to the MT plus ends, or shortly thereafter. A MT end containing tubulin-GTP or tubulin-GDP-P_i is stabilized or "capped," and does no depolymerize easily. Hydrolysis of GTP-bound tubulin and the subsequent release of P_i induce conformational changes that destabilizes the MT polymer.[6]

The GTP hydrolysis induces a conformational change at the inter-dimer interface, which leads to complex destabilization.[30] *In vitro* structural studies of the growing microtubules revealed that plus ends adopt slightly curved, flattened and tapered sheet-like structures, called "**tubulin sheets**", while depolymerizing plus ends display strongly curved, "**peeling**" protofilaments[29] (Figure 6). The precise chemical nature of the stabilizing cap and the mechanism underlying the transition between growth and shrinkage (microtubules rescues and catastrophes) are still poorly understood.[29]

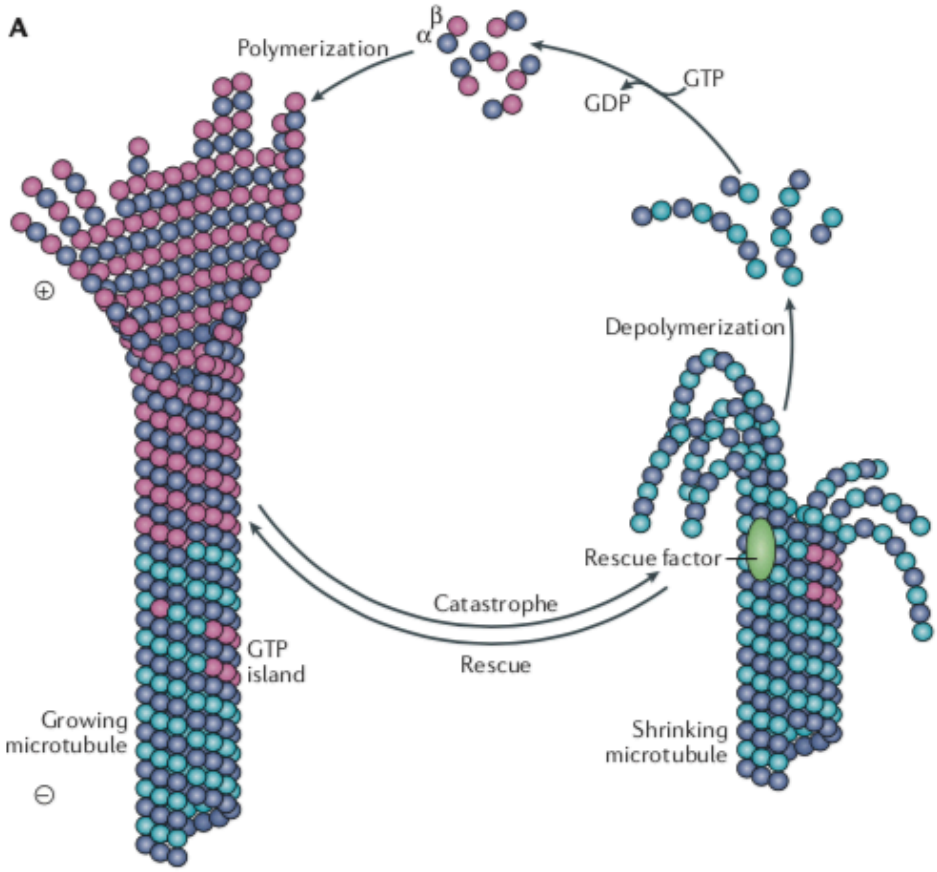

Figure 6. Polymerization and depolymerization of tubulin. The dynamics of this processes is controlled by hydrolysis of the GTP bound to β-tubulin, which enables MTs to switch between the two states: catastrophe and rescue. GTP-bound tubulin dimers are incorporated into growing MTs. A stabilizing CTP-cap is maintained in the growing MT ends, the loss of which leads to a catastrophe and depolymerization. The stability of microtubules is also though be induced by the presence of "rescue factors" in the microtubule lattice.[29]

In living cells, the dynamic instability of microtubules is regulated spatially and temporally by numerous proteins, that are in turn regulated by cell cycle or by their localization inside the cell.[21] The proteins that regulate microtubule dynamics can have either **stabilizing effects** (for example MAPs: microtubule-associated proteins that copurify with tubulin) or **destabilizing effects** (for example Oncoprotein 18 (Op18)/Stathmin) that promote microtubule growth or disassembly.[31] MAPs are generally filamentous, positively charged, and very flexible proteins and include MAP1, MAP2, MAP4 and tau protein.[32] It has been suggested that MAPs bind to tubulin at multiple different binding sites, often cross-bridging multiple subunits, and allowing for increased stabilization of inter-subunit interactions.[21] MAPs are often targeted or regulated by protein kinases, such as p34cdc2 kinase (cyclin-dependent kinase 1, CDK1), that inevitably control changes of MT dynamics in cell-cycle dependant manner.[33] MAPs phosphorylation can lead to their dissociation from MTs, and thus increasing microtubule instability.[34] MAP protein family has four members that include MAP1, MAP2, MAP4 and tau, with MAP4, being the most abundant family member.[35]
The plus-end tracking proteins (+TIPs) belong to another group of MAPs that bind to microtubule plus ends, recruit tubulin dimers and increase the rate of tubulin addition to growing microtubule tips.[34] The **e**nd-**b**inding protein**s** (EBs), a subset of +TIPs proteins, are proteins shown to increase microtubule polymerization rates by modulating the structure of microtubules ends.[36]

In contrast to MAPs there are microtubule-binding proteins that bind to tubulin dimers and promote MT depolymerization. This group of proteins includes Oncoprotein 18 (Op18)/Stathmin, Xenopus kinesin central motor 1 (XKCM1), and katanin.[37] Op18/Stathmin is a prominent microtubule destabilizer which has been studied intensively, but its mechanism of action remains unclear.[38] One model of Op18/Stathmin function suggests that it may promote catastrophe events **indirectly**, it that induces microtubule depolymerization by binding and sequestering tubulin away from the polymer.[39] The second model proposes that Op18/Stathmin is able to cause catastrophe by **directly** destabilizing growing microtubules.[40] Multiple studies reported the Op18/Stathmin's sequestration activity,[41] however the mechanism of any direct action has not been supported thus far.[39] Furthermore, because Op18/Stathmin binds to microtubule very weakly, direct model may be difficult to demonstrate.[41]
Other microtubule binding proteins, in particular MT depolymerizing proteins, are XKCM1 and XKIF2. They belong to kinesin-like protein family and are required for the formation and maintenance of the mitotic spindle.[44] Mitotic spindle organization is another important

biological role of microtubules. The XKCM1 and XKIF2 use their ATPase activity to directly depolymerize MTs from both ends by inducing a destabilizing conformation of the tubulin subunits at the MT ends causing the destabilization of the microtubule lattice.[44]
Last prominent group of proteins involved in regulation and destabilization of MTs is the motor proteins, such as kinesins[45] and dyneins.[46] Kinesins and dyneins form protein complexes that move along MTs, towards the plus and minus ends, respectively, by hydrolyzing ATP.[30]
They can carry membrane-enclosed vesicles/organelles to different locations within the cell, as well as help cytoskeletal filaments to slide against each other and thus facilitate movements important during cell division.[30]
Kinesins and dyneins generally move in the different directions along MTs, and thereby control bi-directional vesicle transport.[30] Kinesins show plus end-directed motility, dyneins show minus end-directed motility.[30]

Over the past years, remarkable progress has been made in the microtubule field with the discoveries of new structural states of αβ-tubulin, the studies of the material properties of microtubules and the investigation about proteins involved in the transition of the different states, increased our understanding of microtubule dynamics. The importance of microtubules in vital cellular functions made them very attractive target for cancer therapies, which will be more discussed in more detail in following sections.

1.3 Microtubule targeting agents

1.3.1 General classification

As described in the previous sections, tubulin and microtubules play an essential role in diverse cellular processes, including cellular replication.[47] Any perturbance in microtubule dynamics can have dire consequences on cell division, and therefore cellular survival. Just to mention few examples, tubulin plays crucial roles in cell cycle, during the process of chromosomal segregation, or in the intracellular trafficking.[47] Function of tubulin in the intracellular trafficking of oncoproteins, its influence on cell migration and endothelial cell shape have been of high interest in disease contexts, including cancer.[48] Because of tubulin's crucial involvement in vital cellular functions governed by microtubules, it represents very attractive chemotherapeutic target.[6]

A large number of natural and synthetic chemical compounds, called “tubulin interactors”, that interfere with the dynamic equilibrium of polymerization and depolymerization have been synthesized and are being studied.[49]

Many of these agents act on tubulin by interacting with different binding sites, and thus influence stability and dynamics of MTs in very diverse ways. Microtubule Targeting Agents (MTAs) can be divided into three main groups: **(1) Microtubule stabilizers (MSAs) -** molecules occupying paclitaxel, laulimalide and others binding domains on tubulin proteins that stabilizing the microtubule structure; **(2) Microtubule destabilizers or inhibitors (MDAs) -** molecules occupying colchicine and vinca binding domain on the tubulin proteins that prevent their assembly into microtubule and/or induce depolymerization at high concentration**;** and **(3) molecules with mixed mechanism of action**[50] (Figure 7).

Despite the specific mechanism of action of tubulin targeting agents, the most important action of these drugs is the suppression of spindle microtubule dynamics, which leads to the slowing or blocking of mitosis and induction of apoptosis otherwise called cell death.[6]

Because of their effects on the mitotic spindle, microtubule damaging agents have also been named “spindle poisons”.[51] Increased division rate is common characteristic of many cancers, therefore, “spindle poison” compounds represent an important class of anticancer drugs. To date number of spindle poison compounds have been proven successful in treating different type of cancers.[52]

Two most important limitations of microtubule-targeting agents include cytotoxicity that indiscriminately effect both tumour and normal cells, and that they lack any selectivity.[52]

Thankfully, because tumour cells often have faster cell proliferation rates, they tend to be more susceptible to at least some microtubule targeting agents.[53] It has been also noted that loss of p53 gene, key cell cycle regulator, sensitizes some cancer cells to microtubule damaging drugs through diverse mechanisms.[54,55]

In the last few years, efforts to identify new microtubule targeting agents that are more specific, and have low side effects have intensified.

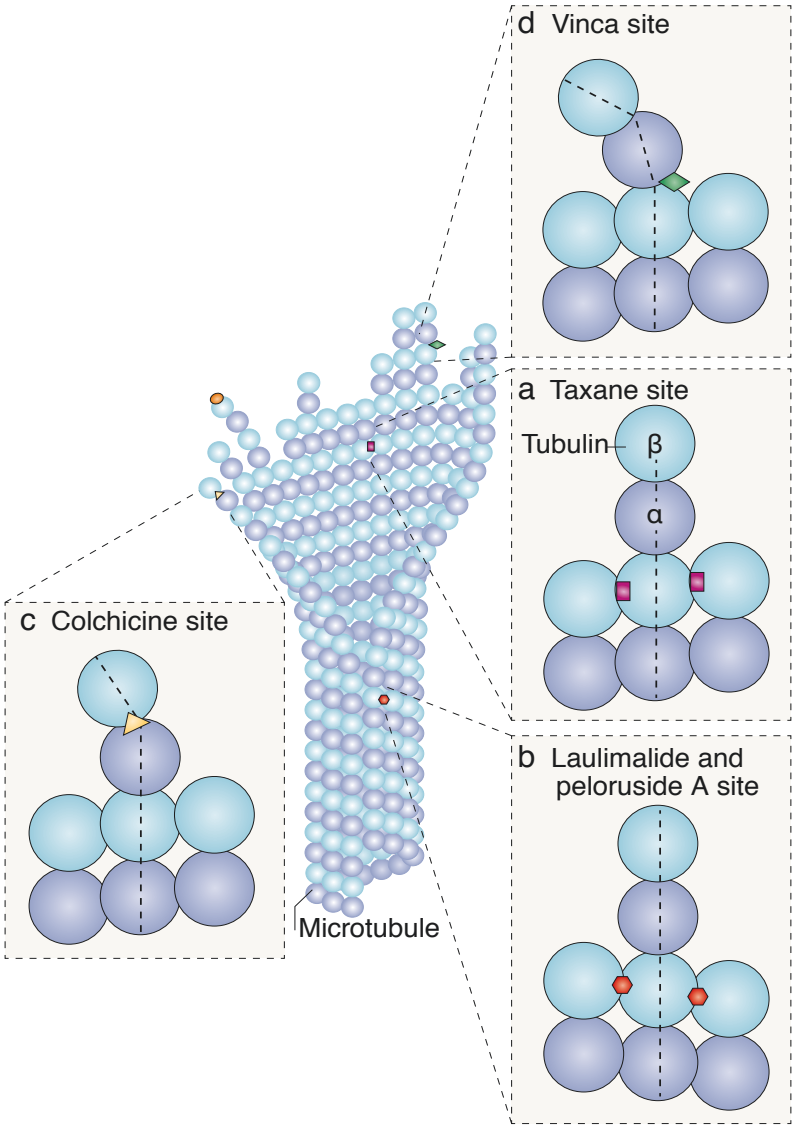

Figure 7. Microtubule targeting agents are divided in microtubule-stabilizing agents (MSAs) and microtubule-destabilizing agents (MDAs). **a)** Most of MSAs, bind along to the "texane site" on β-tubulin. They stabilizing longitudinal and/or lateral tubulin, **b)** Laulimalide and peloruside A bridge two β-tubulin dimers from adjacent protofilaments on the outside surface of the microtubule. **c)** MDAs bind to the "colchicine site" located between α-tubulin and β-tubulin subunits. Colchicine-site MDAs destabilize microtubules. **d)** MDAs can also bind to a different site, such as to the "vinca site".[30]

1.3.2 Microtubule stabilizing agents

Tubulin stabilizing agents constitute a diverse group of compounds that are able to interact with β-tubulin and stimulate polymerization.

Many naturally occurring agents have been described to have tubulin stabilization effects, and to occupy different binding sites on tubulin protein.[56] These agents mainly exert their effects during the G2/M phase of cell cycle, disruptions of which usually leads to cell death.[56] Many of the natural compounds have been derivatized and synthesized as semi-synthetic tubulin stabilizing agents. In the next sections I will discuss some of these synthetic agents based on their target binding site on tubulin protein.

1.3.2.1 *Taxane site binding agents*

The taxanes represent one of the most commonly used classes of microtubule-stabilizing chemotherapy agents over the past several decades. Many studies have indicated that taxanes bind to β-tubulin of inner surface of microtubule lumen, stimulating polymerization reaction[57] (Figure 7). This binding site is known as taxane binding domain.[58] Taxanes bind to soluble tubulin poorly, however they strongly interact with assembled microtubules.[59]

The first microtubule-stabilizing agent used in the treatment of cancer from the taxane group was Paclitaxel (**1**), isolated from the bark of the Pacific yew tree *Taxus brevifolia*.[2]

Paclitaxel binds to the β-tubulin subunit, and promotes microtubules stabilization by inducing conformational changes of a specific loop region of β-tubulin, which result in more stable interactions between protofilaments.[59] Early on after its discovery, clinical application of paclitaxel was impeded by its limited quantities that could be obtained from the yew tree.[60] However, this issue was eventually overcome by advances in the semi-synthesis of 10-deacetylbaccatin III (**2**),[61] that eventually led to the full synthesis of paclitaxel.[62] In 1992 Food and Drug Administration (FDA) approved paclitaxel (Taxol™) for the treatment of metastatic ovarian, breast, and non-small cell lung cancer.[63]

The specific effects of taxol on microtubule polymerization dynamics are complex and depend on the stoichiometry of taxol binding to the microtubule.[64] High concentration of taxol (1-20 μM), both *in vitro* and in cells, increases microtubule polymerization. This characteristic is associated with nearly 1:1 stoichiometric binding of taxol to tubulin in microtubules.[6] However, it has been found that in contrast with the high concentration required to increase microtubule polymerization, over ten-fold less taxol molecules (10-100 nM) is sufficient to powerfully stabilize microtubule dynamics without increasing

microtubule polymerization.[64] As a result of taxol action, suppression of microtubule dynamics leads to mitotic block,[65] preventing the dividing cancer cells from progressing from metaphase into anaphase, and cells eventually die by apoptosis.[66] Both Paclitaxel and its semisynthetic analogue Docetaxel (**3**) are now commonly used as antineoplastic agents.[64] The clinical success of this class of molecules has led to develop other compounds that enhance microtubule polymerization, some of them include: cabazitaxel (**4**), milataxel (**5**) and BMS-275183 (**6**)[60] (Figure 8).

Another family of compounds that compete with paclitaxel for microtubule binding are **Epothilones**.[67] This novel class of microtubule-stabilizing agents is described to promote microtubule assembly.[67] They compete with paclitaxel because they interact with the same taxane-binding site on β-tubulin.[68] Currently there are five epothilone or epothilone-derived compounds undergoing clinical trials.[60] The most promising of them is epothilone B (EPO 906) (developed by Novartis) which is currently in phase III clinical trials for the treatment of different cancer types, including breast, ovarian, carcinoid and endometrial carcinoma.[69] An example epothilone-type compound which is in phase III clinical trial for the treatment of breast cancer is the lactam analogue of epothilone B (Ixabepilone) (**7**) [60] (Figure 8).

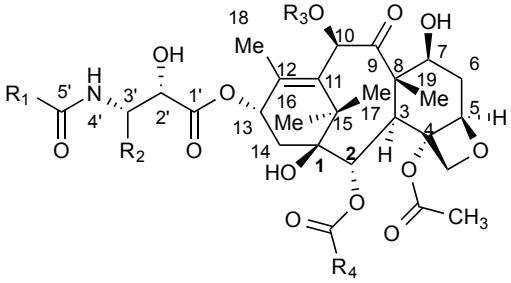

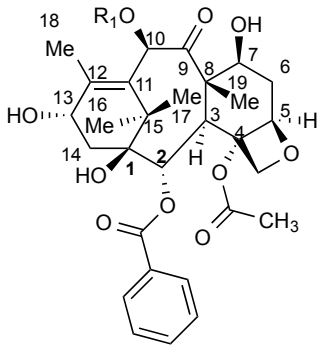

1 Paclitaxel ($R_1 = R_2 = R_4 = Ph$, $R_3 = Ac$)
3 Docetaxel ($R_1 = R_4 = Ph$, $R_2 = t\text{-BuO}$, $R_3 = H$)
4 Cabazitaxel ($R_1 = t\text{-BuO}$, $R_2 = R_4 = Ph$, $R_3 = CH_3$)
5 Milataxel ($R_1 = t\text{-BuO}$, $R_2 = 2\text{-furan}$, $R_3 = H$, $R_4 = Ph$)
6 BMS-275183 ($R_1 = t\text{-BuO}$, $R_2 = t\text{-Bu}$, $R_3 = Ac$, $R_4 = COOCH_3$)

2 Baccatin III ($R_1 = Ac$)

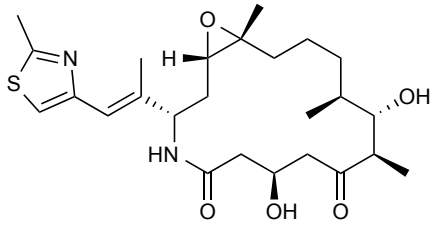

7 Ixabepilone

Figure 8. Taxane binding site tubulin stabilizing agents.

1.3.2.2 *Non-taxane site binding agents*

In addition to the taxane binding site targeting agents, number of molecules that have similar stabilizing effects, but based on different type of tubulin interactions, have been discovered.[56] For example, Laulimalide (**8**) and Peloruside A (**9**) (Figure 9) bind a unique non-taxane site on β-tubulin.[70] (Figure 7). Laulimalide is a macrolide of marine origin, isolated for the first time in 1988 from marine sponge *Hyattella sp*. in Indonesia.[71] Laulimalide shows cytotoxic activity against different cancer cell lines. It has been demonstrated to have antiangiogenic activity, and to be very effective in acting against taxane resistant tumours.[50] However, due to its toxicity, use of Laulimalide is limited.[50]
Another non-taxane agent, Peloruside A, also belongs to macrolide family and has good bioactive profile.[72] Peloruside A binds to the same binding site as laulimide and both laulimalide and peloruside show a synergetic effect with taxoids.[73]

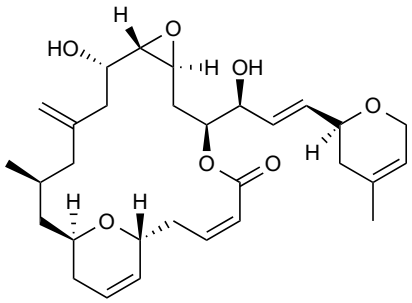

8 Laulimalide

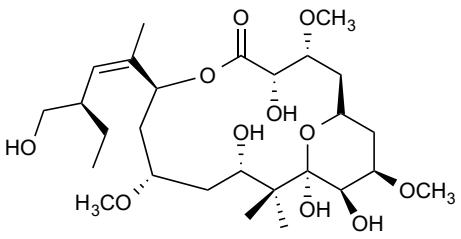

9 Peloruside A

Figure 9. Non-taxane binding site tubulin stabilizing agents.

1.3.3 Microtubule destabilizing agents

In contrast to tubulin-stabilizing agents are the agents that are able to inhibit microtubule polymerization, which are called microtubule destabilizers. Their general mechanisms of action are disruption of microtubule dynamics which halts mitosis and usually leads to cell death.[6]

Microtubule destabilizing compounds can also be classified based on their binding affinities to tubulin, as either **vinca domain-binding** and **colchicine domain-binding**.

1.3.3.1 *Vinca alkaloid site binding agents*

Vinca alkaloids are a relevant group of antimitotic and anticancer agents. Vincristine (**10**) and Vinblastine (**11**) are prominent and naturally occurring members of this family that have been widely used in anticancer therapies, either as a single agent as well as in combination therapies.[74,75]

Promising clinical efficacy of vincristine and vinblastine has led to the development of related semi-synthetic analogues that include – vindesine (**12**), vintripole (**13**), vinxaltin (**14**), vinorelbine (1**5**) and vinflunine (**16**), (Figure 10). The reason for their derivatization was to reduce their main side effects, such as neurotoxicity and myelosuppression – condition in which bone marrow activity is decreased - (as a result of blockage of mitosis and proliferation of the rapidly cycling bone marrow).[76]

The mechanism through which Vinca alkaloids act is highly dependent upon the drug concentration.[57] Jordan and colleagues reported that Vinca alkaloids, at high concentrations (10-100 nmol/L in HeLa cells) used *in vitro* and in cell culture depolymerize microtubules and destroy mitotic spindles, leaving the dividing cells blocked at the metaphase/anaphase transition. At more clinically relevant low concentrations (0.8 nmol/L in HeLa cells), Vinblastine is able to block mitosis without depolymerizing spindle microtubules, and is still causing cell death.[57]

Vinca alkaloids bind to the β-tubulin at a different region than taxanes, called the Vinca-binding domain, which is located very close to the GTP site at the interface between β- and α-tubulin subunits[77] (Figure 7). Vinblastine binds to soluble tubulin rapidly and reversibly in a temperature independent manner, inducing conformational change to stabilize its binding.[78]

Other members of the vinca alkaloid-type compounds includes noscapine (an antitussive drug), maytansine, rhizoxin, spongistatins, podophyllotoxin, antifungal and antihelmintic agents, all of which function in similar fashion, and have been reviewed elsewhere.[56]

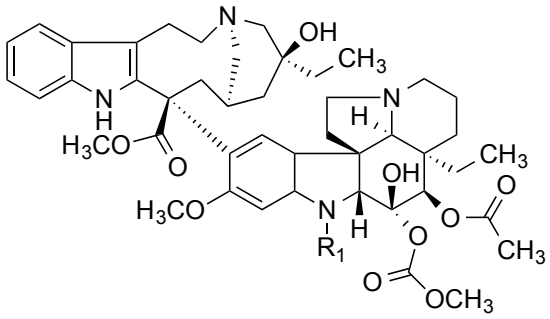

10 Vincristine (R_1 = CHO)
11 Vinblastine (R_1 = CH_3)

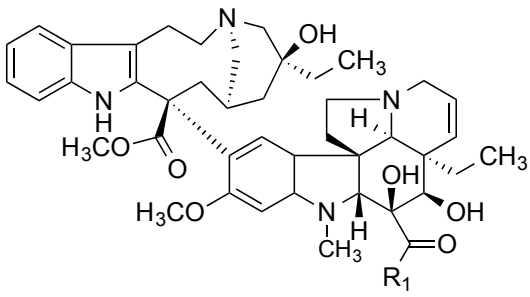

12 Vindesine (R_1 = NH_2)
13 Vintripole (R_1 = L-Trp-OC_2H_5)
14 Vinxaltin (R_1 = D-Vla(P)-$(OC_2H_5)_2$

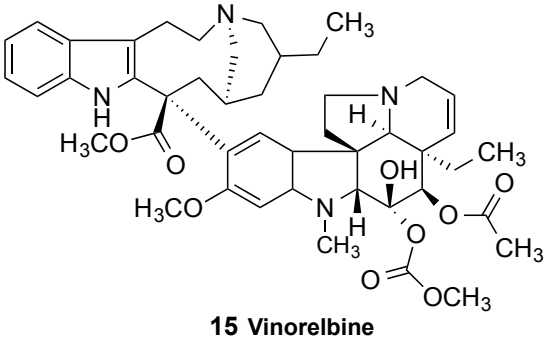

15 Vinorelbine

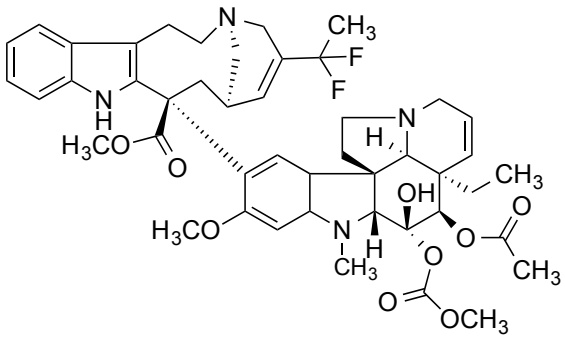

16 Vinflunine

Figure 10. Vinca alkaloid site binding agents.

1.3.3.2 *Colchicine alkaloid site binding agents*

Colchicine (**17**), represents the first known microtubule inhibitor, and it was isolated from the leaves of meadow saffron (*Colchicum autumnale*).[79]

Similar to Vinca alkaloids, the therapeutic effects of colchicine are concentration-dependent. At high concentration colchicine inhibits microtubule and depolymerizes pre-formed microtubules. At the lowest concentration, colchicine inhibits microtubule dynamics, without inducing depolymerization.[57]At first, slow binding step, colchicine interacts with soluble tubulin to form a complex: tubulin-colchicine complex, which then incorporates at the microtubule ends and influences the dynamics.[80]

At low concentration, incorporation of complexes disrupts the tubulin lattice, its dynamics are suppressed, but it does not compromise the ability of tubulin to be incorporated. At high concentration of tubulin-colchicine complex, tubulin addition is completely blocked.

Despite the differences between the different classes, colchicine, similarly to all other microtubule targeting compounds, is able to stabilize microtubule dynamics at low concentrations. In several cell types the outcome of this binding is a block of the mitosis at the metaphase/ anaphase transition, and potentially apoptosis.[6] The mechanism of how colchicine binds to its site has been described using solved crystal structure of TB complexed with *N*-diacetyl-*N*-(2-mercaptoacetyl) colchicine (DAMA-colchicine) by Ravelli *et al.*[81]

In terms of binding, the trimethoxyphenyl unit of ring A of colchicine (Figure 11) is an essential pharmacophore which plays a crucial role in tubulin binding.[50]

In more molecular detail the methoxy group in ring A of colchicine forms a hydrogen-bond with Cysβ241. Simultaneously, ring C of colchicine interacts with the α subunit of tubulin via hydrogen bond between the carbonyl group of ring C and the backbone of Valα181.[82]

The seven-membered B ring and the C7 side chain of colchicine are not believed to be crucial for TB binding, however may affect the conformation of colchinoids and their other TB binding properties.[83,84] Although colchicine is also used clinically in the treatment of gout, it has not found significant use in cancer treatment because its toxicity.[57]

In order to overcome this drawback, some documented attempts to develop molecules interacting with colchicine site have led to a generation of new compounds with improved pharmacological characteristics such as more favourable water solubility, more potent activity, and lower toxicity than colchicine.[56] Some of these compounds include: colchicone (**18**), allocolchicine (**19**), thiocolchicine (**20**), cornigerine (**21**), podophyllotoxin (**22**), combretastatin A-4 (**23**) and related congeners like combretastatin A-4P (**24**) (Figure 11).

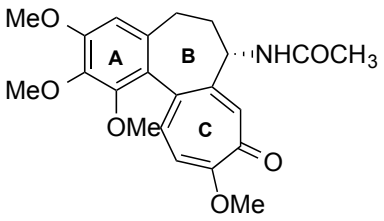

17 Colchicine

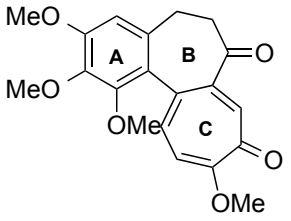

18 Colchicone

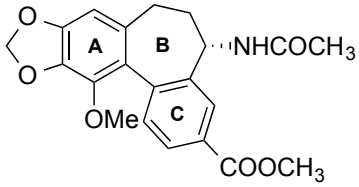

19 Allocolchicine

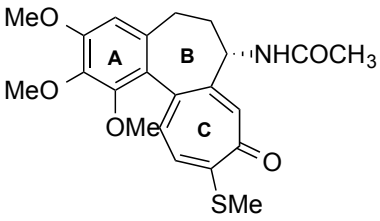

20 Thiocolchicine

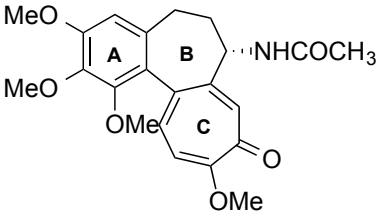

21 Cornigerine

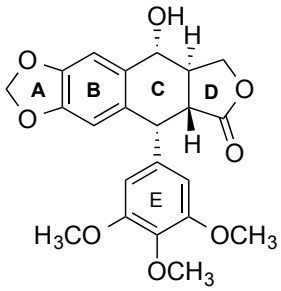

22 Podophyllotoxin

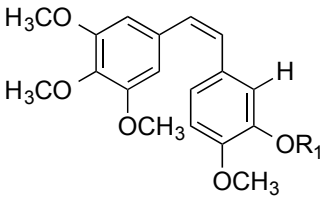

23 Combretastatin A-4 (R_1 = H)
24 Combretastatin A-4P (R_1 = P(=O)(ONa)2)

Figure 11. Colchicine site binding agents.

1.3.4 Combretastatins

Similarly to colchichine, **combretastatins** are powerful microtubule-destabilizing agents, able to inhibit microtubule assembly by binding to β-tubulin subunit at the colchicine binding site[85] (Figure 7).

Combretastatins are cis-stilbenoid natural products isolated from the bark of the South African tree *Combretum caffrum*.[12] In 1982 Pettit and colleagues, in collaboration with National Cancer Institute (NCI), isolated and identified nearly 17 compounds,[12] and in 1988 two other molecules were discovered.[86]

Of all the combretastatins, Combretastatin A-4 (CA-4) (**23**) is reported to have a very high cytotoxicity against a wide range of human cancer cell lines, including multidrug resistant cancer cell lines, with IC_{50}'s values consistently in low nanomolar to sub-nanomolar ranges.[87] The mechanism of action of CA-4, as well as the other combretastatins, is through the inhibition of tubulin polymerization,[88] but in contrast to colchicine that binds tubulin slowly and in temperature-dependent manner, CA-4 interacts with tubulin in a much faster and in temperature independent manner.[89]

In addition to tubulin binding, CA-4 is also able to disrupt the cell signaling pathways, engaged in maintenance of the cytoskeleton of endothelial cells in tumour vasculature.[89] Its vasculature-disrupting effects lead to blood vessel congestion that is followed by loss of blood flow, and eventual loss of oxygen and nutrient supply to tumour cells,[90] (see section 1.4). These anti-vascular and anti-angiogenic effects of CA-4 make it an important anti-cancer agent and a good substrate to guide design of novel derivatives.[90]

CA-4 presents a simple structure features: a 3,4,5-trimethoxyphenyl ring attached to a 4-methoxy-3-hydroxy phenyl group through a double bond (ethene bridge) in the *cis*-configuration, which is essential for its activity[89] (Figure 12).

Due to its relevant biological activity, CA-4 has been extensively studied by number of structural studies that helped to explain aspects of its functioning,[87] and a large number of CA-4 derivatives has been developed and evaluated for their structure-activity relationship (SAR).[91]

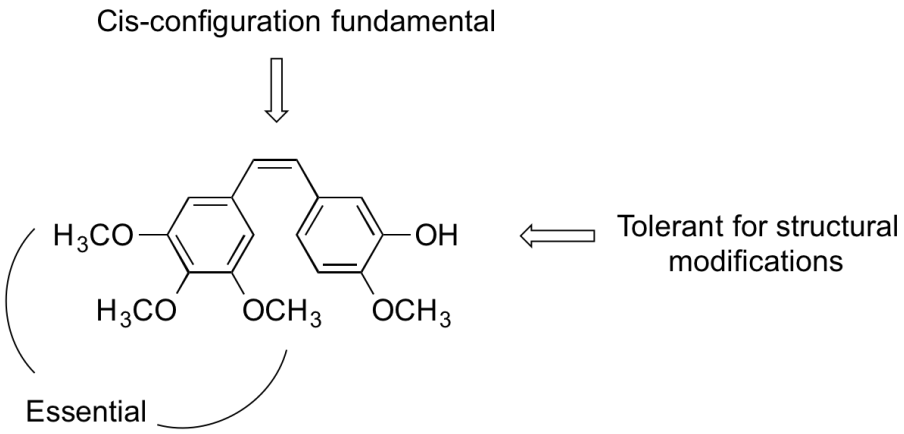

Figure 12. Combretastatin A-4.

These studies underline the importance of the presence of *cis*-configuration of the double bond to achieve high cytotoxicity as well as anti-tubulin activity: when the *cis* double bond in CA-4 isomerizes to form thermally more stable *trans*-isomer, a result is a complete loss of biological activity.[89] In order to address this issue, replacement of the *cis*-double bond by a rigid heterocyclic moiety to hinder the transformation to the *trans*-form has been shown as a viable strategy.[89]

Furthermore, the trimethoxybenzene moiety seems to be important for activity of CA-4,[13] especially when binding to tubulin, while it has been observed that isosteric substitutions on 3-hydroxy 4-methoxy phenyl ring are well tolerated.[92]

All the synthesis efforts are geared towards improving potency and efficacy of CA-4-related compounds as tubulin targeting agents. Some of the main drawbacks of CA-4 compound are its poor pharmacokinetic properties.[89] CA-4 is a lipophilic molecule and has very low water solubility that greatly limits its efficiency *in vivo*.[89]

In order to overcome some of these limitations CA-4 phosphate disodium (CA-4P) (**24**), has been synthetized. It is a water-soluble prodrug form that has been shown promising results.[14] From clinical point of view, CA-4P is under evaluation in phase III trials for the treatment of anaplastic thyroid cancer and in phase II for non-small lung cancer and platinum-resistant ovarian cancer.[14,15]

Tubulin and microtubules play an essential role in diverse cellular processes – including most notably cellular replication. Any perturbance with microtubule dynamics can have dire consequences on cell division, and therefore cellular survival. Because of their vital role in biology, microtubules have been attractive targets for several disease conditions, especially for cancer.

Tubulin targeting agents can be divided into major groups: Microtubule stabilizers (MSAs) that inhibit depolymerization of tubulin and Microtubule destabilizers (MDAs) that inhibit polymerization of tubulin. Paclitaxel and Epothilones are natural tubulin stabilizing agents (MSAs) which were isolated from plant and microorganism. They interact with specific domain of tubulin: taxol binding site.

Vinca alkaloids and Combretastatins, especially Combretastatin A-4, are destabilizing agents (MDAs) which target colchicine binding site. All anti-tubulin drugs interact with different sites on tubulin and at different positions within microtubules, and as a result, these interactions lead to diverse effects on microtubule dynamics. However, aside from individual mechanisms of tubulin targeting agents, the most important effect of these drugs is the suppression of spindle microtubule dynamics, which leads to the slowing or blocking of mitosis and induction of cell death. In conclusion, a broad spectrum of compounds can interact with tubulin. Thanks to the continued development in the chemistry and biology of microtubules, new anti-tubulins agents will emerge in the feature as potent anticancer drugs.

1.4 Antivascular agents

1.4.1 Tumour Vasculature

In all vertebrates, blood vessels serve as a transportation networks for plasma, blood cells, oxygen, or metabolites throughout the whole body.[93] The process of formation of new blood vessels, or “angiogenesis”, occurs in a limited number of physiological circumstances aside from development, which include wound healing or certain reproductive processes.[94] Under normal conditions, angiogenesis is regulated by balanced expression of different pro-angiogenic and anti-angiogenic factors that determine the correct recruitment, migration and proliferation of the blood vessels.[95] However, under abnormal conditions that require the growth of new blood vessels, this balance is lost, and it shifts instead towards the expression of pro-angiogenic factors in an event that is called angiogenic switch.[95]

The most relevant pro-angiogenic factors involved in blood vessel formation include vascular endothelial growth factor family (VEGF), platelet-derived growth factor (PDGF), matrix metalloproteinases (MMPs), hepatocyte growth factor (HGF), and basic fibroblast growth factor (bFGF).[95]

In addition to physical injury, stress such as hypoxia (or lack of oxygen), can also activate angiogenesis. In this case the HIFs transcription factors (hypoxia-inducible transcription factors) turns on the expression of proangiogenic molecules, such as VEGF.[96,97]

Angiogenesis is also a prerequisite for growth of solid tumours and metastasis. To grow, tumours must establish a network of vessels that provides the cancer cells with additional oxygen and nutrients enabling them to grow.[10] A tumour therefore needs to increase its blood vessels. This process has been described to happen through different mechanisms where: (1) progenitor cells from the bone marrow get recruited into existing vessels (in a process called vasculogenesis), or (2) formation of new blood vessels (angiogenesis) is activated. In cancerous tumours angiogenesis is the predominant mechanism of new blood vessel formation.[98]

From an anatomical and functional points of view, the vascular system formed within cancerous tumours is abnormal.[10] Tumour blood vessels are often structurally irregular, chaotic, tortuous, lack of mural cell coverage and have a relatively higher density compared to normal vasculature. As a result, the presence of deviations, dilated regions and excessive branches leads to a disorganized flow.[10] In healthy blood vessels, endothelial cells that make up the vessel walls are distributed in a monolayer and have junctions that limit vascular permeability. In venules and capillaries, very small vessels, this monolayer is closely associated with pericytes – cells required for stabilization of the vascular system.[99,100]

This organization if often absent in tumour vasculature. Structural abnormalities of tumour vasculature have functional consequences that lead to irregularity in the perfusion of the tumour tissue, and creates hypoxic (low oxygen) and necrotic (dead) areas.[98] From the therapeutic point of view, these characteristics of vasculature cause problems with the delivery and penetration of cytotoxic agents into the tumour.[98]

1.4.2 Targeting the Tumour Vasculature

The blood vessels constitute an attractive new target for anticancer therapies for many different reasons.[9] Characteristics and sensitivity of the cancer cells are different depending on the type of cancer and on location of the cells within the same tumour. The vascular system could serve as more stable and homogeneous therapeutic target, because is comprised of endothelial cells that are not variable, sensitivity, or resistance to drugs in the same fashion as cancer cells.[101]

While endothelial cells are normally stable, their proliferation in tumour tissues is increased and they express markers not present in mature endothelial cells of the normal vascular

system.[98] This differential gene expression could allow for the development of unique inhibitors against rapidly proliferating endothelial cells in tumours.[98] Furthermore, because tumour vascular system is in direct contact with the bloodstream, the delivery of the drugs is simplified.[102]

Two different methods of targeting tumour vasculature currently include: (A) antiangiogenic therapies, which targets the vascularization process, and (B) the antivascular therapies, aimed instead at the selective destruction of the newly formed tumour blood vessels. While the targets of agents used in these therapies appear similar, their mechanisms of action are distinct.[98]

1.4.3 Antiangiogenic Agents

Angiogenesis inhibitors prevent the formation of new blood vessels in the tumour.[103] Prolonged inhibition of VEGF signaling has been shown to cause a decrease in vascularization, and to normalize the structure and architecture of residual tumour vessels.[98] Several natural compounds and number of synthetic angiogenesis inhibitors exist and have been developed to date. Naturally occurring antiangiogenic agents are classified as (a) matrix derived and (b) non-matrix derived compounds.[104] Examples of matrix-derived angiogenesis inhibitor include endostatin, endorepellin and thrombospondin 1 and 2, while group of non-matrix agents includes different peptides, metabolites, cytokines, interferons and interleukins.[104]

In recent years, several synthetic inhibitors have also been developed some of which are now in clinical trials.[98] Inhibitors of pro-angiogenic receptor signaling include inhibitors of VEGF receptors, inhibitors of endothelial growth factor receptor (EGFR), inhibitors of fibroblast growth factor receptor (FGFR), and inhibitors of platelet-derived growth receptors (PDGFR).[98]

With a large number of new products in development, the field of antiangiogenic therapy is growing rapidly and future research will focus on determining the tumour types and stages that will benefit most from antiangiogenic therapy.[105]

1.4.4 Vascular Disrupting Agents

Vascular disrupting agents (VDAs) constitute a relatively new group of molecules that act at the level of the tumour vascular system. Use of these agents can cause an interruption of blood flow and consequently lead to necrosis of the tumour tissue.[106] Unlike the

antiangiogenic agents, the VDAs act preferentially at the level of the already formed tumour blood vessels, targeting the cytoskeleton and compromise the integrity of cell junctions.[107] The mechanisms of their selectivity are not completely understood however, they are probably related to the fragile and immature nature of tumour blood vessels at the onset of angiogenesis.[107]

After an exposure to VDA of only few minutes, the newly formed blood vessels have been demonstrated to show the first signs of alterations, causing occlusion of the vessels and marked reduction in blood flow. The cause of death of the vessels is therefore prolonged ischemia, a restriction in blood supply to tissues, causing a shortage of oxygen that is needed for cellular metabolism[108] (Figure 13).

The VDAs differ from the antiangiogenic agents not only in their mechanism of action, but also in their therapeutic applications.[108] While antiangiogenic treatments are usually administered continuously for months to years, the VDAs are typically used at intermittent doses.[108] Vascular disrupting agents can be divided into two major categories that I will discuss about in the next paragraphs: (A) ligand-directed VDAs as agents that use antibodies or peptides to target toxins or pro-coagulants to the tumour endothelium; (B) small molecule VDAs as agents that exploit the differences between normal and tumour endothelium.[11]

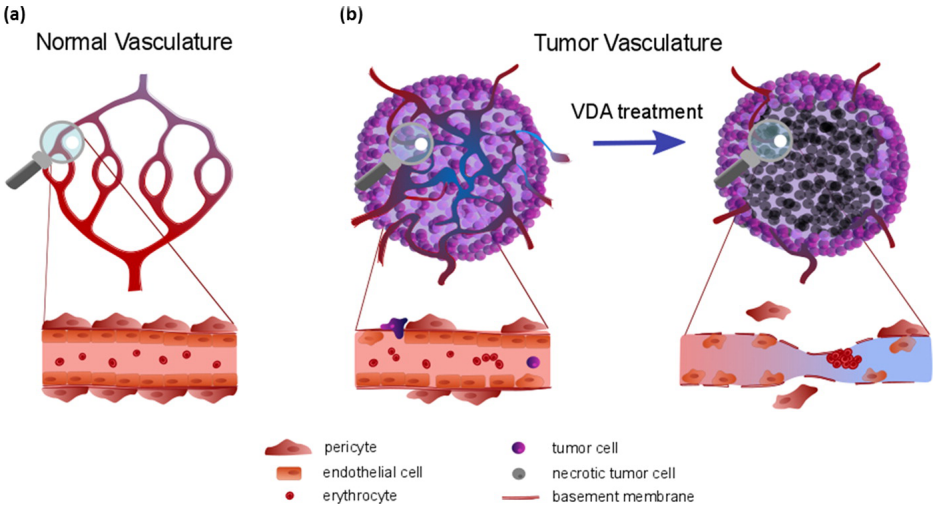

Figure 13. Proposed principle of action for vascular-disrupting agents. **a)** In normal conditions, blood vessels are organized hierarchically and the basement membrane and pericytes provide structure and stability. **b)** Intra-tumoral vessels are chaotic and often lack pericytes and a proper basement membrane. Reduced blood flow renders the tumour center hypoxic, and tumour cells can invade the unstable and leaky vessels. VDA treatment results in disruption of the cytoskeleton and reduced cell–cell junctions. This triggers a cascade of events, resulting in a reduction of blood flow, vessel occlusion, and necrosis in the tumour center.[10]

1.4.4.1 *Ligand-directed VDAs*

The first class of ligand-directed VDAs uses a targeting molecule, for example, an antibody or a peptide, that carry pro-coagulant and pro-apoptotic toxins, which selectively tracks to tumour endothelium.[11]

Vascular endothelial cells often express unique surface markers, making it possible to develop a selective tumour therapy.[108]

This strategy is aided by the fact that endothelial cells in the tumour are accessible to circulatory system, which significantly simplifies drug delivery. The antigenic determinants (epitopes) expressed selectively at the level of tumour neo-vasculature, like endoglin, vascular endothelial growth factor receptors (VEGF), αν-integrins and prostate-specific membrane antigen, have been identified to be the targets of this class of antivascular agents.[108]

1.4.4.2 *Small molecule VDAs*

The second category of antivascular agents includes molecules that are not specifically located at the level of tumour endothelium. Instead, they exploit the differences between the endothelium of healthy tissue and the tumour to induce alterations of blood vessels selectively.[98]

There are two main groups of small-molecule VDAs: (A)Tubulin-binding agents, and (B) Flavonoids. Interest in the vascular disrupting properties of agents capable of binding to tubulin was inspired by studies of colchicines and vinca alkaloids (discussed in previous sections). These two compounds were shown to induce vascular damage in preclinical tumour models.[90] Currently, the most relevant compounds belonging to this class are combretastatin A-4 disodium phosphate (CA-4P) (**24**), ZD6126 (**25**) and AVE8062 (**26**), all of which are capable of inducing anti-vascular and anti-tumour effects[108] (Figure 14).

Moreover, the shutdown of blood flow caused by these molecules specifically affects the newly formed tumour vessels, while the healthy tissues are largely unaffected.[109] Flavonoids are a second group of VDAs.[110] It has been suggested that these compounds exert their effects on blood vessels via the release of tumour necrosis factor alpha (TNFα), from macrophages activated in the tumour tissue.[111] The role of TNFα as a potent anti-tumour agent has been demonstrated by depletion of TNFα using anti-TNFα antibodies, which led to inhibition of flavone acetic acid (FAA) (**27**) and caused consecutive vascular collapse.[111] Compound DMXAA, 5,6-dimethylxantenone-4-acetic acid (**28**), is considered the most

interesting compound belonging to the class of flavonoid VDAs, it has been shown to be the only compound able to stimulate both human and mouse macrophages.[110]

In conclusion, the unique characteristics of the tumour vasculature allow us to target tumour growth and vascularization in a specific and selective ways. The vasculature is easily accessible to therapeutic agents whose activity causes tumour cells to die in nutrient-starved environment. Currently there are two different approaches of targeting tumour vasculature: (A) using antiangiogenic therapies, which target the vascularization process, or (B) the anti-vascular therapies, that are aimed at the selective destruction of the newly formed tumour blood vessels. The second approach includes microtubule-targeting agents that, in addition to their cell cycle regulatory roles discussed in section 1.3, are also able to shut down existing tumour vasculature. Currently multiple clinical trials are underway to determinate the safety and efficacy of anti-vascular agents, both used alone and in combination with other therapies.

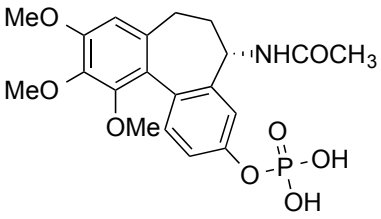

25 ZD6126

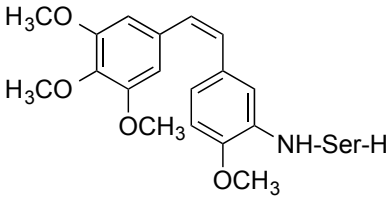

26 AVE-8062

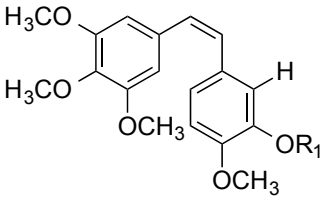

23 Combretastatin A-4 (R_1 = H)
24 Combretastatin A-4P (R_1 = P(=O)(ONa)2)

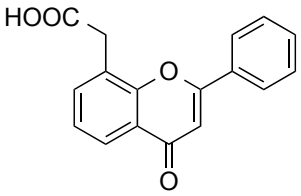

27 FAA

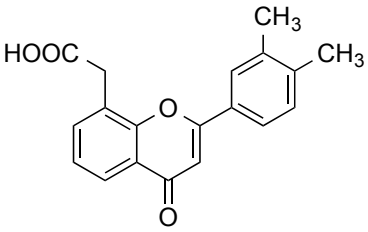

28 DMXAA

Figure 14. Main antivascular agents.

1.5 References

1. Cragg, G. M. & Newman, Da. J. Natural products: A continuing source of novel drug leads. Biochimica et Biophysica Acta (BBA) - General Subjects 1830, 3670–3695 (2013).
2. Denis, J. et al. Highly efficient, practical approach to natural taxol. Journal of the American Chemical Society 110, 5917–5919 (2002).
3. Atanasov, A. et al. Discovery and resupply of pharmacologically active plant-derived natural products: A review. Biotechnology Advances 33, 1582–1614 (2015).
4. Chari, R. V. Targeted Cancer Therapy: Conferring Specificity to Cytotoxic Drugs. Accounts Chem Res 41, 98–107 (2008).
5. Kucuksayan, E. & Ozben, T. Hybrid Compounds as Multitarget Directed Anticancer Agents. Curr Top Med Chem 17, 907–918 (2017).
6. Jordan, M. & Wilson, L. Microtubules as a target for anticancer drugs. Nature Reviews Cancer 4, 253–265 (2004).
7. Stanton, R. A., Gernert, K. M., Nettles, J. H. & Aneja, R. Drugs that target dynamic microtubules: a new molecular perspective. Medicinal research reviews 31, 443–481 (2011).
8. Avila, J. Microtubule functions. Life sciences 50, 327–334 (1992).
9. Keshet, E. & Ben-Sasson, S. A. Anticancer drug targets: approaching angiogenesis. J Clin Invest 104, 1497–1501 (1999).
10. Pérez-Pérez, M.-J. et al. Blocking Blood Flow to Solid Tumors by Destabilizing Tubulin: An Approach to Targeting Tumor Growth. Journal of medicinal chemistry 59, 8685–8711 (2016).
11. Gaya, A. & Rustin, G. Vascular disrupting agents: a new class of drug in cancer therapy. Clinical oncology (Royal College of Radiologists (Great Britain)) 17, 277–290 (2005).
12. Pettit, G., Singh, S., Niven, M., Hamel, E. & hmidt, J. Isolation, structure, and synthesis of combretastatins A-1 and B-1, potent new inhibitors of microtubule assembly, derived from Combretum caffrum. Journal of natural products 50, 119–131 (1987).
13. Shan, Y., Zhang, J., Liu, Z., Wang, M. & Dong, Y. Developments of combretastatin A-4 derivatives as anticancer agents. Current Medicinal Chemistry 18, 523–538 (2011).

14. Zweifel, M. et al. Phase II trial of combretastatin A4 phosphate, carboplatin, and paclitaxel in patients with platinum-resistant ovarian cancer. Annals of Oncology 22, 2036–2041 (2011).
15. Rustin, G. et al. A Phase Ib trial of CA4P (combretastatin A-4 phosphate), carboplatin, and paclitaxel in patients with advanced cancer. British journal of cancer 102, 1355–1360 (2010).
16. Fojo, T. The role of microtubules in cell biology neurobiology and oncology. Humana Press. 1–629 (2008).
17. Benarroch, E. E. Dynamics of microtubules and their associated proteins: Recent insights and clinical implications. Neurology 86, 1911–1920 (2016).
18. Dutcher, S. K. The tubulin fraternity: alpha to eta. Curr Opin Cell Biol 13, 49–54 (2001).
19. Nogales, E., Wolf, S. G. & Downing, K. H. Structure of the αβ tubulin dimer by electron crystallography. Nature 391, 199–203 (1998).
20. Bryan, J. & Wilson, L. Are Cytoplasmic Microtubules Heteropolymers Proc National Acad Sci 68, 1762–1766 (1971).
21. Horio, T. & Murata, T. The role of dynamic instability in microtubule organization. Frontiers in plant science 5, 511 (2014).
22. Manka, S. W. & Moores, C. A. The role of tubulin–tubulin lattice contacts in the mechanism of microtubule dynamic instability. Nat Struct Mol Biol 25, 607–615 (2018).
23. Desai, A. & Mitchison, T. J. Microtubule polymerization dynamics. Annual Review of Cell and Developmental Biology 13, 83–117 (2003).
24. Mitchison, T. Localization of an exchangeable GTP binding site at the plus end of microtubules. Science 261, 1044–1047 (1993).
25. Dumontet, C. & Jordan, M. Microtubule-binding agents: a dynamic field of cancer therapeutics. Nature Reviews Drug Discovery 9, 790–803 (2010).
26. Löwe, J., Li, H., Downing, K. & Nogales, E. Refined structure of αβ-tubulin at 3.5 Å resolution. Journal of Molecular Biology 313, 1045–1057 (2001).
27. Sammak, P., Gorbsky, G. & Borisy, G. Microtubule dynamics in vivo: a test of mechanisms of turnover. J Cell Biology 104, 395–405 (1987).
28. Kirschner, M. & Mitchison, T. Microtubule dynamics. Nature 324, 621–621 (1986).
29. Akhmanova, A. & Steinmetz, M. O. Control of microtubule organization and dynamics: two ends in the limelight. Nature Reviews Molecular Cell Biology 16, 711–726 (2015).

30. Alushin, G. M. et al. High-Resolution Microtubule Structures Reveal the Structural Transitions in αβ-Tubulin upon GTP Hydrolysis. Cell 157, 1117–1129 (2014).
31. Gardiner, J. The evolution and diversification of plant microtubule-associated proteins. The Plant journal: for cell and molecular biology 75, 219–229 (2013).
32. Nogales, E. Structural insights into microtubule function. Annu Rev Biochem 69, 277–302 (2000).
33. Schuyler, S. & Pellman, D. Microtubule 'plus-end-tracking proteins': The end is just the beginning. Cell 105, 421–424 (2001).
34. Akhmanova, A. & Steinmetz, M. O. Tracking the ends: a dynamic protein network controls the fate of microtubule tips. Nature Reviews Molecular Cell Biology 9, 309–322 (2008).
35. Ookata, K. et al. Cyclin B interaction with microtubule-associated protein 4 (MAP4) targets p34cdc2 kinase to microtubules and is a potential regulator of M-phase microtubule dynamics. The Journal of Cell Biology 128, 849–862 (1995).
36. Maurer, S. P. et al. EB1 accelerates two conformational transitions important for microtubule maturation and dynamics. Current biology: CB 24, 372–384 (2014).
37. Andersen, S. Spindle assembly and the art of regulating microtubule dynamics by MAPs and Stathmin/Op18. Trends in cell biology 10, 261–267 (2000).
38. Gupta, K. K. et al. Mechanism for the catastrophe-promoting activity of the microtubule destabilizer Op18/stathmin. Proc National Acad Sci 110, 20449–20454 (2013).
39. Belmont, L. & Mitchison, T. Identification of a protein that interacts with tubulin dimers and increases the catastrophe rate of microtubules. Cell 84, 623–631 (1996).
40. Howell, B., Larsson, N., Gullberg, M. & Cassimeris, L. Dissociation of the tubulin-sequestering and microtubule catastrophe-promoting activities of oncoprotein 18/stathmin. Molecular Biology of the Cell 10, 105–118 (1999).
41. Steinmetz, M. O. Structure and thermodynamics of the tubulin–stathmin interaction. J Struct Biol 158, 137–147 (2007).
42. Desai, A., Verma, S., Mitchison, T. & Walczak, C. Kin I kinesins are microtubule-destabilizing enzymes. Cell 96, 69–78 (1999).
43. Verhey, K. J. & Hammond, J. W. Traffic control: regulation of kinesin motors. Nature Reviews Molecular Cell Biology 10, 765–777 (2009).
44. Vallee, R. B., Williams, J. C., Varma, D. & Barnhart, L. E. Dynein: An ancient motor protein involved in multiple modes of transport. Journal of neurobiology 58, 189–200 (2004).

45. Mitchison, T. Microtubule Dynamics and Kinetochore Function in Mitosis. Annu Rev Cell Dev Bi 4, 527–545 (1988).
46. Parker, A. L., Teo, W., McCarroll, J. A. & Kavallaris, M. An Emerging Role for Tubulin Isotypes in Modulating Cancer Biology and Chemotherapy Resistance. Int J Mol Sci 18, 1434 (2017).
47. Sharma, S., Gupta, M., Saxena, A. & Bedi, P. Thiazolidinone Constraint Combretastatin Analogs as Novel Antitubulin Agents: Design, Synthesis, Biological Evaluation and Docking Studies. Anti-cancer Agent Me 17, 230–240 (2017).
48. Negi, A. S. et al. Natural antitubulin agents: importance of 3,4,5-trimethoxyphenyl fragment. Bioorganic & Medicinal Chemistry 23, 373–389 (2015).
49. Matson, D. R. & Stukenberg, T. P. Spindle poisons and cell fate: a tale of two pathways. Mol Interv 11, 141–50 (2011).
50. Dostál, V. & Libusová, L. Microtubule drugs: action, selectivity, and resistance across the kingdoms of life. Protoplasma 251, 991–1005 (2014).
51. Wahl, A. et al. Loss of normal p53 function confers sensitization to Taxol by increasing G2/M arrest and apoptosis. Nature medicine 2, 72–79 (1996).
52. Vikhanskaya, F. et al. Inactivation of p53 in a human ovarian cancer cell line increases the sensitivity to paclitaxel by inducing G2/M arrest and apoptosis. Experimental cell research 241, 96–101 (1998).
53. Naaz, F., Haider, M. R., Shafi, S. & Yar. Anti-tubulin agents of natural origin: Targeting taxol, vinca, and colchicine binding domains. European Journal of Medicinal Chemistry 171, 310–331 (2019).
54. Jordan, M. Mechanism of action of antitumor drugs that interact with microtubules and tubulin. Curr Medicinal Chem Anti-cancer Agents 2, 1–17 (2002).
55. Manfredi, J., Parness, J. & Horwitz, S. Taxol binds to cellular microtubules. J Cell Biology 94, 688–696 (1982).
56. Nogales, E., Wolf, S., Khan, I., Ludueña, R. & Downing, K. Structure of tubulin at 6.5 A and location of the taxol-binding site. Nature 375, 424–427 (1995).
57. Mukhtar, E., Adhami, V. & Mukhtar, H. Targeting microtubules by natural agents for cancer therapy. Molecular Cancer Therapeutics 13, 275–284 (2014).
58. He, L. et al. A Common Pharmacophore for Taxol and the Epothilones Based on the Biological Activity of a Taxane Molecule Lacking a C-13 Side Chain†. ACS Publications 39, 3972–3978 (2000).
59. Nicolaou, K. et al. Total synthesis of taxol. Nature 367, 630–634 (1994).

60. Eisenhauer, E. & Vermorken, J. The taxoids. Comparative clinical pharmacology and therapeutic potential. Drugs 55, 5–30 (1998).
61. Derry, W., Wilson, L. & Jordan, M. Substoichiometric binding of taxol suppresses microtubule dynamics. Biochemistry 34, 2203–2211 (1995).
62. Yvon, A.-M. C., Wadsworth, P. & Jordan, M. Taxol Suppresses Dynamics of Individual Microtubules in Living Human Tumor Cells. Mol Biol Cell 10, 947–959 (1999).
63. Derry, W., Wilson, L. & Jordan, M. Low potency of taxol at microtubule minus ends: implications for its antimitotic and therapeutic mechanism. Cancer Res 58, 1177–84 (1998).
64. Goodin, S., Kane, M. P. & Rubin, E. H. Epothilones: Mechanism of Action and Biologic Activity. J Clin Oncol 22, 2015–2025 (2004).
65. Hamel, E. Antimitotic natural products and their interactions with tubulin. Med Res Rev 16, 207–231 (1996).
66. dhar Mani et al. The clinical development of new mitotic inhibitors that stabilize the microtubule. Anti-cancer drugs 15, 553–558 (2004).
67. Prota, A. E. et al. Structural Basis of Microtubule Stabilization by Laulimalide and Peloruside A. Angew Chem-ger Edit 126, 1647–1651 (2014).
68. Quinoa, E., Kakou, Y. & Crews, P. Fijianolides, polyketide heterocycles from a marine sponge. The Journal of Organic Chemistry 53, 3642–3644 (2002).
69. West, L. M., Northcote, P. T. & Battershill, C. N. Peloruside A: A Potent Cytotoxic Macrolide Isolated from the New Zealand Marine Sponge Mycale sp. J Org Chem 65, 445–449 (2000).
70. Wilmes, A., Bargh, K., Kelly, C., Northcote, P. T. & Miller, J. H. Peloruside A Synergizes with Other Microtubule Stabilizing Agents in Cultured Cancer Cell Lines. Mol Pharmaceut 4, 269–280 (2007).
71. Moudi, M., Go, R., Yien, C. & Nazre, M. Vinca alkaloids. Int J Prev Medicine 4, 1231–5 (2013).
72. Zhou, X.-J. & Rahmani, R. Preclinical and Clinical Pharmacology of Vinca Alkaloids. Drugs 44, 1–16 (1992).
73. Gidding, C. E. M., Kellie, S. J., Kamps, W. A. & de Graaf, S. S. N. Vincristine revisited. Crit Rev Oncol Hemat 29, 267–287 (1999).
74. Bai, R., Pettit, G. & Hamel, E. Binding of dolastatin 10 to tubulin at a distinct site for peptide antimitotic agents near the exchangeable nucleotide and vinca alkaloid sites. J Biological Chem 265, 17141–9 (1990).

75. Gigant, B. et al. Structural basis for the regulation of tubulin by vinblastine. Nature 435, 519–522 (2005).
76. Niel, E. & Scherrmann, J.-M. Colchicine today. Joint Bone Spine 73, 672–678 (2006).
77. Skoufias, D. & Wilson, L. Mechanism of inhibition of microtubule polymerization by colchicine: inhibitory potencies of unliganded colchicine and tubulin-colchicine complexes. Biochemistry 31, 738–746 (1992).
78. Ravelli, R. B. et al. Insight into tubulin regulation from a complex with colchicine and a stathmin-like domain. Nature 428, 198–202 (2004).
79. Bai, R. et al. Identification of cysteine 354 of beta-tubulin as part of the binding site for the A ring of colchicine. The Journal of biological chemistry 271, 12639–12645 (1996).
80. Andreu, J., Perez-Ramirez, B., Gorbunoff, M., Ayala, D. & Timasheff, S. Role of the colchicine ring A and its methoxy groups in the binding to tubulin and microtubule inhibition. Biochemistry 37, 8356–8368 (1998).
81. Andreu, J. & Timasheff, S. Conformational states of tubulin liganded to colchicine, tropolone methyl ether, and podophyllotoxin. Biochemistry 21, 6465–6476 (1982).
82. Nam, N. Combretastatin A-4 analogues as antimitotic antitumor agents. Current Medicinal Chemistry 10, 1697–1722 (2003).
83. Pettit, G. et al. Isolation and structure of the strong cell growth and tubulin inhibitor combretastatin A-4. Experientia 45, 209–211 (1989).
84. Marrelli, M. et al. Biological Potential and Structure-Activity Relationships of Most Recently Developed Vascular Disrupting Agents: An Overview of New Derivatives of Natural Combretastatin A-4. Curr Med Chem 18, 3035–3081 (2011).
85. Tron, G. et al. Medicinal chemistry of combretastatin A4: present and future directions. Journal of medicinal chemistry 49, 3033–3044 (2006).
86. Bukhari, S., Kumar, G., Revankar, H. & Qin, H.-L. Development of combretastatins as potent tubulin polymerization inhibitors. Bioorg Chem 72, 130–147 (2017).
87. Chaudhary, A. et al. Combretastatin a-4 analogs as anticancer agents. Mini reviews in medicinal chemistry 7, 1186–1205 (2007).
88. Badn, W., Kalliomäki, S., Widegren, B. & Sjögren, H. Low-Dose Combretastatin A4 Phosphate Enhances the Immune Response of Tumor Hosts to Experimental Colon Carcinoma. Clin Cancer Res 12, 4714–4719 (2006).

89. Rajak, H. et al. Design of combretastatin A-4 analogs as tubulin targeted vascular disrupting agent with special emphasis on their cis-restricted isomers. Current Pharmaceutical Design 19, 1923–1955 (2013).
90. Risau, W. & Flamme, I. Vasculogenesis. Annu Rev Cell Dev Bi 11, 73–91 (1995).
91. Zhao, Y. & Adjei, A. A. Targeting Angiogenesis in Cancer Therapy: Moving Beyond Vascular Endothelial Growth Factor. Oncol 20, 660–673 (2015).
92. Hanahan, D. & Folkman, J. Patterns and emerging mechanisms of the angiogenic switch during tumorigenesis. Cell 86, 353–364 (1996).
93. Liu, Y., Cox, S., Morita, T. & Kourembanas, S. Hypoxia regulates vascular endothelial growth factor gene expression in endothelial cells. Identification of a 5' enhancer. Circulation research 77, 638–643 (1995).
94. Shweiki, D., Neeman, M., Itin, A. & Keshet, E. Induction of vascular endothelial growth factor expression by hypoxia and by glucose deficiency in multicell spheroids: implications for tumor angiogenesis. Proceedings of the National Academy of Sciences of the United States of America 92, 768–772 (1995).
95. Citrin, D. & Camphausen, K. Advancement of antiangiogenic and vascular disrupting agents combined with radiation. Canc Treat 139, 153–71 (2008).
96. Baluk, P., Hashizume, H. & nald, D. M. Cellular abnormalities of blood vessels as targets in cancer. Current opinion in genetics & development 15, 102–111 (2005).
97. Gerhardt, H. & Betsholtz, C. Endothelial-pericyte interactions in angiogenesis. Cell and tissue research 314, 15–23 (2003).
98. Drevs, J., Laus, C., Medinger, M., Schmidt-Gersbach, C. & Unger, C. Antiangiogenesis: current clinical data and future perspectives. Onkologie 25, 520–527 (2002).
99. Rüegg, C. et al. The quest for surrogate markers of angiogenesis: a paradigm for translational research in tumor angiogenesis and anti-angiogenesis trials. Current molecular medicine 3, 673–691 (2003).
100. El-Kenawi, A. E. & El-Remessy, A. B. Angiogenesis inhibitors in cancer therapy: mechanistic perspective on classification and treatment rationales. Brit J Pharmacol 170, 712–729 (2013).
101. Nyberg, P., Xie, L. & Kalluri, R. Endogenous inhibitors of angiogenesis. Cancer research 65, 3967–3979 (2005).
102. Siemann, D. W. & Horsman, M. R. Antiangiogenic Agents in Cancer Therapy. 297–310 (2008) doi:10.1007/978-1-59745-184-0_17.

103. Tozer, G. M., Kanthou, C. & Baguley, B. C. Disrupting tumour blood vessels. Nat Rev Cancer 5, 423–435 (2005).
104. Kanthou, C. & Tozer, G. M. Microtubule depolymerizing vascular disrupting agents: novel therapeutic agents for oncology and other pathologies. International Journal of Experimental Pathology 90, 284–294 (2009).
105. Siemann, D. W., Chaplin, D. J. & Horsman, M. R. Vascular-targeting therapies for treatment of malignant disease. Cancer 100, 2491–2499 (2004).
106. Chaplin, D., Pettit, G. & Hill, S. Anti-vascular approaches to solid tumour therapy: evaluation of combretastatin A4 phosphate. Anticancer Res 19, 189–95 (1999).
107. Baguley, B. C. & Ching, L. DMXAA: an antivascular agent with multiple host responses. International journal of radiation oncology, biology, physics 54, 1503–1511 (2002).
108. Philpott, M., Baguley, B. & Ching, L. Induction of tumour necrosis factor-alpha by single and repeated doses of the antitumour agent 5,6-dimethylxanthenone-4-acetic acid. Cancer chemotherapy and pharmacology 36, 143–148 (1995).

2. Synthesis and Biological Evaluation of 2-Methyl-4,5-Disubstituted Oxazoles as a Novel Class of Highly Potent Antitubulin Agents

2.1 Introduction

Cellular microtubules, undergoing constant assembly and disassembly from α, β-tubulin heterodimers, are key components of the cytoskeleton and are involved in a wide range of cellular functions. Perhaps their most important role is formation of the mitotic spindle to direct cell division and proper chromosomal separation.[1] Antimitotic agents represent a major class of cytotoxic drugs for cancer treatment, and tubulin is the target for numerous small natural and synthetic molecules that inhibit the formation of the mitotic spindle.[2-4] Among the naturally occurring anti-microtubule agents, one of the most active is the *cis*-stilbene combretastatin A-4 (CA-4, **1a**, Figure 1), isolated from the African cape bushwillow *Combretum caffrum*.[5] CA-4 inhibits tubulin assembly by interacting with β-tubulin at the colchicine site.[6] The corresponding water-soluble prodrug salt, CA-4 disodium phosphate (CA-4P, **1b**),[7] is currently in Phase II trials for anaplastic thyroid cancer,[8] and it was found to have potent activity in reducing tumour blood flow, thus acting as a vascular disrupting agent (VDA).[9] Its structural simplicity, along with its ability to selectively damage tumour vasculature, makes CA-4 of great interest from the medicinal chemistry point of view.[10]

Previous SAR studies have demonstrated that both the 3',4',5'-trimethoxy substitution pattern on the A-ring and the *cis*-olefin configuration at the bridge were fundamental requirements for optimal activity, while some B-ring structural modifications were tolerated by the target.[11] Numerous researchers have undertaken modification of the relatively unstable *cis*-double bond of CA-4, which is characterized by the tendency to undergo isomerization to the biologically inactive *trans*-form in solution during storage, administration and metabolism.[12] Thus, to retain the appropriate geometry of the two adjacent aryl groups required for potent bioactivity, chemically stable *cis*-restricted derivatives of CA-4 with general structure **2** were obtained by incorporation of the stilbene double bond into vicinally diaryl-substituted five-member aromatic heterocyclic rings, such

as pyrazole,[13] imidazole,[13, 14] thiazole,[15] furazan (1,2,5-oxadiazole),[16] isoxazole,[17] oxazole,[13,14] 1,2,3-thiadiazole,[18] triazole[19] and 1,2,3,4-tetrazole.[20]

Among our efforts focused on modification of the *cis*-double bond of CA-4, we previously described a series of 2-methyl-4-(3',4',5'-trimethoxyphenyl-5-substituted thiazoles with general structure **3** that showed moderate antiproliferative activity against a panel of five cancer cell lines. These compounds were one to three orders of magnitude less active than CA-4, in terms of molar IC_{50} values.[21] These compounds also caused accumulation of HeLa and Jurkat cells in the G2/M phase of the cell cycle, as is typical for antimicrotubule agents. Among the synthesized compounds, derivative **3d** (R_1=naphth-2-yl) was the most active as an inhibitor of tumour cell growth, with IC_{50} values ranging from 33 to 702 nM in the five cell lines examined but was comparable to CA-4 as an inhibitor of tubulin polymerization.

In our ongoing effort to discover novel and potent antimicrotubule agents, these results led us to start a pharmacophore exploration and optimization effort around the 2-methylthiazole derivatives with general formula **3**. Here we describe replacing the thiazole nucleus with the less aromatic and basic bioisosteric equivalent oxazole ring,[22] by the preparation of two different regioisomeric series of 2-methyl-4,5-disubstituted oxazole derivatives with general structures **4** and **5**. In these two series of designed analogues, obtained by interchanging the substitution pattern of ring A and B, we fixed one of the aryl groups as the 3',4',5'-trimethoxyphenyl moiety, identical to the A-ring of CA-4, and examined several substitutions with electron-withdrawing (F and Cl) or electron-releasing (Me, OMe, and OEt) groups (EWG or ERG, respectively) on the other aryl moiety, corresponding to the B-ring of CA-4. In addition, for compounds **4a** and **5a**, the B-ring of CA-4 was replaced with the bulky and lipophilic naphth-2-yl moiety.

It has been previously reported that the replacement of the *meta*-hydroxy group of ring B of CA-4 with halogens such as fluorine or chlorine increased tubulin affinity as well as antiproliferative potency.[23] Since the methoxy and ethoxy groups proved to be favourable for bioactivity, we maintained one of these substituents at the *para*-position and introduced an additional substituent (F and Cl) at the *meta*-position of the phenyl ring.

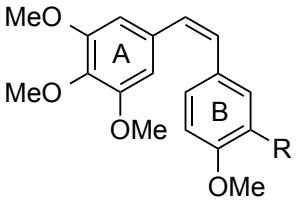

1

R=OH, Combretastatin A-4 (CA-4), **1a**
R=OPO_3Na_2, CA-4P, **1b**

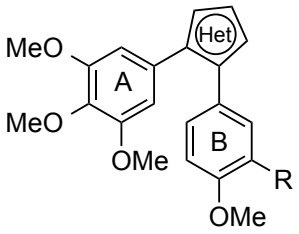

2

R=OH or NH_2
Het=imidazole; pyrazole; thiazole; oxazole; isoxazole; 1,2,3-thiadiazole; 1,2,3- or 1,2,4- or 1,3,4-triazole;1,2,3,4-tetrazole, furazan.

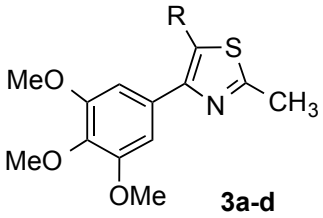

3a-d

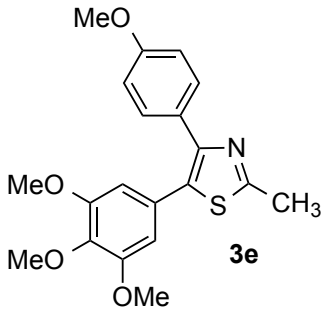

3e

3a, R=4'-Me-C_6H_4 IC_{50}:0.52-1.9 μM
3b, R=4'-OMe-C_6H_4 IC_{50}:0.50-3.4 μM
3c, R=4'-OEt-C_6H_4 IC_{50}:0.043-3.3 μM
3d, R=naphth-2-yl IC_{50}:0.033-0.70 μM

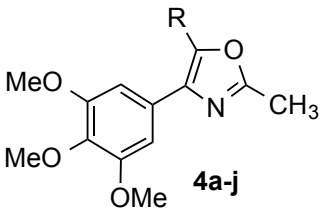

4a-j

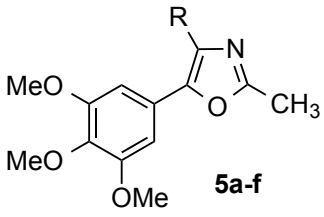

5a-f

4a, R=naphth-2-yl
4b, R=4'-F-C_6H_4
4c, R=4'-Cl-C_6H_4
4d, R=4'-Me-C_6H_4
4e, R=4'-OMe-C_6H_4
4f, R=3'-OMe-C_6H_4
4g, R=4'-OMe-3'-F-C_6H_3
4h, R=4'-OMe-3'-Cl-C_6H_3
4i, R=4'-OEt-C_6H_4
4j, R=4'-OEt-3'-Cl-C_6H_3

5a, R=naphth-2-yl
5b, R=4'-F-C_6H_4
5c, R=4'-Cl-C_6H_4
5d, R=4'-Me-C_6H_4
5e, R=4'-OMe-C_6H_4
5f, R=4'-OEt-C_6H_4

Figure 1. Lead structures of tubulin polymerization inhibitors.

2.2 Chemistry

Synthesis of compounds **4a-j** and **5a-f** was accomplished using a three-step procedure described in Figure 2. 2-Methyl-4-substituted oxazole derivatives **8** or **9a-f** were prepared by the condensation of 2-bromo-1-(3',4',5'-trimethoxyphenyl)ethanone **6** and the appropriate α-bromo acetophenone **7a-f**, respectively, with acetamide at 150 °C for 2 h. The subsequent chemoselective monobromination at the 5-position of derivatives **8** and **9a-f** with *N*-bromosuccinimide in $CHCl_3$ furnished the 2-methyl-4-substituted-5-bromooxazole analogues **10** or **11a-f**, respectively. Finally, these latter intermediates were subjected to Suzuki cross-coupling reaction with the appropriate arylboronic acid under heterogeneous conditions [$PdCl_2$(DPPF), CsF] in 1,4-dioxane at 65 °C, to furnish the target 2-methyl-4-(3',4',5'-trimethoxyphenyl)-5-substituted and isomeric 2-methyl-4-substituted-5-(3',4',5'-trimethoxyphenyl)oxazole derivatives **4a-j** and **5a-f**, respectively.

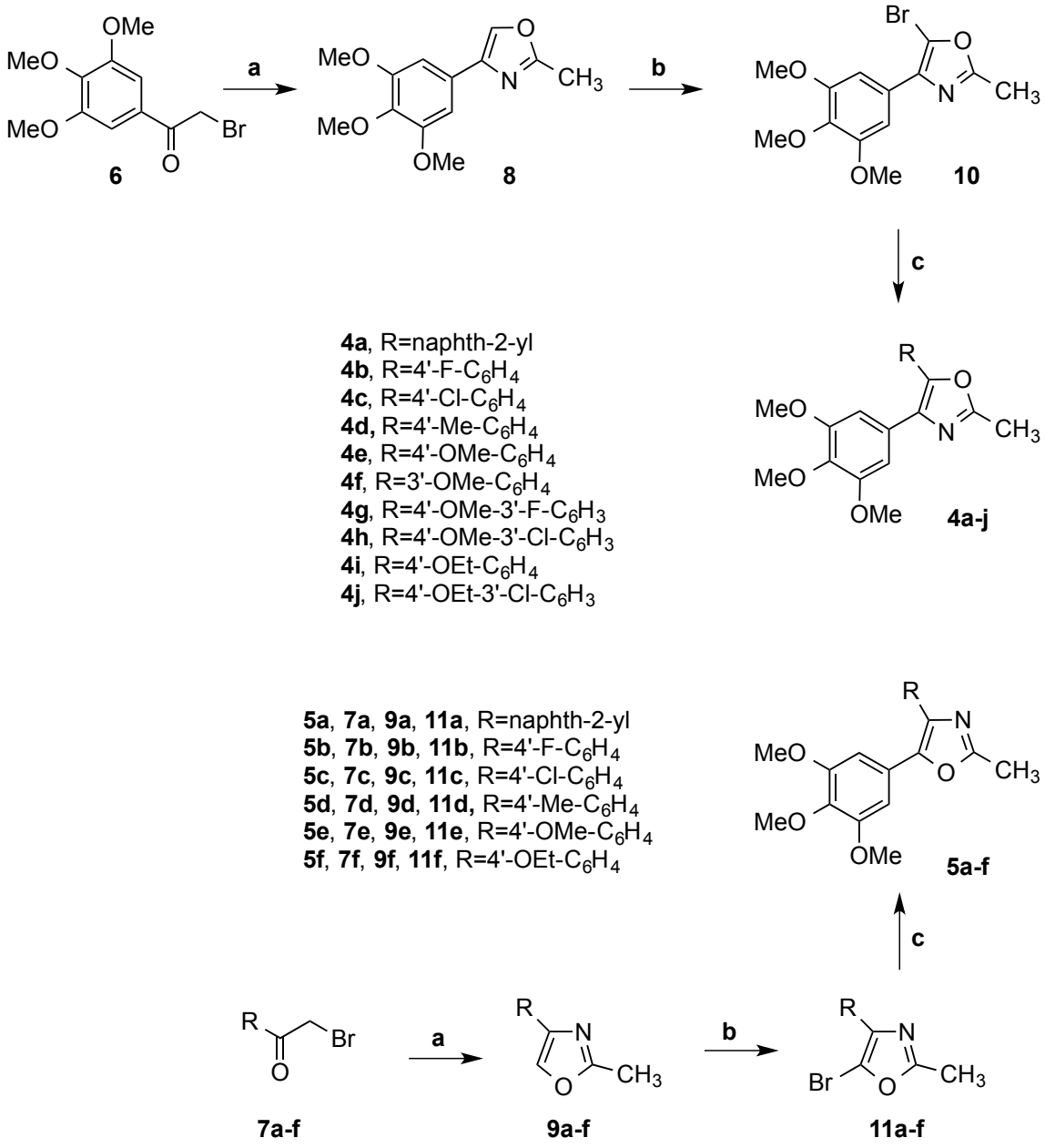

Figure 2. Reagents. a: CH_3CONH_2, 150 °C, 2 h; b: N-bromosuccinimide, $CHCl_3$, rt; c: $PdCl_2$(DPPF), $ArB(OH)_2$, CsF, 1,4-dioxane. 65 °C.

2.3 Biological Results and Discussion

2.3.1 *In vitro* antiproliferative activities

The 2-methyl-4-(3',4',5'-trimethoxyphenyl)-5-substituted oxazoles **4a-j** and the corresponding isomeric 2-methyl-4-substituted-5-(3',4',5'-trimethoxyphenyl) oxazole analogues **5a-f** were evaluated for their antiproliferative activity against a panel of seven human tumour cell lines in comparison with the reference compounds CA-4 and 2-methyl-4-(4'-methoxyphenyl)-5-(3',4',5'-trimethoxyphenyl)thiazole **3e**. Two of the synthesized compounds, **4g** and **4i**, had the best antiproliferative activities against these cell lines and, overall, were significantly more active than the rest of derivatives as well as than CA-4. Specifically, the *m*-fluoro-*p*-methoxyphenyl derivative **4g** and the *p*-ethoxyphenyl analogue **4i** exhibited IC_{50} values of 0.35-4.6 nM and 0.5-20 nM, respectively, as compared with the range 0.8-3100 nM obtained with CA-4. Derivative **4g** was equipotent to CA-4 against Jurkat and SEM cells, while it was from 2- to 940-fold more active against the other five cancer cell lines. Compound **4i** was 2-fold less active than CA-4 against RS4;11 cells, equipotent to CA-4 against Jurkat and SEM cells but 4- to 153-fold more potent against the other four cell lines. Compounds **4a**, **4e**, **4j** and **5f** also inhibited the growth of most of the cancer cell lines at single- to low double-digit nanomolar concentrations.

The relative positions of the two aromatic rings on the 2-methyloxazole core seemed to be critical for antiproliferative activity. In examining the effect of switching the position of the two aromatic rings at the 4- and 5-positions on the 2-methyloxazole system (**4a** *vs.* **5a**, **4b** *vs.* **5b**, **4c** *vs.* **5c**, **4d** *vs.* **5d**, **4e** *vs.* **5e**, **4i** *vs.* **5f**), we observed a considerable difference in potency between the 4'-(3',4',5'-trimethoxyphenyl) derivatives **4a-e** and **4i** and the regioisomeric 5-(3',4',5'-trimethoxyphenyl)oxazole counterparts **5a-f**. Generally, the latter compounds were less active than the former against all the cancer cell lines. Moreover, comparing **3e** and **5e**, which shared common 4'-methoxyphenyl and 3',4',5'-trimethoxyphenyl moieties at their 4 and 5-positions, the thiazole derivative **3e** was from 300- to 11-fold less active than its oxazole congener **5e**.

The 5-(2'-naphthyl)oxazole derivative **4a** was more active than CA-4 in four of the seven cancer cell lines, with activity from single to double digit nanomolar concentrations (IC_{50}: 0.5-73.2 nM). The isomer derivative **5a** was from 4- to 630-fold less active than **4a**, with the greatest reduction of activity against the HT-29 cells.

In comparing the effect of EWG's or ERG's at the *para*-position of the phenyl ring, we observed that compounds with electron-withdrawing substituents such as F (**4b** and **5b**) and

Cl (**4c** and **5c)** showed reduced antiproliferative activity compared to their counterparts with electron-releasing Me, OMe or OEt moieties (**4d-e**, **4i** and **5d-f**).

The *p*-fluorophenyl derivative **4b** and its regioisomer **5b** were the least active compounds of the series, with IC_{50} values over 9 μM against all cell lines screened. Increasing the size of the halide from fluorine to chlorine lead to an increase of activity with all seven cell lines, which was most pronounced against the RS4;11 cell line. Replacing the halogen with the small electron-releasing methyl group at the *p*-position of the phenyl group (**4d**) improved significantly the antiproliferative activity relative to **4b** and **4c**, with IC_{50} values ranging from 25 to 243 nM, with double digit nanomolar activity against HeLa, A549, HT-29 and RS4;11 cells. The *p*-tolyl derivative **4d** was from 3- to 28-fold more potent than isomeric counterpart **5d**, and this difference was most pronounced against A549 and RS4;11.

Replacement of the methyl group with the stronger electron-releasing methoxy group (compounds **4d** and **4e**, respectively) increased the activity from 3- to 9-fold on five of the seven cancer cell lines. For the two 4-(3',4',5'-trimethoxyphenyl)oxazole analogues **4e** and **4f**, the position of methoxy substituent on the 5-phenyl ring had a profound influence on antiproliferative activity. Moving the methoxy group from the *para*- (**4e**) to the *meta*-position (**4f)**, led to a drastic reduction in antiproliferative activity. Compound **4e** was 2- to 3-fold more active than the regioisomeric derivative **5e**, except in HT-29 cells, where **5e** was 3-fold more active than **4e**.

Relative to the activity of **4e**, the insertion of an additional EWG on the *meta*-position of the *p*-methoxyphenyl ring had varying effects on antiproliferative activity. The marked influence of an additional fluorine at the *meta*-position of **4e**, to furnish the *m*-F-*p*-OMe derivative **4g**, led to a 4-276-fold increase in antiproliferative activity, which was most pronounced in the A549 cells. An opposite effect occurred with replacement of *m*-fluorine with *m*-chlorine, to furnish derivative **4h**, which led to a 60-213-fold reduction of activity relative to **4g**. Compound **4h** was also 5-60-fold less active than **4e** against six of the seven cancer cell lines, the exception being the A549 cells.

The *p*-ethoxyphenyl homologue **4i** was 2- to 358-fold more potent than its methoxy counterpart **4e**. The greatest difference in activity was 358-fold against the A549 cells. Since the *p*-ethoxy group of **4i** was favourable for potency, the introduction of an additional electron-withdrawing chlorine group at the *meta*-position of the *p*-ethoxyphenyl ring, resulting in compound **4j**, had variable effects, producing a 5-40-fold reduction in antiproliferative activity against five of the cell lines and increased activity against MCF-7 and HT-29 cells. Compound **4i** was from 2- to 12-fold more potent than the isomeric

derivative **5f** in five of the cell lines, the exceptions being the HT-29 and MCF-7 cells, in which **5f** was 11- and 3-fold more active than **4i**, respectively.

Table 1. *In vitro* cell growth inhibitory effects of compounds **3e**, **4a-j**, **5a-f** and CA-4 (**1**).

Compd	IC_{50} [a](nM)						
	HeLa	A549	HT-29	MCF-7	Jurkat	RS 4;11	SEM
4a	2.1±0.5	12.6±5.4	0.5±0.1	1.1±0.5	73.2±5.2	14.3±6.2	40.2±11.0
4b	>10000	>10000	>10000	>10000	>10000	>10000	9550±2050
4c	2818±169	8785±2309	1397±384	2587±447	5576±888	840±260	2211±256
4d	31.0±16.0	92.3±21.5	53.0±24.6	243.8±74.2	102.2±22.6	25.3±3.2	133.8±39.5
4e	10.8±4.7	179.3±36.3	40.8±19.7	27.7±12.0	18.7±6.0	7.6±2.3	35.6±12.5
4f	>10000	>10000	>10000	>10000	5233±88.2	5333±166.7	3633±171
4g	2.4±0.6	0.65±0.08	3.3±1.1	2.5±0.7	4.6±1.0	0.35±0.15	3.9±0.8
4h	168.8±75.5	138.3±13.7	207.0±93.0	143.8±64.3	512.2±92.7	47.0±13.9	233.3±34.6
4i	0.9±0.3	0.5±0.1	20.2±8.8	4.5±1.8	4.1±1.1	2.1±0.2	6.1±2.3
4j	4.2±1.3	20.3±11.4	0.9±0.5	1.5±0.6	77.7±6.1	20.2±5.4	51.0±13.5
5a	37.0±14.4	45.2±12.5	315.2±145.3	5.2±2.4	638.3±153.5	249.5±89.3	37.0±14.4
5b	>10000	>10000	>10000	>10000	9000±577.4	>10000	>10000
5c	2557±474.6	>10000	>10000	>10000	5250±.934	815±405.9	6567±499.6
5d	148.2±55.3	2579±289	523.3±61.8	360.0±52.6	921.7±76.6	635.2±387.1	351.7±77.8
5e	24.0±10.5	243.3±51.5	12.3±5.9	83.8±20.2	43.6±12.3	17.3±4.2	96.6±22.5
5f	2.0±0.8	1.5±0.44	1.9±0.8	0.4±0.08	50.7±10.8	11.9±6.3	13.3±4.2
3e	1978±779.7	2758±1203	3700±263	1933±448	7200±586	2972±738.3	1978±779.7
CA-4	4±0.1	180±50	3100±100	370±100	5±0.6	0.8±0.2	5±0.1

[a]IC_{50}= compound concentration required to inhibit tumour cell proliferation by 50%. Values are the mean ± SE from the dose-response curves of at least three independent experiments carried out in triplicate.

Effects of test compounds **4a**, **4i** and **5f** in non-tumoral cells

To obtain a preliminary indication of the cytotoxic potential of these derivatives in normal human cells, some of the most active compounds (**4a**, **4i** and **5f**)) were evaluated *in vitro* against peripheral blood lymphocytes (PBL) from healthy donors. All compounds showed an IC_{50} greater than 10 μM both in quiescent lymphocytes and in lymphocytes in an active phase of proliferation induced by phytohematoagglutinin (PHA) a mitogenic stimulus (Table 2). Moreover, we also evaluated the effects of these compounds on primary cultures of human umbilical endothelial cells (HUVECs), and we found that the three compounds were practically inactive, having an IC_{50} values >100 μM. These results indicate that these compounds have very low toxicity in normal cells in comparison to tumour cells, suggesting potential for an excellent therapeutic index.

Table 2. Cytotoxicity of **4n** for nontumoral human cells.

	IC_{50} (μM) [a]		
	4a	**4i**	**5f**
$PBL_{resting}$[b]	15.5±1.5	14.9±3.5	34.5±4.5
PBL_{PHA}[c]	21.1±1.2	18.3±1.5	17.7±2.1
HUVECs	>100	>100	>100

[a] Compound concentration required to reduce cell growth by 50%.
[b] PBL not stimulated with PHA.
[c] PBL stimulated with PHA.
Values are the mean ± SEM for three separate experiments.

2.3.2 Inhibition of tubulin polymerization and colchicine binding

A subset of compounds (**4a, 4d-e, 4g**, **4i-j**, **5a**, **5e-f**) were evaluated for their *in vitro* inhibition of tubulin polymerization and for inhibitory effects on the binding of [^{3}H]colchicine to tubulin (Table 3). CA-4 was also examined in contemporaneous experiments. In the assembly assay, with 10 μM tubulin, one of the most active antiproliferative agents (**4i**), along with compound **4d**, were the best inhibitors of tubulin polymerization, with IC_{50} values of 0.56 and 0.66 μM, respectively, having twice the potency of CA-4 (IC_{50}:1.3 μM). Derivatives **4a**, **4g** and **5f** showed comparable anti-tubulin activity to that of CA-4, while compound **5e** was about half as potent as CA-4. For these new

compounds and CA-4, the order of inhibitory effects on tubulin assembly was **4i**>**4d**>**4e**>**4g**=**4a**=**5f**=CA-4>**5a**>**4j**>**5e**.

In the colchicine binding studies, the same compounds potently inhibited the binding of [^{3}H]colchicine to tubulin, since 54-86% inhibition occurred with these agents and colchicine both at 5 μM. Specifically, derivatives **4d** and **4i** were slightly less active than CA-4 (86 and 82% inhibition, respectively), which in this experiments inhibited colchicine binding by 99%. Inhibition of colchicine binding by compounds **4j**, **5a** and **5e** fall into the 53-64% range.

Table 3. Inhibition of tubulin polymerization and colchicine binding by compounds **4a, 4d-e, 4g**, **4i-j**, **5a**, **5e-f** and CA-4.

Compound	Tubulin assembly[a] IC_{50}±S.D (μM)	Colchicine binding[b] % ±S.D	
		5 μM drug	1 μM drug
4a	1.2±0.1	74±5	47±0.8
4d	0.66±0.0	82±3	55±3
4e	0.95±0.1	78±3	47±4
4g	1.2±0.0	78±0.5	51±1
4i	0.56±0.1	86±1	62±0.4
4j	1.8±0.1	53±3	n.d.
5a	1.6±0.1	64±4	n.d.
5e	2.6±0.3	54±3	n.d.
5f	1.3±0.1	72±2	n.d.
CA-4 (**1**)	1.3±0.1	99±0.7	93±0.8

[a] Inhibition of tubulin polymerisation. Tubulin was at 10 μM.
[b] Inhibition of [^{3}H] colchicine binding. Tubulin and colchicine were at 1 and 5 μM concentrations, respectively.
n.d.=not determined.

While this group of compounds were all highly potent in the biological assays (inhibition of cell growth, tubulin assembly and colchicine binding) correlations between these assay types were imperfect. Thus, while compound **4g** was half as active as an assembly inhibitor as **4d**, these two compounds were equipotent in the colchicine binding assay. Moreover,

compounds **4d** and **4i** were nearly equipotent as inhibitors of tubulin assembly, while **4i** was 2-185-fold more active than **4d** in its effects on cell growth.
Nevertheless, these studies identified tubulin as the molecular target of these compounds, since those with the greatest inhibitory effects on cell growth strongly inhibited tubulin assembly and the binding of colchicine to tubulin.

2.3.3 Molecular modeling

The binding mode in the colchicine site of tubulin of the newly prepared 2-methyloxazole derivatives was elucidated performing a series of molecular docking simulations, following a previous reported procedure.[21] The binding observed for all the derivatives is closely related to the one found for the co-crystallized DAMA-colchicine, and it is consistent with those previously reported for different tubulin polymerization inhibitors.[21,23] The trimethoxyphenyl ring, in both the 4-(*para*-ethoxyphenyl) and isomeric 5-(*para*-ethoxyphenyl)-2-methyloxazole derivatives **4i** and **5f**, respectively, is in close contact with Cys241, while the second substituted phenyl ring occupies a small hydrophobic subpocket (Figure 3, Panels A and B), with the ethoxy substituents lying deep in this pocket. Hydrophobic interactions with the surrounding amino acids (e.g., βMet259, βThr314, βVal181, etc.) of the sub-pocket stabilize the binding of the molecules in the colchicine site.

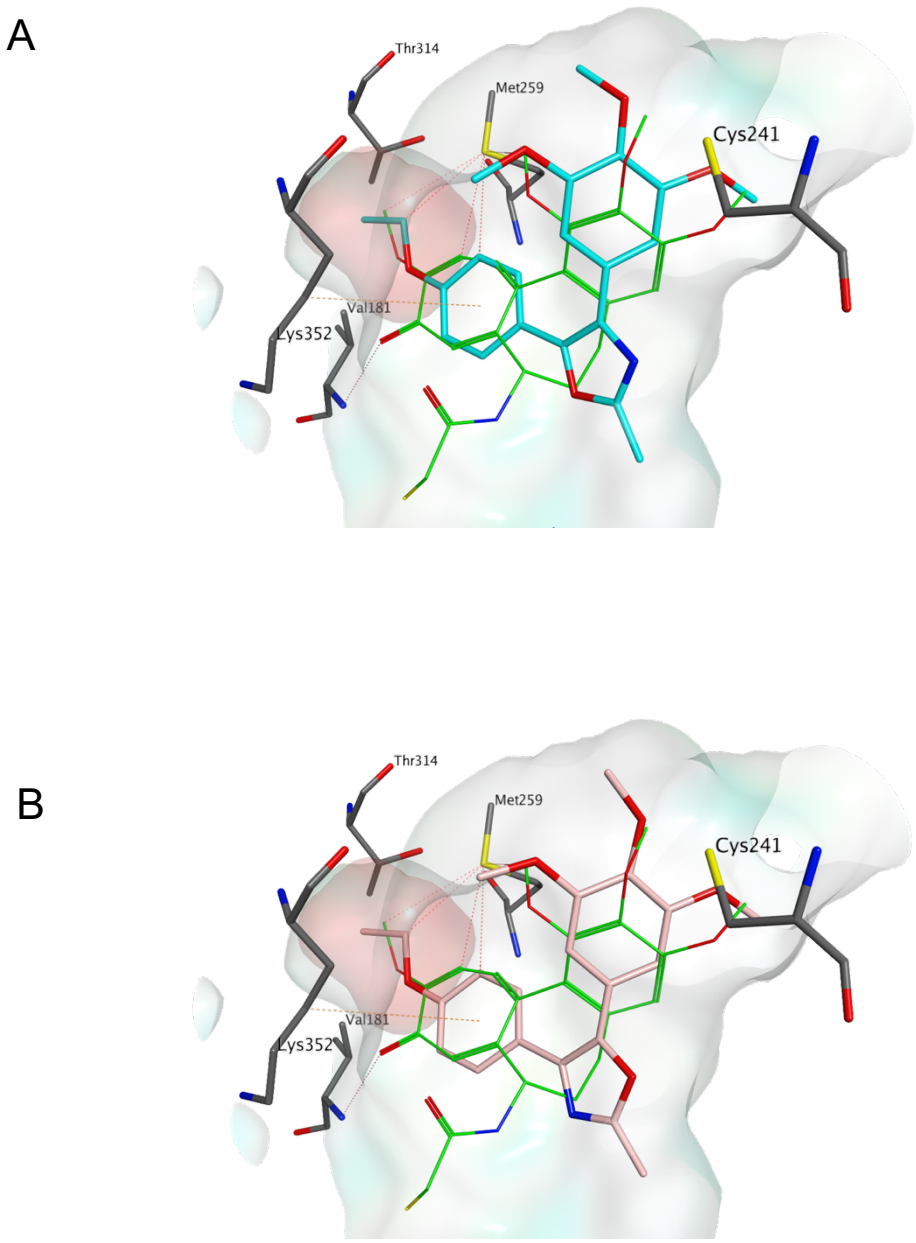

Figure 3. Proposed binding modes for compounds **4i** (carbon atoms in magenta, Figure 1A) and **5f** (carbon atoms in pink, Figure 1B) in the colchicine site. Co-crystallized DAMA-colchicine is shown with carbon atoms in green. The hydrophobic sub-pocket referred to in the text is highlighted with a pink surface.

Analysis of cell cycle effects

The effects of a 24 h treatment with different concentrations of **4a**, **4i** and **5f** on cell cycle progression in Jurkat, and HeLa cells were determined by flow cytometry (Figure 4, Panels A-F). All three compounds caused a significant G2/M arrest in a concentration-dependent manner in the two cell lines examined, with a rise in G2/M cells occurring at a concentration as low as 50 nM, especially with compound **4i**, while at higher concentrations more than 60% of the cells were arrested in G2/M. The cell cycle arrest in G2/M phase was accompanied by a corresponding reduction in cells in the other phases (G1 and S) of the cell cycle. This ability of **4i** to induce G2/M arrest correlates directly with its strong inhibition of tubulin polymerization. With the purpose of evaluating whether **4i** arrested cells in mitosis, Hela cells were stained with an immunofluorescent antibody to p-histone H3, a well-known mitotic marker,[24] as well as with propidium iodide (PI), and analysed by flow cytometry. As shown in Figure 5 (Panel A), in which representative histograms are presented, cells arrested in M phase by treatment with **4i** are readily distinguished from G2 cells by the higher level of p-histone H3. Compound **4i** induced, after a 24 h incubation, a dose-dependent increase in the percentage of mitotic cells, from 1.3% observed in the untreated cells to about 32% and 46% at 50 and 100 nM **4i**, respectively.

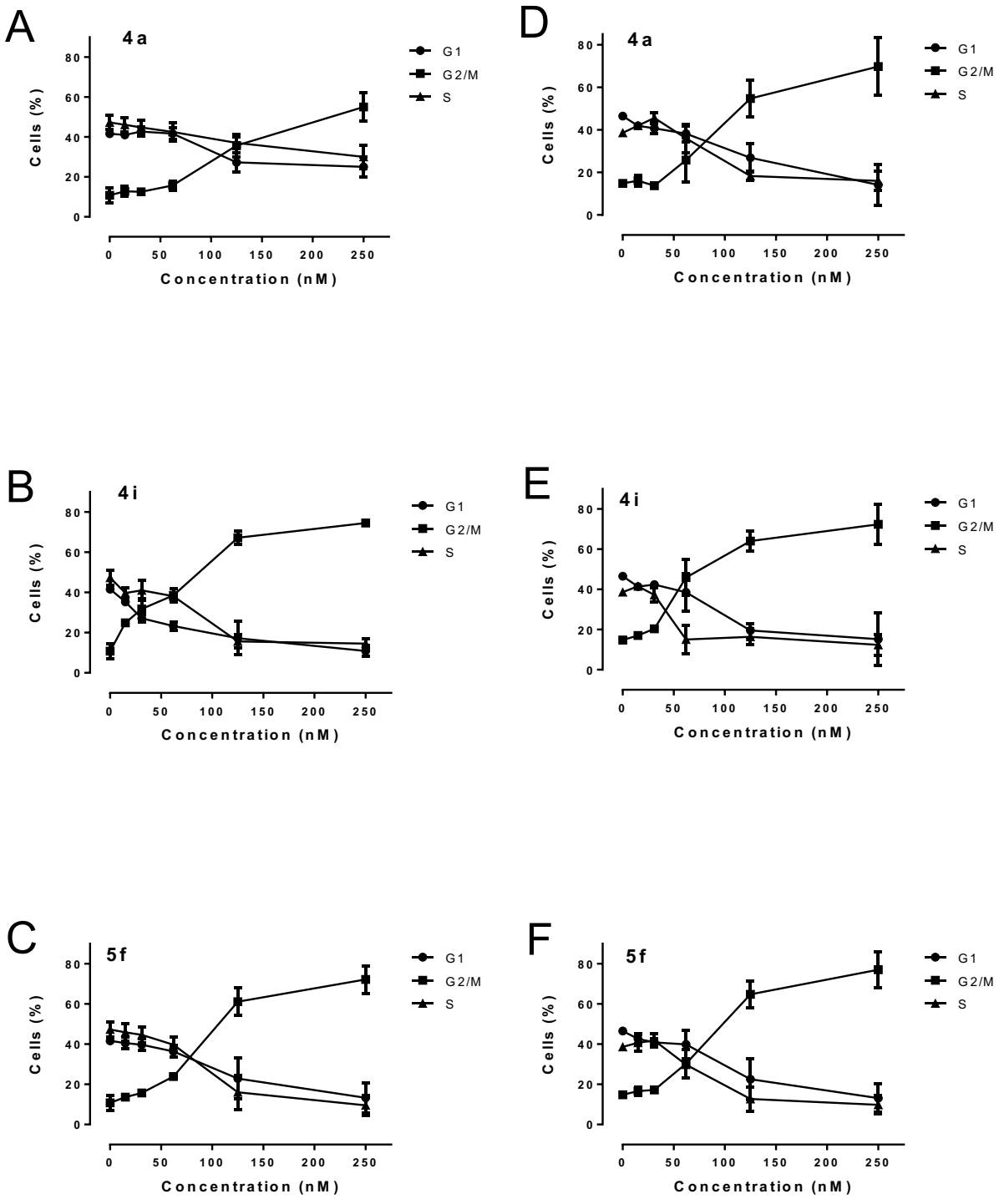

Figure 4. Percentage of cells in each phase of the cell cycle in Jurkat (Panels A-C) and HeLa cells (Panels D-F) treated with the indicated compounds at the indicated concentrations for 24 h. Cells were fixed and labeled with PI and analyzed by flow cytometry as described.

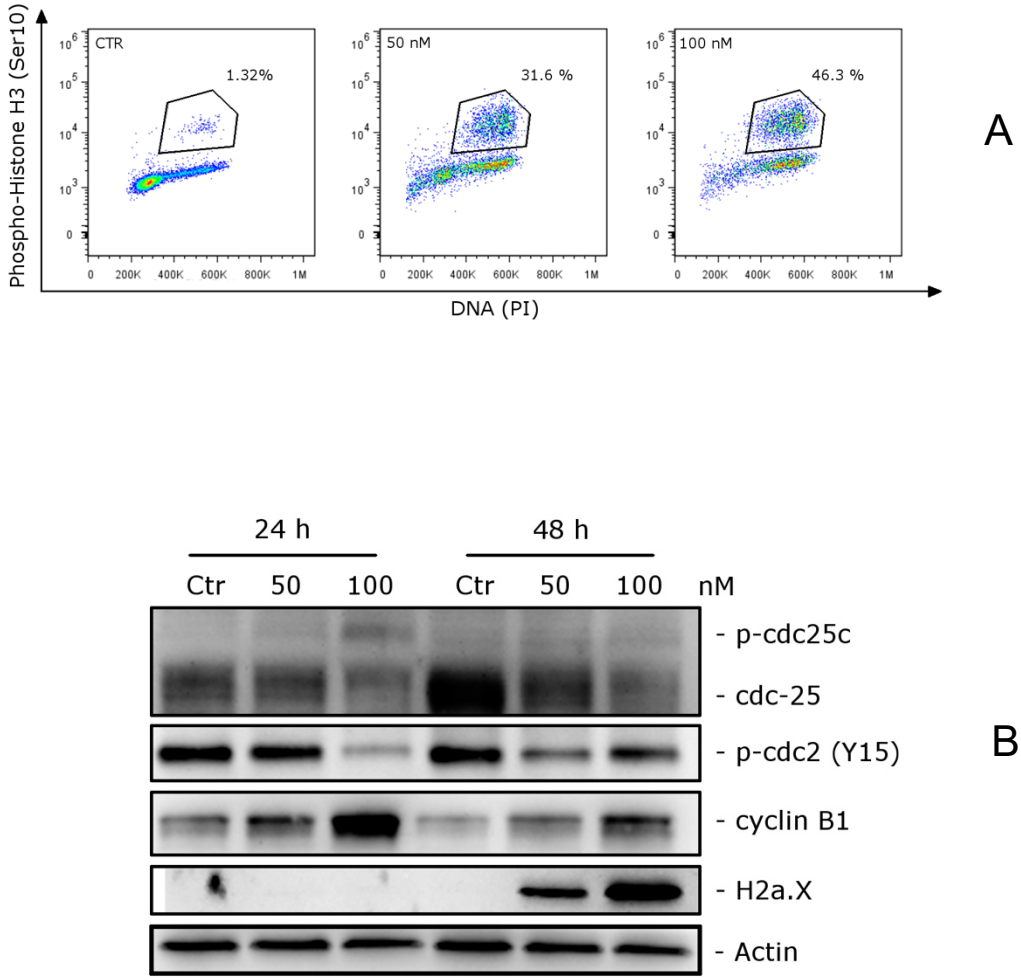

Figure 5. Representative histograms of mitotic cells with phosphorylated histone-H3 after treatment with **4i** at the indicated concentrations in HeLa cells. Data are representative of two experiments with similar results. B. Effect of **4i** on cell cycle checkpoint proteins and expression of p-H2A.X^{Ser139}. HeLa cells were treated for 24 or 48 h with the indicated concentrations of **4i**. The cells were harvested and lysed for detection of the expression of the indicated protein by western blot analysis. To confirm equal protein loading, each membrane was stripped and reprobed with anti-β-actin antibody.

2.3.4 *In vitro* and *in vivo* studies of compound 4i

Compound **4i** induced alteration of cell cycle checkpoint proteins and induced DNA damage

We investigated the effects of **4i** on the expression of proteins involved in regulation of the cell cycle and in spindle assembly. Cyclin B1 is involved in the G2 to M transition as a complex with cdc2, and the activation of the cdc2/cyclin B1 complex through cdc25c-dependent dephosphorylation of phospho-cdc2 and phosphorylation of cyclin B1 triggers cells to enter mitosis.[25,26] As shown in Figure 5 (Panel B) a marked increase of cyclin B1 occurred in a concentration dependent manner 24 and 48 h treatments with **4i**. On the other hand, total cdc25c expression was reduced both at 24 and 48 h after treatment with 100 nM **4i**, and we observed the simultaneous appearance of a slowly migrating form of cdc25c, indicating changes in its phosphorylation state. Furthermore, in good agreement, the expression of phosphorylated cdc2 decreased, most noticeable after the 24 h treatment with 100 nM **4i**. These findings are in good agreement with previous results[21,23] obtained with other antimitotic derivatives and indicate that cdc2/cyclin B1 complexes failed to be activated, preventing cells from exiting mitosis, which would eventually lead to apoptotic cell death.

Moreover, since it is well known that prolonged mitotic arrest induces DNA damage,[27,28] we also examined the expression of phosphorylated histone H2A.X at Ser139 (γH2A.X), a marker of DNA damage.[29] We observed (Figure 5, Panel B) a great increase of the phosphorylation of γH2A.X, after a 48 h treatment, suggesting that DNA damage occurred following treatment with **4i**.

Compound **4i** induced apoptosis

To evaluate the mode of cell death induced by **4i**, we used an annexin-V/PI assay. We treated two cell lines (HeLa and Jurkat) with the test compound with concentrations ranging from 15 to 125 nM for 24 or 48 h. As shown in Figure 6, both HeLa (Panels A, B) and Jurkat (Panels C, D) cells treated with **4i** showed a significant accumulation of annexin-V positive cells in a concentration dependent manner after a 24 h treatment, and the proportions of apoptotic cells further increased at 48 h. Note that **4i** caused the appearance of 70% apoptotic cells at 60 nM in Hela cells, while in the leukemic cell line we observed a lower value (40%) after a 24 h treatment, in good agreement with its cytotoxic activity.

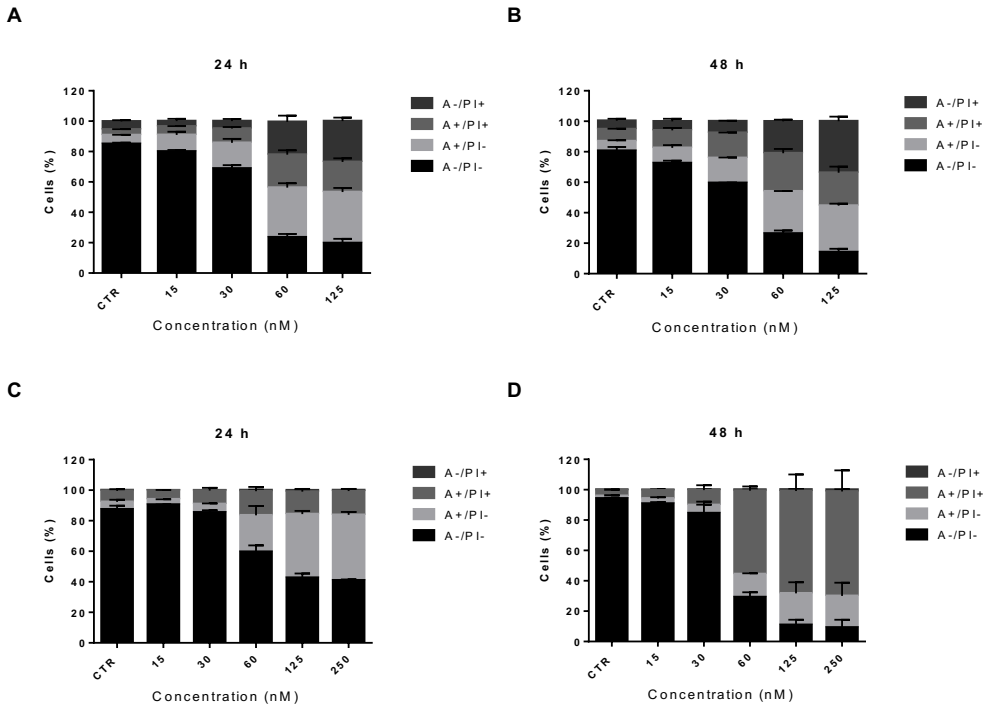

Figure 6. Flow cytometric analysis of apoptotic cells after treatment of HeLa cells (Panels A and B) or Jurkat cells (Panels C and D) with **4i** at the indicated concentrations after incubation for 24 or 48 h. The cells were harvested and labeled with annexin-V-FITC and PI and analyzed by flow cytometry. Data are represented as mean ± SEM of three independent experiments.

Compound **4i** induced apoptosis through the mitochondrial pathway

Since many combretastatin analogues cause apoptosis following the mitochondrial pathway,[19c,20,23] we investigated if **4i** also induced mitochondrial depolarization. Mitochondrial potential was monitored by flow cytometry using the fluorescent dye JC-1. We treated both Hela and Jurkat cells with **4i** at 50 or 100 nM for 24 or 48 h. As shown in Figure 7 (Panels A and B), both HeLa and Jurkat cells treated with **4i** exhibited a marked increase in the percentage of cells with low $\Delta\psi_{mt}$ in a time dependent manner, paralleling the results obtained with the annexin-V apoptotic assay. Since it is well known that dissipation of mitochondrial potential is associated with mitochondrial production of reactive oxygen species (ROS),[30,31] we also evaluated whether ROS production increased after treatment with **4i**. We utilized the dye 2,7-dichlorodihydrofluorescein diacetate (H_2-DCFDA), which is oxidized to the fluorescent compound dichlorofluorescein (DCF) upon ROS induction.

The results shown in Figure 7 (Panels C and D) indicate that **4i** induced ROS production in comparison with the amounts observed in control cells, in both Jurkat and HeLa cells, moving from about 4% of DCF positive cells in untreated samples to about 25-30% in treated

cells at 100 nM, the highest concentration examined. These results are in excellent agreement with the dissipation of $\Delta\psi_{mt}$ described above.

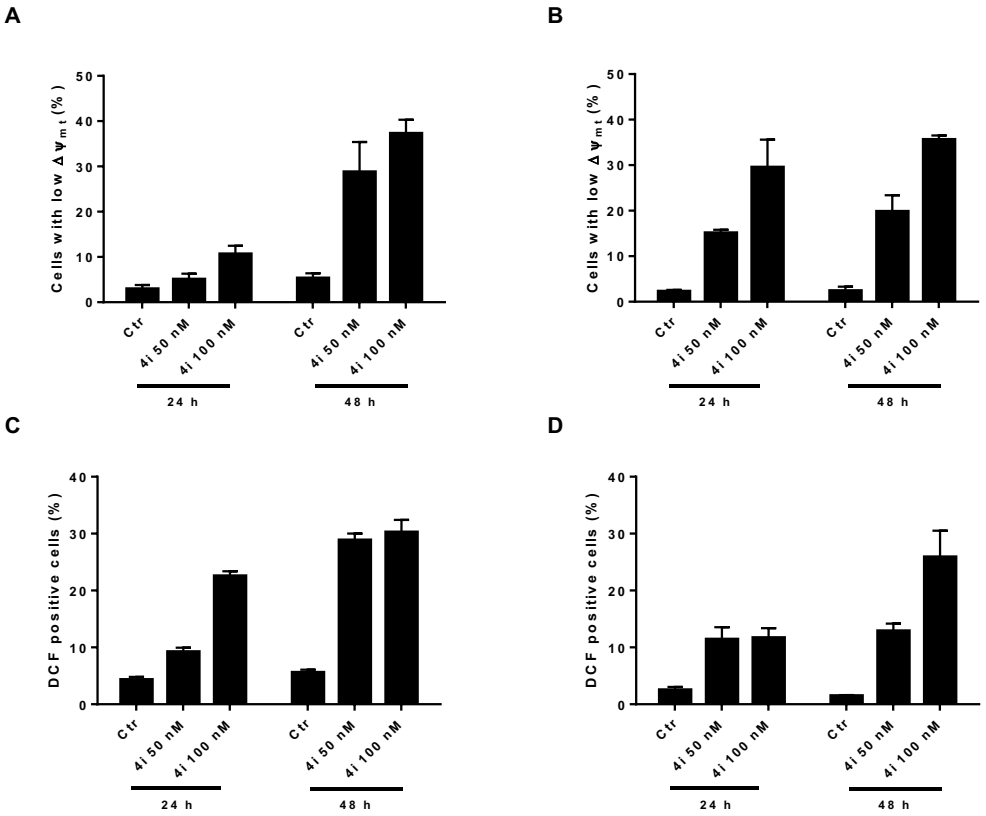

Figure 7. Assessment of mitochondrial membrane potential (Panels A and B) and ROS production after treatment of HeLa cells (A and C) or Jurkat cells (B and D) with compound **4i**. Cells were treated with the indicated concentration of compound for 24 or 48 h and then stained with the fluorescent probes JC-1 or H2-DCFDA and analyzed by flow cytometry. Data are presented as mean ± S.E.M. for three independent experiments.

Compound **4i** induced PARP cleavage and down regulation of anti-apoptotic proteins

To further study the apoptotic process induced by **4i**, we analysed the cleavage of PARP a typical marker of apoptosis.[32] As shown in Figure 8, immunoblot analysis of Hela cells treated with 50 or 100 nM **4i** indicated the activation PARP after both 24 and 48 h, as evidenced by the appearance of its cleavage fragments.

We also investigated the expression of two anti-apoptotic proteins, Mcl-1 and XIAP. Mcl-1 is a member of the Bcl-2 family of anti-apoptotic proteins. Mcl-1 is overexpressed in many

cancers, and it has been reported that sensitivity to antimitotic drugs is regulated by Mcl-1 levels.[33] As shown in Figure 8, the expression of Mcl-1 was only slightly decreased at the highest **4i** concentration used (100 nM).

On the other hand, XIAP, also a member of the IAP family (inhibitors of apoptosis protein) [34], was significantly reduced after both the 24 and 48 h treatments, suggesting that **4i** treatment induced downregulation of these proteins to disable their anti-apoptotic function.

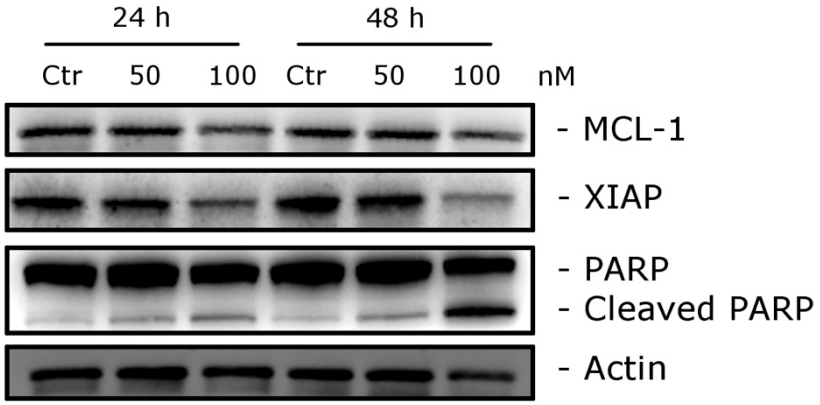

Figure 8. Western blot analysis of caspase-3, PARP, Mcl-1 and XIAP after treatment of HeLa cells with **4i** at the indicated concentrations and for the indicated times. To confirm equal protein loading, each membrane was stripped and reprobed with anti-β-actin antibody.

Evaluation of antivascular activity of **4i** and **4f**

Since many tubulin-binding agents, including CA-4, are endowed with vascular disrupting activity,[9c] we investigated *in vitro* the potential anti-vascular activity of compounds **4i** and **5f**. We tested the anti-vascular effects in HUVECs, evaluating the ability of the compounds to i) interfere with angiogenesis by inhibiting endothelial cell migration and ii) to interfere with the process of capillary-like tube formation. Confluent HUVEC monolayers were scraped with a pipette tip and cellular migration induced to repair the wound was followed by optical microscopy, and the percentage of reduction of wound healing was calculated at different times.[35] As shown in Figure 9 (Panels A and B), after only a 6 h treatment, cell migration was significantly reduced at 100 nM compound **4i** or **5f**. This significant reduction was maintained for a 24 h treatment as well. In contrast, CA-4 was significantly active even at 10 nM, after both the 6 and 24 h treatments.

Endothelial cells seeded on Matrigel are able to form a capillary network miming the first angiogenesis steps.[36] This network is a useful experimental model to assess the action of molecules on vascular morphogenesis.

The antivascular effect induced by the tested compounds is shown in Figure 9 (Panels C and D). In this case, we evaluated the pictures taken after 24 h of incubation by optical microscopy (Figure 9, Panel C) and a quantitative analysis was carried out studying three different dimensional (the area occupied by tubular structures, the capillary length and the mesh area) and two topological parameters (the number of branching points and meshes). Compounds **4i** and **5f** did not show a significant antivascular effect on Matrigel preformed tubular structures (Figure 6, Panel D), even at the highest concentration used (100 nM). In this assay, CA-4 showed, as expected, a significant antivascular activity even at 10 nM. Our findings suggest that these compounds do not possess a good antivascular profile in comparison to the well-known activity of CA-4, since some effects, in particular cellular migration, occurred at a concentration higher than that required for CA-4.

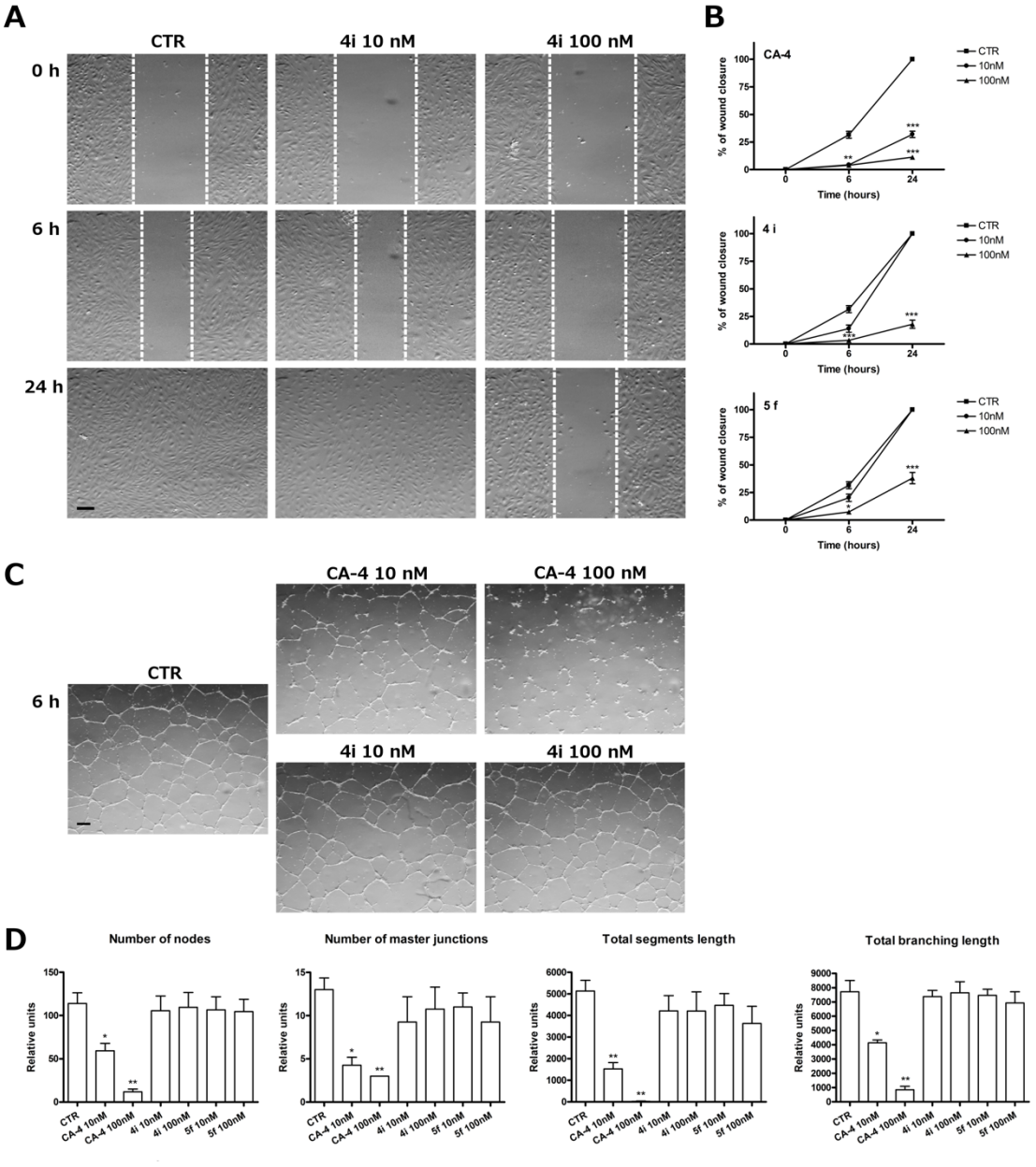

Figure 9. Antivascular activity of compounds **4i** and **4f**. A. Representative images of confluent HUVEC monolayers that were scratch wounded and treated with vehicle (Ctr) or 10 or 100 nM of **4i**, as indicated, after 0, 6 or 24 h from the scratch. After different times, cells were photographed (10x magnification) and the scratch width was quantified (Panel B). **CA-4** was chosen as reference compound. Data are presented as the mean ± SEM of three independent experiments. ***p<0.01 vs control. C. Disruption of capillary-like structures. Representative images of HUVEC cells that were incubated on Matrigel until the formation of capillary-like tubes. The disrupting effects of 10 or 100 nM **4i** are shown (10x magnification). D. Quantification of the effect of compounds **4i**, **5f** and **CA-4** on dimensional and topological parameters of HUVEC morphology in comparison to time zero. Data are presented as the mean ± SEM of three independent experiments. *p<0.01 vs Ctr.

Compound **4i** induced tumour growth reduction in a mouse allograft tumour model

To evaluate its antitumor effect *in vivo*, **4i** was administered by the intraperitoneal route each other day, at two different doses (3.0 and 7.5 mg/kg) in an allograft tumour model developed in mice.[37] As reference compound, CA-4P (**1b**) was used at 30 mg/kg.

As shown in Figure 10, after six days of treatment (doses administered on days 9, 11 and 14), **4i** was able to significantly reduce tumour burden in a dose-dependent manner, even at the lowest dose tested (3.0 mg/kg). We observed reduction of tumour mass of 34.9, and 52.5% at the doses of 3.0 and 7.5 mg/kg, respectively. The reference compound CA-4P at 30 mg/kg induced only a 28.0% reduction of tumour mass. Notably, the *in vivo* efficacy clearly indicates an increased antitumor efficacy of **4i** as compared with CA-4P. Even at the highest dose, **4i** did not show any sign of toxicity and did not cause a decrease in animal body weight (data not shown).

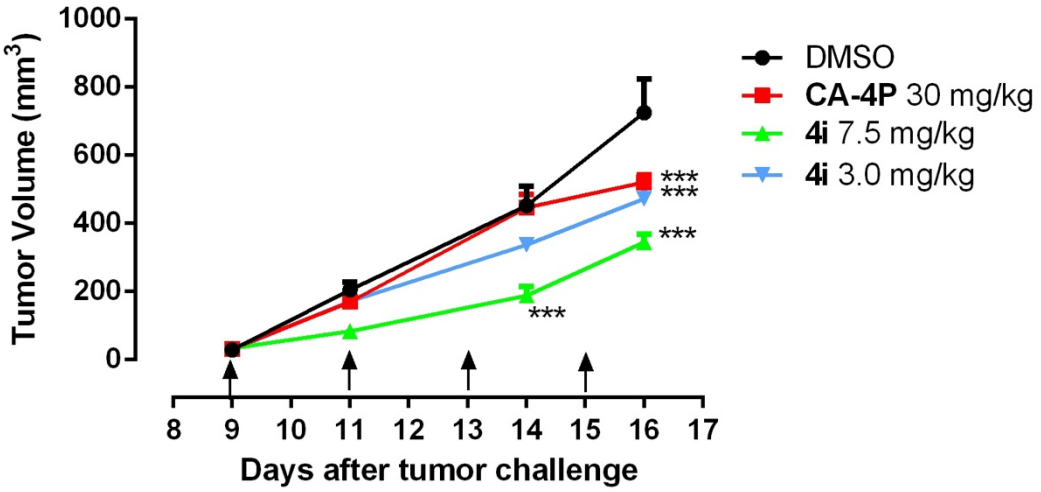

Figure 10. Inhibition of mouse allograft growth *in vivo* by compound **4i**. Male C57BL/6 mice were injected subcutaneously at their dorsal region with 10^7 BL6-B16 murine melanoma cells. Tumor-bearing mice were administered the vehicle, as control, or 3 or 7.5 mg/kg of **4i** or CA-4P as reference compound at the dose of 30 mg/kg. Injections were given intraperitoneally at the days indicated by the arrows. Data are presented as mean ± SEM of tumour volume at each time point for 5 animals per group. ***p<0.001 *vs*. control.

2.4 Conclusions

The isomerization of the *cis*-double bond of CA-4 to its t*rans*-form in solution is one of the major disadvantages of this molecule. The instability of the *Z*-double bond of CA-4 has been resolved incorporating the stilbene double bond in part of the structure of five-member heterocyclic rings. The bioisosteric equivalence between oxazole and thiazole prompted us to synthesize by a three-step procedure two novel series of 2-methyl-4,5-disubstituted oxazole derivatives with general formulas **4** and **5**, in which the oxazole ring replaced the thiazole system of previously published analogues with general structure **3** and could serve as a suitable mimic to retain the bioactive configuration afforded by the *cis*-double bond present in CA-4. For both these series of compounds, the 3',4',5'-trimethoxyphenyl and 2-methyloxazole rings mimic the ring A and *cis*-double bond of CA-4, respectively, while a naphth-2-yl or phenyl ring substituted with electron-releasing or electron-withdrawing groups was utilized as a B-ring surrogate to mimic the 3'-hydroxy-4'-methoxyphenyl group in CA-4. Comparing compounds with the same aryl substitution, the 2-methyl-4-(3',4',5'-trimethoxyphenyl)oxazole derivatives were more active than their isomeric 2-methyl-5-(3',4',5'-trimethoxyphenyl)oxazole counterparts. The results indicated that 2-methyloxazole derivatives **4a**, **4d**-**e**, **4i** and **5e** exhibited more highly potent antiproliferative activity than the corresponding 2-methylthiazole analogues **3a-e** previously described. These marked differences were maintained in all the biological evaluations performed. In particular, it is important to underline that **4i** has very low toxicity in nontumoral cell lines such as PBLs and HUVECs. Although preliminary investigations regarding the potential antivascular activity of these new oxazoles derivatives indicated that they are not vascular disrupting agents, *in vivo* experiments demonstrated that **4i** had excellent antitumor activity that was evident at lower doses than CA-4P and in the absence of obvious toxicity. In summary, the biological characterization of compound **4i** provides compelling evidence to support its further development as an anticancer drug.

2.5 Experimental Section

Chemistry

Materials and Methods. ^{1}H and ^{13}C NMR data were obtained with a Varian VXR 200 spectrometer and a Varian Mercury Plus 400 spectrometer, respectively. Peak positions are given in parts per million (δ) downfield, and J values are given in hertz. Positive-ion

electrospray ionization (ESI) mass spectra were recorded on a double-focusing Finnigan MAT 95 instrument with BE geometry. Melting points (mp) were determined on a Buchi-Tottoli apparatus and are uncorrected. The purity of tested compounds was determined by combustion elemental analyses conducted by the Microanalytical Laboratory of the Chemistry Department of the University of Ferrara with a Yanagimoto MT-5 CHN recorder elemental analyzer. All tested compounds yielded data consistent with a purity of at least 95% as compared with the theoretical values. TLC was carried out using glass plates coated with silica gel 60 F_{254} by Merck, and compounds were visualized by UV detection or with aqueous $KMnO_4$. Flash column chromatography was performed using 230-400 mesh silica gel and the indicated solvent system. Organic solutions were dried over anhydrous Na_2SO_4. Solvents and reagents that are commercially available were purchased from Aldrich (Sigma-Aldrich) or Alfa Aesar (Johnson Matthey Company) and were used without further purification unless otherwise noted.

General procedure A for the preparation of compounds 8 and 9a-f. A mixture of the appropriate 2-bromoacetophenone **6** or **7a-f** (4 mmol) and acetamide (708 mg, 12 mmol) was heated to 150 °C for 2 h. After this time, the mixture was cooled to room temperature, treated with a 2 M aqueous solution of Na_2CO_3 (10 mL), and the suspension was carefully adjusted to pH 12 with Na_2CO_3. The mixture was extracted with EtOAc (2 x 20 mL), the combined organic phase was washed with water (10 mL) and brine (10 mL), dried (Na_2SO_4) and concentrated under reduced pressure. The residue was purified by flash column chromatography on silica gel.

4-(3,4,5-Trimethoxyphenyl)-2-methyloxazole (**8**). Following general procedure A, the crude residue purified by flash chromatography, using EtOAc:petroleum ether 1:1 (v:v) for elution, yielded **8** as a white solid. Yield 72%, mp 98-100 °C. ^{1}H-NMR ($CDCl_3$) δ: 2.57 (s, 3H), 3.87 (s, 3H), 3.93 (s, 6H), 6.96 (s, 2H), 7.79 (s, 1H). MS (ESI): $[M+1]^+$=250.3.

2-Methyl-4-(naphthalen-3-yl)oxazole (**9a**). Following general procedure A, the crude residue purified by flash chromatography, using EtOAc:petroleum ether 1:9 (v:v) for elution, yielded **9a** as an orange solid. Yield 71%, mp 72-73 °C. ^{1}H-NMR ($CDCl_3$) δ: 2.58 (s, 3H), 7.49 (m, 2H), 7.74 (dd, *J*=8.6 and 1.8 Hz, 1H), 7.93 (m, 4H), 8.28 (s, 1H). MS (ESI): $[M+1]^+$=210.3.

4-(4-Fluorophenyl)-2-methyloxazole (**9b**). Following general procedure A, the crude residue purified by flash chromatography, using EtOAc:petroleum ether 3:7 (v:v) for elution, yielded **9b** as an orange solid. Yield 61%, mp 54-56 °C. ^{1}H-NMR ($CDCl_3$) δ: 2.53 (s, 3H), 7.08 (t, *J*=8.8 Hz, 2H), 7.65 (dd, *J*= 8.8 Hz, 2H), 7.76 (s, 1H). MS (ESI): $[M+1]^+$=178.2.

4-(4-Chlorophenyl)-2-methyloxazole (**9c**). Following general procedure A, the crude residue purified by flash chromatography, using EtOAc:petroleum ether 2:8 (v:v) for elution, yielded **9c** as a white solid. Yield 62%, mp 88-90 °C. ^{1}H-NMR ($CDCl_3$) δ: 2.54 (s, 3H), 7.36 (d, *J*=8.8 Hz, 2H), 7.64 (d, *J*= 8.8 Hz, 2H), 7.81 (s, 1H). MS (ESI): $[M+1]^+$=194.7.

2-Methyl-4-*p*-tolyloxazole (**9d**). Following general procedure A, the crude residue purified by flash chromatography, using EtOAc:petroleum ether 3:7 (v:v) for elution, yielded **9d** as an orange solid. Yield 63%, mp 49-51 °C. ^{1}H-NMR ($CDCl_3$) δ: 2.36 (s, 3H), 2.53 (s, 3H), 7.18 (d, *J*=8.2 Hz, 2H), 7.58 (d, *J*=8.2 Hz, 2H), 7.77 (s, 1H). MS (ESI): $[M+1]^+$=174.2.

4-(4-Methoxyphenyl)-2-methyloxazole (**9e**). Following general procedure A, the crude residue purified by flash chromatography, using EtOAc:petroleum ether 4:6 (v:v) for elution, yielded **9e** as a white solid. Yield 67%, mp 68-70 °C. ^{1}H-NMR ($CDCl_3$) δ: 2.66 (s, 3H), 3.84 (s, 3H), 6.94 (d, *J*=8.8 Hz, 2H), 7.68 (d, *J*=8.8 Hz, 2H), 7.77 (s, 1H). MS (ESI): $[M+1]^+$=190.1.

4-(4-Ethoxyphenyl)-2-methyloxazole (**9f**). Following general procedure A, the crude residue purified by flash chromatography, using EtOAc:petroleum ether 3:7 (v:v) for elution, yielded **9f** as a colour cream solid. Yield 62%, mp 76-79 °C. ^{1}H-NMR ($CDCl_3$) δ: 1.42 (t, *J*=6.8 Hz, 3H), 2.56 (s, 3H), 4.01 (q, *J*=6.8 Hz, 2H), 6.90 (d, *J*=8.8 Hz, 2H), 7.62 (d, *J*=8.8 Hz, 2H), 7.73 (s, 1H). MS (ESI): $[M+1]^+$=204.3.

General procedure B for the preparation of compounds 10 and 11a-f. A solution of the appropriate 2-methyl-4-aryloxazole **8** or **9a-f** (4 mmol) in anhydrous $CHCl_3$ (20 mL) was cooled to 0 °C**,** then *N*-bromosuccinimide (783 mg, 4.4 mmol) was added in small portions. The reaction mixture was allowed to warm slowly to room temperature. After 2 h, the resulting mixture was diluted with CH_2Cl_2 (20 mL), washed with a saturated solution of $NaHCO_3$ (10 mL), brine (10 mL), dried ($MgSO_4$) and evaporated. The residue was purified by column chromatography on silica gel.

5-Bromo-4-(3,4,5-trimethoxyphenyl)-2-methyloxazole (10). Following general procedure B, the crude residue purified by flash chromatography, using EtOAc:petroleum ether 4:6 (v:v) for elution, furnished **10** as a white solid. Yield 73%, mp 108-110 °C. ^{1}H-NMR ($CDCl_3$) δ: 2.54 (s, 3H), 3.88 (s, 3H), 3.93 (s, 6H), 7.20 (s, 2H). MS (ESI): $[M]^+$=327.4, $[M+2]^+$=329.5.

5-Bromo-2-methyl-4-(naphthalen-3-yl)oxazole (**11a**). Following general procedure B, the crude residue purified by flash chromatography, using ethyl acetate:petroleum ether 2:8 (v:v) for elution, yielded **11a** as a pink solid. Yield 67%, mp 89-91 °C. ^{1}H-NMR ($CDCl_3$) δ: 2.56 (s, 3H), 7.49 (m, 2H), 7.82 (m, 4H), 8.05 (dd, *J*=8.8 and 1.6 Hz, 1H). MS (ESI): $[M]^+$=268.2, $[M+2]^+$=270.1.

5-Bromo-4-(4-fluorophenyl)-2-methyloxazole (**11b**). Following general procedure B, the crude residue purified by flash chromatography, using EtOAc:petroleum ether 2:8 (v:v) for elution, furnished **11b** as an orange oil. Yield 58%. ^{1}H-NMR ($CDCl_3$) δ: 2.51 (s, 3H), 7.07 (d, *J*=8.8 Hz, 2H), 7.87 (dd, *J*=9.2 and 9.0 Hz, 2H). MS (ESI): $[M]^+$=256.1, $[M+2]^+$=258.1.

5-Bromo-4-(4-chlorophenyl)-2-methyloxazole (**11c**). Following general procedure B, the crude residue purified by flash chromatography, using EtOAc:petroleum ether 4:6 (v:v) for elution, furnished **11c** as an orange solid. Yield 71%, mp 61-62 °C. ^{1}H-NMR ($CDCl_3$) δ: 2.52 (s, 3H), 7.38 (d, *J*=8.4 Hz, 2H), 7.87 (d, *J*=8.4 Hz, 2H). MS (ESI): $[M]^+$=272.6, $[M+2]^+$=274.6.

5-Bromo-2-methyl-4-*p*-tolyloxazole (**11d**). Following general procedure B, the crude residue purified by flash chromatography, using ethyl acetate:petroleum ether 3:7 (v:v) for elution, yielded **11d** as white solid. Yield 58%, mp 72-74 °C. ^{1}H-NMR ($CDCl_3$) δ: 2.38 (s, 3H), 2.53 (s, 3H), 7.21 (d, *J*=8.2 Hz, 2H), 7.84 (d, *J*=8.2 Hz, 2H), 7.77 (s, 1H). MS (ESI): $[M]^+$=252.2, $[M+2]^+$=254.2.

5-Bromo-4-(4-methoxyphenyl)-2-methyloxazole (**11e**). Following general procedure B, the crude residue purified by flash chromatography, using EtOAc:petroleum ether 2:8 (v:v) for elution, furnished **11e** as a white solid. Yield 67%, mp 78-80 °C. ^{1}H-NMR ($CDCl_3$) δ: 2.54 (s, 3H), 3.85 (s, 3H), 6.94 (d, *J*=9.2 Hz, 2H), 7.85 (d, *J*=9.2 Hz, 2H). MS (ESI): $[M]^+$=266.1, $[M+2]^+$=268.0.

5-Bromo-4-(4-ethoxyphenyl)-2-methyloxazole (**11f**). Following general procedure B, the crude residue purified by flash chromatography, using EtOAc:petroleum ether 3:7 (v:v) for elution, yielded **11f** as a pink solid. Yield 59%, mp 64-66 °C. ^{1}H-NMR ($CDCl_3$) δ: 1.44 (t, *J*=7.2 Hz, 3H), 2.52 (s, 3H), 4.01 (q, *J*=7.2 Hz, 2H), 6.92 (dd, *J*=6.8 and 2.2 Hz, 2H), 7.62 (dd, *J*= 6.8 and 2.2 Hz, 2H), 7.73 (s, 1H). MS (ESI): $[M]^+$=282.2, $[M+2]^+$=284.2.

General procedure C for the synthesis of compounds 4a-j and 5a-f. A stirred suspension of 5-bromo-2-methyl-4-aryloxazole **10** or **11a-f** (0.5 mmol) and the appropriate arylboronic acid (0.75 mmol) in dioxane (6 mL containing 2 drops of water) was degassed under a stream of N_2 over 10 min, then treated with $PdCl_2$(DPPF) (41 mg, 0.05 mmol) and CsF (190 mg, 1.25 mmol). The reaction mixture was heated under N_2 at 45 °C for 30 min, then at 65 °C for 6 h. The reaction mixture was cooled to ambient temperature, diluted with CH_2Cl_2 (10 mL), filtered through a pad of celite and evaporated *in vacuo*. The residue was dissolved with CH_2Cl_2 (15 mL), and the resultant solution was washed sequentially with water (5 mL) and brine (5 mL). The organic layer was dried and evaporated, and the residue was purified by column chromatography on silica gel.

4-(3,4,5-Trimethoxyphenyl)-2-methyl-5-(naphthalen-3-yl)oxazole (4a). Following general procedure C, the residue was purified by flash chromatography on silica gel using light petroleum ether:EtOAc 1:1 as eluent, affording compound **4a** as a yellow solid. Yield: 58%, mp 104-116 ºC. ^{1}H-NMR ($CDCl_3$) δ: 2.66 (s, 3H), 3.76 (s, 6H), 3.83 (s, 3H), 6.96 (s, 2H), 7.51 (m, 2H), 7.68 (dd, *J*=8.8 and 1.2 Hz, 1H), 7.84 (m, 3H), 8.1 (d, *J*=1.2 Hz, 1H). ^{13}C NMR (100 MHz, $CDCl_3$) δ: 13.97, 56.16 (2C), 60.98, 105.02 (2C), 109.98, 120.17, 121.16, 122.02, 124.12, 125.94, 126.80, 126.86, 127.81, 128.20, 133.13, 137.08, 139.75, 145.48, 153.38 (2C), 160.79. MS (ESI): $[M]^+$=375.5. Anal. ($C_{23}H_{21}NO_4$) C, H, N.

5-(3,4,5-Trimethoxyphenyl)-4-(4-fluorophenyl)-2-methyloxazole (4b). Following general procedure C, the residue was purified by flash chromatography on silica gel using light petroleum ether:EtOAc 1:1 as eluent, affording compound **4b** as a white solid. Yield: 62%, mp 142-144 ºC. ^{1}H-NMR ($CDCl_3$) δ: 2.60 (s, 3H), 3.78 (s, 6H), 3.83 (s, 3H), 6.85 (s, 2H), 7.06 (t, *J*=8.8 Hz, 2H), 7.60 (dd, *J*=8.8 and 8.6Hz, 2H). ^{13}C NMR (100 MHz, $CDCl_3$) δ: 14.02, 56.18 (2C), 61.03, 104.87 (2C), 115.72, 115.93, 125.14, 127.29, 128.78, 128.86, 134.56, 138.08, 144.40, 153.44 (2C), 160.36 and 163.98 (*J*=144.8 Hz), 161.49. MS (ESI): $[M]^+$=343.4. Anal. ($C_{19}H_{18}FNO_4$) C, H, N.

5-(3,4,5-Trimethoxyphenyl)-4-(4-chlorophenyl)-2-methyloxazole (4c). Following general procedure C, the residue was purified by flash chromatography on silica gel using light petroleum ether:EtOAc 6:4 as eluent, affording compound **4c** as a white solid. Yield: 64%, mp 158–160 ºC. ^{1}H-NMR ($CDCl_3$) δ: 2.66 (s, 3H), 3.80 (s, 6H), 3.84 (s, 3H), 6.87 (s, 2H), 7.34 (d, *J*=8.4 Hz, 2H), 7.56 (d, *J*=8.8 Hz, 2H). ^{13}C NMR (100 MHz, $CDCl_3$) δ: 14.04, 56.21 (2C), 61.04, 105.03 (2C), 126.92, 127.49, 127.82 (2C), 128.90 (2C), 134.32, 135.46, 138.18, 144.14, 153.47 (2C), 160.47. MS (ESI): $[M]^+$=359.6. Anal. ($C_{19}H_{18}ClNO_4$) C, H, N.

4-(3,4,5-Trimethoxyphenyl)-2-methyl-5-*p*-tolyloxazole (4d). Following general procedure C, the residue was purified by flash chromatography on silica gel using light petroleum ether:EtOAc 6:4 as eluent, affording compound **4d** as a white solid. Yield: 51%, mp 110–112 ºC. ^{1}H-NMR ($CDCl_3$) δ: 2.38 (s, 3H), 2.64 (s, 3H), 3.79 (s, 6H), 3.83 (s, 3H), 6.91 (s, 2H), 7.18 (d, *J*=8.2 Hz, 2H), 7.50 (d, *J*=8.2 Hz, 2H). ^{13}C NMR (100 MHz, $CDCl_3$) δ: 14.02, 21.45, 56.16 (2C), 61.01, 104.90 (2C), 126.18, 126.72 (2C), 127.89, 129.32 (2C), 134.29, 137.85, 138.66, 145.44, 153.32 (2C), 159.99. MS (ESI): $[M]^+$=339.7. Anal. ($C_{20}H_{21}NO_4$) C, H, N.

4-(3,4,5-Trimethoxyphenyl)-5-(4-methoxyphenyl)-2-methyloxazole (4e). Following general procedure C, the residue was purified by flash chromatography on silica gel using light petroleum ether:EtOAc 1:1 as eluent, affording compound **4a** as a white solid. Yield: 59%, mp 134-136 ºC. ^{1}H-NMR ($CDCl_3$) δ: 2.63 (s, 3H), 3.79 (s, 6H), 3.80 (s, 3H), 3.84 (s, 3H), 6.90 (s, 2H), 6.91 (d, *J*=8.8 Hz, 2H), 7.54 (d, *J*=8.8 Hz, 2H). ^{13}C NMR (100 MHz, $CDCl_3$) δ: 13.96, 55.33, 56.06 (2C), 60.93, 104.68 (2C), 113.98 (2C), 121.52, 127.86, 128.36 (2C), 133.57, 137.68, 145.21, 153.25 (2C), 159.70, 160.78. MS (ESI): $[M]^+$=355.6. Anal. ($C_{20}H_{21}NO_5$) C, H, N.

5-(3,4,5-Trimethoxyphenyl)-4-(3-methoxyphenyl)-2-methyloxazole (4f). Following general procedure C, the residue was purified by flash chromatography on silica gel using light petroleum ether:EtOAc 1:1 as eluent, affording compound **4f** as a white solid. Yield: 64%, mp 104-106 ºC. ^{1}H-NMR ($CDCl_3$) δ: 2.61 (s, 3H), 3.78 (s, 6H), 3.79 (s, 3H), 3.87 (s, 3H), 6.87 (td, *J*=8.4, 2.8 and 1.2 Hz, 1H), 6.91 (s, 2H), 7.16 (dd, *J*=2.8 and 1.2 Hz, 1H), 7.21 (dt, *J*=8.0 and 1.2 Hz, 1H), 7.27 (dd, *J*=8.4 and 8.0 Hz, 1H). ^{13}C NMR (100 MHz, $CDCl_3$) δ: 14.12, 55.42, 56.26 (2C), 60.47, 61.02, 105.16 (2C), 112.06, 114.78, 119.27, 126.71, 129.79, 134.35, 138.19, 145.28, 153.38 (2C), 159.77, 160.61. MS (ESI): $[M]^+$=355.6. Anal. ($C_{20}H_{21}NO_5$) C, H, N.

5-(3-Fluoro-4-methoxyphenyl)-4-(3,4,5-trimethoxyphenyl)-2-methyloxazole (4g). Following general procedure C, the residue was purified by flash chromatography on silica gel using light petroleum ether:EtOAc 1:1 as eluent, affording compound **4g** as a white solid. Yield: 69%, mp 127-129 ºC. ^{1}H-NMR ($CDCl_3$) δ: 2.66 (s, 3H), 3.80 (s, 6H), 3.84 (s, 3H), 3.88 (s, 3H), 6.89 (s, 2H), 6.96 (d, *J*=8.2 Hz, 1H), 7.36 (m, 2H). ^{13}C NMR (100 MHz, $CDCl_3$) δ: 14.11, 55.26 (2C), 56.33, 61.04, 105.01 (2C), 113.29, 114.47, 121.77, 123.02, 127.04, 134.10, 138.15, 144.14, 147.93, 150.96, 153.44 (2C), 160.28. MS (ESI): $[M]^+$=373.5. Anal. ($C_{20}H_{20}FNO_5$) C, H, N.

5-(3-Chloro-4-methoxyphenyl)-4-(3,4,5-trimethoxyphenyl)-2-methyloxazole (4h). Following general procedure C, the residue was purified by flash chromatography on silica gel using light petroleum ether:EtOAc 6:4 as eluent, affording compound **4h** as a white solid. Yield: 59%, mp 150-152 ºC. ^{1}H-NMR ($CDCl_3$) δ: 2.64 (s, 3H), 3.81 (s, 6H), 3.85 (s, 3H), 3.88 (s, 3H), 6.91 (s, 2H), 6.92 (d, *J*=8.8 Hz, 1H), 7.49 (dd, *J*=8.8 and 2.0 Hz, 1H), 7.07 (d, *J*=2.0 Hz, 1H). ^{13}C NMR (100 MHz, $CDCl_3$) δ: 13.90, 56.11 (2C), 56.21, 60.94, 104.72 (2C), 111.83, 122.28, 122.65, 126.29, 127.23, 128.41, 134.23, 137.97, 143.76, 153.33 (2C), 155.03, 160.09. MS (ESI): $[M]^+$=389.4. Anal. ($C_{20}H_{20}ClNO_5$) C, H, N.

4-(3,4,5-Trimethoxyphenyl)-5-(4-ethoxyphenyl)-2-methyloxazole (4i). Following general procedure C, the residue was purified by flash chromatography on silica gel using light petroleum ether:EtOAc 6:4 as eluent, affording compound **4i** as a white solid. Yield: 65%, mp 95–97 ºC. ^{1}H-NMR ($CDCl_3$) δ: 1.43 (t, *J*=7.0 Hz, 3H), 2.64 (s, 3H), 3.79 (s, 6H), 3.83 (s, 3H), 4.05 (q, *J*=7.0 Hz, 2H), 6.89 (d, *J*=8.8 Hz, 2H), 6.92 (s, 2H), 7.53 (d, *J*=8.8 Hz, 2H). ^{13}C NMR (100 MHz, $CDCl_3$) δ: 14.03, 14.83, 56.14 (2C), 61.01, 63.62, 104.73 (2C), 114.57 (2C), 122.44, 128.01, 128.43 (2C), 133.61, 137.72, 145.35, 153.32 (2C), 159.25, 159.72. MS (ESI): $[M]^+$=369.7. Anal. ($C_{21}H_{23}NO_5$) C, H, N.

5-(3-Chloro-4-ethoxyphenyl)-4-(3,4,5-trimethoxyphenyl)-2-methyloxazole (4j). Following general procedure C, the residue was purified by flash chromatography on silica gel using light petroleum ether:EtOAc 6:4 as eluent, affording compound **4j** as a cream-colored solid. Yield: 63%, mp 124-126 ºC. ^{1}H-NMR ($CDCl_3$) δ: 1.49 (t, *J*=6.8 Hz, 3H), 2.60 (s, 3H), 3.80 (s, 6H), 3.84 (s, 3H), 4.14 (q, *J*=6.8 Hz, 2H), 6.90 (m, 3H), 7.44 (dd, *J*=8.4 and 2.4 Hz, 1H), 7.70 (d, *J*=2.4 Hz, 1H). ^{13}C NMR (100 MHz, $CDCl_3$) δ: 13.93, 14.70, 56.31 (2C), 61.05, 64.95, 104.91 (2C), 113.03, 121.56, 123.16, 126.50, 128.64, 130.04, 133.34,

138.84, 144.27, 153.51 (2C), 154.93, 160.66. MS (ESI): $[M]^+$=403.5. Anal. ($C_{21}H_{22}ClNO_5$) C, H, N.

5-(3,4,5-Trimethoxyphenyl)-2-methyl-4-(naphthalen-3-yl)oxazole (5a). Following general procedure C, the residue was purified by flash chromatography on silica gel using light petroleum ether:EtOAc 6:4 as eluent, affording compound **5a** as a white solid. Yield: 63%, mp 95-97 ºC. ^{1}H-NMR ($CDCl_3$) δ: 2.60 (s, 3H), 3.72 (s, 6H), 3.89 (s, 3H), 6.86 (s, 2H), 7.49 (m, 2H), 7.83 (m, 4H), 8.28 (s, 1H). ^{13}C NMR (100 MHz, $CDCl_3$) δ: 15.46, 56.38 (2C), 61.08, 104.16, 104.67, 124.18, 126.02, 126.48, 127.52, 127.79, 128.08, 128.34, 129.41, 133.13, 133.50, 134.54, 137.66, 138.51, 145.86, 153.45 (2C), 160.44. MS (ESI): $[M]^+$=375.6. Anal. ($C_{23}H_{21}NO_4$) C, H, N.

4-(4-Fluorophenyl)-5-(3,4,5-trimethoxyphenyl)-2-methyloxazole (5b). Following general procedure C, the residue was purified by flash chromatography on silica gel using light petroleum ether:EtOAc 1:1 as eluent, affording compound **5b** as a white solid. Yield: 63%, mp 132-133 ºC. ^{1}H-NMR ($CDCl_3$) δ: 2.66 (s, 3H), 3.72 (s, 6H), 3.88 (s, 3H), 6.76 (s, 2H), 7.05 (t, *J*=8.6 Hz, 2H), 7.65 (dd, *J*=8.8 and 8.6Hz, 2H). ^{13}C NMR (100 MHz, $CDCl_3$) δ: 14.21, 56.20 (2C), 61.05, 103.68 (2C), 115.47 (2C), 124.10, 128.46, 130.06 (2C), 133.76, 138.37, 145.22, 153.46 (2C), 160.19, 163.86. MS (ESI): $[M]^+$=343.7. Anal. ($C_{19}H_{18}FNO_4$) C, H, N.

4-(4-Chlorophenyl)-5-(3,4,5-trimethoxyphenyl)-2-methyloxazole (5c). Following general procedure C, the residue was purified by flash chromatography on silica gel using light petroleum ether:EtOAc 7:3 as eluent, affording compound **5c** as a white solid. Yield: 58%, mp 149-151 ºC. ^{1}H-NMR ($CDCl_3$) δ: 2.61 (s, 3H), 3.77 (s, 6H), 3.89 (s, 3H), 6.77 (s, 2H), 7.33 (d, *J*=8.6 Hz, 2H), 7.62 (d, *J*=8.8 Hz, 2H). ^{13}C NMR (100 MHz, $CDCl_3$) δ: 13.75, 56.29 (2C), 61.04, 104.00 (2C), 123.86, 128.78 (2C), 129.41 (2C), 130.59, 133.34, 134.07, 138.61, 145.67, 153.50 (2C), 160.35. MS (ESI): $[M]^+$=359.6. Anal. ($C_{19}H_{18}ClNO_4$) C, H, N.

5-(3,4,5-Trimethoxyphenyl)-2-methyl-4-*p*-tolyloxazole (5d). Following general procedure C, the residue was purified by flash chromatography on silica gel using light petroleum ether:EtOAc 6:4 as eluent, affording compound **5d** as a white solid. Yield: 55%, mp 128-129 ºC. ^{1}H-NMR ($CDCl_3$) δ: 2.37 (s, 3H), 2.62 (s, 3H), 3.76 (s, 6H), 3.88 (s, 3H), 6.81 (s, 2H), 7.17 (d, *J*=8.2 Hz, 2H), 7.56 (d, *J*=8.2 Hz, 2H). ^{13}C NMR (100 MHz, $CDCl_3$) δ: 14.08, 21.41, 56.16, 56.38, 61.05, 103.65 (2C), 104.68, 124.52, 127.98, 129.20, 129.44,

134.80, 137.67, 138.05, 138.16, 144.88, 153.37, 153.46, 159.95. MS (ESI): $[M]^+$=339.7. Anal. ($C_{20}H_{21}NO_4$) C, H, N.

5-(3,4,5-Trimethoxyphenyl)-4-(4-methoxyphenyl)-2-methyloxazole (5e). Following general procedure C, the residue was purified by flash chromatography on silica gel using light petroleum ether:EtOAc 7:3 as eluent, affording compound **5e** as a white solid. Yield: 62%, mp 108-110 ºC. ^{1}H-NMR ($CDCl_3$) δ: 2.64 (s, 3H), 3.77 (s, 6H), 3.78 (s, 3H), 3.83 (s, 3H), 6.80 (s, 2H), 6.90 (d, *J*=8.8 Hz, 2H), 7.61 (d, *J*=8.8 Hz, 2H). ^{13}C NMR (100 MHz, $CDCl_3$) δ: 14.18, 55.35, 56.16 (2C), 61.00, 103.69 (2C), 114.22 (2C), 122.84, 128.45, 129.63 (2C), 132.01, 139.21, 145.21, 153.49 (2C), 160.24, 161.11. MS (ESI): $[M]^+$=355.5. Anal. ($C_{20}H_{21}NO_5$) C, H, N.

4-(4-Ethoxyphenyl)-5-(3,4,5-trimethoxyphenyl)-2-methyloxazole (5f). Following general procedure C, the residue was purified by flash chromatography on silica gel using light petroleum ether:EtOAc 6:4 as eluent, affording compound **5f** as a white solid. Yield: 68%, mp 116-118 ºC. ^{1}H-NMR ($CDCl_3$) δ: 1.39 (t, *J*=6.8 Hz, 3H), 2.63 (s, 3H), 3.76 (s, 6H), 3.83 (s, 3H), 4.04 (q, *J*=6.8 Hz, 2H), 6.81 (s, 2H), 6.89 (d, *J*=8.8 Hz, 2H), 7.59 (d, *J*=8.8 Hz, 2H). ^{13}C NMR (100 MHz, $CDCl_3$) δ: 12.34, 15.00, 56.37 (2C), 61.19, 63.74, 103.74 (2C), 104.84, 114.72 (2C), 124.38, 129.69 (2C), 144.78, 147.23, 153.56 (2C), 160.13, 160.98, 171.03. MS (ESI): $[M]^+$=369.5. Anal. ($C_{21}H_{23}NO_5$) C, H, N.

Molecular modeling. All molecular modeling studies were performed on a MacPro dual 2.66 GHz Xeon running Ubuntu 14.04. The tubulin structure was downloaded from the PDB data bank (http://www.rcsb.org/; PDB code 1SA0).[38] Hydrogen atoms were added to the protein, using the Protonate 3D routine of the Molecular Operating Environment (MOE).[39] Ligand structures were built with MOE and minimized using the MMFF94x force field until a RMSD gradient of 0.05 kcal mol^{-1} $Å^{-1}$ was reached. The docking simulations were performed using PLANTS.[40]

Biological assays

Materials and Methods

Cell growth conditions and antiproliferative assay. Human T-cell leukemia (Jurkat) and human B-cell leukemia (SEM and RS4;11) cells were grown in RPMI-1640 medium (Gibco, Milano, Italy). Breast adenocarcinoma (MCF-7), human cervix carcinoma (HeLa), human lung adenocarcinoma (A549) and human colon adenocarcinoma (HT-29) cells were grown

in DMEM medium (Gibco, Milano, Italy), all supplemented with 115 units/mL penicillin G (Gibco, Milano, Italy), 115 μg/mL streptomycin (Invitrogen, Milano, Italy), and 10% fetal bovine serum (FBS; Invitrogen, Milano, Italy). Stock solutions (10 mM) of the different compounds were obtained by dissolving them in DMSO. Individual wells of a 96-well tissue culture microtiter plate were inoculated with 100 μL of complete medium containing 8×10^3 cells. The plates were incubated at 37 °C in a humidified 5% CO_2 incubator for 18 h prior to the experiments. After medium removal, 100 μL of fresh medium containing the test compound at different concentrations was added to each well in triplicate and incubated at 37 °C for 72 h. The percentage of DMSO in the medium never exceeded 0.25%. This was also the maximum DMSO concentration in all cell-based assays described below. Cell viability was assayed by the MTT test as previously described.[21] The IC_{50} was defined as the compound concentration required to inhibit cell proliferation by 50%, in comparison with cells treated with the maximum amount of DMSO (0.25%) and considered as 100% viability. Peripheral blood lymphocytes (PBL) from healthy donors were obtained by separation on Lymphoprep (Fresenius KABI Norge AS) gradient. After extensive washing, cells were resuspended (1.0×10^6 cells/mL) in RPMI-1640 with 10% FBS and incubated overnight. For cytotoxicity evaluations in proliferating PBL cultures, non-adherent cells were resuspended at 5×10^5 cells/mL in growth medium, containing 2.5 μg/mL PHA (Irvine Scientific). Different concentrations of the test compounds were added, and viability was determined 72 h later by the MTT test. For cytotoxicity evaluations in resting PBL cultures, non-adherent cells were resuspended (5×10^5 cells/mL) and treated for 72 h with the test compounds, as described above.

Effects on tubulin polymerization and on colchicine binding to tubulin. To evaluate the effect of the compounds on tubulin assembly *in vitro*,[41] varying concentrations of compounds were preincubated with 10 μM bovine brain tubulin in 0.8 M monosodium glutamate (pH adjusted to 6.6 with HCl in a 2.0 M stock solution) at 30 ˚C and then cooled to 0 ˚C. After addition of 0.4 mM GTP, the mixtures were transferred to 0 °C cuvettes in a recording spectrophotometer and warmed to 30 °C. Tubulin assembly was followed turbidimetrically at 350 nm. The IC_{50} was defined as the compound concentration that inhibited the extent of assembly by 50% after a 20 min incubation. The capacity of the test compounds to inhibit colchicine binding to tubulin was measured as described,[42] except that the reaction mixtures contained 1 μM tubulin, 5 μM [^{3}H]colchicine and 1 or 5 μM test compound.

Flow cytometric analysis of cell cycle distribution. 5×10^5 HeLa or Jurkat cells were treated with different concentrations of the test compounds for 24 h. After the incubation period, the cells were collected, centrifuged, and fixed with ice-cold ethanol (70%). The cells were then treated with lysis buffer containing RNase A and 0.1% Triton X-100 and then stained with PI. Samples were analyzed on a Cytomic FC500 flow cytometer (Beckman Coulter). DNA histograms were analyzed using MultiCycle for Windows (Phoenix Flow Systems).

Apoptosis assay. Cell death was determined by flow cytometry of cells double stained with annexin V/FITC and PI. The Coulter Cytomics FC500 (Beckman Coulter) was used to measure the surface exposure of PS on apoptotic cells according to the manufacturer's instructions (Annexin-V Fluos, Roche Diagnostics).

Western blot analysis. HeLa cells were incubated in the presence of **4i** and, after different times, were collected, centrifuged, and washed two times with ice cold phosphate buffered saline (PBS). The pellet was then resuspended in lysis buffer. After the cells were lysed on ice for 30 min, lysates were centrifuged at 15000 x g at 4 °C for 10 min. The protein concentration in the supernatant was determined using the BCA Protein Assay (Pierce, Italy). Equal amounts of protein (10 μg) were resolved using sodium dodecyl sulfate-polyacrylamide gel electrophoresis (SDS-PAGE) (Criterion Precast, BioRad, Italy) and transferred to a PVDF Hybond-P membrane (GE Healthcare). Membranes were blocked with a bovine serum albumin solution (5% in Tween PBS 1X), the membranes being gently rotated overnight at 4 °C. Membranes were then incubated with primary antibodies against caspase-9, PARP, cdc25c, p-H2AX^{Ser139}, cyclin B, p-cdc2^{Tyr15} (all from Cell Signaling) or β-actin (Sigma-Aldrich) for 2 h at room temperature. Membranes were next incubated with peroxidase labeled secondary antibodies for 60 min. All membranes were visualized using ECL Select (GE Healthcare), and images were acquired using an Uvitec-Alliance imaging system (Uvitec, Cambridge, UK). To ensure equal protein loading, each membrane was stripped and reprobed with anti-β-actin antibody.

Antivascular activity. HUVECs were prepared from human umbilical cord veins, as previously described[43] The adherent cells were maintained in M200 medium supplemented with LSGS (Low Serum Growth Supplement), containing FBS, hydrocortisone, hEGF, bFGF, heparin, gentamycin/amphotericin (Life Technologies, Monza, Italy). Once

confluent, the cells were detached by a trypsin–EDTA solution and used in experiments from the first to sixth passages.

The motility assay for HUVECs was based on "scratch" wounding of a confluent monolayer[35] Briefly, HUVECs ($1x10^5$) were seeded onto 6-well plates coated with 0.1% collagen type I (BD Biosciences, Italy) in complete medium until a confluent monolayer was formed. The cells were wounded using a pipette tip, and wells were washed with PBS to remove undetached cells. Then, the cells were treated with the test compounds, and, at different times from the scratch, the cells were photographed under a light microscope. At all indicated time points, the wound width was measured in four areas and compared with the initial width.

Matrigel matrix (Basement Membrane Matrix, BD Biosciences, Italy) was kept at 4 °C for 3 h, when 230 µL of Matrigel solution was added to each well of a 24-well plate. After gelling at 37°C for 30 min, gels were overlaid with 500 µL of medium containing 6×10^4 HUVECs. The cells were incubated over Matrigel for 6 h to allow capillary tubes to form. Different concentrations of test compound were added in the cultures and incubated for different times, and the disappearance of existing vasculature was monitored and photographed (five fields for each well: the four quadrants and the center) at a 10x magnification. Phase contrast images were recorded using a digital camera and saved as TIFF files. Image analysis was carried out using ImageJ image analysis software, and the following dimensional parameters (percent area covered by HUVECs and total length of HUVECs network per field) and topological parameters (number of meshes and branching points per field) were determined.[43] Values were expressed as percent change from control cultures grown with complete medium.

***In vivo* animal studies.** Animal experiments were approved by our local animal ethics committee (OPBA, Organismo Preposto al Benessere degli Animali, Università degli Studi di Brescia, Italy) and were executed in accordance with national guidelines and regulations. Procedures involving animals and their care conformed with institutional guidelines that comply with national and international laws and policies (EEC Council Directive 86/609, OJ L 358, 12 December 1987) and with "ARRIVE" guidelines (Animals in Research Reporting In Vivo Experiments). Six-week-old C57BL/6 mice (Charles River, Calco) were injected subcutaneously into the dorsolateral flank with $2.5x10^5$ BL6-B16 murine melanoma cells in 200 µL of PBS. When tumours were palpable, animals were treated intraperitoneally every other day with different doses of test compounds dissolved in 50 µL of DMSO. Tumours were measured in two dimensions, and tumour volume was calculated according

to the formula $V=(D \times d^2)/2$, where D and d are the major and minor perpendicular tumour diameters, respectively.

Statistical analysis. Unless indicated differently, the results are presented as mean ± SEM. The differences between different treatments were analyzed, using the two-sided Student's t test. P values lower than 0.05 were considered significant.

2.6 References

1. Kueh, H. Y. & Mitchison, T. J. Structural plasticity in actin and tubulin polymer dynamics. *Science* **325**, 960-963 (2009).
2. Liu, Y. M.; Chen, H. L.; Lee, H. Y. & Liou, J. P. Tubulin inhibitors: a patent review. *Expert Opin. Ther. Pat.* **24**, 69-88 (2014).
3. Honore, S.; Pasquier, E. & Braguer, D. Understanding microtubule dynamics for improved cancer therapy. *Cell. Mol. Life Sci.* **62**, 3039-3056 (2005).
4. Nitika, V. & Kapil, K. Microtubule targeting agents: a benchmark in cancer therapy. *Curr. Drug Ther.* **8**, 189-196 (2014).
5. Pettit, G.R. *et al.* Isolation and structure of the strong cell growth and tubulin inhibitor combretastatin A-4. *Experientia* **45**, 209-211 (1989).
6. Lin, C. M.; Ho, H. H.; Pettit, G. R.; Hamel, E. Antimitotic natural products combretastatin A-4 and combretastatin A-2: studies on the mechanism of their inhibition of the binding of colchicine to tubulin. *Biochemistry* **1989**, *28*, 6984-6991.
7. Siemann, D. W.; Chaplin, D. J. & Walike, P. A. A review and update of the current status of the vasculature-disabling agent combretastatin-A4 phosphate (CA4P). *Expert Opin. Investig. Drugs* **18**, 189-197 (2009).
8. Mooney, C. J. *et al.* A phase II trial of fosbretabulin in advanced anaplastic thyroid carcinoma and correlation of baseline serumsoluble intracellular adhesion molecule-1 with outcome. *Thyroid* **19**, 233-240 (2009).
9. Porcù, E.; Bortolozzi, R.; Basso, G. & Viola, G. Recent advances on vascular disrupting agents. *Future Med. Chem.* **6**, 1485-1498 (2014).10. Bibby, M. C. Combretastatin anticancer drugs. *Drugs Future* **27**, 475-480 (2002).
11. Hatanaka, T. *et al.* Novel B-ring modified combretastatin analogues: synthesis and antineoplastic activity. *Bioorg. Med. Chem. Lett.* **8**, 3371-3374 (1998).

12. Rajak, H. *et al.* Design of combretastatin A-4 analogs as tubulin targeted vascular disrupting agent with special emphasis on their *cis*-restricted isomers. *Curr. Pharm. Des.* **19**, 1923-1955 (2013).
13. Wang, L. *et al.* Potent, orally active heterocycle-based combretastatin A-4 analogues: synthesis, structure-activity relationship, pharmaokinetics, and in vivo antitumor activity evaluation. *J. Med. Chem.* **45**, 1697-1711 (2002).
14. Schobert, R.; Biersack, B.; Dietrich, A.; Effenberger, K.; Knauer, S. & Mueller, T. 4-(3-Halo/amino-4,5-dimethoxyphenyl)-5-aryloxazoles and *N*-methylimidazoles that are cytotoxic against combretastatin A resistant tumor cells and vascular disrupting in a cisplatin resistant germ cell tumor model. *J. Med. Chem.* 53, 6595-6002 (2010).
15. Wang, F. *et al.* Synthesis and biological evaluation of diarylthiazole derivatives as antimitotic and antivascular agents with potent antitumor activity. *Bioorg. Med. Chem.* **23**, 3337-3350 (2015).
16. Tron, G. C., Pagliai, F., Del Grosso, E., Genazzani, A. A. & Sorba, G. Synthesis and cytotoxic evaluation of combretafurazans. *J. Med. Chem.* **48**, 3260-3258 (2005).
17. Liu, T. *et al.* Synthesis and biological evaluation of 3,4-biaryl-5-aminoisoxazole derivatives. *Bioorg. Med. Chem.* **17**, 6279-6285 (2009).
18. Wu, M. *et al.* Synthesis and activity of combretastatin A-4 analogues: 1,2,3-thiadiazoles as potent antitumor agents. *Bioorg. Med. Chem. Lett.* **17**, 869-873 (2007).
19. Romagnoli, R *et al.* Synthesis and antitumor activity of 1,5-disubstituted 1,2,4-triazoles as cis-restricted combretastatin analogs, *J. Med. Chem.* **53**, 4248-4258 (2010).
20. Romagnoli, R. *et al.* Synthesis and evaluation of 1,5-disubstituted tetrazoles as rigid analogues of combretastatin A-4 with potent antiproliferative and antitumor activity. *J. Med. Chem*. **55**, 475-488 (2012).
21. Romagnoli, R. *et al.* Synthesis and biological evaluation of 2-substituted-4-(3',4',5'-trimethoxyphenyl)-5-aryl thiazoles as anticancer agents. *Bioorg. Med. Chem.* **20**, 7083-7094 (2012).
22. Lima, L. M. & Barreiro, E. J. Bioisosterism: a useful strategy for molecular modification and drug design. *Curr. Med. Chem.* **12**, 23-49 (2005).
23. Romagnoli, R. *et al.* Convergent synthesis and biological evaluation of 2-amino-4-(3',4',5'-trimethoxyphenyl)-5-arylthiazoles as microtubule targeting agents. *J. Med. Chem.* **54**, 5144-5153 (2011).

24. Goto, H. *et. al.* Identification of a novel phosphorylation site on histone H3 coupled with mitotic chromosome condensation. *J. Biol. Chem.* **274**, 25543-25549 (1999).

25. Weaver, B. A. A. & Cleveland, D. W. Decoding the links between mitosis, cancer, and chemotherapy: the mitotic checkpoint, adaptation, and cell death. *Cancer Cell* **8**, 7-12 (2005).

26. Clarke, P. R. & Allan, L. A. Cell-cycle control in the face of damage- a matter of life or death. *Trends Cell Biol.* **19**, 89-98 (2009).

27. Ganem, N. J. & Pellman, D. Linking abnormal mitosis to the acquisition of DNA damage. *J Cell Biol.* **199**, 871-881 (2012)

28. Orth, J. D.; Loewer, A.; Lahav, G. & Mitchison, T. J. Prolonged mitotic arrest triggers partial activation of apoptosis, resulting in DNA damage and p53 induction. *Mol Biol Cell*. **23**, 567-576 (2012).

29. Fernandez-Capetillo, O., Lee, A., Nussenzweig, M. & Nussenzweig, A. H2AX: the histone guardian of the genome. *DNA Repair* **3**, 959-967 (2004).

30. Zamzami, N. *et al.* Sequential reduction of mitochondrial transmembrane potential and generation of reactive oxygen species in early programmed cell death. *J. Exp. Med*. **182**, 367-377 (1995).

31. Wu, C. C. & Bratton, S. B. Regulation of the intrinsic apoptosis pathway by reactive oxygen species. *Antioxid. Redox Signal*. **19**, 546-558 (2013).

32. Soldani, C. & Scovassi, A. Poly(ADP-ribose) polymerase cleavage during apoptosis: an update. *Apoptosis* **74**, 321-328 (2002).

33. Wertz, I.E. *et al.* Sensitivity to antitubulin chemotherapeutics is regulated by MCL1 and FBW7. *Nature* **471**, 110-114 (2011).

34. Obexer, P. & Ausserlechner, M. J. X-linked inhibitor of apoptosis protein-a critical death resistance regulator and therapeutic target for personalized cancer therapy. *Front. Oncol*. **4**, 197 (2014).

35. Liang, C. C.; Park A. Y. & Guan J. L. In vitro scratch assay: a convenient and inexpensive method for analysis of cell migration in vitro. *Nat. Protoc.* **2**, 329-333 (2007).

36. Staton, C. A., Reed, M. W. & Brown, N. J. A critical analysis of current in vitro and in vivo angiogenesis assays. *Int. J. Exp. Path.* **90**, 195-221 (2009).

37. Ronca, R. *et al.* Long Pentraxin-3 inhibits epithelial-mesenchymal transition in melanoma cells. *Mol. Cancer Ther.* **12**, 2760-2771 (2013).

38. Ravelli, R. B. G. *et al*. Insight into tubulin regulation from a complex with colchicine and a stathmin-like domain. *Nature*. **428**, 198-202 (2004).

39. Molecular Operating Enviroment (MOE 2015.10); Chemical Computing Group, Inc; Montreal, Quebec, Canada, http://www.chemcomp.com. (2015)
40. Korb, O., Stützle, T. & Exner, T. E. PLANTS: Application of ant colony optimization to structure-based drug design. In Ant Colony Optimization and Swarm Intelligence, 5th International Workshop, ANTS (2006).
41. Hamel, E. Evaluation of antimitotic agents by quantitative comparisons of their effects on the polymerization of purified tubulin. *Cell Biochem. Biophys.* **38**, 1-21 (2003).
42. Verdier-Pinard, P. *et al.* Structure-activity analysis of the interaction of curacin A, the potent colchicine site antimitotic agent, with tubulin and effects of analogs on the growth of MCF-7 breast cancer cells. *Mol. Pharmacol.* **53**, 62-67 (1998).
43. Porcù, E. *et al.* TR-644 a novel potent tubulin binding agent induces impairment of endothelial cells function and inhibits angiogenesis *Angiogenesis* **16**, 647-662 (2013).

3. 2-Alkoxycarbonyl-3-arylamino-5-substituted thiophenes as a novel class of anti-microtubule agents: design, synthesis, cell growth and tubulin polymerization inhibition

3.1 Introduction

There has been in recent years an intense effort directed at the discovery and development of novel small molecules, many of which are natural products, able to interfere with tubulin polymerization because of their anti-cancer potential.[1] Microtubules represent a dynamic cellular compartment in both neoplastic and normal cells. The microtubule system of eukaryotic cells plays important roles in regulating cell architecture and has an essential role in cell division, since microtubules are a key component of the mitotic spindle.[2] This dynamicity is characterized by the continuous turnover of αβ-tubulin heterodimers in the polymeric microtubules. Because of their key roles in cell structure and cell division, they are involved in a variety of fundamental cellular functions, such as regulation of motility, cell signaling, formation and maintenance of cell shape, and bidirectional transport of material within the cell.[3-5] The disruption of microtubule dynamics increases the number of cells in metaphase arrest and mitotic catastrophe, and this interference with cell cycle progression has proven to be useful for designing anticancer agents, such as taxanes (paclitaxel, carbazitaxel and docetaxel) and vinca alkaloids (vinblastine, vinorelbine and vincristine), all of which are used clinically.[6-8]

One of the most important microtubule depolymerizing agents is combretastatin A-4 (CA-4, **1;** Chart 1). CA-4, isolated from the bark of the South African tree *Combretum caffrum*,[9] affects microtubule dynamics by binding to the β-subunit of tubulin at the same site as colchicine and thus strongly inhibits tubulin polymerization.[10] This compound has been recognized to act as both a cytotoxic and a vascular disrupting agent (VDA), inducing the collapse of tumour vasculature via rapid microtubule depolymerisation.[11-12] The phosphate prodrug of CA-4, named CA-4P, with improved solubility with respect to CA-4, is in clinical trials as a VDA.[13]

Among the synthetic inhibitors of tubulin polymerization, we previously described the synthesis and biological characterization of two series of compounds based on the 2-alkoxycarbonyl-3-(3',4',5'-trimethoxyanilino)benzo[*b*]thiophene and thieno[2,3-*b*]pyridine molecular skeletons (compounds with general structure **2** and **3**, respectively) that showed strong antiproliferative activity against a panel of cell lines and act as inhibitors of microtubule polymerization by interfering with the colchicine site of tubulin.[14a] To investigate the possible binding mode for this series of compounds, we performed a series of molecular docking simulations in the colchicine site. The results obtained showed that the trimethoxyphenyl unit of these compounds is placed in proximity of βCys241, and it is consistent with that previously reported for different tubulin polymerization inhibitors.[14b] Furthermore, the formation of an intramolecular hydrogen bonding interaction between the anilino and the carbonyl groups in these series of molecules allows the formation of a hydrogen bond between the ester itself and βAla250. This study indicated that important structural requirements that playing a crucial role in enhancing anti-microtubule activity are the presence of an alkoxycarbonyl moiety and a 3',4',5'-trimethoxyanilino function at the 2- and 3-position, respectively, of the thiophene ring fused with benzene or pyridine.

Based on these observations, in this article a new series of 2-alkoxycarbonyl-3-(3',4',5'-trimethoxyanilino)thiophene derivatives with general formula **4** was designed to explore the role of the benzene and pyridine portion of the benzo[*b*]thiophene and thieno[2,3-*b*]pyridine nucleus, respectively, in binding in the colchicine site of tubulin. We examined the replacement of the benzo[*b*]thiophene and thieno[2,3-*b*] pyridine bicyclic systems by a thiophene ring substituted at its 5-position with an aryl or heteroaryl moiety, whereas the 2-methoxycarbonyl group and the 3-(3,4,5-trimethoxyanilino) function were kept unmodified. To evaluate the influence of the new structural modifications on binding in the colchicine site of tubulin, preliminary docking studies were performed, following a previously reported method.[15] The new derivatives occupy the active site in a similar manner as the co-crystallized *N*-deacetyl-*N*-(2-mercaptoacetyl)-colchicine (DAMA-colchicine) (Figure 1A: DAMA-colchicine and 2-methoxycarbonyl-3-(3',4',5'-trimethoxyanilino)-5-phenylthiophene derivative **4a**), and their binding mode is consistent with that reported previously for the thieno[2,3-*b*]pyridine series (Figure 1B: **4a** and thieno[2,3-*b*]pyridine **3a**). The trimethoxyphenyl ring is in proximity to Cys241, while the 5-phenyl ring sits deep in the small hydrophobic pocket and potentially interacts with hydrophobic amino acids Met259, Thr314, Val181 and others. These interactions are similar to those modeled with the heterocycle of the thieno[2,3-*b*]pyridine series (Figure 2: compound **4a** alone). Small substitutions on the 5-phenyl ring could be tolerated and did not affect the binding mode in

a negative manner. As found previously for the benzo[*b*]thiophene and thieno[2,3-*b*] pyridine series, a molecular docking study revealed that the *ortho*-relationship between the alkoxycarbonyl group and the 3,4,5-trimethoxyanilino moiety plays an important role in activity. This allows the formation of an intramolecular hydrogen bond between the hydrogen of the anilino group and the carbonyl oxygen of the alkoxycarbonyl group, resulting in formation of a hydrogen bond between the ester itself and Ala250, further stabilizing these new compounds in the colchicine site. Encouraged by the activity obtained with compound **4a**, we assessed the effects on biological activity of both the nature and position of electron-withdrawing (F, Cl, CF_3 and NO_2) and electron-releasing (CH_3, OCH_3 and OC_2H_5) substituents on the phenyl at the 5-position of the 2-alkoxycarbonyl-3-(3',4',5'-trimethoxyanilino)thiophene system as well as replacement of the phenyl with the bioisosteric thien-2'-yl moiety.

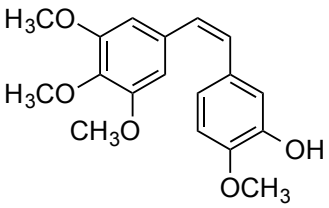

1

Combretastatin A-4 (CA-4)

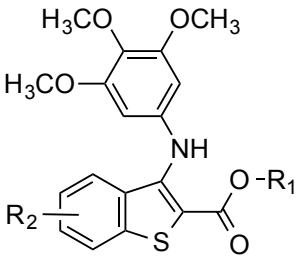

2

R_1=CH_3 or C_2H_5
R_2=H, CH_3 or OCH_3

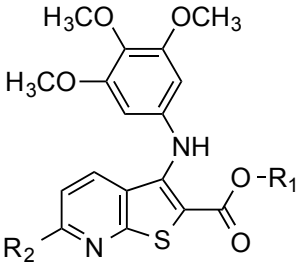

3

3a, R_1=R_2=CH_3

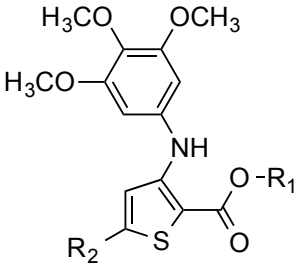

4

4a, R_1=CH_3, R_2=C_6H_5
4b, R_1=C_2H_5, R_2=C_6H_5
4c, R_1=CH_3, R_2=thien-2'-yl
4d, R_1=CH_3, R_2=4'-F-C_6H_4
4e, R_1=C_2H_5, R_2=4'-F-C_6H_4
4f, R_1=CH_3, R_2=4'-Cl-C_6H_4
4g, R_1=C_2H_5, R_2=4'-Cl-C_6H_4
4h, R_1=CH_3, R_2=3',4'-2Cl-C_6H_3
4i, R_1=CH_3, R_2=4'-CH_3-C_6H_4
4j, R_1=C_2H_5, R_2=4'-CH_3-C_6H_4
4k,R_1=CH_3, R_2=4'-OCH_3-C_6H_4
4l, R_1=C_2H_5, R_2=4'-OCH_3-C_6H_4
4m, R_1=CH_3, R_2=4'-OC_2H_5-C_6H_4
4n, R_1=CH_3, R_2=3'-OCH_3-C_6H_4
4o, R_1=CH_3, R_2=3',4'-2OCH_3-C_6H_3
4p, R_1=CH_3, R_2=3',4',5'-3OCH_3-C_6H_2
4q, R_1=CH_3, R_2=4'-CF_3-C_6H_4
4r, R_1=CH_3, R_2=4'-NO_2-C_6H_4

Chart 1. Structures of CA-4 (**1**), benzo[*b*]thiophene and thieno[2,3-*b*]pyridine derivatives **2** and **3** previously published, and novel 2-alkoxycarbonyl-3-(3',4',5'-trimethoxyanilino)-5-aryl/heteroaryl thiophenes **4a-r**.

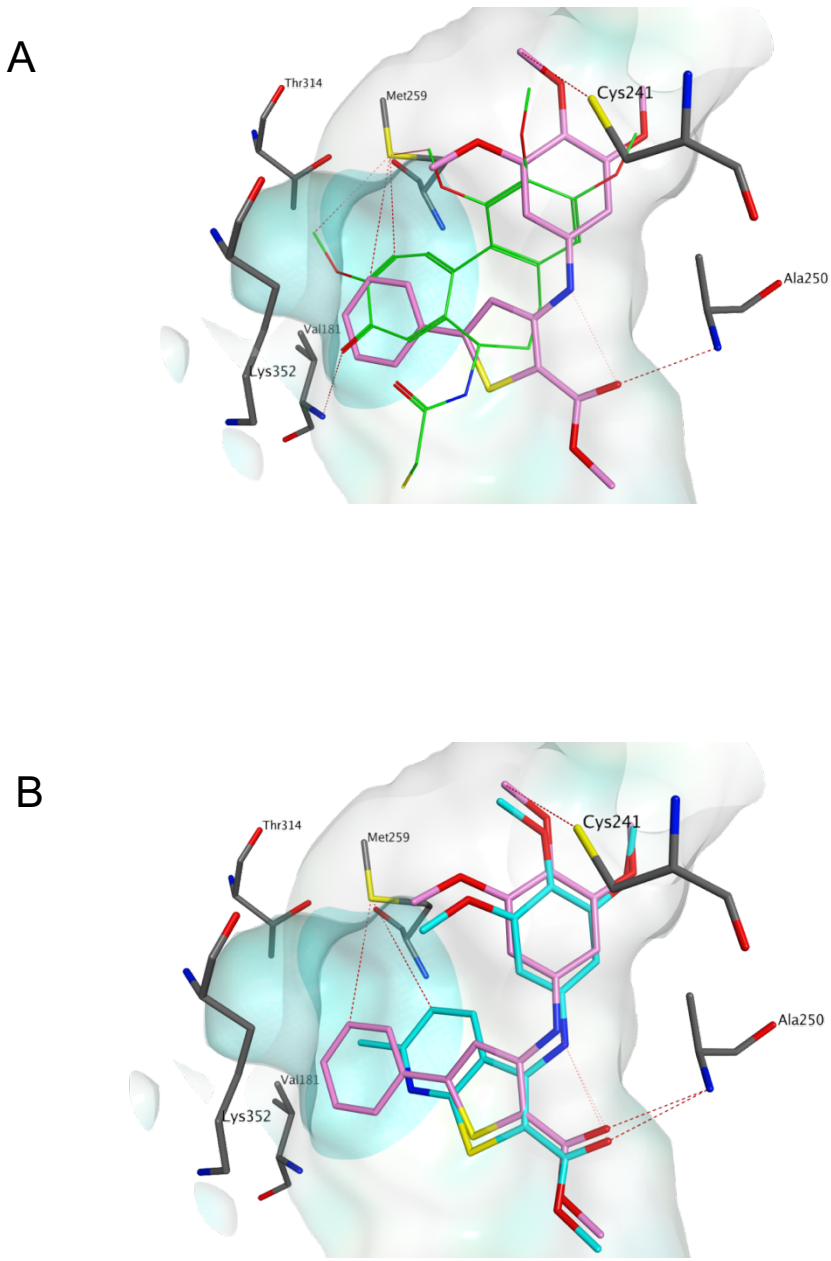

Figure 1. Proposed binding mode for compound **4a** in comparison with DAMA-colchicine (A) and derivative **3a** (B) in the colchicine site. Co-crystallized DAMA-colchicine is shown in green, the carbon atoms of compound **4a** in magenta, and the carbon atoms of compound **3a** in turquoise. The hydrophobic sub-pocket is highlighted with a turquoise-colored surface.

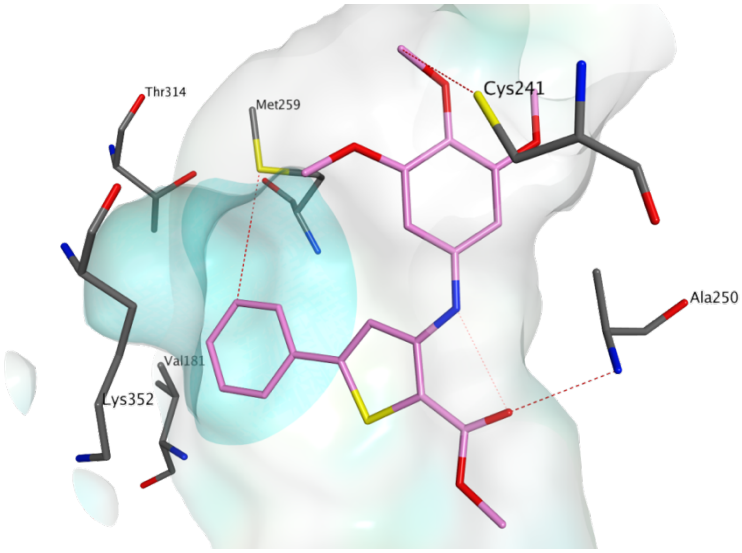

Figure 2. Proposed binding mode for compound **4a** alone in the colchicine site. The hydrophobic sub-pocket is highlighted with a turquoise-colored surface.

3.2 Chemistry

2-Alkoxycarbonyl-3-(3',4',5'-trimethoxyanilino)-5-aryl/heteroaryl thiophene derivatives **4a-r** were synthesized by a four-step procedure summarized in Scheme 1. β-Chloroaryl cinnamonitriles **6a-m** were obtained by a modified Vilsmeier reaction of commercially available acetophenones **5a-m** with phosphorus(V)oxychloride ($POCl_3$) in dimethylformamide, followed by treatment with hydroxylamine hydrochloride ($NH_2OH{\cdot}HCl$).[16] The subsequent condensation of compounds **6a-m** with methyl or ethyl thioglycolate using sodium methoxide (MeONa) as base in a mixture of methanol/DMF furnished in mild conditions the corresponding 2-alkoxycarbonyl-3-amino-5-aryl/heteroaryl thiophene derivatives **7a-r** in good yields through the nucleophilic displacement of chlorine, followed by base-induced ring closure in a single step. Subsequent deaminative bromination using modified Sandmeyer conditions of 3-aminothiophenes **7a-r** using *tert*-butyl nitrite (*t*-BuONO) in acetonitrile in the presence of copper(II)bromide ($CuBr_2$) gave the target bromothiophene **8a-r** in excellent yield. Finally, the novel derivatives **4a-r** were obtained using Buchwald-Hartwig conditions, by coupling of bromide **8a-r** with 3,4,5-trimethoxyaniline in a palladium (II)acetate [$Pd(OAc)_2$], 2,2-bis(diphenylphosphino)1,1'-binaphthyl (BINAP) catalytic system in the presence of cesium carbonate (Cs_2CO_3) as base in toluene at 100 °C for 18 h.

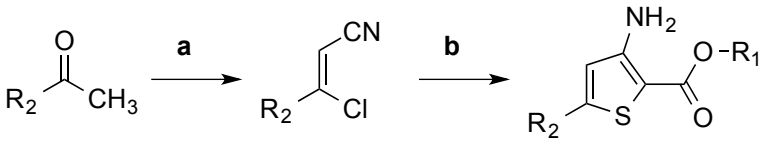

5a-m **6a-m** **7a-r**

5-6a, $R_2=C_6H_5$
5-6b, R_2=thien-2'-yl
5-6c, R_2=4'-F-C_6H_4
5-6d, R_2=4'-Cl-C_6H_4
5-6e, R_2=3',4'--2Cl-C_6H_3
5-6f, R_2=4'-CH_3-C_6H_4
5-6g, R_2=4'-OCH_3-C_6H_4
5-6h, R_2=4'-OC_2H_5-C_6H_4
5-6i, R_2=3'-OCH_3-C_6H_4
5-6j, R_2=3',4'-2(OCH_3)-C_6H_3
5-6k, R_2=2',3',4'--3OCH_3-C_6H_2
5-6l, R_2=4'-CF_3-C_6H_4
5-6m, R_2=4'-NO_2-C_6H_4

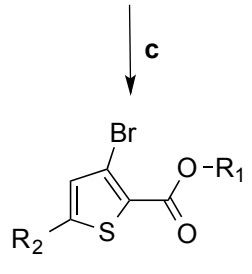

8a-r

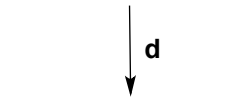

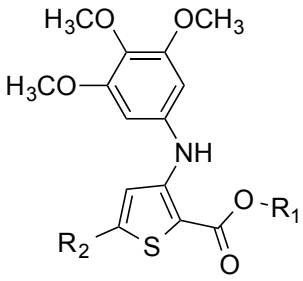

4a-r

4a, **7-8a**, $R_1=CH_3$, $R_2=C_6H_5$
4b, **7-8b**, $R_1=C_2H_5$, $R_2=C_6H_5$
4c, **7-8c**, $R_1=CH_3$, R_2=thien-2'-yl
4d, **7-8d**, $R_1=CH_3$, R_2=4'-F-C_6H_4
4e, **7-8e**, $R_1=C_2H_5$, R_2=4'-F-C_6H_4
4f, **7-8f**, $R_1=CH_3$, R_2=4'-Cl-C_6H_4
4g, **7-8g**, $R_1=C_2H_5$, R_2=4'-Cl-C_6H_4
4h, **7-8h**, $R_1=CH_3$, R_2=3',4'-2Cl-C_6H_3
4i, **7-8i**, $R_1=CH_3$, R_2=4'-CH_3-C_6H_4
4j, **7-8j**, $R_1=C_2H_5$, R_2=4'-CH_3-C_6H_4
4k, **7-8k**, $R_1=CH_3$, R_2=4'-OCH_3-C_6H_4
4l, **7-8l**, $R_1=C_2H_5$, R_2=4'-OCH_3-C_6H_4
4m, **7-8m**, $R_1=CH_3$, R_2=4'-OC_2H_5-C_6H_4
4n, **7-8n**, $R_1=CH_3$, R_2=3'-OCH_3-C_6H_4
4o, **7-8o**, $R_1=CH_3$, R_2=3',4'-2OCH_3-C_6H_3
4p, **7-8p**, $R_1=CH_3$, R_2=3',4',5'-3OCH_3-C_6H_2
4q, **7-8q**, $R_1=CH_3$, R_2=4'-CF_3-C_6H_4
4r, **7-8r**, $R_1=CH_3$, R_2=4'-NO_2-C_6H_4

Scheme 1. **Reagents. a**: $POCl_3$, DMF then $NH_2OH.HCl$; **b**: $HSCH_2CO_2CH_3$ or $HSCH_2CO_2C_2H_5$, MeONa, MeOH/DMF, 60 °C, 4 h; **c**: *t*-BuONO, $CuBr_2$, CH_3CN, 0 °C then room temperature for 2 h; **d**: 3,4,5-trimethoxyaniline, $Pd(OAc)_2$, BINAP, Cs_2CO_3, PhMe, 100 °C, 18 h.

3.3 Biological Results and Discussion

3.3.1 *In vitro* antiproliferative activities

Table 1 summarizes the antiproliferative effects of the 2-alkoxycarbonyl-3-anilino-5-substituted thiophene derivatives **4a-r** against the growth of murine leukemia (L1210), murine mammary carcinoma (FM3A/0), human T-lymphoblastoid leukemia (CEM) and human cervix carcinoma (HeLa) cells as compared with the reference compound CA-4. Comparing compounds which shared a common aryl moiety at the 5-position of the 2-alkoxycarbonyl-3-(3',4',5'-trimethoxyanilino)thiophene scaffold, the 2-methoxycarbonyl derivatives were more potent than the 2-ethoxycarbonyl counterparts (**4a**, **4d**, **4f**, **4i**, **4k** *versus* **4b**, **4e**, **4g**, **4j**, **4l**, respectively). Ignoring compound **4p**, all synthesized compounds possessed significant cell growth inhibitory activity, which was lower than 1 μM for compounds **4a**, **4c-d**, **4i-k**, **4o** and **4r** in all cell lines.

Hydrophobic moieties such as phenyl and thien-2'-yl were well tolerated at the 5-position of the 2-alkoxycarbonyl-3-(3',4',5'-trimethoxyanilino)thiophene scaffold, and variation of the phenyl substituents had variable effects on potency. Replacement of the phenyl ring of compound **4a** by the bioisosteric thien-2'-yl ring, to yield derivative **4c**, increased antiproliferative activity 2-4-fold against L1210 and HeLa cells, while the two compounds showed comparable potency against FM3A and CEM cells. Of all the tested compounds, the thien-2'-yl derivative **4c** possessed the highest overall cytostatic potency and inhibited the growth of the four cancer cell lines with IC_{50} values ranging between 0.13 and 0.16 μM, being 10- to 100-fold less active than the reference compound CA-4. Compound **4i** was virtually as active as **4c**.

SAR was elucidated by substitution with electron-releasing and electron-withdrawing groups on the phenyl moiety at the 5-position of the 2-alkoxycarbonyl-3-(3',4',5'-trimethoxyanilino)thiophene system. In general, a single modification at the *para*-position of the phenyl ring was well tolerated, and *para*-substituted phenyl derivatives showed variable potencies, suggesting an opportunity for further synthetic exploration. In comparing the effect of electron-releasing (ERG's) or electron-withdrawing groups (EWG's) at the *para*-position of the phenyl ring, in all cell lines compounds **4i** and **4k** with electron-donating methyl or methoxy groups, respectively, were generally more cytostatic than those with the electron-withdrawing fluoro or chloro moieties (derivatives **4d** and **4f**, respectively). The same effect was observed for the 2-ethoxycarbonyl derivatives (**4j** and **4l** *vs.* **4e** and **4g**).

Substituents at the *para*-position of the 5-phenyl ring showed antiproliferative activity in the following order: Me>OMe>F>Cl=NO_2>CF_3>>OEt.

Potency was reduced from 4- to 7-fold after the weak ERG *p*-methyl (**4i**) was replaced with the EWG trifluoromethyl in compound **4q**. Turning to the effect of ERG's on the phenyl moiety, with the exception of HeLa cells, we found that *para*-tolyl and *para*-methoxyphenyl groups (compounds **4i** and **4k**, respectively) caused only minor changes in antiproliferative activity relative to the unsubstituted phenyl analogue **4a**.

Relative to the activity of the unsubstituted phenyl analogue **4a**, the introduction of the EWG fluorine at the *para*-position of the phenyl ring (compound **4d**) caused a 2-4-fold reduction of antiproliferative activity in three of the four cancer cell lines. Increasing the size of the halogen from fluorine to chlorine (compounds **4d** and **4f**, respectively) reduced the anti-proliferative activity against L1210 and CEM cells, while the two compounds were equipotent against the FM3A and HeLa cell lines. While a single chlorine atom at the *para*-position of the phenyl group was tolerated for cytostatic activity (**4f**), double substitution by the introduction of a second chlorine atom to furnish the *meta*, *para*-dichlorophenyl derivative **4h** caused a 4-5-fold reduction of potency relative to **4f** in all tumour cell lines. Replacement of the chlorine atom with even stronger EWG's (trifluoromethyl or nitro; derivatives **4q** and **4r**, respectively) had generally little further effect on activity against the four cell lines.

Replacement of the fluorine atom of **4d** with the weak ERG methyl, resulting in *para*-tolyl derivative **4i**, increased antiproliferative activity by 3-4-fold against all tumour cell lines, with a potency similar to that of the thien-2'-yl analogue **4c**.

The number and location of methoxy substituents on the phenyl ring played a profound role in the antiproliferative activity. A comparison between the antiproliferative activities of compounds **4k** and **4n-p**, illustrated the antiproliferative SAR of the number of methoxy groups substituted on the phenyl ring (1>2>>3). The introduction of a single methoxy group at the *para*-position (compound **4k**) caused only minor changes in antiproliferative activity relative to the unsubstituted derivative **4a**. Moving the methoxy group from the *para*- to the *meta*-position, to furnish **4n**, reduced antiproliferative activity 3-4-fold on three of the cancer cell lines. Reduced activity (2-fold) on three cancer cell lines relative to **4k** occurred with the insertion of a second methoxy group, to furnish the *meta*, *para*-dimethoxyphenyl analogue **4o**, while activity was maintained against HeLa cells. This latter compound has antiproliferative activity similar to that of the *meta*-methoxy analogue **4n** against HeLa cells and increased potency against the three other cell lines. These results suggest that the optimal

position for mono-methoxy substitution is the *para*-position, as in compound **4k**. Adding a third methoxy group, to yield derivative **4p**, abolished antiproliferative activity.

These results suggested that the space for accepting substituents on the phenyl at the 5-position of 2-alkoxycarbonyl-3-(3',4',5'-trimethoxyanilino)thiophene system is highly limited and that the phenyl ring is specifically recognized by tubulin in a highly specific manner. In an effort to further understand the steric effect of the alkoxy substitution at the *para*-position of the phenyl ring, replacement of the *para*-methoxy with a *para*-ethoxy homologue (compound **4m**) resulted in a 5-20-fold reduction of cytostatic activity in all cell lines.

Table 1. In vitro inhibitory effects of compounds **4a-r** and CA-4 (**1**) against the proliferation of murine leukemia (L1210), murine mammary carcinoma (FM3A), human T-lymphocyte leukemia (CEM) and human cervix carcinoma (HeLa) cells.

Compound	IC_{50} (μM)[a]			
	L1210	FM3A	CEM	HeLa
4a	0.24±0.01	0.21±0.03	0.20±0.08	0.67±0.40
4b	1.1±0.0	0.98±0.13	0.93±0.08	1.4±0.7
4c	0.13±0.07	0.16±0.01	0.16±0.08	0.16±0.02
4d	0.56±0.38	0.72±0.19	0.53±0.38	0.88±0.16
4e	1.1±0.0	1.0±0.2	0.99±0.24	2.1±1.1
4f	1.1±0.1	0.88±0.08	0.87±0.18	0.87±0.13
4g	6.0±0.0	5.1±0.5	4.6±0.6	9.8±5.0
4h	5.7±0.1	4.6±0.6	3.3±1.7	5.0±1.3
4i	0.15±0.08	0.18±0.01	0.18±0.04	0.26±0.10
4j	0.82±0.31	0.82±0.23	0.76±0.38	0.78±0.06
4k	0.27±0.03	0.25±0.04	0.23±0.10	0.84±0.10
4l	1.2±0.1	1.2±0.1	1.1±0.3	2.3±1.5
4m	6.3±0.0	5.7±0.5	5.4±1.3	4.4±0.2
4n	1.1±0.1	0.99±0.10	0.69±0.46	0.80±0.06
4o	0.48±0.27	0.43±0.29	0.47±0.35	0.89±0.08
4p	>250	>250	>250	162 ±25
4q	1.2±0.1	1.1±0.1	0.81±0.33	1.3±0.2
4r	0.99±0.13	0.93±0.08	0.76±0.21	1.0±0.3
CA-4 (nM)	3±1	42±6	2±1	2±1

IC_{50} = compound concentration required to inhibit tumour cell proliferation by 50%. Data are expressed as the mean ± SD from at least two to three independent experiments.

Evaluation of cytotoxicity of compounds **4a**, **4c** and **4i** in human non-cancer cells

To obtain a preliminary indication of the cytotoxic potential of these derivatives in normal human cells, three of the most active compounds (**4a**, **4c** and **4i**) were evaluated *in vitro* against peripheral blood lymphocytes (PBL) from healthy donors (Table 2). All compounds were practically devoid of significant cytotoxic activity in quiescent lymphocytes, with GI_{50}'s of 30-85 μM, while with the mitogenic stimulus phytohematoaglutinin (PHA), the GI_{50}'s were reduced to about 20-30 μM.

These values, even under proliferation conditions, were more than 100 times those found in the two lines of T lymphoblastic leukemia cells (L1210 and CEM) shown in Table 2. These results indicate that these compounds have little effect in rapidly proliferating normal cells and even less in quiescent cells, as previously observed for other antimitotic derivatives developed by our group.[15,17,18]

Table 2. Cytotoxicity of compounds **4a**,**4c** and **4i** for human peripheral blood lymphocytes (PBL).

	GI_{50} (μM) [a]		
	4a	**4c**	**4i**
$PBL_{resting}$[b]	45.7±10.9	85.7±8.9	31.7±2.0
PBL_{PHA}[c]	19.0±1.7	29.3±1.2	20.0±1.1

[a]Compound concentration required to reduce cell growth inhibition by 50%.
[b] PBL not stimulated with PHA.
[c] PBL stimulated with PHA.
Values are the mean ± SEM from two separate experiments.

3.3.2 Inhibition of tubulin polymerization and colchicine binding

To investigate whether the activities of these molecules were related to an interaction with the microtubule system, the more active compounds (**4a**, **4c**-**d**, **4i**, **4k** and **4o**) and reference compound CA-4 were evaluated for their *in vitro* tubulin polymerization inhibitory activity as well as for their inhibitory effects on the binding of [^{3}H]colchicine to tubulin (in the latter assay, the compounds and colchicine were at 5 μM, and tubulin was at 1 μM) (Table 3). In the tubulin polymerization assay, these compounds showed IC_{50} values in a relatively narrow range (1.2-2.7 μM). Three compounds (**4a**, **4c** and **4i**) showed the best tubulin polymerization assembly inhibition ability (IC_{50}: 1.2-1.3 μM), which is comparable to the IC_{50} of 1.1 μM obtained with CA-4, while derivatives **4d**, **4k** and **4o** were about half as

potent as CA-4. Derivatives **4a**, **4c** and **4i** also displayed the most potent activities against the panel of four cancer cell lines. The results obtained demonstrated that antiproliferative activity correlated well with inhibition of tubulin polymerization.

In the colchicine binding studies, compounds **4a**, **4c** and **4i** were also the best inhibitors of the binding of [^{3}H]colchicine to tubulin. None, however, was quite as potent as CA-4, which in these experiments inhibited colchicine binding by 99%. The potent inhibition observed with these compounds indicated that **4a**, **4c** and **4i** bind to tubulin at a site overlapping the colchicine site. This group of compounds were all highly potent in the biological assays (inhibition of cell growth, tubulin assembly and colchicine binding), and there was a good correlation between the three types of assays. We conclude that the antiproliferative activity of these derivatives derives from an interaction with the colchicine site of tubulin and interference with cellular microtubule assembly.

Table 3. Inhibition of tubulin polymerization and colchicine binding by compounds **4a**, **4c-d**, **4i**, **4k**, **4o** and CA-4.

Compound	Tubulin assembly[a] IC_{50}±SD (μM)	Colchicine binding[b] %±SD
4a	1.3±0.2	57±5
4c	1.2±0.1	62±1
4d	2.2±0.3	41±5
4i	1.2±0.0	70±3
4k	2.0±0.3	46±4
4o	2.7±0.0	30±3
CA-4 (**1**)	1.1±0.1	99±3

[a] Inhibition of tubulin polymerization. Tubulin was at 10 μM.

[b] Inhibition of [^{3}H]colchicine binding. Tubulin, colchicine and tested compound were at 1, 5 and 5 μM, respectively.

3.3.3 *In vitro* studies of compounds 4a, 4c, 4i

Effects of **4a, 4c** and **4i** on the cell cycle

The effects of compounds **4a, 4c** and **4i** on cell cycle progression was examined by flow cytometry in Hela cells. After a 24 h treatment (Figure 3), the three compounds induced a G2/M arrest that became evident at the highest concentration used (500 nM). A concomitant reduction of cells in the G1 phase was also observed, while S phase cells remained essentially constant, although there was a slight increase in S phase cells that occurred at 500 nM with all compounds.

We also studied the association between **4c**-induced G2/M arrest and alterations in G2/M regulatory protein expression in HeLa cells. As shown in Figure 4, compound **4c** caused, in a concentration-dependent manner, an increase in cyclin B1 expression after 24 h, followed by a marked reduction at 48 h, indicating an activation of the mitotic checkpoint following drug exposure.[19] This effect was confirmed by a marked reduction in the expression of phosphatase cdc25c after a 24 h incubation, even at the lowest concentration used (100 nM). In particular, it is worth noting in Figure 4 the appearance of a slowly migrating form of cdc25c, indicating changes in its phosphorylation state, as previously observed for other anti-mitotics synthesized by our group.[15,17,18] The phosphorylation of cdc25c directly stimulates its phosphatase activity, and this is necessary to activate Cdk1/cyclin B on entry into mitosis.[20] Accordingly, we observed a decrease in the phosphorylated form of cyclin dependent kinase-1 (Cdk1) after 24 h and 48 h treatments at 250 nM.

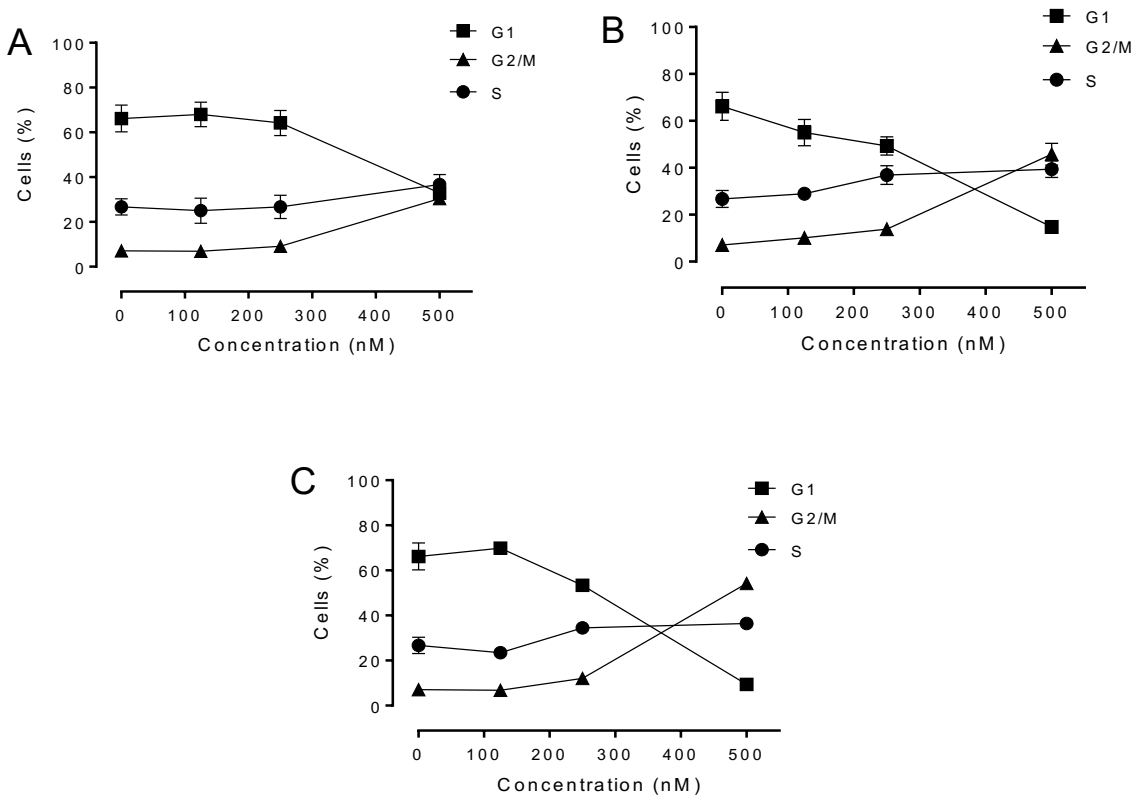

Figure 3. Percentage of cells in each phase of the cell cycle in HeLa cells, treated with compounds **4a** (A), **4c** (B) and **4i** (C) at the indicated concentrations for 24 h. Cells were fixed and labeled with PI and analyzed by flow cytometry as described in the Experimental Section. Data are presented as the mean of two independent experiments ± SEM.

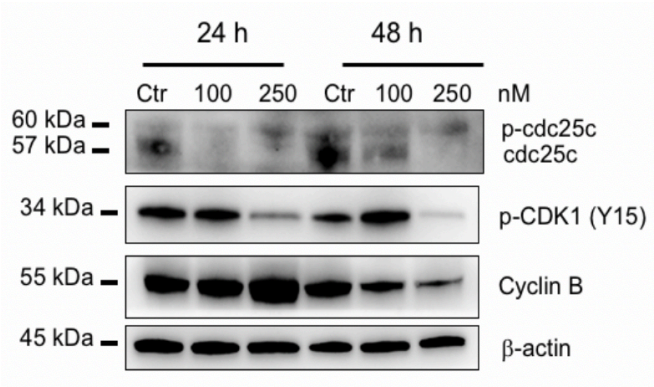

Figure 4. Effect of compound **4c** on cell cycle checkpoint proteins. HeLa cells were treated for 24 or 48 h with the indicated concentrations of **4c**. The cells were harvested and lysed for detection of the expression of the indicated proteins by western blot analysis. To confirm equal protein loading, each membrane was stripped and reprobed with anti-β-actin antibody.

Compounds **4a**, **4c** and **4i** induce apoptosis

To evaluate the mode of cell death, we treated HeLa cells with compounds **4a**, **4c** and **4i**, and, after 24 and 48 h incubations, we performed a biparametric cytofluorimetric analysis using propidium iodide (PI) and annexin-V-FITC, which stain DNA and phosphatidylserine (PS) residues, respectively. As shown in Figure 5, the three compounds induced a significant proportion of apoptotic cells after the 24 h incubation period, and this proportion further increased at 48 h. The most active compounds appear to be **4c** and **4i**, in good agreement with the antiproliferative results presented in Table 1.

Compound **4c** induced mitochondrial depolarization and ROS production

It is well known that mitochondria are involved in the initiation of apoptosis, since, at an early stage, apoptotic stimuli alter the mitochondrial transmembrane potential ($\Delta\psi_{mt}$).[21,22] To determine whether the cells treated with compound **4c** underwent mitochondrial depolarization, we assessed the changes in $\Delta\psi_{mt}$ in HeLa cells by flow cytometry using the fluorescent dye JC-1.[23] HeLa cells treated with compound **4c** (100-250 nM) showed a time-dependent increase in the percentage of cells with low $\Delta\psi_{mt}$ (Figure 6, Panel A). The depolarization of the mitochondrial membrane is associated with the appearance of annexin-V positivity in the treated cells when they are in an early apoptotic stage.[24] One of the major consequences of the increase of mitochondrial membrane permeability is the release into the cytosol of pro-apoptotic molecules such as AIF, Smac/Diablo and, in particular, cytochrome *c*.[21] This release triggers ROS production at the mitochondrial level during the later stages of the cell death program.[24-26] We therefore investigated whether ROS production increased after treatment with compound **4c**. We analyzed ROS production by flow cytometry, using the fluorescence indicator 2,7-dichlorodihydrofluorescein diacetate (H_2-DCFDA). As shown in Figure 6 (Panel B), compound **4c** induced significant production of ROS starting after a treatment of 12-24 h at 250 nM, in good agreement with the mitochondrial depolarization described above.

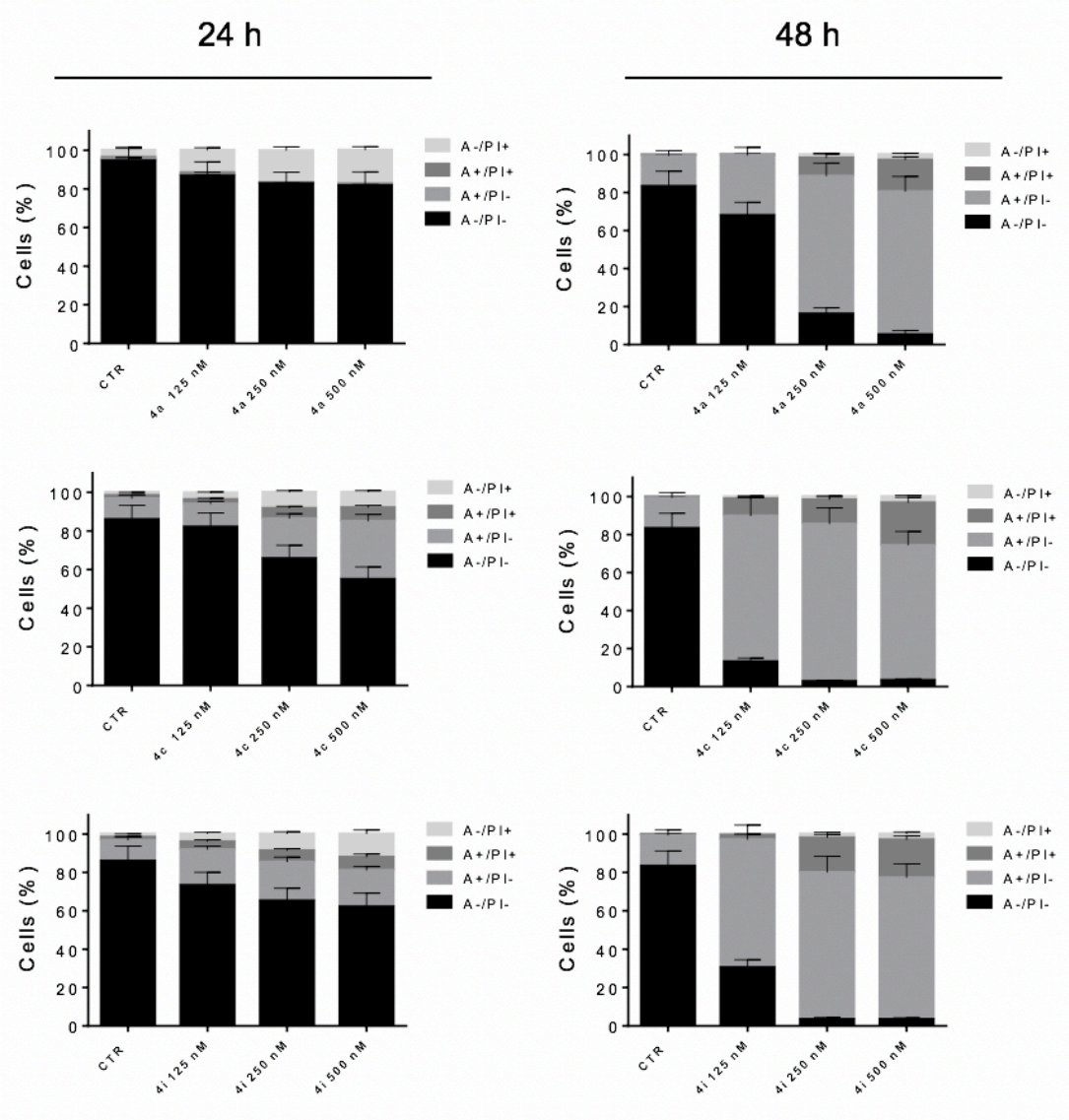

Figure 5. Flow cytometric analysis of apoptotic cells after treatment of HeLa cells with **4a**, **4c** and **4i** at the indicated concentrations after incubation for 24 or 48 h. The cells were harvested and labeled with annexin-V-FITC and PI and analyzed by flow cytometry. Data are presented as mean±SEM of three independent experiments.

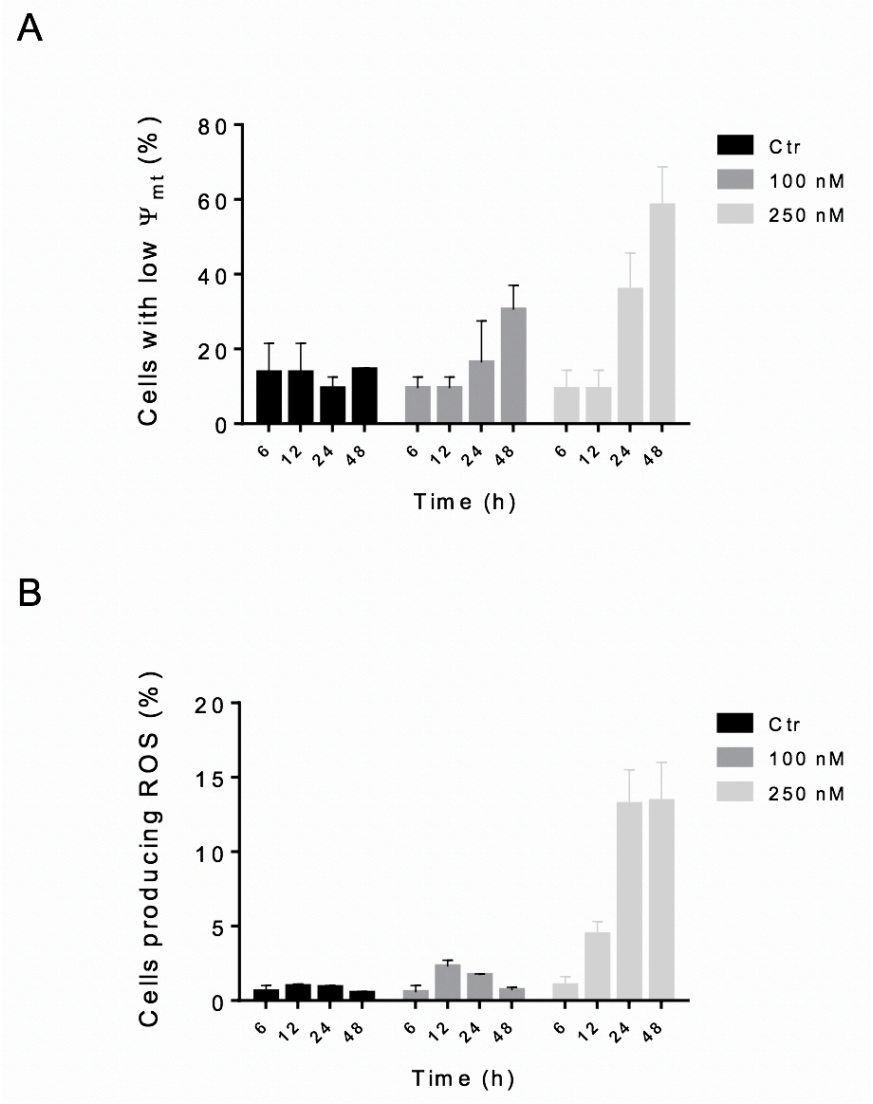

Figure 6. Assessment of mitochondrial membrane potential ($\Delta\psi_{mt}$) after treatment of HeLa cells (Panel A) with compound **4c**. Cells were treated with the indicated concentration of compound for 6, 12, 24 or 48 h and then stained with the fluorescent probe JC-1 for analysis of mitochondrial potential. Cells were then analyzed by flow cytometry as described in the Experimental Section. Data are presented as mean±SEM of three independent experiments. Assessment of ROS production after treatment of HeLa cells with compound **4c** (Panel B). Cells were treated with the indicated concentration for 6, 12, 24 or 48 h and then stained with H_2-DCFDA for evaluation of ROS levels. Cells were then analyzed by flow cytometry as described in the Experimental Section. Data are presented as mean±SEM of three independent experiments.

Compound **4c** induced PARP cleavage and decreased expression of anti-apoptotic proteins

To further investigate the mechanism of apoptosis induction by **4c**, we analyzed the expression of poly (ADP-Ribose) polymerase (PARP), a protein involved in late stage apoptosis, and the expression of two anti-apoptotic proteins belonging to the Bcl-2 family. As shown in Figure 7, compound **4c** in HeLa cells caused a concentration- and time-dependent cleavage of PARP, confirming the pro-apoptotic properties of **4c**.

We also investigated the expression of anti-apoptotic proteins such as Bcl-2 and Mcl-1. It is well-known that antimitotic agents can modulate both expression levels and activity of many proteins of the Bcl-2 family.[27-29] Our results (Figure 7) showed that the expression of both anti-apoptotic proteins Bcl-2 and Mcl-1 were decreased starting after 24 h of treatment, even at the lowest **4c** concentration used (0.1 μM). These studies underline the importance of Mcl-1 phosphorylation and its subsequent degradation in response to antimitotic agents and that this event potentiates cell death.[30,31]

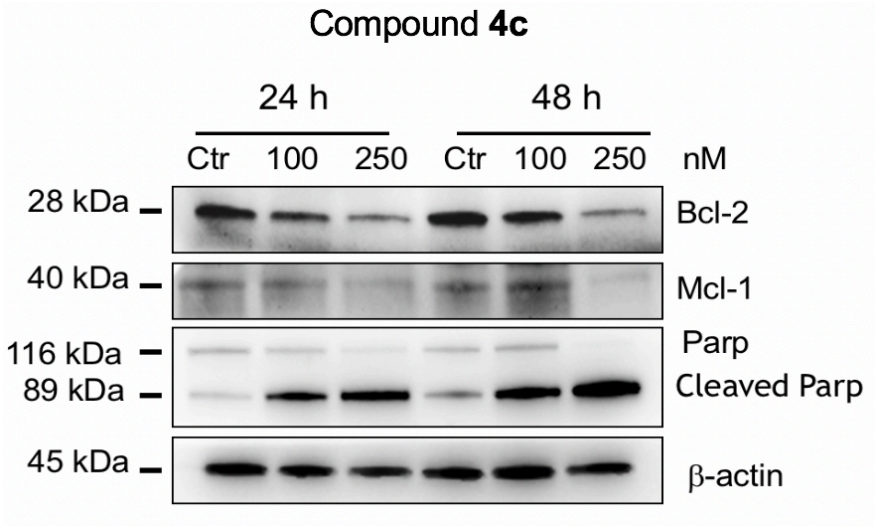

Figure 7. Western blot analysis of Bcl-2, Mcl-1 and PARP after treatment of HeLa cells with **4c** at the indicated concentrations and times. To confirm equal protein loading, each membrane was stripped and reprobed with anti-β-actin antibody.

3.4 Conclusions

In conclusion, we have discovered a new class of simple synthetic inhibitors of tubulin polymerization based on the molecular skeleton of 2-alkoxycarbonyl-3-(3',4',5'-trimethoxyanilino)thiophene. These derivatives were designed and synthesized based on modification of benzo[*b*]thiophene and thieno[2,3-*b*]pyridine analogues previously published. The results demonstrated that the aryl or 2-thienyl moieties at the 5-position of the 2-alkoxycarbonyl-3-(3',4',5'-trimethoxyanilino)thiophene system could replace either the benzene or the pyridine portion of benzo[*b*]thiophene and thieno[2,3-*b*]pyridine derivatives with general structure **2** and **3**, respectively. We explored SAR by examining various substitutions with EWGs and ERGs on the phenyl at the 5-position of the 2-alkoxycarbonyl-3-(3',4',5'-trimethoxyanilino)thiophene scaffold. The presence of ERGs such as methyl or methoxy was beneficial for antiproliferative activity, as these compounds proved to be more potent than the corresponding derivatives with the EWGs fluorine or chlorine. Generally, it was found that most substituents in the *para*-position resulted in lower activity as compared to the unsubstituted parent compound **4a**, with the least deleterious being methyl and methoxy moieties (compounds **4i** and **4k**, respectively).

It is clear that the substitution pattern on the phenyl at the 5-position of the 2-methoxycarbonyl-3-(3',4',5'-trimethoxyanilino)thiophene system plays an important role for antitubulin and antiproliferative activities, and this was supported by the molecular docking studies. SAR studies showed that the 2-methoxycarbonyl-3-(3',4',5'-trimethoxyanilino)-5-phenylthiophene derivative **4a**, its bioisosteric thien-2'-yl analogue **4c** as well as the *para*-tolyl and *para*-methoxyphenyl analogues **4i** and **4k**, respectively, displayed high antiproliferative activities, with IC_{50} values ranging between 0.13-0.24, 0.16-0.25, 0.16-0.23 and 0.16-0.84 μM, respectively, against the L1210, FM3A, CEM and HeLa cell lines. Of all the tested compounds, derivative **4c** possessed the highest overall cytostatic potency with IC_{50} values ranging from 0.13 to 0.16 μM against the panel of four cancer cell lines. The antiproliferative activity was considerably increased by replacing the EWG fluorine with the ERG methyl group (compounds **4d** and **4i**, respectively), with the latter compound being about 3-6-fold more active than the former. By comparing **4d** and **4f**, replacement of the *para*-fluoro group in **4d** with the chloro (derivative **4f**) led to little change in activity against FM3A and HeLa cells, while **4f** was less potent than **4d** in L1210 and CEM cells. Replacement of the EWG *para*-chlorine atom of **4f** with the ERG *para*-methyl moiety, to furnish derivative **4i**, resulted in 4-6-fold enhancement in antiproliferative activity against the four cancer cell lines. Replacement of the methyl with a methoxy group

(derivative **4k**) produced a 2- and 3-fold reduction in potency against L1210 and HeLa cells, respectively, while the difference between **4i** and **4k** were minimal for FM3A and CEM cells.

The antiproliferative activity of the thiophene derivatives **4k** and **4n-p** can be further characterized in terms of the substitution pattern and the number of methoxy groups on the phenyl ring. The introduction of a single methoxy group at the *para*-position caused only minor changes in antiproliferative activity relative to the unsubstituted derivative **4a**. Reduced activity occurred in three of the four cancer cell lines when the methoxy substituent was moved from the *para*- to the *meta*-position (**4n**), with the exception of HeLa cells. As previously observed comparing the activities of *para*-chloro and *meta*, *para*-dichloro derivatives **4f** and **4h**, respectively, the introduction of a second methoxy group at the *meta*-position of *para*-methoxyphenyl derivative **4k**, to furnish the *meta*, *para*-dimethoxyphenyl analogue **4o**, decreased potency in three of the four cancer cell lines by 2-fold, with the exception of the HeLa cells. The 3',4',5'-trimethoxyphenyl derivative **4p** was not active, and this result suggested the space for accepting substituents on the phenyl ring at the 5-position of the 2-alkoxycarbonyl-3-(3',4',5'-trimethoxyanilino)thiophene scaffold is highly limited. This conclusion was supported by comparing the reduced activity (on average 20-fold) of the *para*-ethoxy homologue **4m** relative to the *para*-methoxy analogue **4k**.

The results we obtained indicated that compound **4c** could induce tumour cell apoptosis through reducing the mitochondrial membrane potential and regulating the expression of apoptosis-related proteins in tumour cells.

3.5 Experimental section

Chemistry

Materials and Methods. ^{1}H-NMR experiments were recorded on either a Bruker AC 200 or a Varian 400 Mercury Plus spectrometer, while ^{13}C-NMR spectra were recorded on a Varian 400 Mercury Plus spectrometer. Chemical shifts (δ) are given in ppm upfield from tetramethylsilane as internal standard, and the spectra were recorded in appropriate deuterated solvents, as indicated. Positive-ion electrospray ionization (ESI) mass spectra were recorded on a double-focusing Finnigan MAT 95 instrument with BE geometry. Melting points (mp) were determined on a Buchi-Tottoli apparatus and are uncorrected. All products reported showed ^{1}H and ^{13}C-NMR spectra in agreement with the assigned structures. The purity of tested compounds was determined by combustion elemental

analyses conducted by the Microanalytical Laboratory of the Chemistry Department of the University of Ferrara with a Yanagimoto MT-5 CHN recorder elemental analyzer. All tested compounds yielded data consistent with a purity of at least 95% as compared with the theoretical values. Reaction courses and product mixtures were routinely monitored by TLC on silica gel (precoated F_{254} Merck plates), and compounds were visualized with aqueous $KMnO_4$. Flash chromatography was performed using 230-400 mesh silica gel and the indicated solvent system. Organic solutions were dried over anhydrous Na_2SO_4.

General procedure A for the synthesis of compounds 7a-r. To a solution of methyl/ethyl thioglycolate (10 mmol) in methanol (5 mL) was added a solution of sodium methoxide (0.54 g, 10 mmol) in methanol (5 mL), and the mixture was stirred for 1 h. To the above mixture, a solution of the corresponding 3-chloroacrylonitrile **6a-m** (7.5 mmol) in DMF (5 mL) was added dropwise for 10 min at room temperature and stirred at 60 °C for 2 h. Then, a solution of sodium methoxide (1.08 g, 20 mmol) in methanol (10 mL) was added dropwise at room temperature, and stirring was continued for 2 h at 60 °C. The mixture was poured into cold water and stirred for 10 min. The solution was extracted with CH_2Cl_2 (3 x 20 mL), and the combined CH_2Cl_2 layer was washed with water (20 mL), brine (20 mL), and dried. The solution was filtered, and, after concentration under reduced pressure, the residue was purified by silica gel column chromatography to furnish the corresponding thiophene derivatives **7a-r.**

Methyl 3-amino-5-phenylthiophene-2-carboxylate (7a). Following general procedure A, the crude residue was purified by flash chromatography, using ethyl acetate:petroleum ether 1:9 (v:v) as the eluting solution, to furnish **7a** as a yellow solid (54% yield), mp 130-132 °C. ^{1}H-NMR ($CDCl_3$) δ: 3.85 (s, 3H), 5.47 (bs, 2H), 6.77 (s, 1H), 7.38 (m, 3H), 7.57 (m, 2H). MS (ESI): $[M+1]^+$=234.2.

Ethyl 3-amino-5-phenylthiophene-2-carboxylate (7b). Following general procedure A, the crude residue was purified by flash chromatography, using ethyl acetate:petroleum ether 2:8 (v:v) as the eluting solution, to furnish **7b** as a brown solid (95% yield), mp 90-91 °C. ^{1}H-NMR ($CDCl_3$) δ: 1.33 (t, *J*=7.0 Hz, 3H), 4.26 (q, *J*=7.0 Hz, 2H), 5.46 (bs, 2H), 6.77 (s, 1H), 7.36 (m, 3H), 7.57 (m, 2H). MS (ESI): $[M+1]^+$=248.3.

Methyl 4-amino-[2,2'-bithiophene]-5-carboxylate (7c). Following general procedure A, the crude residue was purified by flash chromatography, using ethyl acetate:petroleum ether

3:7 (v:v) as the eluting solution, to furnish **7c** as a brown solid (78% yield), mp 105-107 °C. ^{1}H-NMR ($CDCl_3$) δ: 3.86 (s, 3H), 5.73 (bs, 2H), 7.38 (m, 2H), 7.45 (m, 1H), 7.86 (dd, *J*=5.0 and 1.2 Hz, 1H). MS (ESI): $[M+1]^+$=240.3.

Methyl 3-amino-5-(4-fluorophenyl)thiophene-2-carboxylate (7d). Following general procedure A, the crude residue was purified by flash chromatography, using ethyl acetate:petroleum ether 2:8 (v:v) as the eluting solution, to furnish **7d** as a white solid (84% yield), mp 164-166 °C. ^{1}H-NMR (d_6-DMSO) δ: 3.71 (s, 3H), 6.59 (bs, 2H), 6.92 (s, 1H), 7.27 (t, *J*=8.8 Hz, 2H), 7.63 (dd, *J*=8.8 and 5.4 Hz, 2H). MS (ESI): $[M+1]^+$=252.3.

Ethyl 3-amino-5-(4-fluorophenyl)thiophene-2-carboxylate (7e). Following general procedure A, the crude residue was purified by flash chromatography, using ethyl acetate:petroleum ether 2:8 (v:v) as the eluting solution, to furnish **7e** as a yellow solid (78% yield), mp 110-112 °C. ^{1}H-NMR ($CDCl_3$) δ: 1.37 (t, *J*=7.0 Hz, 3H), 4.29 (q, *J* =7.0 Hz, 2H), 5.46 (bs, 2H), 6.70 (s, 1H), 7.03 (t, *J* =8.8 Hz, 2H), 7.52 (dd, *J*=8.8 and 5.4 Hz, 2H). MS (ESI): $[M+1]^+$=266.3.

Methyl 3-amino-5-(4-chlorophenyl)thiophene-2-carboxylate (7f). Following general procedure A, the crude residue was purified by flash chromatography, using ethyl acetate:petroleum ether 2:8 (v:v) as the eluting solution, to furnish **7f** as a cream-colored solid (66% yield), mp 134-136 °C. ^{1}H-NMR ($CDCl_3$) δ: 3.84 (s, 3H), 5,48 (bs, 2H), 6.74 (s, 1H), 7.33 (d, *J*=8.8 Hz, 2H), 7.48 (d, *J*=8.8 Hz, 2H). MS (ESI): $[M+1]^+$=268.7.

Ethyl 3-amino-5-(4-chlorophenyl)thiophene-2-carboxylate (7g). Following general procedure A, the crude residue was purified by flash chromatography, using ethyl acetate:petroleum ether 3:7 (v:v) as the eluting solution, to furnish **7g** as a yellow solid (72% yield), mp 103-105 °C. ^{1}H-NMR ($CDCl_3$) δ: 1.36 (t, *J*=7.2 Hz, 3H), 4.29 (q, *J*=7.2 Hz, 2H), 5.46 (bs, 2H), 6.74 (s, 1H), 7.33 (d, *J*=8.8 Hz, 2H), 7.50 (d, *J*=8.8 Hz, 2H). MS (ESI): $[M+1]^+$=282.8.

Methyl 3-amino-5-(3,4-dichlorophenyl)thiophene-2-carboxylate (7h). Following general procedure A, the crude residue was purified by flash chromatography, using ethyl acetate:petroleum ether 3:7 (v:v) as the eluting solution, to furnish **7h** as a grey solid (58% yield), mp 154-156 °C. ^{1}H-NMR ($CDCl_3$) δ: 3.85 (s, 3H), 5.48 (bs, 2H), 6.75 (s, 1H), 7.40

(dd, *J*=8.4 and 2.0 Hz, 1H), 7.44 (d, J=8.4 Hz, 1H), 7.65 (d, *J*=2.0 Hz, 1H). MS (ESI): $[M]^+$=303.2.

Methyl 3-amino-5-(p-tolyl)thiophene-2-carboxylate (7i). Following general procedure A, the crude residue was purified by flash chromatography, using ethyl acetate:petroleum ether 1:9 (v:v) as the eluting solution, to furnish **7i** as an orange solid (54% yield), mp 140-142 °C. ^{1}H-NMR ($CDCl_3$) δ: 2.37 (s, 3H), 3.84 (s, 3H), 5.46 (bs, 2H), 6.73 (s, 1H), 7.17 (d, *J*=8.2 Hz, 2H), 7.46 (d, *J*=8.2 Hz, 2H). MS (ESI): $[M+1]^+$=248.2.

Ethyl 3-amino-5-(p-tolyl)thiophene-2-carboxylate (7j). Following general procedure A, the crude residue was purified by flash chromatography, using ethyl acetate:petroleum ether 1:9 (v:v) as the eluting solution, to furnish **7j** as a yellow solid (80% yield), mp 103-105 °C. ^{1}H-NMR ($CDCl_3$) δ: 1.36 (t, *J*=7.0 Hz, 3H), 2.37 (s, 3H), 4.29 (q, *J*=7.0 Hz, 2H), 5.45 (bs, 2H), 6.73 (s, 1H), 7.17 (d, *J*=7.8 Hz, 2H), 7.46 (d, *J*=7.8 Hz, 2H). MS (ESI): $[M+1]^+$=262.3.

Methyl 3-amino-5-(4-methoxyphenyl)thiophene-2-carboxylate (7k). Following general procedure A, the crude residue was purified by flash chromatography, using ethyl acetate:petroleum ether 3:7 (v:v) as the eluting solution, to furnish **7k** as a yellow solid (95% yield), mp 118-120 °C. ^{1}H-NMR ($CDCl_3$) δ: 3.84 (s, 6H), 5.46 (bs, 2H), 6.67 (s, 1H), 6.89 (d, *J*=9.2 Hz, 2H), 7.51 (d, *J*=9.2 Hz, 2H). MS (ESI): $[M+1]^+$=264.3.

Ethyl 3-amino-5-(4-methoxyphenyl)thiophene-2-carboxylate (7l). Following general procedure A, the crude residue was purified by flash chromatography, using ethyl acetate:petroleum ether 3:7 (v:v) as the eluting solution, to furnish **7l** as a yellow solid (82% yield), mp 132-134 °C. ^{1}H-NMR ($CDCl_3$) δ: 1.36 (t, *J* =7.2 Hz, 3H), 3.83 (s, 3H), 4.28 (q, *J* =7.2 Hz, 2H), 6.66 (s, 3H), 6.88 (d, *J* =9.0 Hz, 2H), 7.51 (d, *J* =9.0 Hz, 2H). MS (ESI): $[M+1]^+$=278.3.

Methyl 3-amino-5-(4-ethoxyphenyl)thiophene-2-carboxylate (7m). Following general procedure A, the crude residue was purified by flash chromatography, using ethyl acetate:petroleum ether 3:7 (v:v) as the eluting solution, to furnish **7m** as a pink solid (82% yield), mp 153-155 °C.-^{1}H-NMR ($CDCl_3$) δ: 1.39 (t, *J*=6.8 Hz, 3H), 3.83 (s, 3H), 4.04 (q, *J*=6.8 Hz, 2H), 5.48 (bs, 2H), 6.66 (s, 1H), 6.87 (d, *J*=8.8 Hz, 2H), 7.48 (d, *J*=8.8 Hz, 2H). MS (ESI): $[M+1]^+$=278.3.

Methyl 3-amino-5-(3-methoxyphenyl)thiophene-2-carboxylate (7n). Following general procedure C, the crude residue was purified by flash chromatography, using ethyl acetate:petroleum ether 3:7 (v:v) as the eluting solution, to furnish **7n** as a yellow oil (95% yield). ^{1}H-NMR ($CDCl_3$) δ: 3.84 (s, 6H), 5.47 (bs, 2H), 6.76 (s, 1H), 6.93 (m, 1H), 7.09 (t, *J*=1.8 Hz, 1H), 7.19 (m, 1H), 7.26 (t, *J*=7.8 Hz, 1H). MS (ESI): $[M+1]^+$=263.4.

Methyl 3-amino-5-(3,4-dimethoxyphenyl)thiophene-2-carboxylate (7o). Following general procedure A, the crude residue was purified by flash chromatography, using ethyl acetate:petroleum ether 3:7 (v:v) as the eluting solution, to furnish **7o** as a brown solid (95% yield), mp 88-90 °C. ^{1}H-NMR ($CDCl_3$) δ: 3.84 (s, 3H), 3.91 (s, 3H), 3.92 (s, 3H), 5.47 (bs, 2H), 6.68 (s, 1H), 6.85 (d, *J*=8.6 Hz, 1H), 7.06 (d, *J*=2.0 Hz, 1H), 7.15 (dd, *J*=8.6 and 2.0 Hz, 1H). MS (ESI): $[M+1]^+$=284.3.

Methyl 3-amino-5-(3,4,5-trimethoxyphenyl)thiophene-2-carboxylate (7p). Following general procedure A, the crude residue was purified by flash chromatography, using ethyl acetate:petroleum ether 4:6 (v:v) as the eluting solution, to furnish **7p** as a brown solid (95% yield), mp 143-145 °C. ^{1}H-NMR ($CDCl_3$) δ: 3.84 (s, 3H), 3.87 (s, 3H), 3.90 (s, 6H), 5.47 (bs, 2H), 6.7 (s,1H), 6.78 (s, 2H). MS (ESI): $[M+1]^+$=324.4.

Methyl 3-amino-5-(4-(trifluoromethyl)phenyl)thiophene-2-carboxylate (7q). Following general procedure A, the crude residue was purified by flash chromatography, using ethyl acetate:petroleum ether 2:8 (v:v) as the eluting solution, to furnish **7q** as a brown solid (63% yield), mp 139-140 °C. ^{1}H-NMR ($CDCl_3$) δ: 3.86 (s, 3H), 5.49 (bs, 2H), 6.83 (s, 1H), 7.61 (d, *J*=9.0 Hz, 2H), 7.68 (d, *J*=9.0 Hz, 2H). MS (ESI): $[M+1]^+$=302.3.

Methyl 3-amino-5-(4-nitrophenyl)thiophene-2-carboxylate (7r). Following general procedure A, the crude residue was purified by flash chromatography, using ethyl acetate:petroleum ether 3:7 (v:v) as the eluting solution, to furnish **7r** as a yellow solid (61% yield), mp 219-220 °C. ^{1}H-NMR ($CDCl_3$) δ: 3.86 (s, 3H), 5.68 (bs, 2H), 6.90 (s, 1H), 7.69 (d, *J*=9.2 Hz, 2H), 8.23 (d, *J*=9.0 Hz, 2H). MS (ESI): $[M+1]^+$=302.3.

General procedure B for the synthesis of compounds 8a-r. To a solution of *tert*-butyl nitrite (360 μL, 3 mmol) in anhydrous acetonitrile (10 mL) at 0 °C under an Ar atmosphere in a dry three-necked round-bottom flask, was added anhydrous $CuBr_2$ (536 mg, 2.4 mmol). Derivative **7a-r** (2 mmol) was then slowly added portion-wise to the mixture, which was

stirred at 0 °C for 1 h. The dark mixture was allowed to reach room temperature, stirred for 2 h and then poured into an aqueous HCl solution (10%, 10 mL). The mixture was extracted with CH_2Cl_2 (3 x 15 mL). The organic phase was washed with brine (10 mL), dried and concentrated at reduced pressure to furnish a residue that was purified by flash chromatography on silica gel to give **8a-r**.

Methyl 3-bromo-5-phenylthiophene-2-carboxylate (8a). Following general procedure B, the crude residue was purified by flash chromatography, using ethyl acetate:petroleum ether 1:9 (v:v) as the eluting solution, to furnish **8a** as a yellow oil (69% yield). ^{1}H-NMR ($CDCl_3$) δ: 3.91 (s, 3H), 7.29 (s, 1H), 7.42 (m, 3H), 7.58 (m, 2H). MS (ESI): $[M+1]^+$ = 296.1 and 298.1.

Ethyl 3-bromo-5-phenylthiophene-2-carboxylate (8b). Following general procedure B, the crude residue was purified by flash chromatography, using ethyl acetate:petroleum ether 1:9 (v:v) as the eluting solution, to furnish **8b** as a yellow solid (63% yield), mp 80-81 °C. ^{1}H-NMR ($CDCl_3$) δ: 1.32 (t, *J*=7.4 Hz, 3H), 4.30 (q, *J*=7.6 Hz, 2H), 7.32 (m, 4H), 7.38 (s, 1H), 7.48 (m, 1H). MS (ESI): $[M+1]^+$=327.1 and 329.1.

Methyl 4-bromo-[2,2'-bithiophene]-5-carboxylate (8c). Following general procedure B, the crude residue was purified by flash chromatography, using ethyl acetate:petroleum ether 1:9 (v:v) as the eluting solution, to furnish **8c** as a yellow oil (55% yield). ^{1}H-NMR ($CDCl_3$) δ: 3.89 (s, 3H), 7.18 (s, 1H), 7.30 (m, 1H), 7.41 (dd, *J*=5.2 and 2.8 Hz, 1H), 7.51 (m, 1H). MS (ESI): $[M+1]^+$=302.1 and 304.2.

Methyl 3-bromo-5-(4-fluorophenyl)thiophene-2-carboxylate (8d). Following general procedure B, the crude residue was purified by flash chromatography, using ethyl acetate:petroleum ether 1:9 (v:v) as the eluting solution, to furnish **8d** as a yellow solid (58% yield), mp 126-128 °C. ^{1}H-NMR ($CDCl_3$) δ: 3.91 (s, 3H), 7.08 (t, *J*=8.8 Hz, 2H), 7.22 (s, 1H), 7.53 (dd, *J*=8.8 and 5.2 Hz, 2H). MS (ESI): $[M+1]^+$=314.9 and 316.9.

Ethyl 3-bromo-5-(4-fluorophenyl)thiophene-2-carboxylate (8e). Following general procedure B, the crude residue was purified by flash chromatography, using ethyl acetate:petroleum ether 1:9 (v:v) as the eluting solution, to furnish **8e** as a yellow solid (67% yield), mp 90-92 °C. ^{1}H-NMR ($CDCl_3$) δ: 1.36 (t, *J*=7.0 Hz, 3H), 4.33 (q, *J* =7.0 Hz, 2H),

7.07 (t, *J* =8.8 Hz, 2H), 7.22 (s, 1H), 7.53 (dd, *J*=8.8 and 5.2 Hz, 2H). MS (ESI): $[M+1]^+$=329.1 and 331.1.

Methyl 3-bromo-5-(4-chlorophenyl)thiophene-2-carboxylate (8f). Following general procedure B, the crude residue was purified by flash chromatography, using ethyl acetate:petroleum ether 0.5:9.5 (v:v) as the eluting solution, to furnish **8f** as a brown solid (64% yield), mp 122-124 °C. ^{1}H-NMR ($CDCl_3$) δ: 3.91 (s, 3H), 7.26 (s, 1H), 7.42 (d, *J*=8.4 Hz, 2H), 7.52 (d, *J*=8.4 Hz, 2H). MS (ESI): $[M+1]^+$=330.9 and 332.9.

Ethyl 3-bromo-5-(4-chlorophenyl)thiophene-2-carboxylate (8g). Following general procedure B, the crude residue was purified by flash chromatography, using ethyl acetate:petroleum ether 1:9 (v:v) as the eluting solution, to furnish **8g** as a yellow solid (58% yield), mp 98-100 °C. ^{1}H-NMR ($CDCl_3$) δ: 1.36 (t, *J*=7.0 Hz, 3H), 4.36 (q, *J*=7.0 Hz, 2H), 7.232 (s, 1H), 7.37 (d, *J*=8.8 Hz, 2H), 7.51 (d, *J*=8.6 Hz, 2H). MS (ESI): $[M+1]^+$=344.9 and 346.9.

Methyl 3-bromo-5-(3,4-dichlorophenyl)thiophene-2-carboxylate (8h). Following general procedure B, the crude residue was purified by flash chromatography, using ethyl acetate:petroleum ether 2:8 (v:v) as the eluting solution, to furnish **8h** as a yellow solid (51% yield), mp 122-124 °C. ^{1}H-NMR ($CDCl_3$) δ: 3.92 (s, 3H), 7.28 (s, 1H), 7.42 (dd, *J*=8.4 and 2.0 Hz, 1H), 7.48 (d, J=8.4 Hz, 1H), 7.68 (d, *J*=2.0 Hz, 1H). MS (ESI): $[M]^+$=364.9 and 366.9.

Methyl 3-bromo-5-(p-tolyl)thiophene-2-carboxylate (8i). Following general procedure B, the crude residue was purified by flash chromatography, using ethyl acetate:petroleum ether 1:9 (v:v) as the eluting solution, to furnish **8i** as a yellow solid (75% yield), mp 90-92 °C. ^{1}H-NMR ($CDCl_3$) δ: 2.38 (s, 3H), 3.89 (s, 3H), 7.20 (d, *J*=8.2 Hz, 2H), 7.26 (s, 1H), 7.47 (d, *J*=8.2 Hz, 2H). MS (ESI): $[M+1]^+$=312.1 and 314.1.

Ethyl 3-bromo-5-(p-tolyl)thiophene-2-carboxylate (8j). Following general procedure B, the crude residue was purified by flash chromatography, using ethyl acetate:petroleum ether 1:9 (v:v) as the eluting solution, to furnish **8j** as a yellow solid (54% yield), mp 98-100 °C. ^{1}H-NMR ($CDCl_3$) δ: 1.36 (t, *J*=7.2 Hz, 3H), 2.38 (s, 3H), 4.36 (q, *J*=7.2 Hz, 2H), 7.20 (d, *J*=8.2 Hz, 2H), 7.24 (s, 1H), 7.47 (d, *J*=8.2 Hz, 2H). MS (ESI): $[M+1]^+$=325.1 and 327.1.

Methyl 3-bromo-5-(4-methoxyphenyl)thiophene-2-carboxylate (8k). Following general procedure B, the crude residue was purified by flash chromatography, using ethyl acetate:petroleum ether 2:8 (v:v) as the eluting solution, to furnish **8k** as a yellow solid (58% yield), mp 106-108 °C. ^{1}H-NMR ($CDCl_3$) δ: 3.85 (s, 3H), 3.90 (s, 3H), 6.92 (d, *J*=8.8 Hz, 2H), 7.18 (s, 1H), 7.51 (d, *J*=8.8 Hz, 2H). MS (ESI): $[M+1]^+$=327.1 and 329.1.

Ethyl 3-bromo-5-(4-methoxyphenyl)thiophene-2-carboxylate (8l). Following general procedure B, the crude residue was purified by flash chromatography, using ethyl acetate:petroleum ether 2:8 (v:v) as the eluting solution, to furnish **8l** as a yellow solid (76% yield), mp 75-77 °C. ^{1}H-NMR ($CDCl_3$) δ: 1.36 (t, *J* =7.2 Hz, 3H), 3.82 (s, 3H), 4.36 (q, *J* =7.2 Hz, 2H), 6.91 (d, *J* =8.8 Hz, 2H), 7.17 (s, 1H), 7.52 (d, *J* =8.8 Hz, 2H). MS (ESI): $[M+1]^+$=341.1 and 343.1.

Methyl 3-bromo-5-(4-ethoxyphenyl)thiophene-2-carboxylate (8m). Following general procedure B, the crude residue was purified by flash chromatography, using ethyl acetate:petroleum ether 3:7 (v:v) as the eluting solution, to furnish **8m** as a yellow solid (46% yield), mp 106-108 °C. ^{1}H-NMR ($CDCl_3$) δ: 1.40 (t, *J*=7.2 Hz, 3H), 3.90 (s, 3H), 4.05 (q, *J*=7.2 Hz, 2H), 6.90 (d, *J*=8.8 Hz, 2H), 7.18 (s, 1H), 7.49 (d, *J*=8.8 Hz, 2H). MS (ESI): $[M+1]^+$=341.1 and 343.1.

Methyl 3-bromo-5-(3-methoxyphenyl)thiophene-2-carboxylate (8n). Following general procedure B, the crude residue was purified by flash chromatography, using ethyl acetate:petroleum ether 2:8 (v:v) as the eluting solution, to furnish **8n** as a yellow oil (84% yield). ^{1}H-NMR ($CDCl_3$) δ: 3.82 (s, 3H), 3.86 (s, 3H), 6.96 (td, *J*=8.0, 2.2 and 1.0 Hz, 1H), 7.11 (t, *J*=2.2 Hz, 1H), 7.20 (m, 1H), 7.28 (s, 1H), 7.34 (d, *J*=8.0 Hz, 1H). MS (ESI): $[M+1]^+$=327.2 and 329.2.

Methyl 3-bromo-5-(3,4-dimethoxyphenyl)thiophene-2-carboxylate (8o). Following general procedure B, the crude residue was purified by flash chromatography, using ethyl acetate:petroleum ether 3:7 (v:v) as the eluting solution, to furnish **8o** as an orange solid (77% yield), mp 105-107 °C. ^{1}H-NMR ($CDCl_3$) δ: 3.89 (s, 3H), 3.90 (s, 3H), 3.92 (s, 3H), 6.87 (d, *J*=8.6 Hz, 1H), 7.05 (d, *J*=2.0 Hz, 1H), 7.19 (m, 2H). MS (ESI): $[M+1]^+$=358.1 and 360.1.

Methyl 3-bromo-5-(3,4,5-trimethoxyphenyl)thiophene-2-carboxylate (8p). Following general procedure B, the crude residue was purified by flash chromatography, using ethyl acetate:petroleum ether 2:8 (v:v) as the eluting solution, to furnish **8p** as a yellow solid (48% yield), mp 143-145 °C. ^{1}H-NMR ($CDCl_3$) δ: 3.88 (s, 3H), 3.90 (s, 3H), 3.92 (s, 3H), 6.78 (s, 2H), 7.26 (s, 1H). MS (ESI): $[M+1]^+$=389.1 and 391.1.

Methyl 3-bromo-5-(4-(trifluoromethyl)phenyl)thiophene-2-carboxylate (8q). Following general procedure B, the crude residue was purified by flash chromatography, using ethyl acetate:petroleum ether 1:9 (v:v) as the eluting solution, to furnish **8q** as a brown solid (58% yield), mp 98-100 °C. ^{1}H-NMR ($CDCl_3$) δ: 3.93 (s, 3H), 7.36 (s, 1H), 7.69 (s, 4H). MS (ESI): $[M+1]^+$=364.1 and 366.2.

Methyl 3-bromo-5-(4-nitrophenyl)thiophene-2-carboxylate (8r). Following general procedure B, the crude residue was purified by flash chromatography, using ethyl acetate:petroleum ether 2:8 (v:v) as the eluting solution, to furnish **8r** as a yellow solid (67% yield), mp 224-226 °C. ^{1}H-NMR ($CDCl_3$) δ: 3.94 (s, 3H), 7.43 (s, 1H), 7.73 (d, *J*=8.2 Hz, 2H), 8.27 (d, *J*=8.8 Hz, 2H). MS (ESI): $[M+1]^+$=364.1 and 366.1.

General procedure C for the preparation of compounds 4a-r. A dry Schlenk tube was charged with dry toluene (5 mL), bromo derivative **8a-r** (0.5 mmol), $Pd(OAc)_2$ (13 mol%, 15 mg), *rac*-BINAP (4 mol%, 15 mg), Cs_2CO_3 (230 mg, 0.7 mmol, 1.4 equiv.) and 3,4,5-trimethoxyaniline (137 mg, 0.75 mmol, 1.5 equiv.) under Ar, and the mixture was heated at 100 °C for 18 h. After cooling, the mixture was filtered through a pad of celite and the filtrate diluted with EtOAc (10 mL) and water (5 mL). The organic phase was washed with brine (5 mL), dried and concentrated under vacuum. The residue was purified by column chromatography on silica gel to furnish **4a-r**.

Methyl 5-phenyl-3-[(3,4,5-trimethoxyphenyl)amino]thiophene-2-carboxylate (4a). Following general procedure C, the crude residue was purified by flash chromatography, using ethyl acetate:petroleum ether 2:8 (v:v) as the eluting solution, to furnish **4a** as a yellow solid (52% yield), mp 120-121 °C. ^{1}H-NMR ($CDCl_3$) δ: 3.85 (s, 9H), 3.89 (s, 3H), 6.47 (s, 2H), 7.37 (m, 4H), 7.61 (m, 2H), 8.67 (s, 1H). ^{13}C-NMR ($CDCl_3$) δ: 56.30 (2x), 61.14, 65.96, 99.13 (2x), 113.70, 114.57, 126.08 (2C), 127.87, 129.16 (2C), 129.28, 133.46, 134.52, 137.47, 149.73, 152.32, 153.88 (2C). MS (ESI): $[M+1]^+$=400.5. Anal. calcd for $C_{21}H_{21}NO_5S$. C, 63.14; H, 5.30; N, 3.51; found: C, 63.01; H, 5.13; N, 3.36.

Ethyl 5-phenyl-3-[(3,4,5-trimethoxyphenyl)amino]thiophene-2-carboxylate (4b). Following general procedure C, the crude residue was purified by flash chromatography, using ethyl acetate:petroleum ether 3:7 (v:v) as the eluting solution, to furnish **4b** as a yellow solid (81% yield), mp 124-125 °C. ^{1}H-NMR ($CDCl_3$) δ: 1.36 (t, *J*=7.6 Hz, 3H), 3.85 (s, 9H), 4.33 (q, *J*=7.6 Hz, 2H), 6.46 (s, 2H), 7.37 (m, 4H), 7.56 (m, 2H), 8.70 (s, 1H). ^{13}C-NMR ($CDCl_3$) δ: 14.63, 56.29 (2C), 60.47, 61.14, 99.02 (2C), 113.71, 114.52, 126.07 (2C), 127.78, 129.15 (2C), 129.22, 133.52, 134.48, 137.55, 149.51, 152.17, 153.88 (2C). MS (ESI): $[M+1]^+$=414.4. Anal. calcd for $C_{22}H_{23}NO_5S$: C, 63.90; H, 5.61; N, 3.39; found: C, 63.76; H, 5.45; N, 3.29.

Methyl 4-[(3,4,5-trimethoxyphenyl)amino]-[2,2'-bithiophene]-5-carboxylate (4c). Following general procedure C, the crude residue was purified by flash chromatography, using ethyl acetate:petroleum ether 2:8 (v:v) as the eluting solution, to furnish **4c** as a yellow solid (58% yield), mp 167-169 °C. ^{1}H-NMR ($CDCl_3$) δ: 3.85 (s, 9H), 3.88 (s, 3H), 6.45 (s, 2H), 7.13 (s, 1H), 7.26 (m, 1H), 7.35 (dd, *J*=5.2 and 3.0 Hz, 1H), 7.48 (m, 1H), 8.67 (s, 1H). ^{13}C-NMR ($CDCl_3$) δ: 51.53, 56.29 (2C), 61.14, 99.16 (2C), 113.65, 122.10, 125.82, 127.03, 134.54, 134.97, 137.43, 144.32, 152.27, 152.88, 153.86 (2C), 165.29. MS (ESI): $[M+1]^+$=405.9. Anal. calcd for $C_{19}H_{19}NO_5S_2$: C, 56.28; H, 4.72; N, 3.45; found: C, 56.20; H, 4.59; N, 3.36.

Methyl 5-(4-fluorophenyl)-3-[(3,4,5-trimethoxyphenyl)amino]thiophene-2-carboxylate (4d). Following general procedure C, the crude residue was purified by flash chromatography, using ethyl acetate:petroleum ether 2:8 (v:v) as the eluting solution, to furnish **4d** as a yellow solid (82% yield), mp 160-161 °C. ^{1}H-NMR ($CDCl_3$) δ: 3.85 (s, 9H), 3.89 (s, 3H), 6.46 (s, 2H), 7.05 (t, *J*=8.8 Hz, 2H), 7.17 (s, 1H), 7.52 (dd, *J*=8.8 and 5.2 Hz, 2H), 8.66 (s, 1H). ^{13}C-NMR ($CDCl_3$) δ: 51.59, 56.32 (2x), 61.14, 99.31 (2x), 113.69, 115.57, 116.12 (2C), 116.34 (2C), 127.87, 127.95, 135.32, 137.37, 148.53, 151.13, 152.42, 153.89 (2C). MS (ESI): $[M+1]^+$=418.2. Anal. calcd for $C_{21}H_{20}FNO_5S$: C, 60.42; H, 4.83; N, 3.36; found: C, 60.29; H, 4.69; N, 3.30.

Ethyl 5-(4-fluorophenyl)-3-[(3,4,5-trimethoxyphenyl)amino]thiophene-2-carboxylate (4e). Following general procedure C, the crude residue was purified by flash chromatography, using ethyl acetate:petroleum ether 2:8 (v:v) as the eluting solution, to furnish **4e** as a yellow solid (77% yield), mp 150-151 °C. ^{1}H-NMR ($CDCl_3$) δ: 1.39 (t, *J*=7.2 Hz, 3H), 3.84 (s, 6H), 3.85 (s, 3H), 4.32 (q, *J* =7.2 Hz, 2H), 6.45 (s, 2H), 7.06 (t, *J* =8.8 Hz,

2H), 7.18 (s, 1H), 7.53 (dd, *J*=8.8 and 5.2 Hz, 2H), 8.68 (s, 1H). ^{13}C-NMR ($CDCl_3$) δ: 10.59, 52.28 (2C), 56.45, 57.10, 95.17 (2C), 109.66 (2C), 112.06 (2C), 112.27, 123.79 (J=33.6 Hz), 125.78, 130.55, 133.42, 144.28, 148.21, 149.85, 158.03, 160.90 (2C). MS (ESI): $[M+1]^+$=432.2. Anal. calcd for $C_{22}H_{22}FNO_5S$: C, 61.24; H, 5.14; N, 3.25; found: C, 61.09; H, 5.02; N, 3.13.

Methyl 5-(4-chlorophenyl)-3-[(3,4,5-trimethoxyphenyl)amino]thiophene-2-carboxylate (4f). Following general procedure C, the crude residue was purified by flash chromatography, using ethyl acetate:petroleum ether 2:8 (v:v) as the eluting solution, to furnish **4f** as a yellow solid (62% yield), mp 164-166 °C. ^{1}H-NMR ($CDCl_3$) δ: 3.85 (s, 9H), 3.89 (s, 3H), 6.45 (s, 2H), 7.21 (s, 1H), 7.34 (d, *J*=8.6 Hz, 2H), 7.48 (d, *J*=8.6 Hz, 2H), 8.65 (s, 1H). ^{13}C-NMR ($CDCl_3$) δ: 51.61, 56.32 (2C), 61.14, 99.35 (2C), 113.95, 127.27 (2C), 129.35 (2C), 131.98, 134.72, 135.18, 137.32, 148.19, 151.09, 152.40, 153.89 (2C), 165.20. MS (ESI): $[M+1]^+$=434.2. Anal. calcd for $C_{21}H_{20}ClN_2O_5S$: C, 58.13; H, 4.65; N, 3.23; found: C, 58.01; H, 4.55; N, 3.12.

Ethyl 5-(4-chlorophenyl)-3-[(3,4,5-trimethoxyphenyl)amino]thiophene-2-carboxylate (4g). Following general procedure C, the crude residue was purified by flash chromatography, using ethyl acetate:petroleum ether 3:7 (v:v) as the eluting solution, to furnish **4g** as a yellow solid (64% yield), mp 137-139 °C. ^{1}H-NMR ($CDCl_3$) δ: 1.36 (t, *J*=7.0 Hz, 3H), 3.84 (s, 6H), 3.85 (s, 3H), 4.30 (q, *J*=7.0 Hz, 2H), 6.45 (s, 2H), 7.21 (s, 1H), 7.34 (d, *J*=8.6 Hz, 2H), 7.49 (d, *J*=8.6 Hz, 2H), 8.67 (s, 1H). ^{13}C-NMR ($CDCl_3$) δ: 14.62, 56.32 (2C), 60.54, 61.13, 99.25 (2C), 113.97, 127.25 (2C), 129.35 (2C), 132.05, 134.70, 135.12, 137.41, 147.98, 151.00, 152.24, 153.89 (2C), 164.91. MS (ESI): $[M+1]^+$=448.2. Anal. calcd for $C_{22}H_{22}ClN_2O_5S$: C, 58.99; H, 4.95; N, 3.13; found: C, 58.79; H, 4.82; N, 3.01.

Methyl 5-(3,4-dichlorophenyl)-3-[(3,4,5-trimethoxyphenyl)amino]thiophene-2-carboxylate (4h). Following general procedure C, the crude residue was purified by flash chromatography, using ethyl acetate:petroleum ether 2:8 (v:v) as the eluting solution, to furnish **4h** as a yellow solid (78% yield), mp 167-168 °C. ^{1}H-NMR (*d_6*-DMSO) δ: 3.64 (s, 3H), 3.78 (s, 6H), 3.82 (s, 3H), 6.60 (s, 2H), 7.69 (d, *J*=8,2 Hz, 1H), 7.71 (m, 2H), 8.09 (d, *J*=2.0 Hz, 1H), 8.70 (s, 1H). ^{13}C-NMR ($CDCl_3$) δ: 51.53, 55.75 (2C), 59.97, 99.22 (2C), 101.78, 116.26, 125.99, 127.58, 131.14, 131.64, 131.96, 133.06, 133.31, 136.75, 145.28, 150.98, 153.22 (2C), 163.63. MS (ESI): $[M]^+$=468.2. Anal. calcd for $C_{21}H_{19}Cl_2NO_5S$: C, 53.85; H, 4.09; N, 2.99; found: C, 53.68; H, 3.97; N, 2.79.

Methyl 5-(p-tolyl)-3-[(3,4,5-trimethoxyphenyl)amino]thiophene-2-carboxylate (4i). Following general procedure C, the crude residue was purified by flash chromatography, using ethyl acetate:petroleum ether 3:7 (v:v) as the eluting solution, to furnish **4i** as a yellow solid (85% yield), mp 135-136 °C. ^{1}H-NMR ($CDCl_3$) δ: 2.37 (s, 3H), 3.84 (s, 3H), 3.85 (s, 6H), 3.88 (s, 3H), 6.46 (s, 2H), 7.18 (d, *J*=8.2 Hz, 2H), 7.26 (s, 1H), 7.48 (d, *J*=8.2 Hz, 2H), 8.67 (s, 1H). ^{13}C-NMR ($CDCl_3$) δ: 21.39, 51.51, 56.28 (2C), 61.14, 99.06 (2C), 113.17, 125.96 (2C), 129.82 (2C), 130.68, 134.46, 137.51, 139.50, 149.98, 152.36, 152.88, 153.86 (2C), 165.33. MS (ESI): $[M+1]^+$=414.0, Anal. calcd for $C_{22}H_{23}NO_5S$: C, 63.90; H, 5.61; N, 3.39; found: C, 63.78; H, 5.51; N, 3.27.

Ethyl 5-(p-tolyl)-3-[(3,4,5-trimethoxyphenyl)amino]thiophene-2-carboxylate (4j). Following general procedure C, the crude residue was purified by flash chromatography, using ethyl acetate:petroleum ether 2:8 (v:v) as the eluting solution, to furnish **4j** as a yellow solid (80% yield), mp 141-143 °C. ^{1}H-NMR ($CDCl_3$) δ: 1.36 (t, *J*=7.2 Hz, 3H), 2.37 (s, 3H), 3.84 (s, 9H), 4.33 (q, *J*=7.2 Hz, 2H), 6.45 (s, 2H), 7.17 (d, *J*=8.4 Hz, 2H), 7.23 (s, 1H), 7.46 (d, *J*=8.4 Hz, 2H), 8.70 (s, 1H). ^{13}C-NMR ($CDCl_3$) δ: 14.62, 21.36, 56.26 (2C), 60.38, 61.11, 98.93 (2C), 113.17, 125.92 (2C), 129.79 (2C), 130.71, 134.37, 137.58, 139.41, 149.73, 152.16, 152.88, 153.83 (2C), 165.00. MS (ESI): $[M+1]^+$=428.2. Anal. calcd for $C_{23}H_{25}NO_5S$: C, 64.62; H, 5.89; N, 3.28; found: C, 64.51; H, 5.74; N, 3.16.

Methyl 5-(4-methoxyphenyl)-3-[(3,4,5-trimethoxyphenyl)amino]thiophene-2-carboxylate (4k). Following general procedure C, the crude residue was purified by flash chromatography, using ethyl acetate:petroleum ether 3:7 (v:v) as the eluting solution, to furnish **4k** as a yellow solid (78% yield), mp 134-136 °C. ^{1}H-NMR ($CDCl_3$) δ: 3.84 (s, 6H), 3.85 (s, 6H), 3.88 (s, 3H), 6.46 (s, 2H), 6.89 (d, *J*=8.6 Hz, 2H), 7.16 (s, 1H), 7.47 (d, *J*=8.6 Hz, 2H), 8.68 (s, 1H). ^{13}C-NMR ($CDCl_3$) δ: 51.49, 55.51, 56.29 (2x), 61.14, 99.10 (2x), 112.60, 114.52, 126.18, 127.44 (2C), 136.32, 137.53 (2C), 148.34, 149.85, 151.13, 153.85 (2C), 160.59. MS (ESI): $[M+1]^+$=430.1. Anal. calcd for $C_{22}H_{23}NO_6S$: C, 61.52; H, 5.40; N, 3.26; found: C, 61.43; H, 5.30; N, 3.15.

Ethyl 5-(4-methoxyphenyl)-3-[(3,4,5-trimethoxyphenyl)amino]thiophene-2-carboxylate (4l). Following general procedure C, the crude residue was purified by flash chromatography, using ethyl acetate:petroleum ether 2:8 (v:v) as the eluting solution, to furnish **4l** as a yellow solid (76% yield), mp 150-151 °C. ^{1}H-NMR ($CDCl_3$) δ: 1.37 (t, *J* =7.2 Hz, 3H), 3.84 (s, 6H), 3.85 (s, 6H), 4.32 (q, *J* =7.2 Hz, 2H), 6.46 (s, 2H), 6.90 (dd, *J* =6.8

and 2.0 Hz, 2H), 7.16 (s, 1H), 7.51 (dd, *J* =6.8 and 2.0 Hz, 2H), 8.71 (s, 1H). ^{13}C-NMR ($CDCl_3$) δ: 14.66, 55.49, 56.29 (2C), 60.37, 61.14, 98.99 (2C), 112.61, 114.50 (2C), 126.26, 127.41 (2C), 134.40, 137.60, 146.24, 148.36, 149.62, 152.30, 153.85 (2C), 160.54, 165.03. MS (ESI): $[M+1]^+$=444.3. Anal. calcd for $C_{23}H_{25}NO_6S$: C, 62.29; H, 5.68; N, 3.16; found: C, 62.10; H, 5.54; N, 3.02.

Methyl 5-(4-ethoxyphenyl)-3-[(3,4,5-trimethoxyphenyl)amino]thiophene-2-carboxylate (4m). Following general procedure C, the crude residue was purified by flash chromatography, using ethyl acetate:petroleum ether 3:7 (v:v) as the eluting solution, to furnish **4m** as a yellow solid (74% yield), mp 147-149 °C. ^{1}H-NMR ($CDCl_3$) δ: 1.43 (t, *J*=7.0 Hz, 3H), 3.82 (s, 3H), 3.85 (s, 6H), 3.87 (s, 3H), 4.04 (q, *J*=7.0 Hz, 2H), 6.46 (s, 2H), 6.88 (d, *J*=8.8 Hz, 2H), 7.15 (s, 1H), 7.48 (d, *J*=8.8 Hz, 2H), 8.68 (s, 1H). ^{13}C-NMR ($CDCl_3$) δ: 14.82, 51.46, 56.28 (2C), 61.12, 63.71, 99.10 (2C), 112.50, 114.99 (2C), 125.97, 127.39 (2C), 130.54, 134.46, 137.52, 149.43, 152.46, 153.83 (2C), 159.97, 165.31. MS (ESI): $[M+1]^+$=444.2. Anal. calcd for $C_{23}H_{25}NO_6S$: C, 62.29; H, 5.68; N, 3.16; found: C, 62.09; H, 5.51; N, 3.00.

Methyl 5-(3-methoxyphenyl)-3-[(3,4,5-trimethoxyphenyl)amino]thiophene-2-carboxylate (4n). Following general procedure C, the crude residue was purified by flash chromatography, using ethyl acetate:petroleum ether 3:7 (v:v) as the eluting solution, to furnish **4n** as a yellow solid (65% yield), mp 127-129 °C. ^{1}H-NMR ($CDCl_3$) δ: 3.84 (s, 6H), 3.85 (6H), 3.89 (s, 3H), 6.46 (s, 2H), 6.89 (td, *J*=8.0, 2.2 and 1.0 Hz, 1H), 7.09 (t, *J*=2.2 Hz, 1H), 7.15 (m, 1H), 7.24 (d, *J*=5.8 Hz, 1H), 7.31 (d, *J*=8.0 Hz, 1H), 8.64 (s, 1H). ^{13}C-NMR ($CDCl_3$) δ: 51.57, 55.45, 56.28 (2x), 61.14, 99.09 (2x), 111.79, 113.91, 114.68, 118.60, 130.21, 134.52, 134.77, 137.44, 149.54, 152.24, 152.38, 152.78, 153.87 (2C), 160.07. MS (ESI): $[M+1]^+$=430.1. Anal. calcd for $C_{22}H_{23}NO_6S$: C, 61.52; H, 5.40; N, 3.26; found: C, 61.40; H, 5.26; N, 3.11.

Methyl 5-(3,4-dimethoxyphenyl)-3-[(3,4,5-trimethoxyphenyl)amino]thiophene-2-carboxylate (4o). Following general procedure C, the crude residue was purified by flash chromatography, using ethyl acetate:petroleum ether 3:7 (v:v) as the eluting solution, to furnish **4o** as a yellow solid (80% yield), mp 160-162 °C. ^{1}H-NMR ($CDCl_3$) δ: 3.84 (s, 6H), 3.85 (s, 3H), 3.88 (s, 3H), 3.91 (s, 6H), 6.47 (s, 2H), 6.86 (d, *J*=8.6 Hz, 1H), 7.05 (d, *J*=2.2 Hz, 1H), 7.15 (m, 2H), 8.68 (s, 1H). ^{13}C-NMR ($CDCl_3$) δ: 51.47, 56.03, 56.22 (2C), 61.10, 99.01 (2C), 112.60, 100.72, 109.18, 111.41, 112.76, 118.89, 126.40, 134.42, 137.47, 149.26,

149.89, 150.15, 152.31, 153.82 (2C), 165.21. MS (ESI): $[M+1]^+$=460.1. Anal. calcd for $C_{23}H_{25}NO_7S$: C, 60.12; H, 5.48; N, 3.05; found: C, 59.96; H, 5.38; N, 2.88.

Methyl 5-(3,4,5-trimethoxyphenyl)-3-[(3,4,5-trimethoxyphenyl)amino]thiophene-2-carboxylate (4p). Following general procedure C, the crude residue was purified by flash chromatography, using ethyl acetate:petroleum ether 4:6 (v:v) as the eluting solution, to furnish **4p** as a yellow solid (80% yield), mp 200-201 °C. ^{1}H-NMR ($CDCl_3$) δ: 3.84 (s, 6H), 3.85 (s, 3H), 3.87 (s, 9H), 3.89 (s, 3H), 6.47 (s, 2H), 6.77 (s, 2H), 7.17 (s, 1H), 8.67 (s, 1H). ^{13}C-NMR ($CDCl_3$) δ: 51.54, 56.25 (2C), 56.31 (2C), 61.06, 61.12, 99.12 (2C), 103.56 (2C), 113.50, 129.15, 134.55, 136.26, 137.43, 139.26, 149.82, 152.18, 153.66 (2C), 153.89 (2C), 165.17. MS (ESI): $[M+1]^+$=490.2. Anal. calcd for $C_{24}H_{27}ClNO_8S$: C, 58.88; H, 5.56; N, 2.86; found: C, 58.76; H, 5.39; N, 2.72.

Methyl 5-(4-trifluorophenyl)-3-[(3,4,5-trimethoxyphenyl)amino]thiophene-2-carboxylate (4q). Following general procedure C, the crude residue was purified by flash chromatography, using ethyl acetate:petroleum ether 4:6 (v:v) as the eluting solution, to furnish **4q** as a yellow solid (80% yield), mp 223-225 °C. ^{1}H-NMR (d_6-DMSO) δ: 3.64 (s, 3H), 3.78 (s, 6H), 3.83 (s, 3H), 6.62 (s, 2H), 7.70 (s, 1H), 7.77 (d, *J*=8.4 Hz, 2H), 7.97 (d, *J*=8.4 Hz, 2H), 8.71 (s, 1H). ^{13}C-NMR (d_6-DMSO) δ: 51.55, 55.78 (2C), 59.98, 98.26 (2C), 102.09, 116.26 (2C), 126.02, 126.57 (2C), 129.34, 133.35, 136.23, 136.79, 146.09, 147.23, 150,98, 153.25 (2C), 163.62. MS (ESI): $[M+1]^+$=468.2. Anal. calcd for $C_{22}H_{20}F_3NO_5S$: C, 56.53; H, 4.31; N, 3.00; found: C, 56.42; H, 4.18; N, 2.87.

Methyl 5-(4-nitrophenyl)-3-[(3,4,5-trimethoxyphenyl)amino]thiophene-2-carboxylate (4r). Following general procedure C, the crude residue was purified by flash chromatography, using ethyl acetate:petroleum ether 3:7 (v:v) as the eluting solution, to furnish **4r** as an orange solid (76% yield), mp 158-160 °C. ^{1}H-NMR (d_6-DMSO) δ: 3.65 (s, 3H), 3.78 (s, 6H), 3.84 (s, 3H), 6.62 (s, 2H), 7.77 (s, 1H), 8.02 (d, *J*=8.8 Hz, 2H), 8.23 (d, *J*=8.8 Hz, 2H), 8.70 (s, 1H). ^{13}C-NMR (d_6-DMSO) δ: 51.71, 55.85 (2C), 60.07, 98.49 (2C), 112.60, 117.28, 124.38 (2C), 127.00 (2C), 136.82, 138.57, 144.64. 145.22, 147.32, 151.09, 153.35 (2C), 163.63. MS (ESI): $[M+1]^+$=445.1. Anal. calcd for $C_{21}H_{20}N_2O_7S$: C, 56.75; H, 4.54; N, 6.30; found: C, 56.67; H, 4.44; N, 6.13.

Biological assays and computational studies

Cell growth conditions and antiproliferative assay. Murine leukemia L1210, murine mammary carcinoma FM3A, human T-lymphocyte leukemia CEM and human cervix carcinoma (HeLa) cells were suspended at 300,000-500,000 cells/mL of culture medium, and 100 μL of a cell suspension was added to 100 μL of an appropriate dilution of the test compounds in wells of 96-well microtiter plates. After incubation at 37 °C for two (L1210 and FM3A), three (CEM) or 4 (HeLa) days, cell number was determined using a Coulter counter. The IC_{50} value was defined as the compound concentration required to inhibit cell proliferation by 50%.

Peripheral blood lymphocytes (PBL) from healthy donors were obtained by separation on Lymphoprep (Fresenius KABI Norge AS) gradient. After extensive washing, cells were resuspended (1.0×10^6 cells/mL) in RPMI-1640 with 10% fetal bovine serum and incubated overnight. For cytotoxicity evaluations in proliferating PBL cultures, non-adherent cells were resuspended at 5×10^5 cells/mL in growth medium, containing 2.5 μg/mL PHA (Irvine Scientific), whereas for cytotoxicity evaluations in resting PBL cultures, non-adherent cells were resuspended (5×10^5 cells/mL) in the same medium without PHA. Different concentrations of the test compounds were added, and viability was determined 72 h later by the MTT assay as described previously.[32]

Effects on tubulin polymerization and on colchicine binding to tubulin. To evaluate the effect of the compounds on tubulin assembly *in vitro*,[33] varying concentrations of compounds were preincubated with 10 μM bovine brain tubulin in 0.8 M monosodium glutamate (pH adjusted to 6.6 with HCl in a 2.0 M stock solution) at 30 ˚C and then cooled to 0 ˚C. After addition of 0.4 mM GTP, the mixtures were transferred to 0 °C cuvettes in a recording spectrophotometer and warmed to 30 °C. Tubulin assembly was followed turbidimetrically at 350 nm. The IC_{50} was defined as the compound concentration that inhibited the extent of assembly by 50% after a 20 min incubation. The capacity of the test compounds to inhibit colchicine binding to tubulin was measured as described.[34] The reaction mixtures contained 1 μM tubulin, 5 μM [^{3}H]colchicine and 5 μM test compound.

Molecular modeling. All molecular modeling studies were performed on a MacPro dual 2.66 GHz Xeon running Ubuntu 14.04. The tubulin structure was downloaded from the PDB data bank (http://www.rcsb.org/; PDB code 1SA0).[35] Hydrogen atoms were added to the protein, using the Protonate 3D routine of the Molecular Operating Environment (MOE).[36] Ligand structures were built with MOE and minimized using the MMFF94x force field until

a RMSD gradient of 0.05 kcal mol^{-1} $Å^{-1}$ was reached. The docking simulations were performed using PLANTS.[37] A RMSD value of 1.5 Å was obtained when comparing the docked pose of DAMA-colchicine to its conformation present in the crystal structure.

Flow cytometric analysis of cell cycle distribution. 5×10^5 HeLa cells were treated with different concentrations of the test compounds for 24 h. After the incubation period, the cells were collected, centrifuged, and fixed with ice-cold ethanol (70%). The cells were then treated with lysis buffer containing RNase A and 0.1% Triton X-100 and then stained with PI. Samples were analyzed on a Cytomic FC500 flow cytometer (Beckman Coulter). DNA histograms were analyzed using MultiCycle for Windows (Phoenix Flow Systems).

Apoptosis assay. Cell death was determined by flow cytometry of cells double stained with annexin V/FITC and PI. The Coulter Cytomics FC500 (Beckman Coulter) was used to measure the surface exposure of PS on apoptotic cells according to the manufacturer's instructions (Annexin-V Fluos, Roche Diagnostics).

Analysis of mitochondrial potential and reactive oxygen species (ROS). The mitochondrial membrane potential was measured with the lipophilic cation JC-1 (Molecular Probes, Eugene, OR, USA), while the production of ROS was followed by flow cytometry using the fluorescent dye H_2DCFDA (Molecular Probes), as previously described.[35]

Western blot analysis. HeLa cells were incubated in the presence of **4c** and, after different times, were collected, centrifuged, and washed two times with ice-cold phosphate buffered saline (PBS). The pellet was then resuspended in lysis buffer. After the cells were lysed on ice for 30 min, lysates were centrifuged at 15000 x g at 4 °C for 10 min. The protein concentration in the supernatant was determined using the BCA protein assay reagents (Pierce, Italy). Equal amounts of protein (10 µg) were resolved using sodium dodecyl sulfate-polyacrylamide gel electrophoresis (Criterion Precast, BioRad, Italy) and transferred to an Immobilon-P membrane (Millipore). Membranes were blocked with a bovine serum albumin solution (3% in Tween PBS 1X) for at least 2 h at room temperature. Membranes were then incubated with primary antibodies against Bcl-2, PARP, cdc25c, cyclin B, p-$cdc2^{Tyr15}$, Mcl-1 (all from Cell Signaling) and β-actin (Sigma-Aldrich) and gently rotated overnight at 4 °C. Membranes were next incubated with peroxidase labeled secondary antibodies for 60 min. All membranes were visualized using ECL Select (GE Healthcare), and images were acquired using an Uvitec-Alliance imaging system (Uvitec, Cambridge,

UK). To ensure equal protein loading, each membrane was stripped and reprobed with anti-β-actin antibody.

3.6 References

1. R.J. van Vuuren, M.H. Visagie, A.E. Theron, A.M. Joubert. Antimitotic drugs in the treatment of cancer. Cancer Chemother Pharmacol. 76 (2015) 1101-1112.
2. A. Akhmanova, M.O. Steinmetz. Control of microtubule organization and dynamics: two ends in the limelight. Nat. Rev. Mol. Cell. Biol. 16 (2015) 711-726.
3. C. Janke. The tubulin code: molecular components, readout mechanisms, and functions. J. Cell Biol. 206 (2014) 461-472.
4. H.Y. Kueh, T.J. Mitchison. Structural plasticity in actin and tubulin polymer dynamics. Science. 325 (2009) 960-963.
5. G.J. Brouhard, L.M. Rice. The contribution of αβ-tubulin curvature to microtubule dynamics. J. Cell Biol. 207 (2014) 323-334.
6. E. Mukhtar, V.M. Adhami, H. Mukhtar. Targeting microtubules by natural agents for cancer therapy. Mol. Cancer Ther. 13 (2014) 275-284.
7. N. G. Vindya, N. Sharma, M. Yadav, K.R. Ethiraj. Tubulins-the target for anticancer therapy. Curr. Top. Med. Chem. 125 (2015) 73-82.
8. V. Nitika, K. Kapil. Microtubule targeting agents: a benchmark in cancer therapy. Curr. Drug Ther. 8 (2014) 189-196.
9. G. R. Pettit, S. B. Singh, E. Hamel, C. M. Lin, D. S. Alberts, D. Garcia-Kendall. Isolation and structure of the strong cell growth and tubulin inhibitor combretastatin A-4. Experientia 45 (1989) 209-211.
10. C. M. Lin, H. H. Ho, G. R. Pettit, E. Hamel. Antimitotic natural products combretastatin A-4 and combretastatin A-2: studies on the mechanism of their inhibition of the binding of colchicine to tubulin. Biochemistry 28 (1989) 6984-6991.
11. Y. T. Ji, Y. N. Liu, Z. P. Liu. Tubulin colchicine binding site inhibitors as vascular disrupting agents in clinical developments. Curr. Med. Chem. 22 (2015) 1348-1360.
12. L. M. Greene, M. J. Meegan, D. M. Zisterer. Combretastatins: more than just vascular targeting agents? J. Pharmacol. Exp. Ther. 355 (2015) 212-227.
13. M.-J. Pérez-Pérez, E. M. Priego, O. Bueno, M. S. Martins, M. D. Canela, S. Liekens, Blocking blood flow to solid tumors by destabilizing tubulin: an approach to targeting tumor growth, J. Med. Chem. 59 (2016) 8685-8711

14. a) R. Romagnoli, P. G. Baraldi, M. Kimatrai Salvador, D. Preti, M. Aghazadeh Tabrizi, M. Bassetto, A. Brancale, E. Hamel, I. Castagliuolo, R. Bortolozzi, G. Basso, G. Viola. Synthesis and biological evaluation of 2-alkoxycarbonyl-3-Anilino benzo[*b*]thiophenes and thieno[2,3-*c*]pyridines as new potent anticancer agents. J. Med. Chem. 56 (2013) 2606-2618; b) G. F. Mangiatordi , D. Trisciuzzi, D. Alberga, N. Denora, R. M. Iacobazzi, D. Gadaleta, M. Catto, O. Nicolotti. Novel chemotypes targeting tubulin at the colchicine binding site and unbiasing P-glycoprotein. Eur. J. Med. Chem. 139 (2017) 792-803.
15. R. Romagnoli, P. G. Baraldi, M.K. Salvador, M.E. Camacho, D. Preti, M. Aghazadeh Tabrizi, M. Bassetto, A. Brancale, E. Hamel, R. Bortolozzi, G. Basso, G. Viola. Synthesis and biological evaluation of 2-substituted-4-(3',4',5'-trimethoxyphenyl)-5-aryl thiazoles as anticancer agents. Bioorg. Med. Chem. 20 (2012) 7083-7094.
16. For the characterization of compounds **6a-f** see: R. Romagnoli, P. G. Baraldi, V. Remusat, M. D. Carrion, C. Lopez Cara, D. Preti, F. Fruttarolo, M. G. Pavani, M. Aghazadeh Tabrizi, M. Tolomeo, S. Grimaudo, J. Balzarini, M. A. Jordan, E. Hamel. Synthesis and biological evaluation of 2-(3',4',5'-trimethoxybenzoyl)-3-amino 5-aryl thiophenes as a new class of tubulin inhibitors. J. Med. Chem. 49 (2006) 6425-6428.
17. R. Romagnoli, P. G. Baraldi, A. Brancale., A. Ricci, E. Hamel, R. Bortolozzi, G. Basso, G. Viola. Convergent synthesis and biological evaluation of 2-amino-4-(3',4',5'-trimethoxyphenyl)-5-arylthiazoles as microtubule targeting agents. J. Med. Chem. 54 (2011) 5144-5153.
18. R. Romagnoli, P. G. Baraldi, F. Prencipe, P. Oliva, S. Baraldi, M. Kimatrai Salvador, L. C. Lopez Cara, A. Brancale, S. Ferla, R. Ronca, R. Bortolozzi, E. Mariotto, E. Porcù, G. Basso, G. Viola. Synthesis and biological evaluation of 2-methyl-4,5-disubstituted oxazoles as a novel class og highly potent tubulin polymerization inhibitors. derivatives as novel anticancer agents. Sci Rep. (2017) 7:46356.
19. B. A. A. Weaver, D. W. Cleveland. Decoding the links between mitosis, cancer, and chemotherapy: the mitotic checkpoint, adaptation, and cell death. Cancer Cell 8 (2005) 7-12.
20. P. R. Clarke, L. A. Allan. Cell-cycle control in the face of damage- a matter of life or death. Trends Cell Biol. 19 (2009) 89-98.
21. Y. Tsujimoto, S. Shimizu. Role of the mitochondrial membrane permeability transition in cell death. Apoptosis. 12 (2007) 835-840.

22. S. Xiong, T. Mu, G. Wang, X Jiang. Mitochondria-mediated apoptosis in mammals. Protein Cell 5 (2014) 737-749.

23. E. Lugli, L. Troiano, A. Cossarizza. Polychromatic analysis of mitochondrial membrane potential using JC-1. Curr Protoc Cytom. 2007 Jul;Chapter 7:Unit 7.32.

24. N. Zamzami, P. Marchetti, M. Castedo, D. Decaudin, A. Macho, T. Hirsch, S. A. Susin, P. X. Petit, B. Mignotte, G. Kroemer. Sequential reduction of mitochondrial transmembrane potential and generation of reactive oxygen species in early programmed cell death. J. Exp. Med. 182 (1995) 367-377.

25. J. Cai, D. P. Jones Superoxide in apoptosis. Mitochondrial generation triggered by cytochrome c loss. J. Biol. Chem. 273 (1998) 11401-11404.

26. A. Rovini, A. Savry, D. Braguer, M. Carré. Microtubule-targeted agents: when mitochondria become essential to chemotherapy. Biochim. Biophys. Acta - Bioenerg. 6 (2011) 679–688.

27. R. Romagnoli, P. G. Baraldi. C. Lopez-Cara, D. Preti, M. Aghazadeh Tabrizi, J. Balzarini, M. Bassetto, A. Brancale, F. Xian-Hua, Y. Gao, J. Li, S.-Z. Zhang, E. Hamel, R. Bortolozzi, G. Basso, G. Viola. Concise synthesis and biological evaluation of 2-aroyl-5-amino benzo[*b*]thiophene derivatives as a novel class of potent antimitotic agents. J. Med. Chem. 56, (2013), 9296-9309.

28. R. Romagnoli, P. G. Baraldi, M. Kimatrai Salvador, S. Schiaffino Ortega, F. Prencipe, A. Brancale, E. Hamel, I. Castagliuolo., S. Mitola., R. Ronca, R. Bortolozzi, E. Porcù, G. Basso, G. Viola. Design, synthesis, in vitro and in vivo anticancer and antiangiogenic activity of novel 3-arylamino benzofuran derivatives targeting the colchicine site on tubulin. J. Med. Chem. 58 (2015) 3209-3222.

29. M. D. Haschka, C. Soratroi, S. Kirschnek, G. Häcker, R. Hilbe, S. Geley, A Villunger, L. L. Fava. The NOXA-MCL1-BIM axis defines lifespan on extended mitotic arrest. Nat. Commun. 6 (2015) 6891.

30. M. E. Harley, L. A. Allan, H. S. Sanderson, P. R. Clarke. Phosphorylation of Mcl-1 by CDK1-cyclin B1 initiates its Cdc20-dependent destruction during mitotic arrest. EMBO J. 29 (2010) 2407-2420.

31. I. E. Wertz, S. Kusam, C. Lam, T. Okamoto, W. Sandoval, D. J. Anderson, E. Helgason, J. A. Ernst, M. Eby, J. Liu, L. D. Belmont, J. S. Kaminker, K. M. O'Rourke, K. Pujara, P. B. Kohli, A. R. Johnson, M. L. Chiu, J. R. Lill, P. K. Jackson, W. J. Fairbrother, S. Seshagiri, M. J. Ludlam, K. G. Leong, E. C. Dueber, H. Maecker, D. C. Huang, V. M. Dixit. Sensitivity to antitubulin chemotherapeutics is regulated by MCL1 and FBW7. Nature 471 **(**2011) 110-114.

32. M. G. Ferlin, R. Bortolozzi, P. Brun, I. Castagliuolo, E. Hamel, G. Basso, G. Viola. Synthesis and in vitro evaluation of 3*H*-pyrrolo[3,2-*f*]-quinolin-9-one derivatives that show potent and selective anti-leukemic activity. ChemMedChem, 5 (2010), 1373-1385.

33. E. Hamel. Evaluation of antimitotic agents by quantitative comparisons of their effects on the polymerization of purified tubulin. Cell Biochem. Biophys. 38 (2003) 1-21.

34. P. Verdier-Pinard, J.-Y. Lai, H.-D. Yoo, J. Yu, B. Marquez, D. G. Nagle, M. Nambu, J. D. White, J. R. Falck, W. H. Gerwick, B. W. Day, E. Hamel. Structure-activity analysis of the interaction of curacin A, the potent colchicine site antimitotic agent, with tubulin and effects of analogs on the growth of MCF-7 breast cancer cells. Mol. Pharmacol. 53 (1998) 62-67.

35. R. B. G. Ravelli, B. Gigant, P. A. Curmi, I. Jourdain, S. Lachkar, A. Sobel, M. Knossow. Insight into tubulin regulation from a complex with colchicine and a stathmin-like domain. Nature 428 (2004) 198-202.

36. Molecular Operating Enviroment (MOE 2015.10); Chemical Computing Group, Inc; Montreal, Quebec, Canada, 2015; http://www.chemcomp.com.

37. O. Korb, T. Stützle, T. E. Exner. PLANTS: Application of ant colony optimization to structure-based drug design. In *Ant Colony Optimization and Swarm Intelligence*, 5th International Workshop, ANTS 2006, Brussels, Belgium, Sep 4-7, 2006. M. Dorigo, L.M. Gambardella, M. Birattari, A.; Martinoli, R. Poli, T. Sttzle. Eds.; Springer: Berlin, 2006; LNCS 4150, 247-258.

4. Design, Synthesis and Biological Evaluation of 6-Substituted Thieno[3,2-*d*]pyrimidine Analogues as Dual Epidermal Growth Factor Receptor Kinase and Microtubule Inhibitors

4.1 Introduction

Cellular microtubules are formed by the non-covalent polymerization of α- and β-tubulin heterodimers and act as an essential element of the cytoskeleton. Microtubules are crucial for multiple functions in cells, especially the development and function of the mitotic spindle during mitosis, but also for establishing the shape of the cell, intracellular transport, secretion, and cell movement.[1] Their importance for cell structure and function, together with their long history of utility in cancer chemotherapy, has kept microtubules important for anticancer drug discovery, and agents that target them are among the most reliable chemotherapeutics.[2] A substantial number of compounds, representing many chemotypes, bind to tubulin or microtubules and inhibit or enhance tubulin polymerization.[3] Moreover, several small molecules inhibiting tubulin polymerization are able to damage the already existing vasculature in developing tumour, acting as vascular disrupting agents (VDAs).[4]

Originally derived from a South African tree,[5] combretastatin A-4 (CA-4, **1a**, Figure 1) is a widely studied molecule that inhibits tubulin assembly by binding to the colchicine site.[6] The disodium phosphate prodrug of CA-4 (CA-4P, **1b**) is water-soluble, and there have been promising results with **1b** as a tumour VDA in phase II clinical trials.[7] The properties of CA-4, including its simple structure and its potent destructive effects on tumour blood vessels, has made **1a** widely studied by medicinal chemists.[8]

A growing body of evidence has shown that antimitotic agents, and in particular microtubule destabilizing drugs, have multiple effects beyond mitosis.[9] Several lines of evidence suggested mixed mechanisms that are not so far fully understood to explain the activities of tubulin binding agents, and these mechanisms probably extend beyond simple antimitotic effects. Moreover, there is evidence that the efficacy of microtubule targeting agents also involve interphase effects.[10]

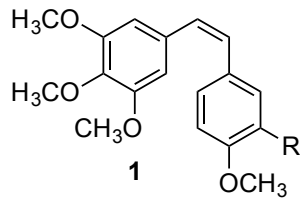

1

R=OH, Combretastatin A-4 (CA-4), **1a**
R=OPO_3Na_2, CA-4P, **1b**

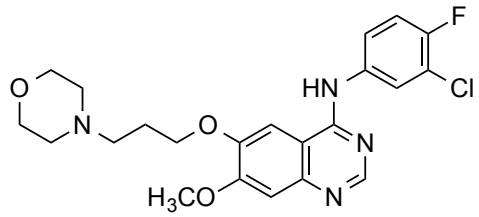

Gefitinib (**2a**)

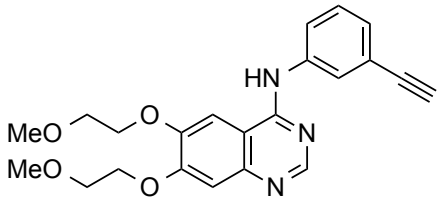

Erlotinib (**2b**)

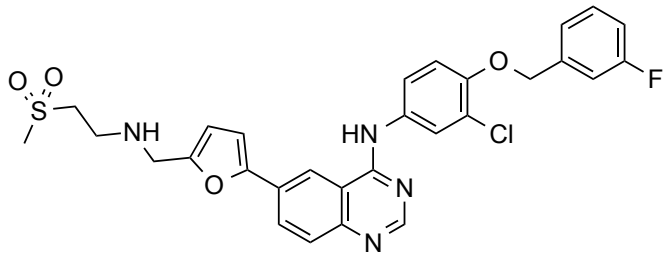

Lapatinib (**2c**)

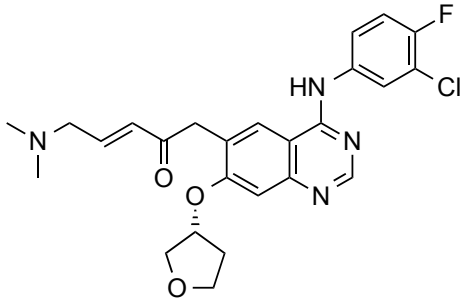

Afatinib (**2d**)

Figure 1. Structures of tubulin depolymerizing agents CA-4 and CA-4P and selected EGFR (**2a-d**) and VEGFR-2 (**2e**) tyrosine kinase inhibitors.

Signal transduction in mammalian cells involves many receptor kinases. Particularly important is the epidermal growth factor receptor, which is a *trans*-membrane bound molecule that has important regulatory functions affecting tumour growth and progression. These include cell proliferation, differentiation, migration, apoptosis and angiogenesis.[11] EGFR kinase, consisting of ErB1 and HER1, belongs to the ErbB family of kinases, which also includes human epidermal growth factor receptor-2 (subunits: HER2 and ErbB-2), human epidermal growth factor receptor-3 (subunits: HER3 and ErbB-3), and human epidermal growth factor receptor-4 (subunits: HER4 and ErbB-4).[12] Among the known receptor tyrosine kinases (RTKs), the ErbB family, in particular EGFR and HER2, have been extensively studied and clinically validated as targets for cancer therapies, being over-

expressed in a wide number of human tumours and associated with cancer proliferation, angiogenesis and metastasis.[13] With no bound ligand, EGFR is in monomeric form of the cell surface. When ligand is bound, EGFR forms homodimers with itself and heterodimers with other ErbB family members.[14] There are currently eight drugs approved by the FDA targeting this family: four monoclonal antibodies (trastuzumab, cetuximab, panitumumab and pertuzumab) and four small-molecule inhibitors based on a central 4-aminoarylquinazoline core [Gefitinb (**2a**), erlotinib (**2b**), lapatinib (**2c**) and afatinib (**2d**)].[15] These latter synthetic EGFR inhibitors have been approved by the FDA for the treatment of patients with non-small cell lung cancer (NSCLC).[16] Unfortunately, the duration of benefit derived from tyrosine kinase inhibitor based-therapy is relatively short, due to the development of acquired resistance.[17a] The development of multi-targeted inhibitors represents a valid approach to overcome the acquired drug resistance to tyrosine kinase inhibitors.[17b] Twelve clinical trials were found on clinicaltrials.gov site (accessed in October 2018) in which the FDA approved the EGFR kinase inhibitors gefitinib, erlotinib and lapatinib were being used in combination with the microtubule targeting agents docetaxel, vinorelbine, paclitaxel and other chemotherapeutic agents for the treatment of a variety of cancers including, lung cancer, head and neck cancer and hepatocellular carcinoma.[18]

A large number of thienopyrimidine derivatives have been reported to show remarkable antitumor activity against different cancer types by means of inhibiting multiple enzymes, as well as by modulating the activity of many receptors.[19] In an effort to develop non-quinazoline EGFR inhibitors, using the strategy known as “scaffold hopping”, bio isosteric thieno[2,3-*d*]pyrimidine and thieno[3,2-*d*]pyrimidine scaffolds have been reported as interesting structural elements employed for the development of novel EGFR or EGFR with vascular growth factor receptor-2 (VEGFR-2) dual inhibition.[20]

Munchhof et al. reported the design and structure-activity relationship (SAR) of a series of 6-aryl substituted thieno[3,2-*d*]pyrimidines with general structure **3**, identified as VEGFR-2 and EGFR dual inhibitors (Figure 2).[21] Kemnitzer and colleague reported the discovery of *N*-methyl-4-(methoxyanilino)thieno[3,2-*d*]pyrimidine **4** as a potent apoptosis inducer through inhibition of tubulin assembly, with IC_{50}<1 μM in the tubulin polymerization assay.[22] This compound inhibited the growth of a panel of five cancer cell lines (T-47D, HT-29, H-1299, MX-1 and MDAAMB 435) with IC_{50} values ranging from 4 to 40 nM. Much research has been conducted on the structural modification of the thieno[3,2-*d*]pyrimidine skeleton, with the 4-, 6- and 7-positions as the main targets for chemical modifications to increase antitumor activity.[23]

Lin et al. have also reported a series of 2,7-diaminothiazolo[4,5-*d*]pyrimidines with general formula **5**, with various structural modifications at the 2- and 7-positions, as potent EGFR inhibitors, with IC_{50} values ranging from micromolar to single digit nanomolar.[24] Compound **5a**, characterized by potent and selective EGFR activity (IC_{50}: 12 nM), proved to be active *in vitro* as an antiproliferative agent against the human ovarian adenocarcinoma (SK-OV-3) cell line, with an IC_{50} of 0.57 μM. Unfortunately, compound **5a** showed no *in vivo* antitumour efficacy in a tumour xenograft model in nude mice.

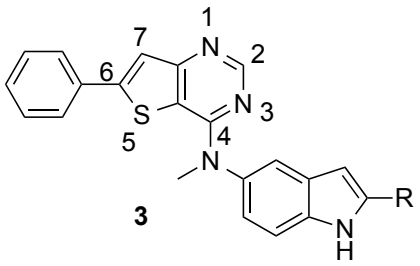

3

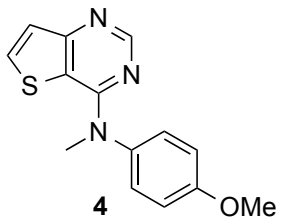

4

3a, R=H, VEGFR-2 IC_{50}: 80 nM, EGFR IC_{50}: 3 nM
3b, R=Me, VEGFR-2 IC_{50}: 140 nM, EGFR IC_{50}: 100 nM

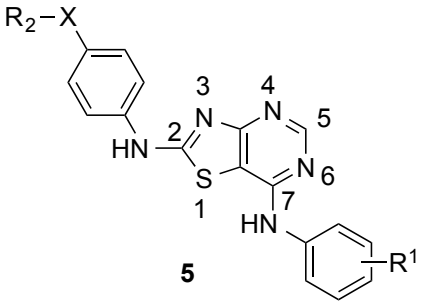

5

X=nothing, O, CH_2 or CH_2CH_2
R^1=halogen
R^2=H, SO_2NH_2, morpholine, pyrrolidine, piperidine, imidazole.
5a, X=CH_2, R^1=3'-Cl, 4'-F; R^2=*N*-morpholine

Figure 2. Chemical structures of representative thieno[3,2-*d*]pyrimidines and thiazolo[4,5-*d*]pyrimidines as known tubulin polymerization (**4**) and EGFR kinase (**3** and **5**) inhibitors.

Our findings caused us to use the thieno[3,2-*d*]pyrimidine scaffold for optimization of the pharmacophore, which was maintained for the discovery of new antitumor agents. We replaced the 5'-aminoindole side chain at the C-4 position of 6-phenylthieno[2,3-*d*]pyrimidine derivatives with general structure **3** with a 3',4',5'-trimethoxyanilino moiety, to furnish a first series of 4-(3',4',5'-trimethoxyanilino)-6-aryl/heteroaryl thieno[3,2-*d*]pyrimidine derivatives with general structure **6** (Figure 3). By maintaining the 3',4',5'-trimethoxyanilino group at the 4-position, the first stage of our study was to evaluate the steric and electronic effects of different substituents on the benzene portion at the C-6 position of the 4-(3',4',5'-trimethoxyanilino)thieno[2,3-*d*]pyrimidine nucleus. Besides the hydrogen, the examined substituents included electron withdrawing groups (EWGs), such

as F, Cl, Br, I and NO_2, and the electron releasing methyl and methoxy groups (ERGs). The bioisosteric replacement of phenyl with the thien-2-yl ring was also explored.

The newly synthesized agents all contained the 3',4',5'-trimethoxyanilino moiety at the common C-4 position of the thieno[2,3-*d*]pyrimidine nucleus and isomeric thieno[3,2-*d*]pyrimidine nucleus, as well as at the C-7 position of the thiazolo[4,5-*d*]pyrimidine system. The rationale for this was the well-documented requirement for a trimethoxyphenyl group in numerous colchicine site inhibitors.[25]

In the second small series of compounds, the thiophene nucleus was replaced by the bioisosteric thiazole ring, to obtain the derivatives **7a-d**, characterized by the presence of an anilino moiety at its C-7 position. The electron-withdrawing chlorine atom (**7b**) and the electron-releasing methyl and methoxy groups (**7c** and **7d**, respectively) were introduced at the *para*-position of the phenyl portion of the anilino moiety.

In a third series of compounds **8a-l**, we explored the replacement of the thieno[3,2-d]pyrimidine system, which characterizes derivatives with general structure **6**, by the isomeric thieno[2,3-*d*]pyrimidine nucleus. The SAR was investigated by the insertion of different substituents (Cl, Me or OMe) on the phenyl at the C-5 or C-6 positions of the 4-(3',4',5'-trimethoxyanilino) thieno[2,3-*d*]pyrimidine core.

These three series of compounds, obtained by replacing the thieno[3,2-*d*]pyrimidine scaffold with the isomeric thieno[2,3-*d*]pyrimidine and the bioisosteric thiazolo[4,5-*d*]pyrimidine skeletons, were designed to determine the potential of incorporating in a single molecule both VEGFR-2 and/or EGFR kinase inhibition and anti-tubulin activity.

The biososteric replacement of the thiophene ring of the structure motif of the thieno[2,3-*d*]pyrimidine nucleus with a furan or pyrrole provided two series of furo[2,3-*d*]pyrimidine and pyrrolo[3,2-*d*]pyrimidine derivatives, respectively, identified by Gangjee et al. as multitarget receptor tyrosine kinase and microtubule inhibitors.[26-28] A literature search also revealed that recent studies have yielded different series of chemically diverse small molecules acting as EGFR kinase and tubulin polymerization inhibitors derived from anthranilic acid[29] or benzo[*b*]furan[30] or obtained by replacing the quinazoline core of compounds **2a-d** with a quinazolinone[31,32] or triazolo[4,3-*a*]quinoxaline[33] scaffold.

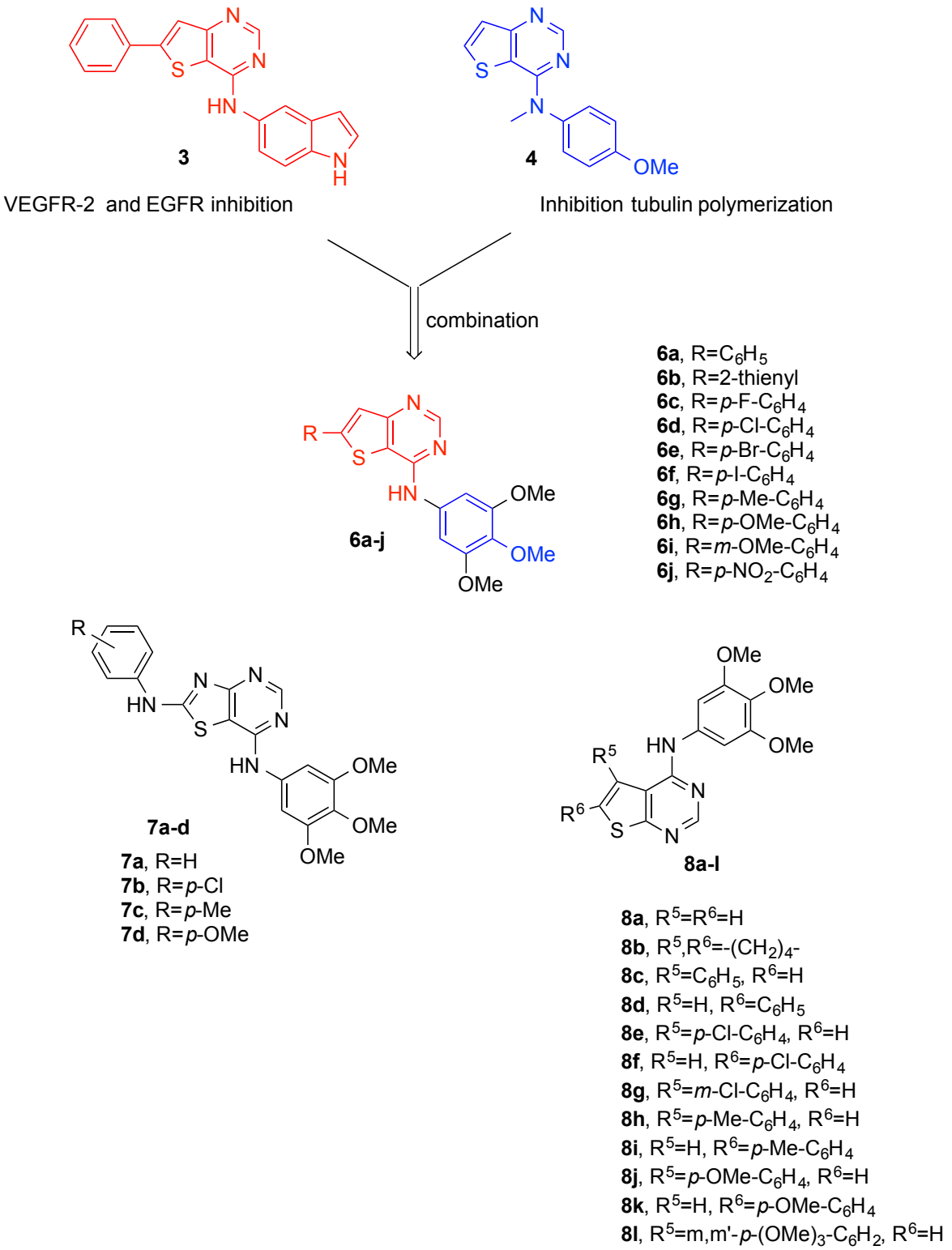

Figure 3. Design strategy for thieno[3,2-*d*]pyrimidines **6a-j**. Target compounds containing the thiazolo[4,5-*d*]pyrimidine (**7a-d**) and thieno[2,3-*d*]pyrimidine (**8a-l**) scaffolds.

4.2 Chemistry

Preparation of thieno[3,2-*d*]pyrimidine and thiazolo[4,5-*d*]pyrimidine derivatives **6a-j** and **7a-d**, respectively, was accomplished using the general convergent synthetic route shown in Scheme 1. Cyclization of methyl 5-aryl/heteroayl-3-aminothiophene-2-carboxylate and ethyl 2-anilino-4-aminothiazole-5-carboxylate **9a-j** and **9k-n**, respectively, with formamide ($HCONH_2$) yielded the corresponding 6-aryl/heteroaryl-thieno[3,2-*d*]pyrimidin-4(3*H*)-ones **10a-j** and 2-arylaminothiazolo[4,5-*d*]pyrimidin-7(6*H*)-ones **10k-n**. The subsequent chlorination of the carbonyl group with phosphorus oxychloride ($POCl_3$) provided 4-chlorothieno[3,2-*d*]pyrimidine and 7-chlorothiazolo[4,5-*d*]pyrimidine derivatives **11a-j** and **11k-n**, respectively. Finally, the nucleophilic substitution with 3,4,5-trimethoxyaniline in refluxing isopropanol furnished the final compounds **6a-j** and **7a-d**, respectively.

Scheme 1. Synthesis of thieno[3,2-*d*]pyrimidines **6a-j** and thiazolo[4,5-*d*]pyrimidines **7a-d**[a]

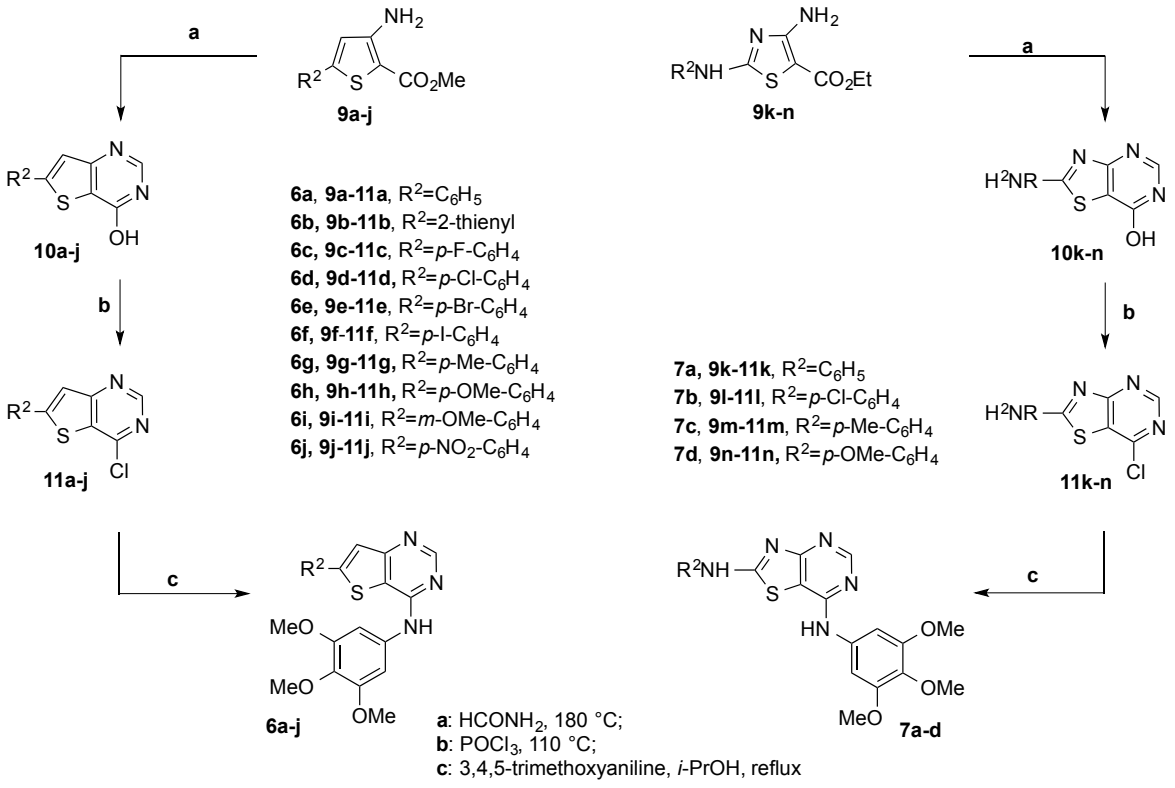

[a]*Reagents and conditions*. **a**: $HCONH_2$, 180 °C; **b**: $POCl_3$, 110 °C; **c**: 3,4,5-trimethoxyaniline, isopropanol, reflux.

The isomeric 4-(3',4',5'-trimethoxyanilino)-thieno[2,3-*d*]pyrimidine derivatives **8a-l** were synthesized following the procedure reported in Scheme 2. Thieno[2,3-*d*]pyrimidin-4(3*H*)-one derivatives **13a-l** variously substituted at their C-5 or C-6 position were prepared by the cyclo-condensation of ethyl 2-aminothiophene-3-carboxylate derivatives **12a-l** with $HCONH_2$ at 180 °C for 8-12 h. These intermediates were subjected to chlorination by the action of $POCl_3$ at reflux to furnish the 4-chlorothieno[2,3-*d*]pyrimidine analogues **14a-l**. The final step of the synthesis involved nucleophilic displacement of the 4-chloride atom of **14a-l** with 3,4,5-trimethoxyaniline in refluxing isopropanol to obtain the 4-(3',4',5'-trimethoxyanilino) thieno[3,2-*d*]pyrimidine derivatives **8a-l**.

Scheme 2. Synthesis of thieno[2,3-*d*]pyrimidines (**8a-l**)[a].

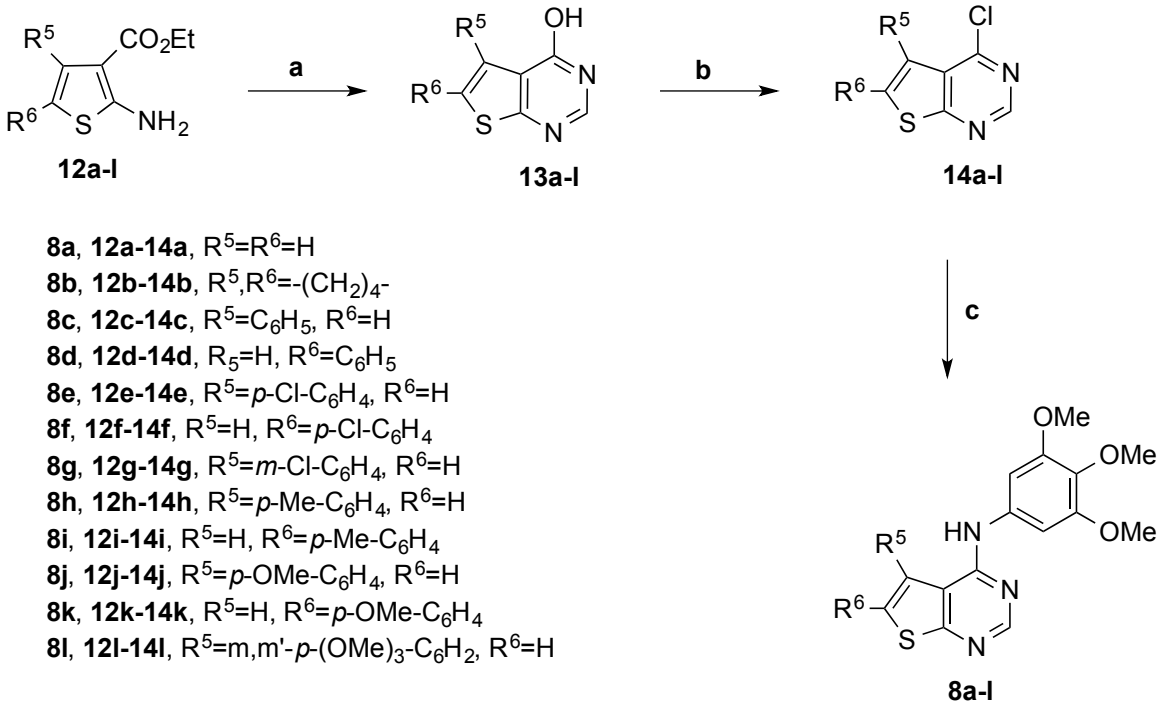

8a, **12a-14a**, R^5=R^6=H
8b, **12b-14b**, R^5,R^6=-$(CH_2)_4$-
8c, **12c-14c**, R^5=C_6H_5, R^6=H
8d, **12d-14d**, R_5=H, R^6=C_6H_5
8e, **12e-14e**, R^5=*p*-Cl-C_6H_4, R^6=H
8f, **12f-14f**, R^5=H, R^6=*p*-Cl-C_6H_4
8g, **12g-14g**, R^5=*m*-Cl-C_6H_4, R^6=H
8h, **12h-14h**, R^5=*p*-Me-C_6H_4, R^6=H
8i, **12i-14i**, R^5=H, R^6=*p*-Me-C_6H_4
8j, **12j-14j**, R^5=*p*-OMe-C_6H_4, R^6=H
8k, **12k-14k**, R^5=H, R^6=*p*-OMe-C_6H_4
8l, **12l-14l**, R^5=m,m'-*p*-$(OMe)_3$-C_6H_2, R^6=H

[a]**Reagents and conditions. a**: $HCONH_2$, 180 °C; **b**: $POCl_3$, 110 °C; **c**: 3,4,5-trimethoxyaniline, isopropanol, reflux.

4.3 Biological Results and Discussion

4.3.1 *In vitro* antiproliferative activities

Table 1 summarizes the antiproliferative effects of 4-(3',4',5'-trimethoxyanilino)-6-substituted thieno[3,2-d]pyrimidine derivatives **6a-j** against a panel of five human cancer cell lines [including EGFR wild-type ($EGFR^{wt}$) NSCLC A549 cells], using CA-4 as the reference compound. The corresponding thieno[2,3-*d*]pyrimidine isomers **7a-d** and the 2-anilino-7-(3',4',5'-trimethoxyanilino)thiazolo[4,5-*d*]pyrimidine **8a-l** were also evaluated for their activities on the same panel of cells, but because they were all inactive (IC_{50}>10 μM), with only a few exceptions on selected cancer cell lines (derivatives **6h**, **6k** and **6l**).

The unsubstituted phenyl derivative **6a** was weakly active (IC_{50}: 2.3 μM) against A549, moderately potent against HeLa, HT-29 and RS4;11 with IC_{50} values of 0.17, 0.35 and 0.26 μM, respectively, but showed high activity (IC_{50}: 10 nM) against Jurkat cells. The bioisosteric 2-thienyl analogue **6b** was 2-, 8- and 10- fold less active than **6a** against A549, Jurkat and HeLa cells, respectively, while the difference in potency between **6a** and **6b** was minimal in RS4;11 cells. Only in HT29 cells **6a** was less active than **6b**, with IC_{50} values of 0.35 and 0.21 μM, respectively.

Table 1. In vitro cell growth inhibitory effects of compounds **6a-j** and CA-4.

Compound	IC_{50} [a](μM)				
	A549	HeLa	HT29	Jurkat	RS4;11
6a	2.3±0.7	0.17±0.02	0.35±0.06	0.01±0.006	0.26±0.10
6b	5.1±1.9	1.7±0.8	0.21±0.07	0.08±0.03	0.36±0.1
6c	13.5±3.0	0.45±0.09	1.9±0.8	0.26±0.04	1.9±0.3
6d	0.60±0.11	0.09±0.03	0.087±0.033	0.003±0.001	0.005±0.002
6e	0.53±0.16	0.22±0.09	0.15±0.04	0.03±0.005	0.19±0.04
6f	0.77±0.26	0.28±0.15	0.25±0.13	0.30±0.06	0.17±0.04
6g	0.019±0.008	0.001±0.0005	0.02±0.007	0.001±0.0005	0.002±0.001
6h	0.43±0.13	0.17±0.08	0.06±0.04	0.005±0.001	0.004±0.001
6i	8.8±1.9	3.2±0.1	3.3±0.8	3.0±1.0	5.4±1.3
6j	1.1±0.3	4.9±1.4	6.3±1.4	2.0±0.3	1.3±0.4
CA-4	0.18±0.05	0.004±0.0001	3.1±0.1	0.005±0.0001	0.001±0.0001

[a]IC_{50}= compound concentration required to inhibit tumour cell proliferation by 50%. Data are expressed as the mean ± SE from the dose-response curves of at least three independent experiments.

The introduction of electron-releasing or electron-withdrawing substituents at the *para*-position of the phenyl ring at the C-6 position of the thieno[3,2-d]pyrimidine nucleus appeared to have considerable biological effects, enhancing antiproliferative activity compared with the unsubstituted phenyl analogue **6a**. These compounds include the *p*-Cl (**6d**; IC_{50}: 3-600 nM), *p*-Me (**6g**; IC_{50}: 1-20 nM) and *p*-OMe (**6h**; IC_{50}: 4-430 nM) derivatives. The *p*-tolyl derivative **6g** displayed the strongest growth inhibitory activity against A549, HeLa, HT29, Jurkat and RS4:11, with IC_{50} values of 19, 1, 20, 1 and 2 nM, respectively.

A *para*-fluoro group in the phenyl ring (compound **6c**) caused a reduction of activity of 2-26-fold relative to the unsubstituted phenyl derivative **6a**, while the presence of other halogen groups led to an improvement in antiproliferative activity. As the bulk of the halide group increased from a fluoro to a chloro moiety, resulting in compound **6d**, produced a 5- to 87-fold increase in antiproliferative activity in the five cell lines. Replacing chlorine with bromine (**6e**), reduced activity 2-38-fold against four of the five cancer cell lines, but **6d** and **6e** were equally potent against A549 cells. For the *p*-Br and *p*-I derivatives **6e** and **6f**, respectively, nearly identical activities were observed in three of the five cancer cell lines, the exception being the HT-29 and Jurkat cells, in which **6f** was 2- and 10-fold more potent than **6e**, respectively.

The small and weak electron-releasing methyl group at the *para*-position of the phenyl ring, to yield derivative **6g**, improved significantly antiproliferative activity relative to **6a**. Derivative **6g** exhibited the greatest cell growth inhibitory effects among the tested compounds, with IC_{50} values of 1-20 nM against all cell lines, as compared with the range 0.8-3100 nM obtained with CA-4. Compound **6g** was equipotent with CA-4 against RS4;11 cells, while it was from 2- to $1.5x10^5$ times more active against the other four cancer cell lines.

A *para*-methoxy group in the phenyl ring (**6h**), a more potent electron-releasing group than the methyl of **6h**, caused a marked reduction (2-170x) in activity against the tumour cell lines. Thus, the two substituents, despite their structural similarity, are not biologically equivalent. The reduction in activity was more evident, 23- and 170-fold, against A549 and HeLa, respectively, while only a 2-, 3- and 5-fold reduced activity was observed against RS4;11, HT-29 and Jurkat cells.

Compound **6i**, with a methoxy group at the *meta*-position of the phenyl ring, was one to four orders of magnitude less active than the *para*-methoxy isomer **6h**, indicating that the position of the methoxy group was important for *in vitro* activity.

Among the strong electron-withdrawing groups, the small polar nitro substituent, intermediate in size between chlorine and bromine, when placed in the *para*-position of the phenyl ring, furnished a compound (**6j**) with reduced antiproliferative activity (IC_{50}: 1.1-6.3 μM) relative to the unsubstituted phenyl derivative **6a**.

4.3.2 Inhibition of tubulin polymerization and colchicine binding

We anticipated that at least some of the compounds would have anti-tubulin activity, and **6a-b** and **6d-h** were examined for inhibitory effects on tubulin assembly and on the binding of colchicine to tubulin in comparison with CA-4 (Table 2).

Table 2. Inhibition of tubulin polymerization and colchicine binding by compounds **6a-b, 6d-h** and CA-4 (**1a**).

Compound	Tubulin assembly[a] IC_{50}±SD (μM)	Colchicine binding [b] % inhibition±SD
6a	10±2	n.d.
6b	18±1	n.d
6d	3.3±0.3	36±3
6e	2.5±0.3	35±4
6f	2.5±0.2	35±2
6g	0.71±0.05	76±0.7
6h	2.8±0.2	31±3
CA-4	1.2±0.1	98±0.7

[a] Inhibitory effects on the assembly of 10 μM purified tubulin.

[b] In the experiments to evaluate compound effects on the binding of [^{3}H] colchicine to purified tubulin, the protein was at 1.0 μM and the radiolabeled colchicine and inhibitory compound were both at 5.0 μM.

n.d.: Not done.

Compounds **6e-h** strongly inhibited tubulin assembly, with derivative **6g** as the most active of the series, being almost 2-fold more active than CA-4 in this assay (IC_{50}: 0.71 and 1.2 μM for **6g** and CA-4, respectively). Compounds **6e**, **6f** and **6h** were half as active (IC_{50}: 2.5, 2.5 and 2.8 μM, respectively) and **6d** about one-third as active (IC_{50}: 3.3 μM) as CA-4. Compounds **6a** and **6b** showed weak antitubulin polymerization activities (IC_{50}: 10 and 18 μM, respectively), which were consistent with their low antiproliferative activity. Thus, in

the two tubulin biochemical assays, compound activities were similar, with **6g** the most active (even more active than CA-4 in the polymerization assay) and **6a** and **6b** the least active in the polymerization assay. These data are consistent with the conclusion that tubulin was an intracellular target of the tested compounds.

4.3.3 Activity on EGFR and VEGFR-2 kinase

EGFR and VEGFR-2 kinase inhibitory activity assay

Compounds **6a-b** and **6d-h** were further evaluated for their EGFR and VEGFR-2 kinase inhibitory activities. The approved VEGFR-2 and EGFR inhibitory agents sunitinib and erlotinib (**2b**), respectively, were used as positive controls. The data compiled in Table 3 showed potent inhibition of $EGFR^{wt}$ kinase by compounds **6a-b** and **6f-h**, but no inhibition of VEGFR-2 (IC_{50}>1 μM) was observed. All tested molecules, with the exception of **6d** and **6e**, were more potent than sunitinib as EGFR kinase inhibitors, with the 2-thienyl derivative **6b** as the most potent compound of the series. All evaluated molecules showed lower potency than erlotinib, with **6b** about 1.7-fold less potent. Three of these compounds (**6f-h**) were discovered to possess dual EGFR and tubulin polymerization inhibitory activity, and the good correlation between cytotoxicity and anti-tubulin activity extends to inhibition of EGFR activity.

Table 3. EGFR inhibitory activities by compounds **6a-b, 6e-h,** sunitinib and erlotinib (**2b**).

Compound	Inhibition of $EGFR^{wt}$ kinase[a] IC_{50}±SD (nM)
6a	23±4
6b	2.5±0.3
6d	273±35
6e	326±46
6f	10±3
6g	30±5
6h	52±6
Sunitinib (2e)	140±19
Erlotinib (2b)	1.5±2

[a]Values are expressed as the mean ± SD from the dose-response curves of at least two independent experiments.

Compound **6g**, with the most potent effect on tubulin polymerization, also exhibited excellent EGFR inhibitory activity, with IC_{50} values of 0.71 μM and 30 nM, respectively. In contrast, compound **6b**, the most active compound as an EGFR inhibitor (IC_{50}: 2.5 nM), was less potent as an inhibitor of tubulin polymerization (IC_{50}: 18 μM). As shown in Table 3, compounds **6d** and **6e**, showed moderate EGFR inhibitory activities (IC_{50}: 273 and 326 nM, respectively) and similar potent anti-tubulin potency (IC_{50}: 3.3 and 2.5 μM), while for compound **6h** a good correlation was observed between both its EGFR and anti-tubulin activities. The SAR analysis derived from the antiproliferative activities of compounds **6d** and **6e** was more consistent with their tubulin inhibition activities, probably due to their potent inhibitory activities against tubulin polymerization but moderate activities against EGFR.

Compound **6g** induced inhibition of EGFR activation in HeLa cells

In order to test the inhibition on the phosphorylation of EGFR and the downstream signaling pathway, we evaluated by western blot analysis the inhibition of EGFR phosphorylation by **6g** in HeLa cells. The cells were treated with different concentration of **6g** (10-1000 nM) and then stimulated with epidermal growth factor (EGF) (50 ng/mL) for 15 min. The results (Figure 4) showed that **6g** strongly inhibited the phosphorylation of EGFR in a concentration dependent manner starting at 50 nM. Erlotinib (1 μM) was taken as reference compound, and erlotinib showed similar inhibitory activity as compound **6g**. These results demonstrated that **6g**, in addition to its antimitotic activity (see below), is also a potent EGFR inhibitor.

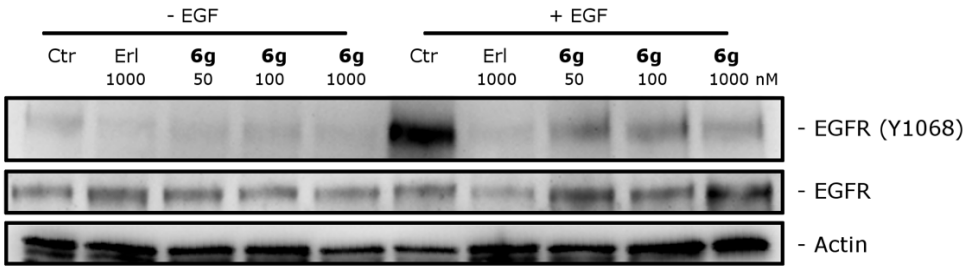

Figure 4. Effects of **6g** on EGFR signaling in HeLa cells. Cells were treated with the indicated concentrations of **6g** for 6 h and then stimulated by EGF (30 ng/mL) for 15 min. Cells were harvested for Western blot analysis for both EGFR and its phosphorylation at Y1068. Erlotinib (Erl) was used as the reference compound. We established that each gel lane had similar quantities of protein by determining their β-actin content.

4.3.4 Molecular modeling

A series of docking simulations were conducted on the newly designed 4-(3',4',5'-trimethoxyanilino)-6-substituted thieno[3,2-*d*]pyrimidines to evaluate their potential interaction at the binding site for colchicine on tubulin.[34] The results showed that the compounds bind in the active site with considerable overlap with *N*-deacetyl-*N*-(2-mercaptoacetyl)-colchicine (DAMA-colchicine), which was the ligand in the crystal structure, and the binding mode is consistent with the one previously reported for a thieno[2,3-*b*]pyridine series,[35] with the trimethoxyphenyl group in proximity of βCys241. The thieno[3,2-d]pyrimidine core overlapped with the central part of DAMA-colchicine, with the substituted phenyl ring placed in a small hydrophobic sub-pocket, potentially interacting with the surrounding amino acids βThr314, βVal181 and especially βMet259. This small sub-pocket appears to be able to interact with phenyl rings bearing different substituents, but only the *para* methyl derivative **6g** has the correct combination of size/electronic properties to stably occupy and properly fit that area of the binding site (Figure 5C), suggesting a better inhibition of tubulin assembly. Replacement with a larger methoxy group (**6h**) does not allow the efficient occupation of the sub-pocket, indicating a potential reduction of the inhibition of tubulin polymerization. A similar decrease in activity is seen when the methyl group is replaced by different electron withdrawing atoms (**6d-f**), but in this case the decrease in activity could be associated with the electronic properties of the substituent rather than its size, since they can occupy the sub-pocket very similarly to **6g** (Figure 5C). Compounds where the *para* substituent has been removed (**6a**) or the phenyl ring has been replaced with a smaller 5-member thiophene ring, do not entirely fill the sub-pocket, potentially causing the 10-18-fold activity reduction found for these derivatives (Figure 5A).

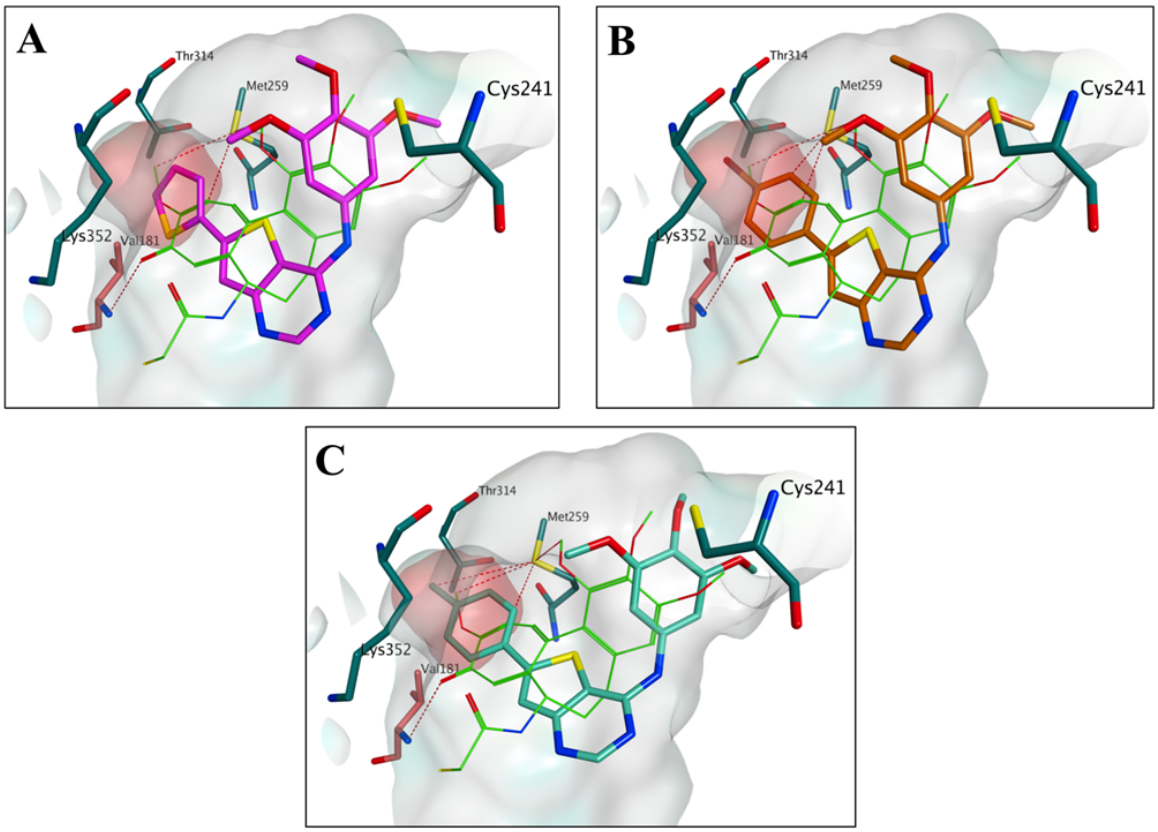

Figure 5. Proposed binding modes for compounds **6b** (**A**), **6e** (**B**) and **6g** (**C**) in comparison with DAMA-colchicine in the colchicine site (PDB ID: 1SA0). Carbons of the co-crystallized DAMA-colchicine are shown in green, of compound **6b** in purple, of compound **6e** in orange and of compound **6g** in turquoise. The residues from the α-tubulin chain are shown in salmon, whereas residues from β-tubulin are coloured in teal. The sub-pocket is highlighted with a red surface.

In an attempt to clarify the potential binding mode of the new derivatives in the EGFR kinase domain, docking of the new molecules was performed using the crystal structure of the EGFR kinase domain in complex with the inhibitor (*R*)-6-(4-((4-ethylpiperazin-1-yl)methyl)phenyl)-*N*-(1-phenylethyl)-7*H*-pyrrolo[2,3-*d*]pyrimidin-4-amine (AEE788).[36] The 6-phenyl-thieno[3,2-*d*]pyrimidine core of the molecules perfectly overlaps with the phenyl pyrrolo[2,3-*d*]pyrimidine core of the co-crystallized inhibitor, making the same interactions with Gln791, Met793 and Leu844 that seem to anchor the molecule to the binding site (Figure 6). The trimethoxyphenyl group is placed in the same area occupied by the methyl moiety of AEE788, in proximity of Asp855.

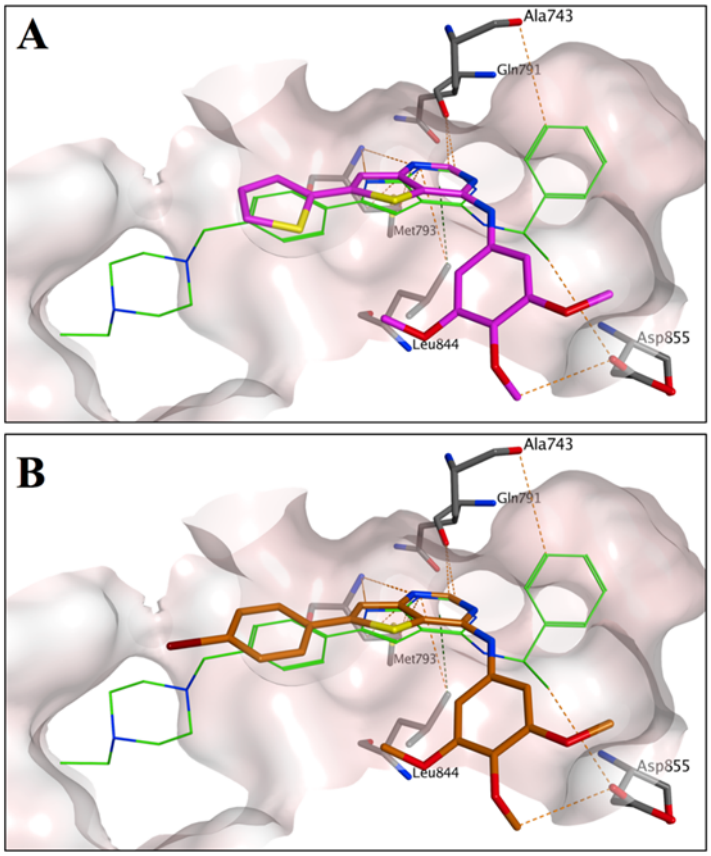

Figure 6. Proposed binding modes for compounds **6b** (**A**) and **6e** (**B**) in comparison with the inhibitor AEE788 in the crystal structure of the EGFR kinase domain (PDB ID: 2J6M). The carbons of the co-crystallized AEE788 are shown in green, of compound **6b** in purple and of compound **6e** in orange. The phenyl ring of **6e** and the thiophene of **6b** are not involved in any interaction with the surrounding residues.

Overall, the binding mode proposed for these compounds is very similar to that of the co-crystallized ligand and also to another previously published thienopyrimidine EGFR inhibitor.[23] All the new compounds occupy the active site in an identical manner. However, from these results, it is not possible to fully rationalize the role of the substitution on the phenyl ring in the anti-EGFR activity, since that part of the molecule does not seem to be involved in any specific interactions with the binding pocket.

4.3.5 *In vitro* and *in vivo* studies of compound 6g

Effects of compound **6g** on the cell cycle

Cell cycle effects of the highly active **6g** were examined in HeLa and Jurkat cells, using flow cytometry (Figure 7). After 24 h, G2/M arrest occurred in both cells lines at 25 nM **6g**, as shown by propidium iodide (PI) staining. That the arrest occurred in mitosis was established by staining the cells with an immunofluorescent antibody to p-histone H3.[37] Typical histograms show that HeLa cells arrested in mitosis by **6g** are easily distinguished from G2 cells with the p-histone H3 stain (Figure 7D). The increase in mitotic cells (from 1.5% in the control) was especially dramatic with 50 (38%) and 100 (50%) nM **6g**.

A

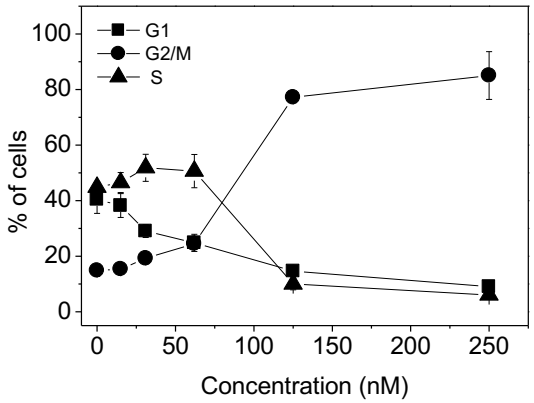

B

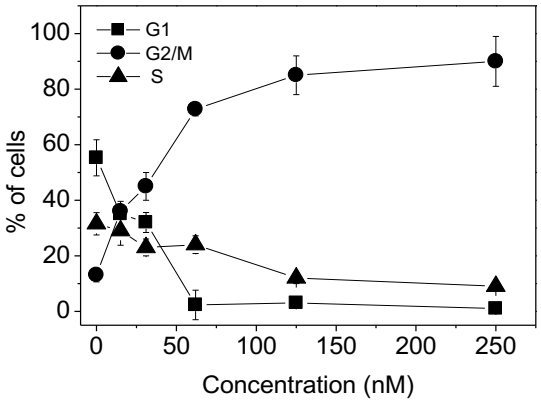

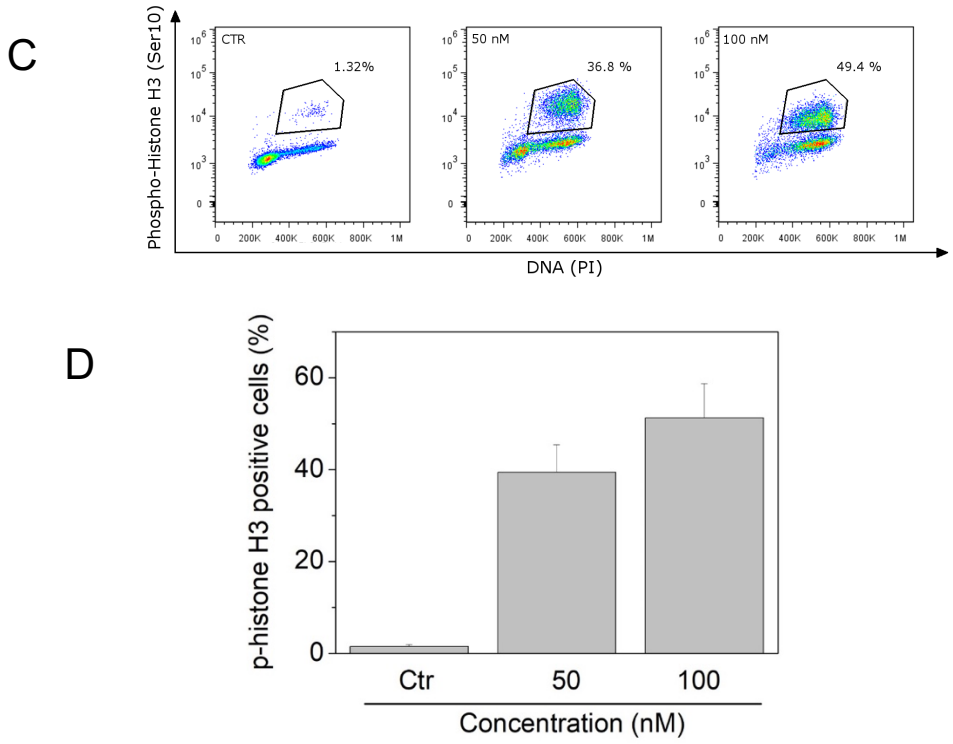

Figure 7. Cell cycle effects caused by **6g**. A) HeLa cells treated with varying concentrations of **6g**, stained with PI, and examined by flow cytometry. B) Jurkat cells treated with varying concentrations of **6g**, stained with PI, and examined by flow cytometry. G1 cells are indicated by the symbol ■, G2/M cells by the symbol ●, and S cells by the symbol ▲. Three independent experiments were performed, and the S.E.M. values are indicated. C) Typical flow cytometric patterns are shown of mitotic HeLa cells immune-fluorescently stained with an antibody to p-histone H3, following treatment with 0 (left-hand pattern), 50 (middle pattern, or 100 (right-hand pattern) nM **6g**. D) Histogram presentation of the data from Panel C (two experiments, with S.E.M. values indicated).

Compound **6g** induced apoptosis in different cell lines

The mechanism of cell death was evaluated by two-dimensional cell sorting by staining DNA with PI and staining phosphatidylserine (PS) with a fluorescent annexin V derivative. We used two cell lines, Hela and Jurkat, in which we evaluated the effects of compound **6g** after both 24 and 48 h treatments. As shown in Figure 8, in both cell lines, **6g** caused apoptosis that increased with time and with **6g** concentration, with an apoptotic effect observed at 50 nM, the lowest concentration used, shown in the (3-(4,5-dimethylthiazol-2-yl)-2,5-diphenyl tetrazolium bromide (MTT) test (Table 1).

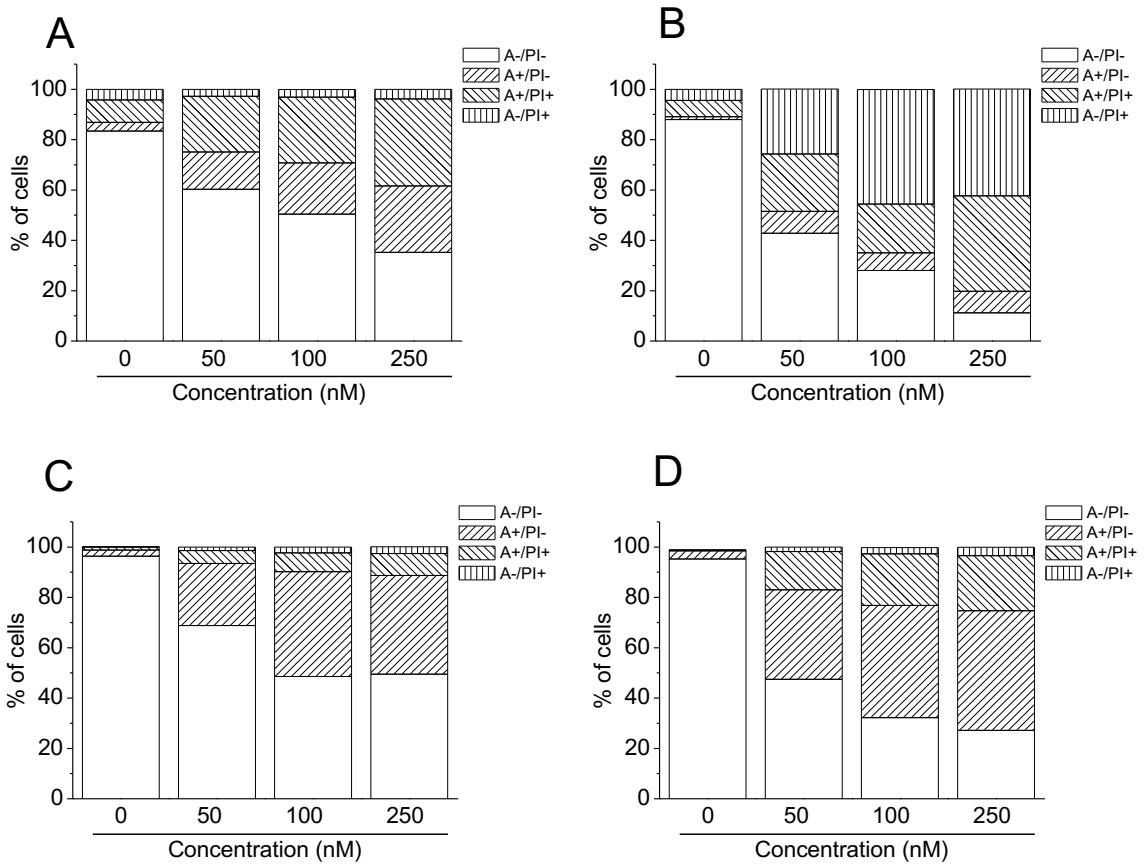

Figure 8. Apoptotic effects caused by **6g**. A) Apoptosis examined by flow cytometry after treatment of HeLa cells for 24 h with **6g**, as indicated. B) Apoptosis examined by flow cytometry after treatment of HeLa cells for 48 h with **6g**, as indicated. C) Apoptosis examined by flow cytometry after treatment of Jurkat cells for 24 h with **6g**, as indicated. D) Apoptosis examined by flow cytometry after treatment of Jurkat cells for 48 h with **6g**, as indicated. In all cases cells were stained with annexin-V linked to fluorescence and with PI.

Mitochondrial depolarization and formation of reactive oxygen species caused by treatment with **6g**

Mitochondria are critical for the occurrence of apoptosis.[38,39] Early in the process, the mitochondrial transmembrane potential ($\Delta\psi_{mt}$) changes. We measured by flow cytometry these changes through use of 5,5',6,6'-tetrachloro-1,1',3,3'-tetraethylbenzimidazolcarbocyanine (JC-1). As shown in Figure 9 (Panel A), cells treated with different concentration of **6g** (50, 100 and 250 nM) showed a concentration- and a time-dependent increase in the percentage of cells with low $\Delta\psi_{mt}$. The depolarization of the mitochondrial membrane is already evident at early times of drug exposure (3-6 h), in good agreement with findings of many microtubule active agents that a fall in $\Delta\psi_{mt}$ occurs early in apoptosis in many types of cells.[40-42] We also established that this drop in $\Delta\psi_{mt}$ is

associated with generation of ROS[43] (Figure 9B) following **6g** treatment for as short a time as 12 h with as little as 50 nM **6g**.

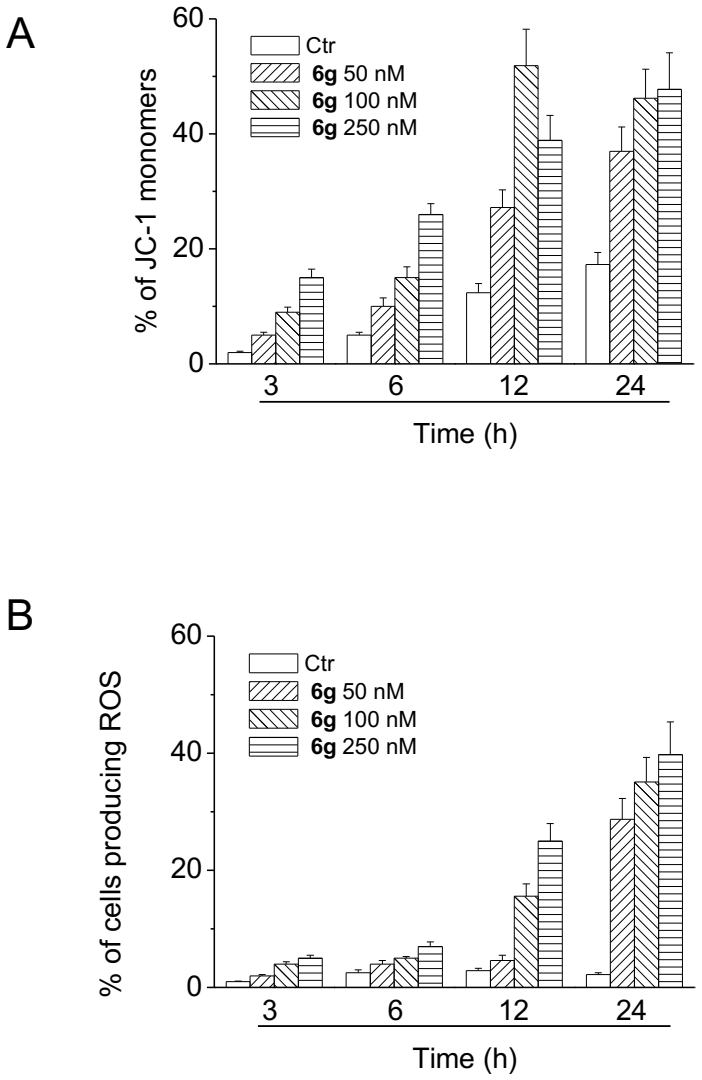

Figure 9. Flow cytometric measurement of $\Delta\psi_{mt}$ and ROS following treatment of HeLa cells with **6g**. Treatment times and **6g** concentrations as indicated. A) Measurement of $\Delta\psi_{mt}$ by JC-1 fluorescence. B) Measurement of ROS by fluorescence of 2,7-dichlorodihydrofluorescein diacetate.

Compound **6g** induced PARP activation and caused a decrease in the expression of anti-apoptotic proteins

To gain a better insight into the mechanism of action of **6g**, we evaluated the cleavage of poly (ADP-ribose) polymerase (PARP) during the apoptotic process induced by this compound. As shown in Figure 10, compound **6g** in HeLa cells caused a concentration and time-dependent cleavage of PARP, confirming its pro-apoptotic activity. Moreover, the

expression of two anti-apoptotic proteins, Bcl-2 and Mcl-1, was also studied.[44,45] Immunoblot analysis, shown in Figure 10, demonstrated that the expression of the anti-apoptotic protein Bcl-2 was decreased starting after a 24 h treatment at both 50 and 100 nM. The decrease in expression of Mcl-1 was even greater, both at the lowest concentration and after the 24 h treatment.

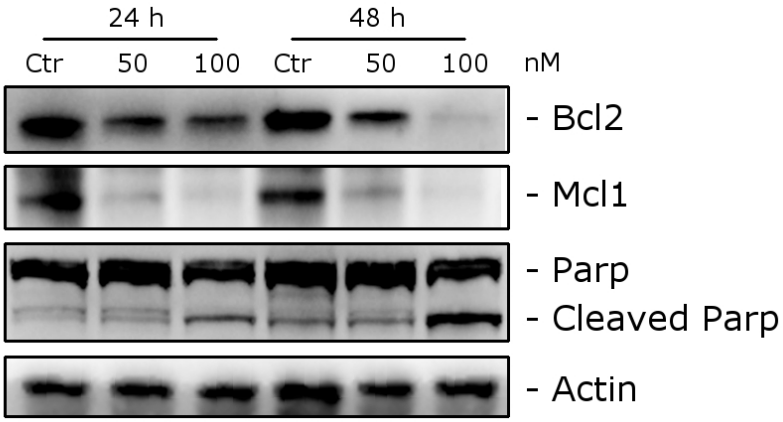

Figure 10. Western blot demonstrating PARP, Bcl-2 and Mcl-1 levels. HeLa cells were treated with **6g** as indicated. Equivalent protein loading was confirmed by evaluating anti-β-actin levels in the gel slots.

Antivascular activity of **6g**

Combined use of cytotoxic drugs with agents showing antiangiogenic or antivascular effects to increase treatment effects is a relatively recent therapeutic strategy.[4] Many anti-tubulin drugs, especially CA-4P, were found to have vascular disrupting effects against tumour endothelial cells.[46-49] We therefore examined effects of **6g** on human umbilical vein endothelial cells (HUVECs) to evaluate potential effects on angiogenesis. We specifically studied HUVECs growing in Matrigel, a substance rich in pro-angiogenic compounds, for their ability to alter their shape to resemble capillaries. Preliminary experiments carried out on these cells, with the aim to evaluate the cytotoxicity of the test compound, indicated that **6g** had a GI_{50} of 56 nM after a 48h treatment. Thus, to evaluate antivascular activity, we used a concentration of **6g** that did not induce cellular death.

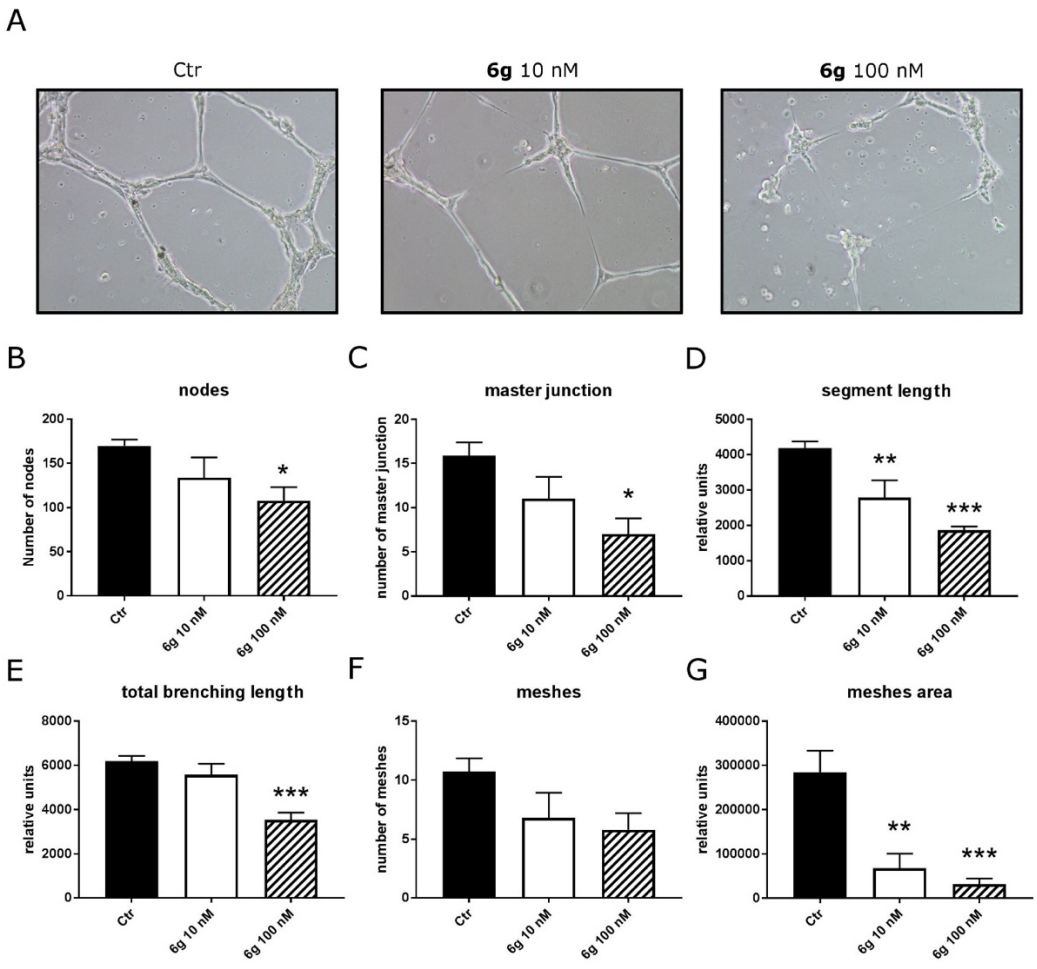

Figure 11. Antivascular effects of **6g** treatment on HUVECS. A) Typical images after 1 h of growth on Matrigel of untreated cells (left-hand image), of cells treated with 10 nM **6g** (middle image), and of cells treated with 100 nM **6g** (right-hand image). B-G) Quantitative evaluation of **6g** on standard parameters of HUVEC tubule formation, as indicated, at the indicated **6g** concentrations. Mean ± SEM, 3 experiments. **p<0.01; ***p<0.001.

We examined the effects of 10 nM (noncytotoxic concentration) and 100 nM (cytotoxic concentration) **6g** on HUVECs after a 1 h treatment (Figure 11A). Both concentrations of **6g** disrupted the network formation observed in the untreated HUVECs. Standard image analysis[45] was performed to obtain the parameters usually evaluated: 1) nodes (Figure 11B); 2) master junctions (Figure 11C); 3) segment length (Figure 11D); 4) total branching length (Figure 11E); 5) number of meshes (Figure 11F); and 6) meshes area (Figure 11G).

The results for segment length and meshes area were statistically significant effects for the lowest concentration used, suggesting, the high potential for vascular disrupting activity of **6g**.

6g induced tumour growth reduction in a mouse allograft tumour model

In *in vivo* studies, tumour bearing animals were dosed with **6g** q.o.d. intraperitoneally, beginning on day 9. Two different doses (3.0 and 7.5 mg/kg) were studied, and CA-4P (30 mg/kg) was used as a reference compound. The murine allograft model was B16 murine melanoma cells injected into the flanks of mice.[50,51] The B16 melanoma cell line was used because it has high levels of EFGR kinase,[52] and, in initial experiments, we had found that the IC_{50} of **6g** was 23.4 ± 3.8 nM (MTT assay).

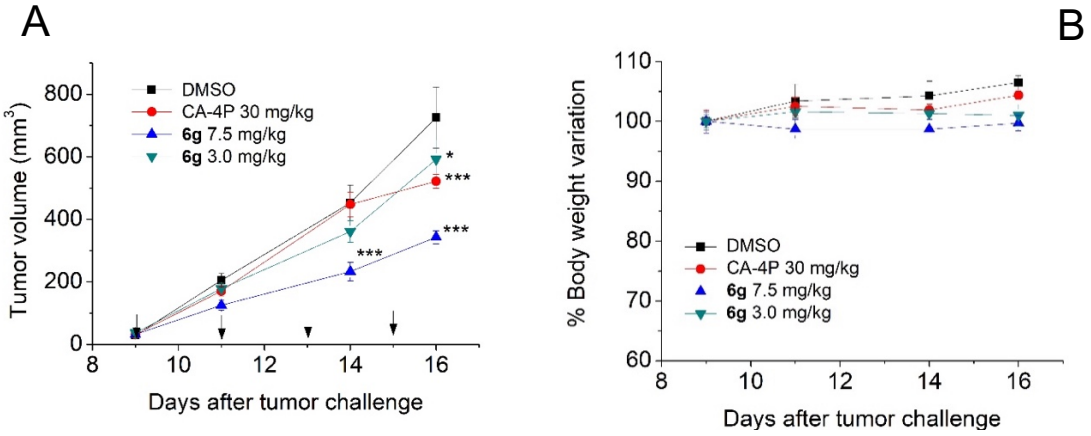

Figure 12. *In vivo* activity of **6g** in the treatment of murine B16 melanoma in an allograft model. A) Each male C57BL/6 mouse was injected s.q. in its dorsum with 2.5 x 10^5 murine melanoma cells. On the days indicated by the arrows, mice were administered i.p. either vehicle, 3.0 mg/kg **6g**, 7.5 mg/kg **6g**, or 30 mg/kg CA-4P. B) Body weight variation after treatment with compound **6g** or CA-4P as described above. The data are plotted as mean ± S.E.M. of tumour volume at each time point for five animals per group, *$p < 0.05$; *** $p < 0.001$ *vs.* control.

Figure 12A demonstrates that after four doses of **6g**, given on days 9, 11, 13, and 15, tumour burden was reduced 28% with 3.0 mg/kg and 52.5% with 7.5 mg/kg, as compared with a 34.9% reduction with 30 mg/kg of CA-4P. No toxicity, based on no weight loss, was observed in any of the experimental groups (Figure 12B).

4.4 Conclusions

An effective strategy to develop anticancer agents is the discovery of synergistic multi-targeting properties of new molecules. The thiophene ring has been employed as an isostere for benzene-fused pyrimidines in the design of molecules that possess tyrosine kinase inhibitory activity. In this study we report the design and synthesis of a new series 4-(3',4',5'-trimethoxyanilino)-6-substituted thieno[3,2-d]pyrimidines, some of which possess both tubulin polymerization and EGFR kinase inhibitory properties. Optimal structure at the phenyl at the C-6 position of the 4-(3',4',5'-trimethoxyanilino)-thieno[3,2-d]pyrimidine system was explored by various substituents, with either electron-releasing or electron-withdrawing properties. The importance of the specific substituent is demonstrated by the data summarized in Table 1.

Three of the 4-(3',4',5'-trimethoxyanilino)-6-substituted thieno[3,2-*d*]pyrimidine derivatives, corresponding to *p*-Cl (**6d**), *p*-Me (**6g**) and *p*-OMe (**6h**), were the most potent compounds found in this study, with IC_{50} values of, respectively, 3-600, 1-20 nM and 4-430 nM in the five cell lines. The 4-(3',4',5'-trimethoxyanilino)-6-(*p*-tolyl)thieno[3,2-*d*]pyrimidine derivative **6g** was the most potent compound of the whole series, exhibiting an IC_{50} value of 19 nM against the NSCLC A549 cell line, which harbors $EGFR^{WT}$ and K-ras mutations. Comparing the *p*-tolyl derivative **6g** with the *p*-methoxy phenyl compound **6h**, the latter was 2-170-fold less active than **6g**, with the greatest differences in activity being 23- and 170-fold in A549 and Hela cells, respectively.

The corresponding thieno[2,3-*d*]pyrimidine isomers and the 2-anilino-7-(3',4',5'-trimethoxyanilino) thiazolo[4,5-d]pyrimidine derivatives generally had little activity, with IC_{50} values usually greater than 10 μM. There was a considerable difference in potency between 4-(3',4',5'-trimethoxyanilino)-6-arylthieno[3,2-*d*]pyrimidine derivatives **6a**, **6d** (*p*-Cl), **6g** (*p*-Me) and **6h** (*p*-OMe) and the regioisomeric 4-(3',4',5'-trimethoxyanilino)-6-arylthieno[2,3-*d*]pyrimidine analogues **8d**, **8f**, **8i** and **8k**, respectively, with these latter being considerably less active than the former in all cancer cell lines examined.

The inhibitory activity against EGFR and VEGFR-2 kinases of selected compounds **6a-b** and **6d-h** showed that these molecules were selective EGFR inhibitors. Compounds **6f-h** inhibited both EGFR kinase and tubulin polymerization, while derivative **6b** only inhibited EGFR kinase. Compounds **6a-b** and **6d-h** showed lower potency than erlotinib, with derivative **6b** having the greatest inhibitory activity against EGFR kinase, being only slightly less potent than erlotinib (IC_{50}: 2.5 and 1.5 nM, respectively). Besides its potent antiproliferative activity and highly competitive inhibitory activity on EGFR, compound **6g**

also inhibited tubulin assembly through an interaction at the colchicine site, thereby combining EGFR inhibition with anti-tubulin activity. The IC_{50} of 0.7 μM obtained with **6g** in the tubulin assembly assay was almost half that obtained in simultaneous experiments with CA-4 (IC_{50}: 1.2 μM).

In our results with compounds **6f-h** there was a high correlation between the *in vitro* antiproliferative activity against the cancer cell lines and inhibition of tubulin polymerization and EGFR kinase, which suggested that targeting both tubulin and EGFR kinase played major roles in the cancer cell growth inhibitory effects of these three molecules.

4.5 Experimental Section

Chemistry

General materials and methods. A Varian VXR 200 spectrometer was used to obtain ^{1}H NMR; a Varian Mercury Plus 400 spectrometer was used to obtain ^{13}C NMR data. Peak positions are provided in ppm (δ) downfield, and *J* values in hertz. Mass spectra were obtained on a Waters ZQ 2000 ESI single quadrupole mass spectrometer, with values given as $[M+1]^{+}$. Melting points (mp) (uncorrected) were obtained on a Buchi-Tottoli instrument. Purity (≥ 95%) was verified by combustion elemental analyses performed at the Microanalytical Laboratory of the Department of Chemistry and Pharmaceutical Sciences of the University of Ferrara using a Yanagimoto MT-5 CHN recorder elemental analyzer. TLC was performed on glass plates from Merck coated with silica gel 60 F_{254}, with compounds visualized by UV detection or with aqueous $KMnO_4$. Flash column chromatography was performed with 230-400 mesh silica gel and solvents as indicated. Organic solutions were dried over anhydrous Na_2SO_4. Commercial solvents and reagents were from Aldrich (Sigma-Aldrich) or Alfa Aesar (Johnson Matthey Company) and were used as supplied. Compounds **12a** and **12b** are commercially available. General procedures and references related to the preparation of methyl 3-aminothiophene-5-aryl/heteroaryl-2-carboxylate **9a-j**, ethyl 5-amino-2-anilinothiazole-4-carboxylate **9k-n** and ethyl 2-aminothiophene-3-carboxylate derivatives **12c-l** are reported in the Supporting Information section. Active compounds were not recognized as PAINS according to the Free ADME-Tox Filtering Tool (FAF-Drugs4) program (http://fafdrugs4.mti.univ-paris-diderot.fr/).

General procedure for the synthesis of compounds 6a-j, 7a-d and 8a-l. A mixture of the appropriate 4-chlorothieno[3,2-*d*]pyrimidine **11a-j**, 7-chlorothiazolo[4,5-*d*]pyrimidine **11k-n** or 4-chlorothieno[2,3-*d*]pyrimidine **14a-l** (1 mmol) and 3,4,5-trimethoxyaniline (2 mmol, 366 mg, 2 equiv.) in *iso*-propanol (5 mL) with a drop of concentrated HCl was refluxed for 18 h and then evaporated to dryness *in vacuo*. The residue was dissolved with dichloromethane, and the organic solution was washed with water, followed by brine, and dried over Na_2SO_4, and the solvent was evaporated. The crude residue was purified by column chromatography on silica gel to furnish the desired compound.

6-Phenyl-N-(3,4,5-trimethoxyphenyl)thieno[3,2-d]pyrimidin-4-amine (6a). The crude residue was purified by flash chromatography, using ethyl acetate as eluent, to furnish **6a** as a yellow solid. Yield: 80%, mp 176 °C. ^{1}H-NMR (*d*$_6$-DMSO) δ: 3.67 (s, 3H), 3.79 (s, 6H), 7.22 (s, 2H), 7.51 (m, 3H), 7.85 (m, 2H), 7.90 (s, 1H), 8.59 (s, 1H), 9.64 (s, 1H). ^{13}C-NMR (*d*$_6$-DMSO) δ: 55.84 (2C), 60.16, 100.17 (2C), 114.74, 120.50, 126,26 (2C), 129.42 (2C), 129.73, 132.62, 133.91, 135.03, 149.41, 152,57 (2C), 154.46, 154.81, 161.03. MS (ESI): $[M+1]^+$=394.5. Anal. ($C_{21}H_{19}N_3O_3S$) C, H, N.

6-(Thiophen-2-yl)-N-(3,4,5-trimethoxyphenyl)thieno[3,2-d]pyrimidin-4-amine (6b). The crude residue was purified by flash chromatography, using ethyl acetate:petroleum ether 9:1 (v:v) as eluent, to furnish **6b** as a yellow solid. Yield: 69%, mp 211 °C. ^{1}H-NMR ($CDCl_3$) δ: 3.67 (s, 3H), 3.79 (s, 6H), 7.21 (s, 2H), 7.62 (dd, J=5.0 and 1.2 Hz, 1H), 7.76 (m, 1H), 7.78 (s, 1H), 8.06 (dd, J=5.0 and 1.2 Hz, 1H), 8.57 (s, 1H), 9.59 (s, 1H). ^{13}C-NMR ($CDCl_3$) δ: 55.73 (2C), 60.06, 99.97 (2C), 113.98, 120.09, 123.76, 126.04, 128.28, 133.74, 134.07, 135.00, 144.26, 152.47 (2C), 154.36, 154.67, 160.94. MS (ESI): $[M+1]^+$=400.5. Anal. ($C_{19}H_{17}N_3O_3S_2$) C, H, N.

6-(4-Fluorophenyl)-N-(3,4,5-trimethoxyphenyl)thieno[3,2-d]pyrimidin-4-amine (6c). The crude residue was purified by flash chromatography, using ethyl acetate as eluent, to furnish **6c** as a brown solid. Yield: 68%, mp 192 °C. ^{1}H-NMR (*d*$_6$-DMSO) δ: 3.65 (s, 3H), 3.77 (s, 6H), 7.19 (s, 2H), 7.37 (t, J=9.2 Hz, 2H), 7.86 (s, 1H), 7.88 (m, 2H), 8.57 (s, 1H), 9.63 (bs, 1H). ^{13}C-NMR (*d*$_6$-DMSO) δ: 56.30 (2C), 60.62, 10.67 (2C), 115.18, 116.81, 117.03, 121.13, 128.95, 129.04, 129.75, 134.38, 135.44, 148.68, 153.02, 154.97, 155.26, 161.54, 162.07, 164.53. MS (ESI): $[M+1]^+$=412.4. Anal. ($C_{21}H_{18}FN_3O_3S$) C, H, N.

6-(4-Chlorophenyl)-N-(3,4,5-trimethoxyphenyl)thieno[3,2-d]pyrimidin-4-amine (6d). The crude residue was purified by flash chromatography, using ethyl acetate as eluent, to furnish **6d** as a white solid. Yield: 65%, mp 215 °C. ^{1}H-NMR (*d*$_6$-DMSO) δ: 3.67 (s, 3H), 3.79 (s, 6H), 7.20 (s, 2H), 7.58 (d, J=7.2 Hz, 2H), 7.86 (d, J=7.2 Hz, 2H), 7.93 (s, 1H), 8.59 (s, 1H), 9.66 (s, 1H). ^{13}C-NMR (*d*$_6$-DMSO) δ: 55.74 (2C), 60.06, 100.14 (2C), 114.80, 121.08 (2C), 127.86 (2C), 129.34 (2C), 131.43, 133.78, 134.18, 134.84, 147.80, 152.47, 154.44, 154.74, 160.87. MS (ESI): $[M+1]^+$=428.9. Anal. ($C_{21}H_{18}ClN_3O_3S$) C, H, N.

6-(4-Bromophenyl)-N-(3,4,5-trimethoxyphenyl)thieno[3,2-d]pyrimidin-4-amine (6e). The crude residue was purified by flash chromatography, using ethyl acetate as eluent, to furnish **6e** as a yellow solid. Yield: 68%, mp 219 °C. ^{1}H-NMR (*d*$_6$-DMSO) δ: 3.67 (s, 3H), 3.79 (s, 6H), 7.20 (s, 2H), 7.71 (d, J=7.8 Hz, 2H), 7.80 (d, J=7,8 Hz, 2H), 7.95 (s, 1H), 8.59 (s, 1H), 9.66 (s, 1H). ^{13}C-NMR (*d*$_6$-DMSO) δ: 55.75 (2C), 60.06, 100.14 (2C), 114.81, 121.08, 122.86, 128.09 (2C), 131.79, 132.25 (2C), 133.87, 134.86, 147.88, 152.47 (2C), 154.46, 154.75, 160.89. MS (ESI): $[M+1]^+$=520.4. Anal. ($C_{21}H_{18}BrN_3O_3S$) C, H, N.

6-(4-Iodophenyl)-N-(3,4,5-trimethoxyphenyl)thieno[3,2-d]pyrimidin-4-amine (6f). The crude residue was purified by flash chromatography, using ethyl acetate:petroleum ether 8:2 (v:v) as eluent, to furnish **6f** as a yellow solid. Yield: 61%, mp 199 °C. ^{1}H-NMR (*d*$_6$-DMSO) δ: 3.67 (s, 3H), 3.79 (s, 6H), 7.20 (s, 2H), 7.84 (d, J=8.4 Hz, 2H), 7.88 (d, J=8.4 Hz, 2H), 7.94 (s, 1H), 8.59 (s, 1H), 9.65 (s, 1H). ^{13}C-NMR (*d*$_6$-DMSO) δ: 55.73 (2C), 60.05, 100.11 (2C), 114.72, 120.91 (2C), 126.14, 127.98 (2C), 129.33, 132.03, 133.84, 134.85, 138.07, 148.14, 152.46, 154.43, 154.72, 160.87. MS (ESI): $[M+1]^+$=520.4. Anal. ($C_{21}H_{18}IN_3O_3S$) C, H, N.

6-(p-Tolyl)-N-(3,4,5-trimethoxyphenyl)thieno[3,2-d]pyrimidin-4-amine (6g). The crude residue was purified by flash chromatography, using ethyl acetate as eluent, to furnish **6g** as a yellow solid. Yield: 75%, mp 202 °C. ^{1}H-NMR (*d*$_6$-DMSO) δ: 2.37 (s, 3H), 3.67 (s, 3H), 3.79 (s, 6H), 7.22 (s, 2H), 7.33 (d, J=8.0 Hz, 2H), 7.74 (d, J=8.0 Hz, 2H), 7.83 (s, 1H), 8.58 (s, 1H), 9.60 (s, 1H). ^{13}C-NMR (*d*$_6$-DMSO) δ: 20.77, 55.73 (2C), 60.05, 99.99 (2C), 114.32, 119.63, 126.04 (2C), 129.78, 129.97 (2C), 133.75, 134.99, 139.47, 149.51, 152.46 (2C), 154.30, 154.64, 161.02. MS (ESI): $[M+1]^+$=408.5. Anal. ($C_{22}H_{21}N_3O_3S$) C, H, N.

6-(4-Methoxyphenyl)-N-(3,4,5-trimethoxyphenyl)thieno[3,2-d]pyrimidin-4-amine (6h). The crude residue was purified by flash chromatography, using ethyl acetate as eluent,

to furnish **6h** as a brown solid. Yield: 54%, mp 182 °C. ^{1}H-NMR (d_6-DMSO) δ: 3.67 (s, 3H), 3.79 (s, 6H), 3.83 (s, 3H), 7.07 (d, J=8.4 Hz, 2H), 7.21 (s, 2H), 7.76 (s, 1H), 7.83 (d, J=8.8 Hz, 2H), 8.56 (s, 1H), 9.56 (s, 1H). ^{13}C-NMR (d_6-DMSO) δ: 55.31, 55.75 (2C), 60.08, 99.97 (2C), 105.88, 109.63, 114.73 (2C), 118.87 (2C), 125.06, 127.64 (2C), 135.06, 149.46, 152.49, 154.30, 154.58, 160.39, 161.22. MS (ESI): $[M+1]^+$=424.5. Anal. ($C_{22}H_{21}N_3O_4S$) C, H, N.

6-(3-Methoxyphenyl)-N-(3,4,5-trimethoxyphenyl)thieno[3,2-d]pyrimidin-4-amine (6i). The crude residue was purified by flash chromatography, using ethyl acetate as eluent, to furnish **6i** as a yellow solid. Yield: 62%, mp 163 °C. ^{1}H-NMR (d_6-DMSO) δ: 3.67 (s, 3H), 3.78 (s, 6H), 3.86 (s, 3H), 7.08 (m, 1H), 7.14 (s, 2H), 7.43 (m, 3H), 7.94 (s, 1H), 8.59 (s, 1H), 9.63 (s, 1H). ^{13}C-NMR (d_6-DMSO) δ: 55.35, 55.85 (2C), 60.16, 100.05 (2C), 111.47, 114.77, 115.56, 118.55, 120.85, 130.61, 133.86, 133.95, 135.08, 149.22, 152.57 (2C), 154.48, 154.78, 159.86, 160.95. MS (ESI): $[M+1]^+$=424.5. Anal. ($C_{22}H_{21}N_3O_4S$) C, H, N.

6-(4-Nitrophenyl)-N-(3,4,5-trimethoxyphenyl)thieno[3,2-d]pyrimidin-4-amine (6j). The crude residue was purified by flash chromatography, using ethyl acetate as eluent, to furnish **6j** as a yellow solid. Yield: 79%, mp >300 °C. ^{1}H-NMR (d_6-DMSO) δ: 3.67 (s, 3H), 3,80 (s, 6H), 7.21 (s, 3H), 8.12 (d, J=9.0 Hz, 2H), 8.17 (s, 1H), 8.35 (d, J=9.0 Hz, 2H), 8.63 (s, 1H), 9.78 (s, 1H). ^{13}C-NMR ($CDCl_3$) δ: 55.77 (2C), 60.06, 78.53, 78.86, 79.19, 100.32 (2C), 123.48, 124.54 (2C), 127.27 (2C), 134.67, 138.68, 147.53, 152.50 (2C), 154.68, 154.91, 160.63. MS (ESI): $[M+1]^+$=439.4. Anal. ($C_{21}H_{18}N_4O_5S$) C, H, N.

General procedure for the preparation of compounds 10a-n and 13a-l. A mixture of the appropriate methyl 3-aminothiophene-5-aryl/heteroaryl-2-carboxylate **9a-j**, ethyl 5-amino-2-anilinothiazole-4-carboxylate **9k-n** or ethyl 2-aminothiophene-3-carboxylate derivatives **12a-l** (10 mmol) and formamide (15 mL) was heated at 180 °C for 18 h. After cooling to room temperature, cooled water (15 mL) was added to the reaction mixture. The solid was removed by filtration, washed with water and dried under vacuum for 12 h. The crude residue was suspended in ethyl ether, stirred for 30 min and filtered. The solid was used for the next reaction without further purification.

6-Phenylthieno[3,2-d]pyrimidin-4(3H)-one (10a). Yellow solid, yield: 71%, mp 294 °C. ^{1}H-NMR (d_6-DMSO) δ: 7.48 (m, 3H), 7.35 (m, 3H), 8.17 (s, 1H), 12.6 (bs, 1H). MS (ESI): $[M+1]^+$=229.3.

6-(Thiophen-2-yl)thieno[3,2-d]pyrimidin-4(3H)-one (10b). Black solid, yield: 95%, mp 170 °C. ^{1}H-NMR (d_6-DMSO) δ: 7.63 (dd, J=2.6 and 1,6 Hz, 1H), 7.74 (dd, J=2.6 and 1,6 Hz, 1H), 8.01 (s, 1H), 8.10 (m, 1H), 8.15 (s, 1H), 12.2 (bs, 1H). MS (ESI): $[M+1]^+$=235.3.

6-(4-Fluorophenyl)thieno[3,2-d]pyrimidin-4(3H)-one (10c). Brown solid, yield: 81%, mp >300 °C. ^{1}H-NMR (d_6-DMSO) δ: 7.34 (d, J=8.8 Hz, 2H), 7.83 (s, 1H), 7.93 (m, 2H), 8.17 (s, 1H), 12.6 (bs, 1H). MS (ESI): $[M+1]^+$=247.3.

6-(4-Chlorophenyl)thieno[3,2-d]pyrimidin-4(3H)-one (10d). Brown solid, yield: 89%, mp >300 °C. ^{1}H-NMR (d_6-DMSO) δ: 7.54 (d, J=8.8 Hz, 2H), 7.87 (m, 3H), 8.17 (s, 1H), 11.6 (bs, 1H). MS (ESI): $[M+1]^+$=263.7.

6-(4-Bromophenyl)thieno[3,2-d]pyrimidin-4(3H)-one (10e). Yellow solid, yield: 78%, mp >300 °C.^{1}H-NMR (d_6-DMSO) δ: 7.67 (d, J=8.6 Hz, 2H), 7.80 (d, J=8.6 Hz, 2H), 7.90 (s, 1H), 8.17 (s, 1H), 12.6 (bs, 1H). MS (ESI): $[M+1]^+$=308.2.

6-(4-Iodophenyl)thieno[3,2-d]pyrimidin-4(3H)-one (10f). Yellow solid, yield: 95%, mp >300 °C. ^{1}H-NMR (d_6-DMSO) δ: 7.63 (d, J=8.8 Hz, 2H), 7.87 (m, 3H), 8.17 (s, 1H), 11.4 (bs, 1H). MS (ESI): $[M+1]^+$=279.7.

6-(4-Tolyl)thieno[3,2-d]pyrimidin-4(3H)-one (10g). Brown solid, yield: 83%, mp >300 °C. ^{1}H-NMR (d_6-DMSO) δ: 2.36 (s, 3H), 7.29 (d, J=7.8 Hz, 2H), 7.73 (m, 3H), 8.15 (s, 1H), 12.5 (bs, 1H). MS (ESI): $[M+1]^+$=243.3.

6-(4-Methoxyphenyl)thieno[3,2-d]pyrimidin-4(3H)-one (10h). Brown solid, yield: >95%, mp >300 °C. ^{1}H-NMR (d_6-DMSO) δ: 3.82 (s, 3H), 7.03 (d, J=8.8 Hz, 2H), 7.71 (s, 1H), 7.78 (d, J=8.8 Hz, 2H), 8.14 (s, 1H), 11.8 (bs, 1H). MS (ESI): $[M+1]^+$=259.3.

6-(3-Methoxyphenyl)thieno[3,2-d]pyrimidin-4(3H)-one (10i). Brown solid, yield: >95%, mp 212 °C. ^{1}H-NMR (d_6-DMSO) δ: 3.84 (s, 3H), 7.04 (m, 1H), 7.39 (m, 2H), 7.88 (s, 1H), 7.94 (d, J=8.6 Hz, 1H), 8.17 (s, 1H), 12.0 (bs, 1H). MS (ESI): $[M+1]^+$=259.3.

6-(4-Nitrophenyl)thieno[3,2-d]pyrimidin-4(3H)-one (10j). Brown solid, yield: >95% yield, mp >300 °C. ^{1}H-NMR (d_6-DMSO) δ: 7.18 (d, J=8.8 Hz, 2H), 7.43 (d, J=8.8 Hz, 2H), 7.94 (s, 1H), 10.5 (bs, 1H), 11.4 (bs, 1H). MS (ESI): $[M+1]^+$=274.3.

General procedure for the preparation of compounds 11a-n and 14a-l. A mixture of the appropriate thieno[3,2-*d*]pyrimidin-4(3*H*)-one **10a-j**, thiazolo[4,5-*d*]pyrimidin-7(6*H*)-one **10k-n** or thieno[2,3-*d*]pyrimidin-4(3*H*)-one **13a-l** (5 mmol) and $POCl_3$ (30 mL) with 2-3 drops of DMF was refluxed for 6 h. The mixture was cooled, $POCl_3$ was removed under vacuum, the residue obtained was poured into a saturated solution of $NaHCO_3$ and the suspension neutralized with solid $NaHCO_3$. The mixture was extracted with dichloromethane, the organic phase washed with water, brine, dried over Na_2SO_4 and concentrated *in vacuo*. The crude product was stirred for 15 min with ethyl ether (15 mL), and the desired product was obtained after removal of the ether by filtration.

4-Chloro-6-phenylthieno[3,2-d]pyrimidine (11a). Brown solid, yield: 71%, mp 152 °C. ^{1}H-NMR (d_6-DMSO) δ: 7.57 (m, 3H), 6.01 (m, 2H), 8.25 (s, 1H), 9.03 (s, 1H). MS (ESI): $[M+1]^+$=247.7.

4-Chloro-6-(thiophen-2-yl)thieno[3,2-d]pyrimidine (11b). Orange solid, yield: 60%, mp 176 °C. ^{1}H-NMR (d_6-DMSO) δ: 7.79 (m, 2H), 8.11 (s, 1H), 8.36 (dd, J=2.6 and 1,6 Hz, 1H), 9.00 (s, 1H). MS (ESI): $[M+1]^+$=252.7.

4-Chloro-6-(4-fluorophenyl)thieno[3,2-d]pyrimidine (11c). Brown solid, yield: 83%, mp >300 °C. ^{1}H-NMR ($CDCl_3$) δ: 7.37 (d, J=8.8 Hz, 2H), 8.04 (m, 2H), 8.11 (s, 1H), 9.03 (s, 1H). MS (ESI): $[M+1]^+$=265.7.

4-Chloro-6-(4-chlorophenyl)thieno[3,2-d]pyrimidine (11d). Yellow solid, yield: 68%, mp 188 °C.^{1}H-NMR ($CDCl_3$) δ: 7.47 (d, J=8.8 Hz, 2H), 7.69 (m, 3H), 8.96 (s, 1H). MS (ESI): $[M+1]^+$=282.2.

6-(4-Bromophenyl)-4-chlorothieno[3,2-d]pyrimidine (11e). Yellow solid. Yield: 55%, mp 201 °C. ^{1}H-NMR (d_6-DMSO) δ: 7.75 (d, J=9.0 Hz, 2H), 7.93 (d, J=9.0 Hz, 2H), 8,29 (s, 1H), 9.04 (s, 1H). MS (ESI): $[M+1]^+$=326.6.

4-Chloro-6-(4-iodophenyl)thieno[3,2-d]pyrimidine (11f). Yellow solid, yield: 54%, mp >300 °C. ^{1}H-NMR ($CDCl_3$) δ: 7.81 (d, J=8.4 Hz, 2H), 7.95 (d, J=8.4 Hz, 2H), 8.29 (s, 1H), 9.04 (s, 1H). MS (ESI): $[M+1]^+$=373.6.

4-Chloro-6-(p-tolyl)thieno[3,2-d]pyrimidine (11g). Brown solid, yield: 84%, mp >300 °C. ^{1}H-NMR (d_6-DMSO) δ: 2.39 (s, 3H), 7.36 (d, J=7.8 Hz, 2H), 7.87 (d, J=7.8 Hz, 2H), 8.18 (s, 1H), 9.01 (s, 1H). MS (ESI): $[M+1]^+$=261.7.

4-Chloro-6-(4-methoxyphenyl)thieno[3,2-d]pyrimidine (11h). Yellow solid, yield: 72%, mp 181 °C. ^{1}H-NMR ($CDCl_3$) δ: 3.89 (s, 3H), 7.04 (d, J=8.8 Hz, 2H), 7.69 (s, 1H), 7.71 (d, J=8.8 Hz, 2H), 8.93 (s, 1H). MS (ESI): $[M+1]^+$=277.7.

4-Chloro-6-(3-methoxyphenyl)thieno[3,2-d]pyrimidine (11i). Brown solid, yield: 61%, mp 153 °C. ^{1}H-NMR ($CDCl_3$) δ: 3.87 (s, 3H), 7.14 (m, 1H), 7.76 (m, 3H), 8.29 (s, 1H), 9.04 (s, 1H). MS (ESI): $[M+1]^+$=277.7.

4-Chloro-6-(4-nitrophenyl)thieno[3,2-d]pyrimidine (11j). Orange solid, yield: >95%, mp >300 °C. ^{1}H-NMR (d_6-DMSO) δ: 8.32 (d, J=8.8 Hz, 2H), 8.36 (d, J=8.8 Hz, 2H), 8.51 (s, 1H), 9.10 (s, 1H). MS (ESI): $[M+1]^+$=292.7.

Biology

Materials and Methods

Cytotoxicity assays. The cell lines and culture media used were described previously, as were the cell culture methodologies.[35] The 10 mM compound stock solutions were prepared with DMSO, and the DMSO concentration in cytotoxicity and all cell-based assays was always ≤ 0.25%.

Tubulin assays. Assessment of compound effects on tubulin polymerization was described in detail previously,[53a] as was measurement of the binding of [^{3}H] colchicine to tubulin.[53b] The polymerization assay contained 10 μM purified bovine brain tubulin, and the extent of assembly after a 20 min incubation at 30 °C was the parameter measured. The reaction components in the colchicine assay included 1.0 μM tubulin, 5.0 μM [^{3}H] colchicine, and potential inhibitors at 1.0 or 5.0 μM.

EGFR and VEGFR kinase activity assays. Kinase assays were performed using the bioluminescent ADP-Glo™ kinase assay (Promega, Milano Italy), following the manufacturer's instructions. The assay was performed with the test compounds at different scalar concentrations. The IC_{50} values reported are based on the average of at least 2 titration curves. As reference compounds erlotinib (Sigma-Aldrich) and sunitinib (Selleckchem, USA) were used.

Molecular modeling. Hardware, software and general methodology were described in detail previously.[51,54,55] Protein structures were downloaded from the PDB data bank (http://www.rcsb.org/; PDB codes 1SA0 and 2J6M, respectively, for tubulin and the EGFR kinase domain). The two proteins were pre-processed using the Schrödinger Protein Preparation Wizard by assigning bond orders, adding hydrogens and performing a restrained energy minimization of the added hydrogens using the OPLS_2005 force field. Ligand structures were built with MOE and minimized using the MMFF94x force field. The ligands were then prepared using the Maestro LigPrep tool by energy minimizing the structures (OPLS_2005 force filed), generating possible ionization states at pH 7±2, generating tautomers and low-energy ring conformers. A 12 Å docking grid (inner-box 10 Å and outer-box 22 Å) was prepared using as centroid the co-crystallized DAMA-colchicine for the tubulin structure. A 15 Å docking grid (inner-box 10 Å and outer-box 25 Å) was prepared using as centroid the co-crystallized AEE788 for the EGFR structure. Molecular docking was performed using Glide SP precision keeping the default parameters and setting 5 as the number of output poses per input ligand to include in the solution. The docking results were visually inspected on MOE for their ability to bind the active sites.

Cell cycle distribution evaluated by flow cytometry. HeLa or Jurkat cells (50,000 cells) were exposed to compounds for 24 h. Cells were harvested by centrifugation and fixed with 70% (v/v) ethanol (0 °C). Cells were lysed with 0.1% (v/v) Triton X-100 containing RNase A and stained with PI. A Beckman-Coulter Cytomic FC500 instrument and MultiCycle for Windows software from Phoenix Flow Systems were used to analyze the cells.

Measurement of apoptosis by flow cytometry. In these studies, the Cytomics FC500 instrument was used. The cells were stained with both PI, to stain DNA, and annexin V-FITC, to stain membrane PS on the cell surface (which occurs in apoptosis). The latter was done following the instructions of the manufacturer (Roche Diagnostics) of the Annexin-V Fluos reagent.

Evaluation of cellular protein expression with western blots. Following growth for various times in the presence of **6g**, HeLa cells were harvested by centrifugation and washed twice in 0 °C phosphate-buffered saline (PBS). In some experiments Hela cells were treated with **6g** or erlotinib (Sigma-Aldrich) and stimulated with EGF (R&D Systems, Minneapolis MN, USA) 50 ng/mL for 15 min and then processed as described above. Cells were lysed with 0.1% (v/v) Triton X-100 containing RNase A at 0 °C, and supernatants were obtained by centrifuging the lysed cells at 15000 x g for 10 min at 4 °C. The protein content of the solutions was measured, and 10 µg of protein from each sample was subjected to sodium dodecyl sulfate-polyacrylamide gel electrophoresis. Proteins were transferred by electroblotting to a polyvinylidene difluoride Hybond-P membrane from GE Healthcare. The membranes were treated with 5% bovine serum albumin in PBS containing 0.1% Tween 20 overnight at 4 °C. The membranes were then exposed for 2 h at room temperature to primary antibodies directed against PARP, Mcl-1, Bcl-2, (all from Cell Signaling) or β-actin (Sigma-Aldrich; to verify equal protein loading) and subsequently for 1 h to peroxidase labeled secondary antibodies. The membranes were visualized using ECL Select (GE Healthcare), and images were acquired using an Uvitec-Alliance imaging system.

Use of HUVECS as a model for antivascular activity. Adherent HUVECs, were obtained and cultured as before.[46,49] Once confluent, the cells were removed from the culture matrix with a trypsin-EDTA solution and used up to the sixth passage.

Matrigel matrix (Basement Membrane Matrix, BD Biosciences) was prepared and left for 3h at 4 °C. At this point, 230 µL of the matrix preparation was added to each well of a 24-well plate. The matrix was allowed to gel at 37 °C for 30 min. The matrix in each well was overlaid with 500 µL of medium containing 6000 HUVECs, which was incubated for 6 h to allow formation of capillary tubes. Different concentrations of **6g** were added, and the cultures were incubated for another hour to monitor the disappearance of existing vasculature. The cultures were photographed (the four quadrants and the center of each well) at 10x magnification (phase contrast). The images were saved as TIFF files and analyzed with ImageJ image analysis software. Standard dimensional parameters (percent area covered by HUVECs and total length of HUVECs network per field) were noted, and standard topological parameters (number of meshes and branching points per field) were estimated.[46,49]

***In vivo* activity of 6g.** Animal procedures and care were performed in accord with institutional guidelines complying with all national and international laws and policies (EEC

Council Directive 86/609, OJ L 358, 12 December 1987) and with "ARRIVE" guidelines (Animals in Research Reporting In Vivo Experiments). Six-week old C57BL/6 mice (from Charles River) were injected s.q. into the dorsolateral flank with 200 µL of PBS containing 25,000 BL6-B16 murine melanoma cells. Tumours became palpable on the ninth day, and animals were given q.o.d. x 4 i.p. injections of test compounds dissolved in 50 µL of DMSO at desired doses. Tumours were measured in two dimensions, and tumour volume was calculated using the formula $V= (D \times d^2)/2$, where D and d are the major and minor perpendicular tumour diameters.

4.6 References

1. a) Akhmanova, A.; Steinmetz, M. O. Control of microtubule organization and dynamics: two ends in the limelight. Nat. Rev. *Mol. Cell. Biol.* **2015**, *16*, 711-726; b) Brouhard, G. J.; Rice, L. M. The contribution of αβ-tubulin curvature to microtubule dynamics. *J. Cell Biol.* **2014**, *207*, 323-334.
2. a) Vindya, N. G.; Sharma, N.; Yadav, M.; Ethiraj, K. R. Tubulins-the target for anticancer therapy. *Curr. Top. Med. Chem.* **2015**, *15*, 73-82; b) Nitika, V.; Kapil, K. Microtubule targeting agents: a benchmark in cancer therapy. *Curr. Drug Ther.* **2014**, *8*, 189-196.
3. a) Patil, P. O.; Patil, A. G.; Rane, R. A.; Patil, P. C.; Deshmukh, P. K.; Bari, S. B.; Patil, D. A.; Naphade, S. S. Recent advancement in discovery and development of natural product combretastatin-inspired anticancer agents. *Anticancer Agents Med. Chem.* **2015**, *15*, 955-969; b) Mukhtar, E.; Adhami, V. M.; Mukhtar, H. Targeting microtubules by natural agents for cancer therapy. *Mol. Cancer Ther.* **2014**, 13, 275-284.
4. a) Porcù, E.; Bortolozzi, R.; Basso, G.; Viola, G. Recent advances in vascular disrupting agents in cancer therapy. *Future Med. Chem.* **2014**, *6*, 1485-1498, b) Mita, M. M.; Sargsyan, L.; Mita, A. C.; Spear, M. Vascular disrupting agents in oncology. *Expert. Opin. Invest. Drugs* **2013**, *22*, 317-328.
5. a) Pettit, G. R.; Singh, S. B.; Hamel, E.; Lin, C. M.; Alberts, D. S.; Garcia-Kendall, D. Isolation and structure of the strong cell growth and tubulin inhibitor combretastatin A-4. *Experientia* **1989**, *45*, 209-211; b) Pettit, G. R.; Cragg, G. M.; Herald, D. L.; Schmidt, J. M.; Lohavanijaya, P. Isolation and structure of combretastatin. *Can. J. Chem.* **1982**, *60*, 1374-1376.

6. Lin, C. M.; Ho, H. H.; Pettit, G. R.; Hamel, E. Antimitotic natural products combretastatin A-4 and combretastatin A-2: studies on the mechanism of their inhibition of the binding of colchicine to tubulin. *Biochemistry* **1989**, *28*, 6984-6991.
7. Liu, P.; Qin, Y.; Wu, L.; Yang, S.; Li, N.; Wang, H.; Xu, H.; Sun, K.; Zhang, S.; Han, X.; Sun, Y.; Shi, Y. A phase I clinical trial assessing the safety and tolerability of combretastatin A4 phosphate injections. *Anti-Cancer Drugs* **2014**, *25*, 462-471.
8. a) Patil, P. O.; Patil, A. G.; Rane, R. A.; Patil, P. C.; Deshmukh, P. K.; Bari, S. B.; Patil, D. A.; Naphade, S. S. Recent advancement in discovery and development of natural product combretastatin-inspired anticancer agents. *Anticancer Agents Med. Chem.* **2015**, *15*, 955-969; b) Rajak, H.; Dewangan, P. K.; Patel, V.; Jain, D. K.; Singh, A.; Veerasamy, R.; Sharma, P. C.; Dixit, A. design of combretastatin A-4 analogs as tubulin targeted vascular disrupting agent with special emphasis on their cis-restricted isomers. *Curr. Pharm. Des.* **2013**, *19*, 1923-1955.
9. Greene, L. M.; Meegan, M. J.; Zisterer, D. M. Combretastatins: more than just vascular targeting agents? *J. Pharmacol. Exp. Ther.* **2015**, *355*, 212-227.
10. Field, J. J.; Kanakkanthara, A.; Miller, J. H. Microtubule-targeting agents are clinically successful due to both mitotic and interphase impairment of microtubule function. *Bioorg. Med. Chem.* **2014,** *22*, 5050-5059.
11. a) Goffin, J. R.; Zbuk, K. Epidermal growth factor receptor: pathway, therapies, and pipeline. *Clin. Ther.* **2013**, *35*, 1282-1303; b) Reardon, D. A.; Wen, P. Y.; Mellinghoff, I. K. Targeted molecular therapies against epidermal growth factor receptor: past experiences and challenges. *Neuro Oncol.* **2014**, *16*, viii7-viii13.
12. Hynes, N. E.; Horsch, K.; Olayioye, M. A.; Badache, A. The ErbB receptor tyrosine family as signal integrators. *Endocr. Relat. Cancer* **2001**, *8*, 151-159.
13. a) Hynes, N. E.; Lane, H. A. ERBB receptors and cancer: the complexity of targeted inhibitors. *Nat. Rev. Cancer* **2005**, *5*, 341-354; b) Arteaga, C. L. Epidermal growth factor receptor dependence in human tumors: more than just expression? *Oncologist* **2002**, *4*, 31-39.
14. Olayioye, M. A.; Neve, R. M.; Lane, H. A. N.; Hynes, N. E. The ErbB signaling network: receptor heterodimerization in development and cancer. *EMBO J.* **2000**, *13*, 3159-3167.
15. a) Zhang, H. Three generations of epidermal growth factor receptor tyrosine kinase inhibitors developed to revolutionize the therapy of lung cancer. *Drug Des. Devel. Ther.* **2016**, *10*, 3867-3872; b) Hossam, M.; Lasheen, D. S.; Abouzid, K. A. Covalent EGFR inhibitors: binding mechanisms, synthetic approaches, and clinical profiles.

Arch. Pharm. **2016**, *349*, 573-593; c) Liu, F.; Tang, B.; Liu, H.; Li, L.; Liu, G.; Cheng, Y.; Xu, Y.; Chen, W.; Huang, Y. 4-Anilinoquinazoline derivatives with epidermal growth factor receptor inhibitor activity. *Anticancer Agents Med. Chem.* **2016**, *16*, 1652-1664.

16. a) Herbst, R. S.; Heymach, J. V.; Lippman, S. M. Lung cancer. *N. Engl. J. Med.* **2008**, *13*, 1367-1380; b) Di Maio, M.; Gridelli, C.; Normanno, N.; Perrone, F.; Ciardiello, F. Trying to compose the puzzle with all the pieces: epidermal growth factor tyrosine kinase inhibitors in non-small cell lung cancer. *J. Cell. Physiol.* **2005**, *205*, 355-363: c) Cataldo, V. D.; Gibbons, D. L.; Perez-Soler, R.; Quintas-Cardama, A. Treatment of non-small-cell lung cancer with erlotinib or gefitinib. *N. Engl. J. Med.* **2011**, *364*, 947-955.

17. a) Yun, C. H.; Mengwasser, K. E. Toms, A. V.; Woo, M. S.; Greulich, H.; Wong, K. K.; Meyerson, M., Eck, M. J. The T790M mutation in EGFR kinase causes drug resistance by increasing the affinity for ATP. *Proc. Natl. Acad. Sci. U.S.A.* **2008**, *105*, 2070-2075; b) Trusolino, L.; Bertotti, A. Compensatory pathways in oncogenic kinase signaling and resistance to targeted therapies: six degrees of separation. *Cancer Discovery* **2012**, *2*, 876-880.

18. The identification numbers in https://clinicaltrials.gov (accessed Oct 25, 2018) websites are: NCT02326285, NCT00720304, NCT00049283, NCT02319577, NCT00083057, NCT01405079, NCT01755923, NCT00532441, NCT01749072, NCT01050322, NCT00446225 and NCT00553358.

19. a) Litvinov, V. P. The chemistry of thienopyrimidines. *Adv. Heterocycl. Chem.* **2006**, 92, 83-143, b) El-Ansary, A. K.; Kamal, A. M.; Al-Ghorafi, M. A. Synthesis and evaluation of 4-anilinoquinazoline bioisosteres as potential anti-breast cancer agents. *Eur. J. Med. Chem.* **2014**, *86*, 202-210; c) Liu, Z.; Wu, S.; Wang, Y.; Li, R.; Wang, J.; Wang, L.; Zhao, Gong, P. Design, synthesis and biological evaluation of novel thieno[3,2-*d*]pyrimidine derivatives possessing diaryl semicarbazone scaffolds as potent antitumor agents. *Eur. J. Med. Chem.* **2014**, *87*, 782-799.

20. a) Bugge, S,; Kaspersen, S. J.; Larsen, S.; Nonstad, U.; Bjørkøy, G.; Sundby, E.; Hoff, B. H, Structure-activity study leading to identification of a highly active thienopyrimidine based EGFR inhibitor. *Eur. J. Med. Chem.* **2014**, *75*, 354-374; b) Rheault, T. R.; Caferro, T. R.; Dickerson, S. H.; Donaldson, K. H.; Gaul, M. D.; Goetz, A. S.; Mullin, R. J.; McDonald, O. B.; Petrov, K. G.; Rusnak, D. W.; Shewchuk, L. M.; Spehar, GH. M.; Truesdale, A. T.; Vanderwall, D. E.; Wood, E. R.; Uehling, D. E. Thienopyrimidine-based dual EGFR/ErbB-2 inhibitors. *Bioorg.*

Med. Chem. Lett. **2009**, *19*, 817-820; c) Beckers, T.; Sellmer, A.; Eichhorn, E.; Pongratz, H.; Schaechtele, C.; Totzke, F.; Kelter, G.; Krumbach, R.; Fiebig, H. H.; Boehmer, F. D.; Mahboobi, S. Novel inhibitors of epidermal growth factor receptor: (4-(arylamino)-7*H*-pyrrolo[2,3-*d*]pyrimidin-6-yl)(1*H*-indol-2-yl)methanones and (1*H*-indol-2-yl)(4-(phenylamino) thieno[2,3-*d*]pyrimidin-6-yl)methanones. *Bioorg. Med. Chem.* **2012**, *20*, 125-136; d) Milik, S.A., Abdel-Aziz, A.K.; Lasheen, D.S.; Serya, R.A.T.; Minucci, S.; Abouzid, K.A.M. Surmounting the resistance against EGFR inhibitors through the development of thieno[2,3-*d*]pyrimidine-based dual EGFR/HER2 inhibitors. *Eur. J. Med. Chem.* **2018**, *155*, 316-336.

21. Munchhof, M. J.; Beebe, J. S.; Casavant, J. M.; Cooper, B. A.; Doty, J. L.; Higdon, R. C.; Hillerman, S. M.; Soderstrom, C. I.; Knauth, E. A.; Marx, M. A.; Rossi, A. M.; Sobolov, S. B.; Sun, J. Design and SAR of thienopyrimidine and thienopyridine inhibitors of VEGFR-2 kinase activity. *Bioorg. Med. Chem. Lett.* **2004**, *14*, 21-24.
22. Kemnitzer, W.; Sirisoma, N.; May, C.; Tseng, B.; Drewe, J. ; Xiong Cai, S. Discovery of 4-anilino-*N*-methylthieno[3,2-*d*]pyrimidines and 4-anilino-*N*-methylthieno[2,3-*d*]pyrimidines as potent apoptosis inducers. *Bioorg. Med. Chem. Lett.* **2009**, *19*, 3536-3540.
23. Bugge, S.; Formo Buene, A.; Jurisch-Yaksi, N.; Ullestad Moen, I.; Skjønsfjell, E. M.; Sundby, E.; Hoff, B. H. Extended structure-activity study of thienopyrimidine-based EGFR inhibitors with evaluation of drug-like properties. *Eur. J. Med. Chem.* **2016**, *107*, 255-274.
24. Lin, R.; Johnson, S. G.; Connolly, P. J.; Wetter, S. K.; Binnun, E.; Hughes, T. V.; Murray, W. V.; Pandey, N. B.; Moreno-Mazza, S. J.; Adams, M.; Fuentes-Pesquera, A. R.; Middleton, S. A. Synthesis and evaluation of 2,7-diamino-thiazolo[4,5-*d*]pyrimidine analogues as anti-tumor epidermal growth factor receptor (EGFR) tyrosine kinase inhibitors. *Bioorg. Med. Chem. Lett.* **2009**, *19*, 2333-2337.
25. a) Cushman, M.; Nagarathnam, D.; Gopal, D.; He, H.-M.; Lin, C. M.; Hamel, E. Synthesis and evaluation of analogues of (*Z*)-1-(4-methoxyphenyl)-2-(3,4,5-trimethoxyphenyl)ethene as potential cytotoxic and antimitotic agents. *J. Med. Chem.* **1992**, *35*, 2293-2306; b) Hatanaka, T.; Fujita, K.; Ohsumi, K.; Nakagawa, R.; Fukuda, Y.; Nihei, Y.; Suga, Y.; Akiyama, Y.; Tsuji, T. Novel B-ring modified combretastatin analogues: synthesis and antineoplastic activity. *Bioorg. Med. Chem. Lett.* **1998**, *8*, 3371-3374; c) Negi, A. S.; Gautam, Y.; Alam, S.; Chanda, D.; Luqman, S.; Sarkar, J.; Khan, F.; Konwar, R. Natural antitubulin agents: Importance of 3,4,5-trimethoxyphenyl fragment. *Bioorg. Med. Chem.* **2015**, *23*, 373-389.

26. Devambatla, R. K. V.; Choudhary, S.; Ihnat, M.; Hamel, E.; Mooberry, S. L. Gangjee, A. Design, synthesis and preclinical evaluation of 5-methyl-N^4-aryl-furo[2,3-*d*]pyrimidines as single agents with combination chemotherapy potential. *Bioorg. Med. Chem. Lett.* **2018**, *28*, 3085-3093.
27. Pavana, R. K.; Choudhary, S.; Bastian, A.; Ihnat, M. A.; Bai, R.; Hamel, E.; Gangjee, A. Discovery and preclinical evaluation of 7-benzyl-*N*-(substituted)-pyrrolo[3,2-*d*]pyrimidin-4-amines as single agents with microtubule targeting effects along with triple-acting angiokinase inhibition as antitumor agents. *Bioorg Med Chem.* **2017**, *25*, 545-556.
28. Zhang, X.; Raghavan, S.; Ihnat, M.; Hamel, E.; Zammiello, C.; Bastian, A.; Mooberry, S. L.; Gangjee, A. The design, synthesis and biological evaluation of conformationally restricted 4-substituted-2,6-dimethylfuro[2,3-*d*]pyrimidines as multi-targeted receptor tyrosine kinase and microtubule inhibitors as potential antitumor agents. *Bioorg. Med. Chem.* **2015**, *23*, 2408-2423.
29. Ihmaid, S.; Ahmed, H. E. A.; Zayed, M. F. The design and development of potent small molecules as anticancer agents targeting EGFR TK and tubulin polymerization. *Int. J. Mol. Sci.* **2018**, *19*, 408.
30. Mphahlele, M. J.; Maluleka, M. M.; Parbhoo, N.; Malindisa, S. T. Synthesis, evaluation for cytotoxicity and molecular docking studies of benzo[*c*]furan-chalcones for potential to inhibit tubulin polymerization and/or EGFR-tyrosine kinase phosphorylation. *Int. J. Mol. Sci.* **2018**, *19*, 2552.
31. Zayed, M. F.; Ahmed, S.; Ihmaid, S.; Ahmed, H. E. A.; Rateb, H. S.; Ibrahim, S. R. M. Design, synthesis, cytotoxic evaluation and molecular docking of new fluoroquinazolinones as potent anticancer agents with dual EGFR kinase and tubulin polymerization inhibitory effects. *Int. J. Mol. Sci.* **2018,** *19*, 1731.
32. Zayed, M. F.; Rateb, H. S.; Ahmed, S.; Khaled, O. A.; Ibrahim, S. R. M. Quinazolinone-amino acid hybrids as dual inhibitors of EGFR kinase and tubulin polymerization. *Molecules* **2018**, *23*, 1699.
33. Alswah, M.; Bayoumi, A.H.; Elgamal, K.; Elmorsy, A.; Ihmaid, S.; Ahmed, H. E. A. Design, synthesis and cytotoxic evaluation of novel chalcone derivatives bearing triazolo[4,3-*a*]-quinoxaline moieties as potent anticancer agents with dual EGFR kinase and tubulin polymerization inhibitory effects. *Molecules* **2018**, *23*, 48.
34. Ravelli, R.B.; Gigant, B.; Curmi, P.A.; Jourdain, I.; Lachkar, S.; Sobel, A.; Knossow. M. Insight into tubulin regulation from a complex with colchicine and a stathmin-like domain. *Nature* **2004**, *428*, 198-202.

35. Romagnoli, R.; Baraldi, P. G.; Kimatrai Salvador, M.; Preti, D.; Aghazadeh Tabrizi, M.; Bassetto, M.; Brancale, A.; Hamel, E.; Castagliuolo, I.; Bortolozzi, R.; Basso, G.; Viola, G. . Synthesis and biological evaluation of 2-alkoxycarbonyl-3-anilino benzo[*b*]thiophenes and thieno[2,3-*c*]pyridines as new potent anticancer agents. *J. Med. Chem.* **2013**, *56*, 2606-2618.

36. Yun, C.-H.; Boggon, T. J.; Li, Y.; Woo, S.; Greulich, H.; Meyerson, M.; Eck, M. J. Structures of lung cancer-derived EGFR mutants and inhibitor complexes: mechanism of activation and insights into differential inhibitor sensitivity. *Cancer Cell* **2007**, *11*, 217-227.

37. Goto, H; Tomono, Y.; Ajiro, K.; Kosako H.; Fujita M.; Sakurai, M.; Okawa K.; Iwamatsu, A.; Okigaki, T.; Takahashi, T., Inagaki, M. Identification of a novel phosphorylation site on histone H3 coupled with mitotic chromosome condensation. *J. Biol. Chem.* **1999**, *274*, 25543-25549.

38. Xiong, S., Mu, T.; Wang, G.; Jiang, X. Mitochondria-mediated apoptosis in mammals. *Protein Cell* **2014**, *5*, 737-749.

39. Rovini, A., Savry, A., Braguer, D., Carré, M. Microtubule-targeted agents: when mitochondria become essential to chemotherapy. *Biochim. Biophys. Acta-Bioenerg.* **2011**, *1807*, 679-688.

40. Mendez, G., Policarpi, C., Cenciarelli, C., Tanzarella, C.; Antoccia, A. Role of Bim in apoptosis induced in H460 lung tumor cells by the spindle poison combretastatin-A4. *Apoptosis* **2011**, *16*, 940-949.

41. Romagnoli, R.; Baraldi, P. G.; Kimatrai Salvador, M.; Preti, D.; Tabrizi, M. A.; Brancale, A.; Fu, X.-H.; Li, J.; Zhang, S.-Z.; Hamel, E.; Bortolozzi, R.; Porcù, E.; Basso, G.; Viola, G. Discovery and optimization of a series of 2-aryl-4-amino-5-(3’,4’,5’-trimethoxybenzoyl)thiazoles as novel anticancer agents. *J. Med. Chem.* **2012**, *55*, 5433-5445.

42. Romagnoli, R.; Baraldi, P. G.; Kimatrai Salvador, M.; Prencipe, F.; Bertolasi, V.; Cancellieri, M.; Brancale, A.; Hamel, E.; Castagliuolo. I.; Consolaro, F.; Porcù, E.; Basso, G.; Viola, G. Synthesis, antimitotic and antivascular activity of 1-(3',4',5'-trimethoxybenzoyl)-3-arylamino-5-amino-1,2,4-triazoles. *J. Med. Chem.* **2014**, *57*, 6795-6808.

43. Zamzami, N.; Marchetti, P.; Castedo, M.; Decaudin, D.; Macho, A.; Hirsch, T.; Susin, S.A.; Petit, P. X.; Mignotte, B.; Kroemer, G. Sequential reduction of mitochondrial transmembrane potential and generation of reactive oxygen species in early programmed cell death. J. *Exp. Med.* **1995**, *182*, 367-377.

44. Wertz, I. E.; Kusam, S.; Lam, C., Okamoto, T.; Sandoval, W., Anderson, D. J.; Helgason, E., Ernst, J. A.; Eby, M.; Liu, J.; Belmont, L. D.; Kaminker, J. S.; O'Rourke, K. M.; Pujara, K.; Kohli, P. B.; Johnson, A. R.; Chiu, M. L.; Lill, J. R.; Jackson, P. K.; Fairbrother, W. J.; Seshagiri, S.; Ludlam, M. J.; Leong, K. G., Dueber, E. C.; Maecker, H.; Huang, D. C.; Dixit, V. M.. Sensitivity to antitubulin chemotherapeutics is regulated by MCL1 and FBW7. *Nature* **2011**, *471*, 110-114.

45. Czabotar, P. E., Lessene, G., Strasser, A.; Adams, J. M. Control of apoptosis by the BCL-2 protein family: implications for physiology and therapy. *Nature Rev. Mol. Cell Biol.* **2014**, *15*, 49-63.

46. Porcù, E.; Viola, G.; Bortolozzi, R.; Mitola, S.; Ronca, R.; Presta, M.; Persano, L.; Romagnoli, R.; Baraldi, P. G.; Basso, G. TR-644 a novel potent tubulin binding agent induces impairment of endothelial cells function and inhibits angiogenesis. *Angiogenesis* **2013**, *16*, 647-662.

47. Romagnoli, R.; Baraldi, P.G.; Kimatrai Salvador, M.; Prencipe, F.; Bertolasi, V.; Cancellieri, M.; Brancale, A.; Hamel, E.; Castagliuolo, I.; Consolaro, F.; Porcù, E.; Basso, G.; Viola, G. Synthesis, antimitotic and antivascular activity of 1-(3',4',5'-trimethoxybenzoyl)-3-arylamino-5-amino-1,2,4-triazoles. *J. Med. Chem.* **2014**, *57*, 6795-6808.

48. Romagnoli, R.; Baraldi, P.G.; Kimatrai Salvador, M.; Schiaffino Ortega, S.; Prencipe, F.; Brancale, A.; Hamel, E.; Castagliuolo, I.; Mitola, S.; Ronca, R.; Bortolozzi, R.; Porcù, E.; Basso, G.; Viola, G. Design, synthesis, *in vitro* and *in vivo* anticancer and antiangiogenic activity of novel 3-arylamino benzofuran derivatives targeting the colchicine site on tubulin *J. Med, Chem.* **2015**, *58*, 3209-3222.

49. Porcù, E.; Persano, L.; Ronca, R.; Mitola, S.; Bortolozzi, R., Romagnoli, R., Oliva, P., Basso, G., Viola, G. The novel antitubulin agent TR-764 strongly reduces tumor vasculature and inhibitis HIF-1α activation. *Sci. Rep.* **2016**, *6*, 27886.

50. Ronca, R.; Di Salle, E.; Giacomini, A.; Leali, D.; Alessi, P.; Coltrini, D.; Ravelli, C.; Matarazzo, S.; Ribatti, D.; Vermi, W.; Presta, M. Long pentraxin-3 inhibits epithelial-mesenchymal transition in melanoma cells. *Mol. Cancer Ther.* **2013**, *12*, 2760-2771.

51. Romagnoli, R.; Baraldi, P. G.; Prencipe, F.; Lopez-Cara L. C.; Ferla, S.; Brancale, A.; Hamel, E.; Ronca, R.; Bortolozzi, R.; Mariotto. E.; Basso, G.; Viola, G. Design and synthesis of potent in vitro and in vivo anticancer agents based on 1-(3',4',5'-trimethoxyphenyl)-2-aryl-1*H*-imidazole. *Sci. Rep.* **2016**, *6*, 26602.

52. Xu, Q.; Zhang, X.; Yue, J.; Liu, C.; Cao, C.; Zhong, H.; Qingjun Ma, Q. Human TGFalpha-derived peptide TGFalphaL3 fused with superantigen for immunotherapy of EGFR-expressing tumours. *BMC Biotechnology* **2010**, *10*, 91.

53. a) Hamel, E. Evaluation of antimitotic agents by quantitative comparisons of their effects on the polymerization of purified tubulin. *Cell Biochem. Biophys.* **2003**, *38*, 1-21; b) Verdier-Pinard, P.; Lai J.-Y.; Yoo, H.-D.; Yu, J.; Marquez, B.; Nagle D. G.; Nambu, M.; White, J. D.; Falck, J. R.; Gerwick, W. H.; Day, B. W.; Hamel, E. Structure-activity analysis of the interaction of curacin A, the potent colchicine site antimitotic agent, with tubulin and effects of analogs on the growth of MCF-7 breast cancer cells. *Mol. Pharmacol.* **1998**, *53*, 62-67.

54. Molecular Operating Environment (MOE 2015.10); Chemical Computing Group, Inc.: Montreal, Quebec, Canada; URL http://www.chemcomp.com (2015).

55. Schrödinger Release 2017-1: Maestro, Schrödinger, LLC, New York, NY, 20167.

5. Design, Synthesis, in Vitro and in Vivo Biological Evaluation of 2-Amino-3-Aroyl Benzofuran Derivatives as Highly Potent Tubulin Polymerization Inhibitors

5.1 Introduction

Microtubules, as key components of the cytoskeleton, are dynamic cellular structures in neoplastic and non-neoplastic cells generated by the polymerization of α,β-tubulin heterodimers.[1-3] The microtubule system of eukaryotic cells is a critical element involved in a variety of essential cellular processes besides mitotic spindle assembly, including determination and maintenance of cell shape, regulation of motility, cell signaling, secretion and intracellular transport.[4-6] Due to the essential role of microtubules in mitosis and cell division, tubulin is the target for numerous small natural and synthetic molecules that inhibit the formation of the mitotic spindle.[7-9] More recent studies have demonstrated that several small molecules able to interfere with the dynamic assembly of tubulin in generating the microtubule system are also able to induce extensive morphological changes in the endothelial cells of tumour vasculature. Such agents can thus also be classified as vascular disrupting agents (VDA).[10-12]

Among the natural microtubule depolymerizing agents, combretastatin A-4 (CA-4, **1a;** Figure 1) is one of the more studied compounds. CA-4, isolated from the bark of the South African tree *Combretum caffrum,*[13] strongly inhibits the polymerization of tubulin by binding to the colchicine site.[14] CA-4 inhibits cell growth at low to mid-nanomolar concentrations.[15] The water soluble sodium phosphate prodrug of CA-4 (CA-4P, fosbretabulin or Zybrestat, **1b**) is actually in phase III clinical trials for the treatment of anaplastic thyroid cancer and Phase II trials for non-small-cell lung cancer,[16-17] while the related serine aminoacid prodrug of 3'-amino-deoxycombretastatin A-4 (Ombrabulin or AVE8062, **1c**) was found to have more potent activity compared with CA-4P and is in phase I clinical studies for patients with solid tumours.[18] In addition, CA-4P and AVE8062 demonstrate strong suppressive activity on tumour blood flow, leading to tumour necrosis.[19,20]

Anticancer therapy based on microtubule-targeting agents that bind to tubulin at the colchicine-binding site and disrupt microtubule dynamics have received considerable attention and there is still a need to identify novel molecules that target microtubules.[21-24] Although many synthetic tubulin inhibitors have been synthesized in the last decades, among such compounds there are limited examples of chemically diverse small molecules antimitotic agents based on the benzo[*b*]furan molecular skeleton as the core structure.[25-31] During our continuing search directed at the preparation of new small molecules tubulin inhibitors, we previously reported the discovery of a series of methoxy-substituted 2-(3',4',5'-trimethoxybenzoyl)-3-aminobenzo[*b*]furan derivatives with general structure **2**, as a new class of antimitotic agents.[28] In this series of compounds, potent activity was highly dependent upon the presence and position of four methoxy substituents. A fairly dramatic difference was observed between C-4/5 and C-6/7-methoxy substituted compounds. The greatest activity occurred when the methoxy group was located at the 6- or 7-position, while 4- and 5-methoxy derivatives were inactive. Among the synthesized compounds, derivative **2a**, characterized by the presence of a methoxy group at the 6-position of the benzo[*b*]furan skeleton, displayed the greatest antiproliferative activity with IC_{50} values ranging from 87 to 430 nM against a panel of four different cancer cell lines. This agent inhibited tubulin polymerization by binding to the colchicine site on tubulin (IC_{50}: 1.1 μM for assembly) and caused G2/M phase arrest of the cell cycle.

The 3-(3',4',5'-trimethoxybenzoyl)-6-methoxybenzo[*b*]furan molecular skeleton was the core structure of a series of agents with general structure **3** identified by Pinney and co-workers as potent inhibitors of both tubulin polymerization and cell proliferation of the MCF-7 cancer cell line.[30,31] While at the C-2 position there was a wide tolerance to structural variation with hydrophobic and hydrophilic substituents, at the C-3 position the carbon linker with the 3',4',5'-trimethoxyphenyl substituent was more effective as a carbonyl group than as a carbinol or a simple methylene group.[30] Previous studies have shown that the concomitant presence of a C-6 methoxy substituent significantly contributed to maximize the activity, presumably as a mimic of the 4-methoxy group in the B-ring of CA-4.[30] The introduction of a hydroxyl at the C-7 position was well tolerated and afforded compounds with similar potency for R_2=H, while a 10-fold increase in activity was observed for R_2=OH.[31] Among the synthesized compounds, the C-2 3'-hydroxy-4'-methoxyphenyl analogue **3a** showed potent activity in inhibiting the growth of the MCF-7 human breast cancer cell line (IC_{50}: 4 nM), with a significant effect on inhibition of tubulin polymerization (IC_{50}: 0.8 μM). Replacement of C-2 aryl group with a methyl furnished derivative **3b** (BNC105), a potent and selective antiproliferative (IC_{50}: 3 nM on MCF-7 cells) and

antitubulin (IC_{50}: 3 μM for tubulin assembly) agent, that causes strong tumour vasculature disruption and exhibits tumour growth inhibitory properties in xenograft tumour models.[31,32] These data confirmed that the 4-methoxy-3-hydroxy groups in the B-ring of CA-4 correlates to 6-methoxy-7-hydroxy substituents on the benzene portion of benzo[*b*]furan skeleton.

Compound **3c**, obtained replacing the C-2 methyl group of **3b** with an amino moiety, was characterized by an 2-amino-3-(3',4',5'-trimethoxybenzoy)benzo[b]furan skeleton and can be also considered as a positional isomer of compounds with general structure **2**, switching the position of the amino and 3',4',5'-trimethoxybenzoyl groups. Compound **3c** was able to inhibit the growth of activated and quiescent human umbilical vein endothelial cells (HUVECs), with a selectivity ratio of 4.6, but unfortunately, neither its antiproliferative activity on cancer cell lines nor inhibition of tubulin assembly were reported.[31] This compound has been then re-synthesized by an easy and rapid chemical approach reported in this article, resulting equipotent with CA-4 as inhibitor of tubulin assembly (IC_{50}: 0.59 μM). By comparing activity as inhibitors of tubulin polymerization of **3c** to **3a** and **3b**, the amino moiety of **3c** can be considered a good surrogate for the 4'-methoxy-3'-hydroxyphenyl ring or methyl group present at the 2-position of 3-(3',4',5'-trimethoxybenzoy)benzo[b]furan system of the latter two compounds **3a** and **3b**. We can presume that the presence of the amino group at the C-2 position of benzo[*b*]furan system should be important in restricting the conformation of the adjacent trimethoxybenzoyl moiety into the favoured orientation for binding to tubulin by the formation an intramolecular hydrogen bond between one of the hydrogen of the amino group with the carbonyl oxygen of the adjacent trimethoxybenzoyl function.

The biological evaluation of compound **3c** prompted us to continue our research on this class of compounds in more detail, extending the structure-activity analysis around compound **3c** in an effort to determine if its activity was maintained, or even improved, by the synthesis with a different synthetic approach of a new series of derivatives with general structure **4** that incorporated the structural motif of the 2-amino-3-(3',4',5'-trimethoxybenzoy)benzo[b]furan molecular scaffold modified with respect to position C-4 to C-7 with substituents with different chemical properties, which included electron releasing moieties such as alkoxy (methoxy, ethoxy, *n*-propoxy and benzyloxy) methyl, amino and hydroxy or electron-withdrawing fluorine and bromine groups.

Since the C-6 methoxy moiety proved to be favourable for bioactivity, we evaluated the effect of replacing the strong electron-releasing methoxy with the corresponding ethoxy and n-propoxy homologues, and by the weaker electron-releasing methyl group, which has been well-tolerated in a series of CA-4 analogues published previously.[33] In an effort to design

compounds with improved polarity, we have also replaced the methoxy group at the C-5 or C-6 position of benzo[b]furan ring with the more hydrophilic amino or hydroxyl moieties, respectively.

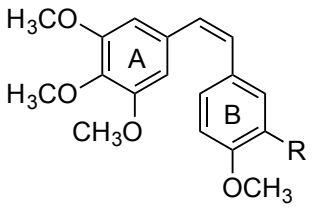

1

R=OH, Combretastatin A-4 (CA-4), **1a**
R=OPO_3Na_2, CA-4P, **1b**
R=NH-Ser, Ombrabulin (AVE8062), **1c**

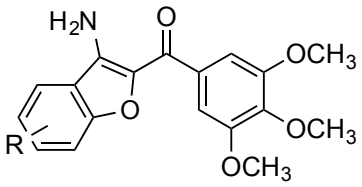

2

R=H or OMe
R=6-OCH_3, **2a**

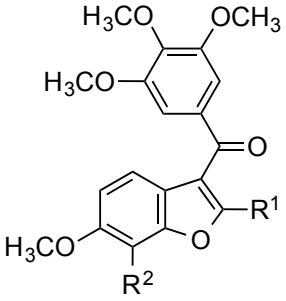

3

R^1=H, Br, CN, CO_2CH_3, alkyl, alkylamine, aryl, heteroaryl
R^2=H or OH
3a, R^1=4'-OMe-3'-OH-C_6H_3, R^2=OH
3b, R^1=CH_3, R^2=OH
3c, R^1=NH_2, R^2=OH

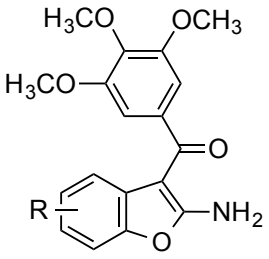

4

R=H, electron-withdrawing (F and Br) or electron-releasing groups such as alkoxy (OCH_3, OC_2H_5, n-OC_3H_7, $OCH_2C_6H_5$), CH_3, OH and NH_2

Figure 1. Chemical structures of CA-4 (**1a**), CA-4P (**1b**) and Ombrabulin (**1c**). General structure of 2-(3',4',5'-trimethoxybenzoyl)-3-aminobenzo[b]furan **2** and 2-substituted-3-(3',4',5'-trimethoxybenzoyl)benzo[b]furan **3**. General molecular formula of synthesized 2-amino-3-(3',4',5'-trimethoxybenzoyl)benzo[b]furan **4**.

5.2 Chemistry

Compounds **4a-n** and **3c** were prepared by an efficient previously described two-step procedure for the synthesis of 2-amino-3-aroyl benzo[*b*]furans,[34] as shown in Scheme 1. α-Azido chalcones **6a-n** were synthesized via Knoevenagel condensation reaction of salicylaldehydes **5a-n**[35-37] with 2-azido-1-(3,4,5-trimethoxyphenyl)ethanone[38] in presence of one equivalent of piperidinium acetate.[34] A solution of α-azido chalcones **6a-n** in CH_3CN was transformed in good yields (60-80%) in the corresponding 2-amino-3-(3',4',5'-trimethoxybenzoyl)benzo[*b*]furan **4a-l**, **7a** and **3c** by heating at reflux in presence of a catalytic amount (0.2 equiv., 20 mol %) of p-toluensulfonic acid (*p*-TSA) for 12 h. The same compounds can be also obtained with a 20-40% reduced yield by a photochemical process replacing the thermal heating with the irradiation for 24 h at room temperature with a 25 W white compact fluorescent lamp (CFL). The 6-hydroxy benzo[b]furan derivative **4m** was obtained by cleavage of the 6-benzyloxy group of **4i** performed by flow hydrogenolysis with H-Cube® over 10% Pd/C catalyst. 5-Amino benzo[b]furan derivative **4n** was generated from the corresponding nitro analogue **7a** by reduction with iron and ammonium chloride in a refluxing mixture of water and ethanol.

Scheme 1. Synthesis of 2-amino-3-(3',4',5'-trimethoxybenzoyl)benzo[*b*]furan **3c**, **4a-n**, **7a**

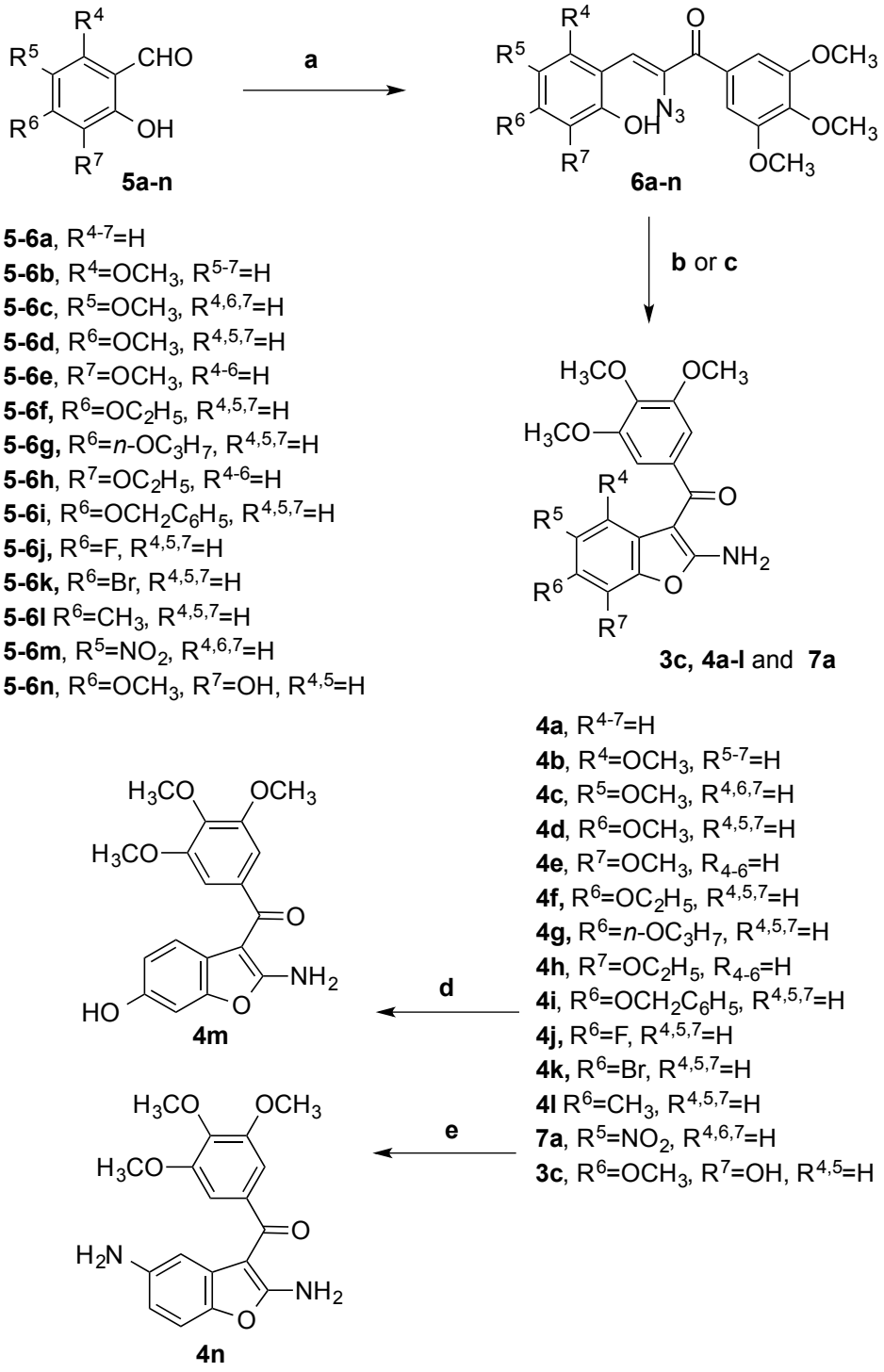

5-6a, R^{4-7}=H
5-6b, R^4=OCH_3, R^{5-7}=H
5-6c, R^5=OCH_3, $R^{4,6,7}$=H
5-6d, R^6=OCH_3, $R^{4,5,7}$=H
5-6e, R^7=OCH_3, R^{4-6}=H
5-6f, R^6=OC_2H_5, $R^{4,5,7}$=H
5-6g, R^6=*n*-OC_3H_7, $R^{4,5,7}$=H
5-6h, R^7=OC_2H_5, R^{4-6}=H
5-6i, R^6=$OCH_2C_6H_5$, $R^{4,5,7}$=H
5-6j, R^6=F, $R^{4,5,7}$=H
5-6k, R^6=Br, $R^{4,5,7}$=H
5-6l R^6=CH_3, $R^{4,5,7}$=H
5-6m, R^5=NO_2, $R^{4,6,7}$=H
5-6n, R^6=OCH_3, R^7=OH, $R^{4,5}$=H

4a, R^{4-7}=H
4b, R^4=OCH_3, R^{5-7}=H
4c, R^5=OCH_3, $R^{4,6,7}$=H
4d, R^6=OCH_3, $R^{4,5,7}$=H
4e, R^7=OCH_3, R_{4-6}=H
4f, R^6=OC_2H_5, $R^{4,5,7}$=H
4g, R^6=*n*-OC_3H_7, $R^{4,5,7}$=H
4h, R^7=OC_2H_5, R_{4-6}=H
4i, R^6=$OCH_2C_6H_5$, $R^{4,5,7}$=H
4j, R^6=F, $R^{4,5,7}$=H
4k, R^6=Br, $R^{4,5,7}$=H
4l R^6=CH_3, $R^{4,5,7}$=H
7a, R^5=NO_2, $R^{4,6,7}$=H
3c, R^6=OCH_3, R^7=OH, $R^{4,5}$=H

Reagents. **a**: 2-azido-1-(3,4,5-trimethoxyphenyl)ethanone, piperidinium acetate, MeOH, rt, 24 h; **b**: *p*-TSA (0.2 equiv., 20 mol %), CH_3CN, reflux, 12 h; **c**: white CFL (25W), *p*-TSA (0.2 equiv., 20 mol %), CH_3CN, rt, 24 h, **d**: 10% Pd/C, EtOH, 40 bar, 60 °C, 30 min; **e**: Fe, NH_4Cl, EtOH-H_2O, reflux, 3 h.

5.3 Biological Results and Discussion

5.3.1 *In vitro* antiproliferative activities

Table 1 summarizes the growth inhibitory effects of 2-amino-3-(3',4',5'-trimethoxybenzoyl)benzo[b]furan derivatives **4a-n** and **3c** against a panel of six human cell lines which were derived from different cancer types, including cervix carcinoma (HeLa), colon adenocarcinoma (HT-29), medulloblastoma (Daoy), promyelocytic leukemia (HL-60), B-cell leukemia (SEM) and T-cell leukemia (Jurkat), using the isomeric 6-methoxy-2-(3',4',5'-trimethoxybenzoyl)-3-aminobenzo[b]furan derivative **2a** and CA-4 (**1a**) as reference compounds.

As shown in Table 1, derivatives with a methoxy (**4d**), an ethoxy (**4f**), a bromine (**4k**) or a methyl (**4l**) at the C-6 position of the benzo[*b*]furan system exhibited the greatest activity among the tested compounds, with IC_{50} values of 0.30-5.6, 0.005-2.8, 2.5-5.6 and 0.3-3.5 nM, respectively, with compound **4f** which showed a remarkable activity (IC_{50}: 5 pM) against Daoy cells as compared with the other cancer cell lines. None of the synthesized compounds was more active than CA-4 against HL-60 cells, while only derivatives **4f** and **4l** were more potent than CA-4 against HeLa, HT-29, Daoy, SEM and Jurkat cells. These latter three cancer cell lines were highly sensitive to compounds **4f** and **4l**, with IC_{50} values ranging from 0.005 to 0.38 nM. Also derivatives **4d** and **3c** resulted active at subnanomolar concentrations against Daoy cells, with **3c** which was potent (IC_{50}:0.34 nM) against Jurkat cells too.

Comparing the two C-6 methoxy derivatives **2a** and **4d**, obtained switching the position of the amino and 3',4',5'-trimethoxybenzoyl moieties at the 2- and 3-positions of benzo[*b*]furan ring, both compounds are equipotent against HL-60, SEM and Jurkat cells, while **4d** resulted 2- and 17-fold more active than **2a** against HeLa and Daoy cells. It is noteworthy to note that the increase in potency was more evident against HT-29 cells (140-fold), with IC_{50} values of 5.6 and 787 nM for **4d** and **2a**, respectively.

In terms of antiproliferative activity, derivative **4a** which was unsubstituted in the benzene portion of the benzo[*b*]furan ring, was active at sub-micromolar concentrations (IC_{50}. 0.25-0.59 μM), resulting less active than derivatives **4c** and **4d** with a methoxy group at C-5 or C-6 position, respectively, equipotent with C-7 methoxy derivative **4e** but more active than C-4 methoxy analogue **4b**.

In the series of methoxy substituted benzo[*b*]furan derivatives **4b-e**, the results presented in Table 1 indicated that potent cancer cell growth inhibition appears to be strongly dependent

from the position of the methoxy group. A fairly dramatic difference was observed between C-4/7 and C-5/6 substituted compounds (**4b** and **4e** versus **4c** and **4d**). The greatest activity occurred with the methoxy group located at the C-5 or C-6 position, the least when located at the C-4 or C-7 positions, with the order being 6-OMe (**4d**)>5-OMe (**4c**)>7-OMe (**4e**)>>4-OMe (**4b**). Thus, compound **4b**, with a methoxy group at the C-4 position, showed modest antiproliferative activity (IC_{50}: 2.8-8.5 μM), resulting the less active compound of this small series of four derivatives. Simply moving the methoxy group from C-4 to C-5 position (**4c**) resulted in a 100-150-fold increased activity, with IC_{50} values ranging from 29 to 56 nM. The activity was further increased of 10-120-fold shifting the methoxy group from C-5 to C-6 position (**4d**), with the greatest difference being with the Daoy cells (IC_{50}: 36.2 and 0.3 nM for **4c** and **4d**, respectively). Moving the methoxy group to the C-7 position (**4e**), the activity decreased of 2-3-orders of magnitude relative to **4d**, with IC_{50} values ranging from 0.2 to 0.5 μM. The substitution of C-5 methoxy group of **4c** with an amino group (**4n**) has a detriment effect on activity, with compound **4n** being from 7- to 15-fold less potent than **4d**. We found that replacement of C-6 methoxy of **4d** with its ethoxy homologue, to furnish compound **4f**, maintained the activity against HeLa and HL-60 cells, which was improved of 2.5-60-fold against four of the six cancer cell lines relative to **4d**, with the difference in activity more pronounced (60-fold) against Daoy cells. **4f** resulted one of the most potent antiproliferative agents among the evaluated compounds, with IC_{50} values of 2.8, 2.1, 0.005, 2.7, 0.31 and 0.28 nM against Hela, HT-29, Daoy, HL-60, SEM and Jurkat cells, respectively. Compound **4f** resulted 3-fold less active than CA-4 against HL-60 cells (IC_{50}: 2.7 and 1.1 nM, respectively), equipotent to CA-4 against HeLa cells and 3- and 16-fold more active than CA-4 against Jurkat and SEM cells. The enhancement in antiproliferative activity was more evident against Daoy cells (2,460-fold), with **4f** which resulted active against HT-29 cells which are refractory to CA-4 (IC_{50}: 2.1 nM and 3.1 μM, respectively). As expected, for compound **4f** the antiproliferative activities against the whole panel of human cancer cell lines were all considerably superior to those of C-7 ethoxy isomer **4h**. A further homologation of ethoxy group of **4f** to *n*-propoxy (**4g**) reduced antiproliferative activity from one to three order of magnitude (IC_{50}: 0005-2.8 and 4.4-41 nM for **4f** and **4g**, respectively), while the C-6 benzyloxy derivative **4i** exhibited no antiproliferative activities against the cancer cell lines at all (IC_{50}: 4-10 μM).

A comparison of the substituent effect revealed that the replacement of C-6 methoxy with the less electron-releasing methyl group (compounds **4d** and **4l**, respectively), caused a 3-14-fold increased activity against HeLa, HT-29, SEM and Jurkat cells relative to **4d**, whereas methyl and methoxy functions can be replaced each other without substantial loss of activity

against Daoy and HL-60 cells. A drastic loss of activity was instead observed replacing the C-6 methoxy group by the weaker electron-donating and more hydrophilic hydroxy (**4m**) or the electron-withdrawing fluorine (**4j**) moieties. For this latter compound, increasing the size of the halide from fluorine with bromine (**4k**) lead to an increase of activity of 71-338-fold with all six cell lines, which was more pronounced against the Daoy cells.

The introduction of an additional hydroxyl group at the C-7 position of **4d**, to furnish **3c**, has contrasting effects, with the activity which was maintained against Daoy and HL-60, while a reduced potency relative to **4d** (4-fold) was observed against HeLa, which was more prominent against HT-29 and SEM cells (76- and 63-fold, respectively). Only against Jurkat cells derivative **3c** resulted more potent (8-fold) than **4d**.

Table 1. *In vitro* cell growth inhibitory effects of compounds **CA-4 (1a)**, **2a**, **3c** and **4a-n**.

	IC_{50} [a](nM)					
Compd	HeLa	HT-29	Daoy	HL-60	SEM	Jurkat
4a	413±40.3	591±29	371±19	339±21	250±28	385±52
4b	5225±312	6512±263	3950±236	4891±445	4557±369	2760±156
4c	56.0±19	62.9±12.9	36.2±6.9	36.2±11	38.9±12	29.2±9.3
4d	2.9±0.3	5.6±0.9	0.30±0.08	3.0±0.2	4.1±0.2	2.7±0.6
4e	496±39	477±42	345±36	233±31	285±26	333±42
4f	2.8±0.3	2.1±0.2	0.005±0.001	2.7±0.2	0.31±0.05	0.28±0.08
4g	22.7±1.8	17.7±1.2	4.4±0.9	41.7±15.9	29.7±8.9	27.2±1.9
4h	1250±98	910±58	1670±87	428±36	385±27	390±39
4i	9670±125	8680±458	>10000	7056±659	3675±298	4390±154
4j	591±26	682±45	846±28	413±56	333±45	299±39
4k	4.5±0.5	5.4±0.3	2.5±0.2	5.6±0.9	3.5±0.1	2.8±0.6
4l	1.1±0.2	0.6±0.02	0.34±0.1	3.5±0.4	0.30±0.03	0.33±0.05
4m	591±63	3420±368	428±45	285±2.5	371±1.5	299±37
4n	635±1.5	790±98	494±56	413±3.8	259±1.8	399±58
2a	6.2±4.0	787±45	5.0±1.2	3.5±0.3	3.6±0.2	3.1±0.9
3c	15.3±1.9	424±36	0.32±0.06	2.8±0.3	259±19	0.34±0.07
1a	4±1	3100±100	12.3±0.9	1±0.2	5±0.1	0.8±0.2

[a]IC_{50}= compound concentration required to inhibit tumour cell proliferation by 50%. Data are expressed as the mean ± SEM from the dose-response curves of at least three independent experiments.

5.3.2 Inhibition of tubulin polymerization and colchicine binding

To investigate whether the antiproliferative activities of these compounds were related to interaction with the microtubule system, seven of the most active compounds (**4c-d**, **4f-g**, **4k-l** and **3c**) were evaluated for their inhibition of the polymerization of purified tubulin and inhibition of the binding of [^{3}H]colchicine to tubulin. In the latter assay, the compounds were examined at two different concentrations (5 and 0.5 μM), with tubulin and colchicine at 1 and 5 μM concentrations, respectively (Table 2).[39,40] For comparison, CA-4 (**1a**) was examined in contemporaneous experiments. All tested compounds strongly inhibited tubulin assembly, with activities comparable or superior to that of the reference compound CA-4. Compounds **4f** and **4l** seemed to be even more potent than CA-4 (IC_{50}, 0.37, 0.39 and 0.54 μM, respectively), while the others were as active as CA-4 as inhibitors of tubulin assembly, with IC_{50}'s ranging from 0.48 to 0.59 μM. This is in agreement with **4f** and **4l** being the derivatives with the greatest antiproliferative activity.

In the colchicine binding studies, all tested compounds potently inhibited the binding of [^{3}H]colchicine to tubulin, with six of them (the exception was **4c**) which were as potent as CA-4, with these agents and radiolabeled colchicine were equimolar (5 μM each) in the reaction mixture. However, only derivatives **4d**, **4f, 4l** and **3c** were quite as potent as CA-4 as inhibitors of colchicine binding with one fifth the concentration of colchicine in the reaction mixture. These data suggested that tested compounds are potent antiproliferative and antitubulin agents acting as microtubule-depolymerizing agents through the colchicine-binding site on tubulin.

Table 2. Inhibition of tubulin polymerization and colchicine binding by compounds **4c-d**, **4f-g**, **4k-l**, **3c** and CA-4 (**1a**).

Compound	Tubulin assembly[a]	Colchicine binding[b]	
	IC_{50}±S.D (μM)	% ±S.D	
		5 μM drug	0.5 μM drug
4c	0.50 ± 0.09	73±0.5	ND
4d	0.48 ± 0.05	99±0.2	79±1
4f	0.37 ± 0.02	99±0.3	86±0.8
4g	0.51 ± 0.1	91±0.3	42±0.4
4k	0.57 ± 0.04	92±1	56±2
4l	0.39 ± 0.04	97±0.4	74±0.1
3c	0.59 ± 0.08	99±1	87±5
CA-4 (**1a**)	0.54 ± 0.06	97±0.8	82±2

ND= not determined.

[a] Inhibition of tubulin polymerisation. Tubulin was at 10 μM.

[b] Inhibition of [^{3}H] colchicine binding. Tubulin and colchicine were at 1 and 5 μM, respectively.

5.3.3 Molecular modeling

The potential interaction between these novel 2-amino-3-(3',4',5'-trimethoxybenzoil) benzo[b]furan derivatives and the colchicine binding site was investigated through molecular docking studies, using GLIDE.[41]

The proposed binding mode for all the new active derivatives is consistent with the co-crystallized colchicine, with the trimethoxyphenyl ring in proximity of βCys241, a key interaction point for tubulin polymerisation inhibition (Figure 2A). The free amino group in position 2 of the benzofuran ring, is interacting with αAsn101, potentially locking the compounds in this favourable binding conformation. The benzofuran ring overlaps with the co-crystallized colchicine central core, placing the different substituents at the C-6 position in a small hydrophobic sub-pocket near βMet259, where the colchicine methoxy group is positioned. This small sub-pocket, accommodating the different substituents in position 6, can function as an important anchor point, stabilising the protein-ligand interaction, resulting in a better inhibition of tubulin assembly and antiproliferative activity. In support of this observation, it should be noted that the compounds without a substituent in this position (e.g. **4a**) loose antiproliferative activity. Interestingly, no plausible docking poses were found for the C-6 benzyloxy derivative **4i** (figure 2b), as the large benzyl group in C-6 position cannot be accommodated in the sub-pocket. This observation justifies the loss of antiproliferative activity observed for this compound.

Finally, based on the modeling results, the loss of activity of C-4 methoxy analogue **4b** could be due to the lack of space in the colchicine site around βLeu255, to accommodate the substituent at the C-4 position of the benzo[*b*]furan. Larger substituent than a hydroxyl group at the C-7 position, such as methoxy and ethoxy moieties for derivatives **4e** and **4h**, respectively, could also be sterically hindered by the amino acids αAla180 and αVal18, impeding the efficient binding to the colchicine site, reducing the antiproliferative activity.

A

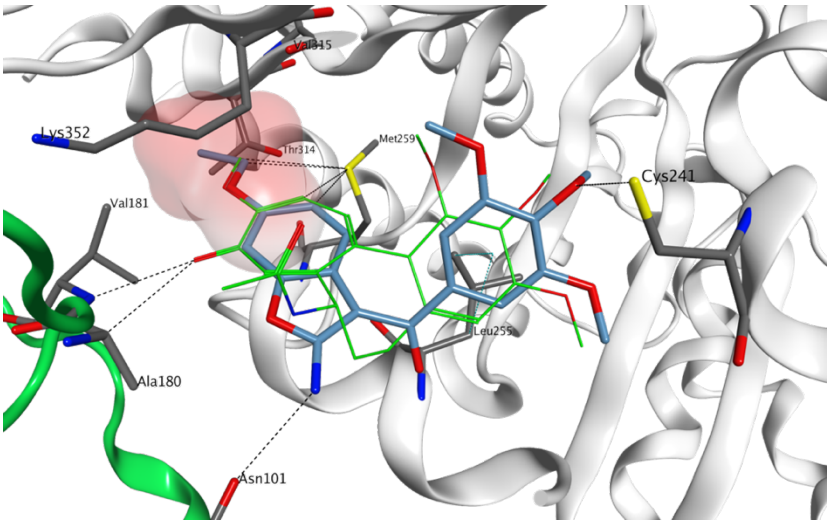

B

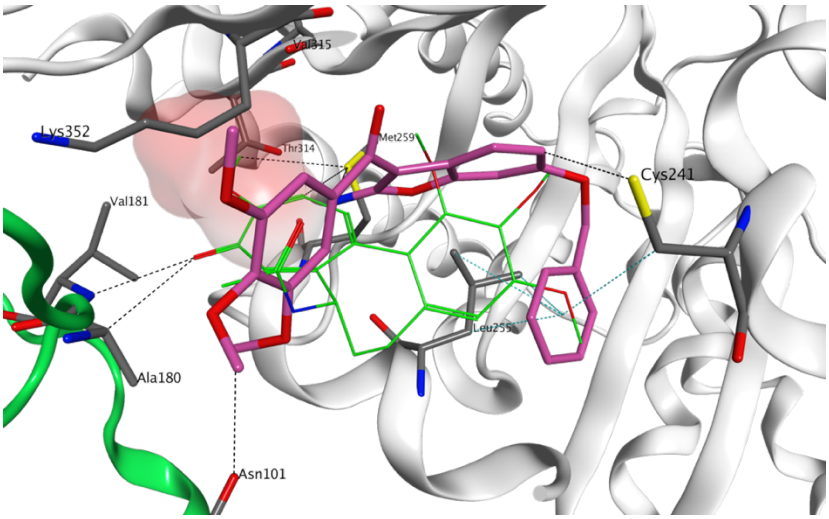

Figure 2. A) Proposed binding for compound **4f** in the colchicine site. The trimethoxyphenyl ring is in proximity of βCys24, while the 6-ethoxy substituent lies in the small sub-pocket. B) The benzyl group at the C-6 position cannot be accommodated in the small sub-pocket, therefore compound **4i** is forced away from the binding site. Co-crystallized colchicine is shown in green. The hydrophobic sub-pocket is highlighted with a red surface. The tubulin α unit is shown as green ribbon, while the β unit is represented in white ribbon. Secondary structure from residue 245 to residue 250 of unit β has been hidden for clarity.

5.4 Conclusions

The benzo[*b*]furan molecular skeleton is the core structure of attractive inhibitors of tubulin polymerization. In this article we have reported the synthesis and evaluation for their biological activity of a new class of 2-amino-3-(3',4',5'-trimethoxybenzoyl)benzo[*b*]furan derivatives as positional isomers of compounds with general structure **2** previously published, obtained switching the position of the amino and 3',4',5'-trimethoxybenzoyl moieties. The structure-activity relationship was investigated by the insertion of electron-withdrawin (F and Br) or electron releasing (OMe, OEt, *n*-OPr, OBn, OH, Me and NH_2) substituents on the benzene fused the furan ring of the benzo[*b*]furan molecular skeleton. Derivatives with a methoxy (**4d**), an ethoxy (**4f**), a bromine (**4k**) or a methyl (**4l**) at the C-6 position of the benzo[*b*]furan system exhibited potent antiproliferative activity, with IC_{50} values from single digit nanomolar to sub-nanomolar range. The C-6 ethoxy derivative **4f** and the C-6 methyl analogue **4l** resulted the two most potent compound of the series, exhibiting IC_{50} values of 0.005-2.8 and 0.3-3.5 nM, respectively, as compared with the range 0.8-3100 nM obtained with CA-4. Only against Jurkat cells, the introduction of a C-7 OH to **4d** afforded a much more potent compound (8-fold), corresponding to derivative **3c** previously reported by Pinney and colleagues. The two compounds **4d** and **3c** are equipotent against Daoy and HL-60 cells, but **3c** was much less active than **4d** against HeLa, HT-229 and SEM cells. The reduction of potency was more evident against these two latter cancer cell lines (76- and 63-fold, respectively). For compound **4d**, moving the methoxy group from the C-6 to C-5 and C-7 position, resulted in a ten- and one-hundred- fold decrease in activity, respectively. The reduction in potency was more evident (three orders of magnitude) between C-6 and C-4 methoxy derivatives.

A comparison of substituent effect at the C-6 position revealed that the antiproliferative effect of the bromine derivative **4k** exceed that of its fluorine counterpart **4j** by two-orders of magnitude.

With four of the six cancer cell lines, the C-6 ethoxy derivative **4f** was 2.5-60-fold more active than its cognate C-6 methoxy analogue **4d**, while these two compounds were equipotent against HeLa and HL-60 cells. It was important to underline that **4f** showed a remarkable activity (IC_{50}: 5 pM) against Daoy cells. Although **4f** was 3-fold less potent than CA-4 against HL-60 cells, it was from 1.5- to 2,460-fold more active than CA-4 against the other five cancer cell lines. As for methoxy, a drastic reduction of antiproliferative activity was observed moving the ethoxy group from C-6 (**4f**) to C-7 position (**4h**). Lengthening

further the C-6 ethoxy substituent of **4f** to a *n*-propoxy group (**4g**) led to a reduced activity (9-990-fold) relative to **4f** against all cancer cell lines.

As cell growth inhibitors, the C-6 methoxy and C-6 methyl derivatives **4d** and **4l**, respectively, were equipotent against HL-60 and Daoy cell, while **4l** was from 3- to 14-fold more potent than **4d** against the other four cancer cell lines.

The results are consistent with the conclusion that tubulin is the intracellular target of these compounds, with the tested molecules (**3c**, **4d**, **4f**, **4g**. **4k** and **4l**) which resulted potent inhibitors of both tubulin-dependent reactions, with activities quantitatively similar to that of CA-4. Two compounds, **4f** and **4l**, were better inhibitors of assembly than CA-4, and six of the seven tested compounds (with the exception of **4c**) were as potent as CA-4 as inhibitors of colchicine binding at the concentration of 5 μM, while only derivatives **4d**, **4f** and **3c** were as potent as CA-4 as an inhibitor of colchicine binding at ten-fold reduced concentration (0.5 μM), a property rarely observed in colchicine site drugs. For the most active compounds (**4d**, **4f** and **4l**), a good correlation was observed between antiproliferative activities, inhibition of tubulin assembly and colchicine binding.

We conclude that the antiproliferative activity of these compounds derives from an interaction with the colchicine site of tubulin and interference with microtubule assembly. This indicates that the cellular actions of these agents would involve mitotic arrest, due to interference with the functions of the mitotic spindle, and an apoptotic cell death.

5.5 Experimental Section

Chemistry

Materials and methods. ^{1}H NMR and ^{13}C NMR spectra were recorded in $CDCl_3$ solution with a Varian Mercury Plus 400 spectrometer at 400 MHz and 100 MHz, respectively. Peak positions are given in parts per million (δ) downfield from tetramethylsilane as internal standard, and *J* values are given in hertz. Positive-ion electrospray ionization (ESI) mass spectra were measured on a double-focusing Finnigan MAT 95 instrument with BE geometry. Analytical HPLC analyses were performed at ambient temperature on a Beckman 125 liquid chromatograph fitted with a Luna C-18 column (4.6 x 100 mm, 3 μm particle size) with 0.1% TFA in H_2O (A) and 0.1% TFA in CH_3CN (B) solvent mixtures and equipped with a Beckman 168 diode array detector. Melting points (mp) were determined on a Buchi-Tottoli apparatus and are uncorrected. The purity of tested compounds was determined by combustion elemental analyses conducted by the Microanalytical Laboratory

of the Chemistry Department of the University of Ferrara with a Yanagimoto MT-5 CHN recorder elemental analyzer. All tested compounds yielded data consistent with a purity of at least 95% as compared with the theoretical values. All reactions were carried out under an inert atmosphere of dry nitrogen, unless otherwise indicated. TLC was performed on silica gel (precoated F_{254} Merck plates), and compounds were visualized with aqueous $KMnO_4$. Flash column chromatography was performed using 230-400 mesh silica gel and the indicated solvent system. Organic solutions were dried over anhydrous Na_2SO_4. All commercial chemicals and solvents were reagent grade and were used without further treatment. With the exception of compounds **5f-g** and **5n**, all salicylaldehydes are commercially available.

General procedure A for the synthesis of compounds 6a-n. A mixture of the appropriate salicylaldehyde **5a-n** (1 mmol), 2-azido-1-(3,4,5-trimethoxyphenyl)ethanone (0.25 g, 1 mmol) and piperidinium acetate (0.15 g, 1 mmol) in methanol (5 mL) was stirred in dark for 24 h under nitrogen atmosphere at room temperature. If the α-azidochalcone was precipitated from the reaction mixture, the solid was filtered, washed with cold methanol, dried in vacuum and used without further any purification for the next reaction. When the α–azidochalcone was not precipitated, the reaction mixture was evaporated to dryness under reduced pressure and the resulting residue portioned between a mixture of ethyl acetate/water. After phase separation, the organic layer was washed with brine, dried over Na_2SO_4 and concentrated under vacuum to give a crude product which was purified by silica-gel column chromatography to yield the appropriate α-azidochalcone.

(*Z*)-2-Azido-3-(2-hydroxyphenyl)-1-(3,4,5-trimethoxyphenyl)prop-2-en-1-one (6a). Following general procedure A, the crude residue purified by flash chromatography, using EtOAc:petroleum ether 1:1 (v:v) for elution, furnished as a yellow oil Yield 64%. ^{1}H-NMR (DMSO-d_6) δ: 3.78 (s, 3H), 3.84 (s, 6H), 6.84 (m, 2H), 7.02 (s, 1H), 7.14 (s, 2H), 7.22 (m, 1H), 8.18 (dd, J=7.2 and 2.4 Hz, 1H), 10.1 (s, 1H).

(*Z*)-2-Azido-3-(2-hydroxy-6-methoxyphenyl)-1-(3,4,5-trimethoxyphenyl)prop-2-en-1-one (6b). Following general procedure A, the precipitate which appeared was filtered and washed with cold methanol, to furnish as a colour cream solid. Yield 63%, mp 130-132 °C. ^{1}H-NMR (DMSO-d_6) δ: 3.77 (s, 6H), 3.86 (s, 6H), 6.49 (d, J=8.2 Hz, 1H), 6.65 (s, 1H), 7.19 (m, 4H), 9.82 (bs, 1H).

(*Z*)-2-Azido-3-(2-hydroxy-5-methoxyphenyl)-1-(3,4,5-trimethoxyphenyl)prop-2-en-1-one (6c). Following general procedure A, the precipitate which appeared was filtered and washed with cold methanol, to furnish as a yellow solid. Yield 69%, mp 97-99 °C. ^{1}H-NMR (DMSO-d_6) δ: 3.72 (s, 3H), 3.78 (s, 3H), 3.84 (s, 6H), 6.82 (m, 2H), 7.00 (s, 1H), 7.12 (s, 2H), 7.74 (d, J=2.6 Hz, 1H), 9.70 (s, 1H).

(*Z*)-2-Azido-3-(2-hydroxy-4-methoxyphenyl)-1-(3,4,5-trimethoxyphenyl)prop-2-en-1-one (6d). Following general procedure A, the crude residue purified by flash chromatography, using EtOAc:petroleum ether 4:6 (v:v) for elution, furnished as a yellow solid. Yield 86%, mp 112-114 °C. ^{1}H-NMR (DMSO-d_6) δ: 3.74 (s, 3H), 3.77 (s, 3H), 3.83 (s, 6H), 6.42 (d, J=2.2 Hz, 1H), 6.46 (dd, J=9.0 and 2,2 Hz, 1H), 7.05 (s, 1H), 7.08 (s, 2H), 8.18 (d, J=9.0 Hz, 1H), 10.3 (s, 1H).

(*Z*)-2-Azido-3-(2-hydroxy-3-methoxyphenyl)-1-(3,4,5-trimethoxyphenyl)prop-2-en-1-one (6e). Following general procedure A, the precipitate which appeared was filtered and washed with cold methanol, to furnish as a white solid. Yield 75%, mp 130-131 °C. ^{1}H-NMR (DMSO-d_6) δ: 3.78 (s, 3H), 3.80 (s, 3H), 3.83 (s, 6H), 6.85 (t, J=8.0 Hz, 1H), 6.98 (dd, J=8.0 and 1.2 Hz, 1H), 7.07 (s, 1H), 7.12 (s, 2H), 7.77 (dd, J=8.0 and 1.2 Hz, 1H), 9.42 (bs, 1H).

(*Z*)-2-Azido-3-(2-hydroxy-4-ethoxyphenyl)-1-(3,4,5-trimethoxyphenyl)prop-2-en-1-one (6f). Following general procedure A, the crude residue purified by flash chromatography, using EtOAc:petroleum ether 4:6 (v:v) for elution, furnished as a yellow solid. Yield 68%, mp 135-137 °C. ^{1}H-NMR (DMSO-d_6) δ: 1.31 (t, J=6.8 Hz, 3H), 3.77 (s, 3H), 3.83 (s, 6H), 4.02 (q, J=6.8 Hz, 2H), 6.41 (d, J=2.2 Hz, 1H), 6.47 (dd, J=8.8 and 2.2 Hz, 1H), 7.05 (s, 1H), 7.07 (s, 2H), 8.17 (d, J=8.8 Hz, 1H), 10.3 (s, 1H).

(*Z*)-2-Azido-3-(2-hydroxy-4-propoxyphenyl)-1-(3,4,5-trimethoxyphenyl)prop-2-en-1-one (6g). Following general procedure A, the crude residue purified by flash chromatography, using EtOAc:petroleum ether 3:7 (v:v) for elution, furnished as a yellow solid. Yield 58%, mp 168-170 °C. ^{1}H-NMR (DMSO-d_6) δ: 0.97 (t, J=7.4 Hz, 3H), 1.74 (m, 2H), 3.76 (s, 3H), 3.83 (s, 6H), 3.91 (q, J=7.4 Hz, 2H), 6.41 (d, J=2.2 Hz, 1H), 6.50 (dd, J=9.0 and 2.2 Hz, 1H), 7.05 (s, 1H), 7.07 (s, 2H), 8.17 (d, J=9.0 Hz, 1H), 10.2 (s, 1H).

(*Z*)-2-Azido-3-(2-hydroxy-3-ethoxyphenyl)-1-(3,4,5-trimethoxyphenyl)prop-2-en-1-one (6h). Following general procedure A, the precipitate which appeared was filtered and

washed with cold methanol, to furnish as a yellow solid. Yield 67%, mp 138-139 °C. ^{1}H-NMR (DMSO-d_6) δ: 1.33 (t, J=7.0 Hz, 3H), 3.77 (s, 3H), 3.84 (s, 6H), 4.03 (q, J=7.0 Hz, 2H), 6.83 (t, J=8.0 Hz, 1H), 6.97 (d, J=8.0 Hz, 1H), 7.08 (s, 1H), 7.13 (s, 2H), 7.76 (d, J=8.0 Hz, 1H), 9.12 (s, 1H).

(*Z*)-2-Azido-3-(2-hydroxy-4-benzyloxyphenyl)-1-(3,4,5-trimethoxyphenyl)prop-2-en-1-one (6i). Following general procedure A, the crude residue purified by flash chromatography, using EtOAc:petroleum ether 1:1 (v:v) for elution, furnished as a yellow solid. Yield 71%, mp 102-104 °C. ^{1}H-NMR (DMSO-d_6) δ: 3.77 (s, 3H), 3.82 (s, 6H), 5.10 (s, 2H), 6.48 (d, J=2.4 Hz, 1H), 6.58 (dd, J=8.8 and 2.4 Hz, 1H), 7.04 (s, 1H), 7.07 (s, 2H), 7.42 (m, 5H), 8.18 (d, J=9.0 Hz, 1H), 10.3 (s, 1H).

(*Z*)-2-Azido-3-(2-hydroxy-4-fluorophenyl)-1-(3,4,5-trimethoxyphenyl)prop-2-en-1-one (6j). Following general procedure A, the crude residue purified by flash chromatography, using EtOAc:petroleum ether 3:7 (v:v) for elution, furnished as a yellow solid. Yield 55%, mp 107-109 °C. ^{1}H-NMR (DMSO-d_6) δ: 3.77 (s, 3H), 3.83 (s, 6H), 6.68 (m, 2H), 6.96 (s, 1H), 7.11 (s, 2H), 8.12 (dd, J=8.4 and 5.6 Hz, 1H), 10.8 (bs, 1H).

(*Z*)-2-Azido-3-(2-hydroxy-4-bromophenyl)-1-(3,4,5-trimethoxyphenyl)prop-2-en-1-one (6k). Following general procedure A, the precipitate which appeared was filtered and washed with cold methanol, to furnish as a white solid. Yield 60%, mp 115-117 °C. ^{1}H-NMR (DMSO-d_6) δ: 3.77 (s, 3H), 3.83 (s, 6H), 6.93 (s, 1H), 7.02 (m, 2H), 7.12 (s, 2H), 8.09 (d, J=8.2 Hz, 1H), 10.2 (bs, 1H).

(*Z*)-2-Azido-3-(2-hydroxy-4-methylphenyl)-1-(3,4,5-trimethoxyphenyl)prop-2-en-1-one (6l). Following general procedure A, the precipitate which appeared was filtered and washed with cold methanol, to furnish as a yellow solid. Yield 56%, mp 100-102 °C. ^{1}H-NMR (DMSO-d_6) δ: 2.24 (s, 3H), 3.77 (s, 3H), 3.83 (s, 6H), 6.68 (m, 2H), 7.05 (s, 1H), 7.09 (s, 2H), 8.08 (d, J=7.8 Hz, 1H), 10.2 (s, 1H).

(*Z*)-2-Azido-3-(2-hydroxy-5-nitrophenyl)-1-(3,4,5-trimethoxyphenyl)prop-2-en-1-one (6m). Following general procedure A, the precipitate which appeared was filtered and washed with cold methanol, to furnish as a yellow solid. Yield 53%, mp 137-138 °C. ^{1}H-NMR (DMSO-d_6) δ: 3.78 (s, 3H), 3.84 (s, 6H), 6.85 (s, 1H), 7.01 (d, J=7.8 Hz, 1H), 7.17 (s, 2H), 8.12 (d, J=7.8 Hz, 1H), 9.02 (s, 1H), 11.8 (s, 1H).

(*Z*)-2-Azido-3-(2,3-dihydroxy-4-methoxyphenyl)-1-(3,4,5-trimethoxyphenyl)prop-2-en-1-one (6n). Following general procedure A, the crude residue purified by flash chromatography, using EtOAc:petroleum ether 1:1 (v:v) for elution, furnished as a yellow solid. Yield 36%, mp 121-123 °C. ^{1}H-NMR (DMSO-d_6) δ: 3.77 (s, 3H), 3.83 (s, 6H), 3.87 (s, 3H), 6.58 (d, J=9.0 Hz, 1H), 7.08 (s, 2H), 7.09 (s, 1H), 7.75 (d, J=9.0 Hz, 1H), 9.13 (s, 1H), 10.3 (s, 1H).

General procedure B for the synthesis of compounds 4a-l, 7a and 3c. A mixture of the appropriate α-azidochalcone **6a-n** (1 mmol) and *p*-TSA (38 mg, 0.2 mmol) in acetonitrile (10 mL) was stirred under Argon at reflux for 12 h (Method A) or irradiated with a 25W white compact fluorescent lamp (CFL) for 24 h at room temperature (Method B). After this time, the reaction mixture was concentrated under reduced pressure to give a residue which was dissolved in dichloromethane (15 mL). washed with water (5 mL) and brine (5 mL). Organic layer was dried on Na_2SO_4, filtered and evaporated. The crude product was purified by silica gel column chromatography to yield compounds **4a-l**, **7a** and **3c.**

(2-Amino-benzofuran-3-yl)(3,4,5-trimethoxyphenyl)methanone (4a). Following general procedure B, the crude residue purified by flash chromatography, using EtOAc:petroleum ether 1:1 (v:v) for elution, furnished **4a** as a yellow solid. Yield: 73% (Method A), 49% (Method B), mp 103-104°C. ^{1}H-NMR (DMSO-d_6) δ: 3.74 (s, 3H), 3.75 (s, 6H), 6.82 (dd, J=6.8 and 1.6 Hz, 1H), 6.89 (s, 2H), 6.99 (m, 2H), 7.30 (dd, J=7.6 and 2.0 Hz, 1H), 8.54 (s, 2H). ^{13}C-NMR (DMSO-d_6) δ: 56.39 (2C), 60.66, 92.43, 105.08 (2C), 110.36, 118.55, 121.78, 123.96, 126.89, 136.85, 139.79, 148.85, 153.15 (2C), 167.25, 188.14. MS (ESI): $[M+1]^+$=328.43. Anal. ($C_{18}H_{17}NO_5$) C, H, N.

(2-Amino-4-methoxybenzofuran-3-yl)(3,4,5-trimethoxyphenyl)methanone (4b). Following general procedure B, the crude residue purified by flash chromatography, using EtOAc:petroleum ether 1:1 (v:v) for elution, furnished **4b** as a yellow solid. Yield: 74% (Method A), 53% (Method B), mp 123-125°C. ^{1}H-NMR (DMSO-d_6) δ: 3.28 (s, 3H), 3.69 (s, 6H), 3.72 (s, 3H), 6.69 (dd, J=6.8 and 2.4 Hz, Hz, 1H), 6.81 (s, 2H), 7.05 (m, 2H), 8.22 (bs, 2H). ^{13}C-NMR (DMSO-d_6) δ: 54.79, 55.67 (2C), 59.99, 91.72, 102.97, 105.52 (2C), 106.22, 115.17, 122.17, 137.32, 139.31, 149.04, 151.21, 151.62 (2C), 165.71, 188.15. MS (ESI): $[M+1]^+$=358.31. Anal. ($C_{19}H_{19}NO_6$) C, H, N.

(2-Amino-5-methoxybenzofuran-3-yl)(3,4,5-trimethoxyphenyl)methanone (4c). Following general procedure B, the crude residue purified by flash chromatography, using EtOAc:petroleum ether 1:1 (v:v) for elution, furnished **4c** as a colour cream solid. Yield: 68% (Method A), 49% (Method B), mp 140-142°C. ^{1}H-NMR (DMSO-d_6) δ: 3.56 (s, 3H), 3.74 (s, 3H), 3.78 (s, 6H), 6.26 (d, J=2.4 Hz, 1H), 6.56 (dd, J=8.8 and 2.4 Hz, 1H), 6.89 (s, 2H), 7.22 (d, J=8.8 Hz, 1H), 8.54 (bs, 2H). ^{13}C-NMR (DMSO-d_6) δ: 55.07, 55.88 (2C), 60.09, 92.30, 103.22, 104.36 (2C), 106.91, 109.98, 127.34, 136.36, 139.09, 142.99, 152.64 (2C), 155.78, 167.23, 187.61. MS (ESI): $[M+1]^+$=358.40. Anal. ($C_{19}H_{19}NO_6$) C, H, N.

(2-Amino-6-methoxybenzofuran-3-yl)(3,4,5-trimethoxyphenyl)methanone (4d). Following general procedure B, the crude residue purified by flash chromatography, using EtOAc:petroleum ether 1:1 (v:v) for elution, furnished **4d** as an orange solid. Yield: 74% (Method A), 52% (Method B),mp 48-50 °C. ^{1}H-NMR (DMSO-d_6) δ: 3.72 (s, 3H), 3.75 (s, 3H), 3.77 (s, 6H), 6.67 (dd, J=9.0 and 2.4 Hz, 1H), 6.73 (d, J=9.0 Hz, 1H), 6.90 (s, 2H), 7.03 (d, J=2.4 Hz, 1H), 8.48 (bs, 2H). ^{13}C-NMR (DMSO-d_6) δ: 55.51, 55.88 (2C), 60.13, 91.58, 96.60, 104.54 (2C), 110.19, 118.18, 119.22, 136.42, 139.21, 149.12, 152.60 (2C), 155.25, 166,712, 187.11. MS (ESI): $[M+1]^+$=358.28. Anal. ($C_{19}H_{19}NO_6$) C, H, N.

(2-Amino-7-methoxybenzofuran-3-yl)(3,4,5-trimethoxyphenyl)methanone (4e). Following general procedure B, the crude residue purified by flash chromatography, using EtOAc:petroleum ether 6:4 (v:v) for elution, furnished **4e** as a white solid. Yield: 72% (Method A), 48% (Method B), mp 164-165 °C. ^{1}H-NMR (DMSO-d_6) δ: 3.75 (s, 3H), 3.76 (s, 6H), 3.88 (s, 3H), 6.43 (d, J=7.6 Hz, 1H), 6.71 (d, J=8.0 Hz, 1H), 6.90 (s, 2H), 6.94 (d, J=8.0 Hz, 1H), 8.51 (bs, 2H). ^{13}C-NMR (DMSO-d_6) δ: 55.68, 55.82 (2C), 60.10, 92.29, 104.64 (2C), 105.11, 110.79, 124.03, 127.87, 136.16, 136.77, 139.25, 143.73, 152.53 (2C), 166.54, 187.68. MS (ESI): $[M+1]^+$=358.39. Anal. ($C_{19}H_{19}NO_6$) C, H, N.

(2-Amino-6-ethoxybenzofuran-3-yl)(3,4,5-trimethoxyphenyl)methanone (4f). Following general procedure B, the crude residue purified by flash chromatography, using EtOAc:petroleum ether 1:1 (v:v) for elution, furnished **4f** as an orange solid. Yield: 78% (Method A), 46% (Method B), mp 83-85 °C. ^{1}H-NMR (DMSO-d_6) δ: 1.29 (t, J=6.8 Hz, 3H), 3.75 (s, 3H), 3.77 (s, 6H), 3.97 (q, J=6.8 Hz, 2H), 6.63 (dd, J=9.0 and 2.4 Hz, 1H), 6.73 (d, J=9.0 Hz, 1H), 6.90 (s, 2H), 7.00 (d, J=2.4 Hz, 1H), 8.46 (bs, 2H). ^{13}C-NMR (DMSO-d_6) δ: 14.55, 55.81 (2C), 60.09, 63.41, 91.56, 97.05, 104.48 (2C), 110.68, 118.15, 119.08, 136.40,

139.14, 149.06, 152.56 (2C), 154.39, 166.65, 187.06. MS (ESI): $[M+1]^+$=372.31. Anal. ($C_{20}H_{21}NO_6$) C, H, N.

(2-Amino-6-propoxybenzofuran-3-yl)(3,4,5-trimethoxyphenyl)methanone (4g). Following general procedure B, the crude residue purified by flash chromatography, using EtOAc:petroleum ether 4:6 (v:v) for elution, furnished **4g** as an orange solid. Yield: 78% (Method A), 52% (Method B), mp 168-170 °C. ^{1}H-NMR (DMSO-*d*$_6$) δ: 0.96 (t, J=7.2 Hz, 3H), 1.68 (m, 2H), 3.75 (s, 3H), 3.77 (s, 6H), 3.88 (q, J=7.6 Hz, 2H), 6.64 (dd, J=8.8 and 2.0 Hz, 1H), 6.73 (d, J=8.8 Hz, 1H), 6.90 (s, 2H), 7.01 (d, J=2.0 Hz, 1H), 8.48 (bs, 2H). ^{13}C-NMR (DMSO-*d*$_6$) δ: 10.33, 21.95, 55.81 (2C), 60.09, 69.36, 91.55, 97.09, 104.49 (2C), 110.68, 118.16, 119.06, 136.38, 139.14, 149.07, 152.55 (2C), 154.55, 166.69, 187.04. MS (ESI): $[M+1]^+$=386.19. Anal. ($C_{21}H_{23}NO_6$) C, H, N.

(2-Amino-7-ethoxybenzofuran-3-yl)(3,4,5-trimethoxyphenyl)methanone (4h). Following general procedure B, the crude residue purified by flash chromatography, using EtOAc:petroleum ether 1:1 (v:v) for elution, furnished **4h** as an orange solid. Yield: 68% (Method A), 43% (Method B),, mp 158-160 °C. ^{1}H-NMR (DMSO-*d*$_6$) δ: 1.37 (t, J=6.8 Hz, 3H), 3.75 (s, 3H), 3.76 (s, 6H), 4.14 (q, J=6.8 Hz, 2H), 6.41 (d, J=8.0 Hz, 1H), 6.69 (d, J=8.0 Hz, 1H), 6.90 (s, 2H), 6.94 (t, J=8.0 Hz, 1H), 8.52 (bs, 2H). ^{13}C-NMR (DMSO-*d*$_6$) δ: 14.69, 55.83 (2C), 60.12, 63.80, 92.31, 104.60 (2C), 105.78, 110.68, 124.06, 127.92, 136.21, 136.57, 139.19, 142.99, 152.53 (2C), 166.58, 187.68. MS (ESI): $[M+1]^+$=372.39. Anal. ($C_{20}H_{21}NO_6$) C, H, N.

(2-Amino-6-benzyloxybenzofuran-3-yl)(3,4,5-trimethoxyphenyl)methanone (4i). Following general procedure B, the crude residue purified by flash chromatography, using EtOAc:petroleum ether 1:1 (v:v) for elution, furnished **4i** as an orange solid. Yield: 75% (Method A), 54% (Method B), mp 123-125 °C^{1}H-NMR (DMSO-*d*$_6$) δ: 3.72 (s, 3H), 3.75 (s, 3H), 3.77 (s, 6H), 6.67 (dd, J=9.0 and 2.4 Hz, 1H), 6.73 (d, J=9.0 Hz, 1H), 6.90 (s, 2H), 7.03 (d, J=2.4 Hz, 1H), 8.48 (bs, 2H). ^{13}C-NMR (DMSO-*d*$_6$) δ: 55.82 (2C), 60.09, 69.69, 91.53, 97.57, 104.49 (2C), 111.07, 118.13, 119.44, 127.71 (2C), 128.28 (2C), 136.37, 136.95, 139.16, 148.96, 152.56 (2C), 154.16, 166.71, 187.07. MS (ESI): $[M+1]^+$=434.37. Anal. ($C_{25}H_{23}NO_6$) C, H, N.

(2-Amino-6-fluorobenzofuran-3-yl)(3,4,5-trimethoxyphenyl)methanone (4j). Following general procedure B, the crude residue purified by flash chromatography, using

EtOAc:petroleum ether 1:1 (v:v) for elution, furnished **4j** as a white solid. Yield: 76% (Method A), 44% (Method B), mp 178-180 °C. ^{1}H-NMR (DMSO-d_6) δ: 3.76 (s, 3H), 3.77 (s, 6H), 6.76 (d, J=8.4 Hz, 1H), 7.21 (dd, J=8.4 and 5.2 Hz, 1H), 6.91 (s, 2H), 7.35 (dd, J=9.2 and 2.8 Hz, 1H), 8.56 (bs, 2H). ^{13}C-NMR (DMSO-d_6) δ: 55.84 (2C), 60.12, 91.28, 98.53 and 98.81 (J_{C-F}=110 Hz), 104.41 (2C), 110.33, 118.11, 122.52, 136.19, 139.21, 147.99, 152.67 (2C), 159.01, 167.11, 187.36. MS (ESI): $[M+1]^+$=346.05. Anal. ($C_{18}H_{16}FNO_5$) C, H, N.

(2-Amino-6-bromobenzofuran-3-yl)(3,4,5-trimethoxyphenyl)methanone (4k). Following general procedure B, the crude residue purified by flash chromatography, using EtOAc:petroleum ether 1:1 (v:v) for elution, furnished **4k** as a yellow solid. Yield: 78% (Method A), 47% (Method B), mp 170-172 °C. ^{1}H-NMR (DMSO-d_6) δ: 3.75 (s, 3H), 3.77 (s, 6H), 6.76 (d, J=8.4 Hz, 1H), 6.90 (s, 2H), 7.21 (dd, J=8.4 and 2.0 Hz, 1H), 7.64 (d, J=2.0 Hz, 1H), 8.66 (bs, 2H). ^{13}C-NMR (DMSO-d_6) δ: 55.86 (2C), 60.13, 91.48, 104.49 (2C), 112.62, 113.06, 119.22, 126.02, 126.34, 136.03, 139.34, 148.64, 152.66 (2C), 166.77, 187.46. MS (ESI): $[M]^+$=405.92, $[M+2]^+$=408.25. Anal. ($C_{18}H_{16}BrNO_5$) C, H, N.

(2-Amino-6-methylbenzofuran-3-yl)(3,4,5-trimethoxyphenyl)methanone (4l). Following general procedure B, the crude residue purified by flash chromatography, using EtOAc:petroleum ether 1:1 (v:v) for elution, furnished **4l** as a yellow solid. Yield: 73% (Method A), 39% (Method B), mp 137-139 °C. ^{1}H-NMR (DMSO-d_6) δ: 2.28 (s, 3H), 3.74 (s, 3H), 3.75 (s, 6H), 6.72 (d, J=8.0 Hz, 1H), 6.85 (dd, J=8.0 and 0.8 Hz, 1H), 6.89 (s, 2H), 7.15 (d, J=0.8 Hz, 1H), 8.49 (bs, 2H). ^{13}C-NMR (DMSO-d_6) δ: 20.71, 55.82 (2C), 60.12, 91.80, 104.53 (2C), 110.29, 117.74, 123.65, 124.19, 130.83, 136.35, 139.15, 148.64, 152.56 (2C), 166.70, 187.33. MS (ESI): $[M+1]^+$=342.20. Anal. ($C_{19}H_{19}NO_5$) C, H, N.

(2-Amino-5-nitrobenzofuran-3-yl)(3,4,5-trimethoxyphenyl)methanone (7a). Following general procedure B, the crude residue purified by flash chromatography, using EtOAc:petroleum ether 8:2 (v:v) for elution, furnished **7a** as a brown solid. Yield; 68% (Method A), 47% (Method B), mp 95-97°C. ^{1}H-NMR (DMSO-d_6) δ: 3.78 (s, 3H), 3.79 (s, 6H), 6.98 (s, 2H), 7.62 (d, J=8.2 Hz, 1H), 7.69 (d, J=2.4 Hz, 1H), 8.00 (dd, J=8.2 and 2.4 Hz, 1H), 8.88 (bs, 2H). MS (ESI): $[M+1]^+$=373.27. Anal. ($C_{18}H_{18}N_2O_5$) C, H, N.

(2-Amino-7-hydroxy-6-methoxybenzofuran-3-yl)(3,4,5-trimethoxyphenyl)methanone (3c). Following general procedure B, the crude residue purified by flash chromatography, using EtOAc:petroleum ether 6:4 (v:v) for elution, furnished **3c** as a yellow solid. Yield:

71% (Method A), 52% (Method B), mp 103-105 °C^{1}H-NMR (DMSO-d_6) δ: 3.73 (s, 3H), 3.75 (s, 6H), 3.77 (s, 3H), 6.21 (d, J=8.8 Hz, 1H), 6.69 (d, J=8.8 Hz, 1H), 6.89 (s, 2H), 8.47 (bs, 2H), 9.25 (s, 1H). ^{13}C-NMR (DMSO-d_6) δ: 55.83 (2C), 56.75, 60.08, 91.92, 104.46 (2C), 107.41, 108.82, 121.28, 122.49, 131.49, 136.49, 139.02, 143.81, 152.51 (2C), 166.90, 187.32. MS (ESI): $[M+1]^+$=374.22.

(2-Amino-6-hydroxybenzofuran-3-yl)(3,4,5-trimethoxyphenyl)methanone (4m). (2-Amino-6-(benzyloxy)benzofuran-3-yl)(3,4,5-trimethoxyphenyl)methanone **4i** (0.12 g, 0.28 mmol) was dissolved in a mixture of methanol (25 mL) and ethanol (25 mL) and passed through a H-Cube Pro flow reactor using a 10% Pd/C 70 mm Catcart at 40 bar and 60 °C. Once the reaction was complete, the solvent was concentrated. The final compound was obtained as a yellow solid. Yield 78%, mp 87-89 °C. ^{1}H-NMR (DMSO-d_6) δ: 3.75 (s, 3H), 3.77 (s, 6H), 6.52 (dd, J=8.4 and 1.6 Hz, 1H), 6.66 (d, J=8.4 Hz, 1H), 6.74 (d, J=1.6 Hz, 1H), 6.90 (s, 2H), 8.42 (bs, 2H), 9.36 (bs, 1H). ^{13}C-NMR (DMSO-d_6) δ: 55.81 (2C), 60.08, 91.72, 97.72, 104.47 (2C), 110.99, 118.00, 118.26, 136.46, 139.37, 149.15, 152.53 (2C), 153.06, 166.50, 186.93. MS (ESI): $[M+1]^+$=344.18.

(2,5-Diaminobenzofuran-3-yl)(3,4,5-trimethoxyphenyl)methanone (4n). To a stirred suspension of (2-amino-5-nitrobenzofuran-3-yl)(3,4,5-trimethoxyphenyl)methanone **7a** (220 mg, 0.59 mmol) in EtOH (10 ml) was added iron powder (230 mg, 4.13 mmol,, 7 equiv.) and a solution of ammonium chloride (126 mg, 2.3 mmol, 4 equiv.) in water (1 mL). The reaction mixture was heated under reflux for 1 h, cooled to room temperature, and filtered through Celite. The filter cake was rinsed with dichloromethane (20 mL) and the filtrate washed with water (5 mL), brine (5 mL), dried over Na_2SO_4 and the solvent removed under reduced pressure. The crude residue was purified by flash chromatography, using EtOAc:petroleum ether 6:4 (v:v) for elution, furnished **4n** as an orange solid. Yield 45%, mp 168-170 °C. ^{1}H-NMR (DMSO-d_6) δ: 3.76 (s, 3H), 3.78 (s, 6H), 4.82 (bs, 2H), 6.20 (dd, J=8.4 and 2.4 Hz, 1H), 6.26 (d, J=2.4 Hz, 1H), 6.93 (s, 2H), 6.96 (d, J=8.4 Hz, 1H), 8.41 (bs, 2H). ^{13}C-NMR (DMSO-d_6) δ: 55.79 (2C), 60.08, 92.38, 103.49, 104.78 (2C), 107.74, 109.59, 126.60, 136.12, 139.30, 145.05, 152.46 (2C), 154.09, 167.22, 187.30. MS (ESI): $[M+1]^+$=343.22.

Biology

Materials and Methods

Effects on tubulin polymerization and on colchicine binding to tubulin. To evaluate the effect of the compounds on tubulin assembly *in vitro*,[39] varying concentrations of compounds were preincubated with 10 μM bovine brain tubulin in glutamate buffer at 30 ˚C and then cooled to 0 ˚C. After addition of 0.4 mM GTP (final concentration), the mixtures were transferred to 0 °C cuvettes in a recording spectrophotometer and warmed to 30 °C. Tubulin assembly was followed turbidimetrically at 350 nm. The IC_{50} was defined as the compound concentration that inhibited the extent of assembly by 50% after a 20 min incubation. The ability of the test compounds to inhibit colchicine binding to tubulin was measured as described,[40] except that the reaction mixtures contained 1 μM tubulin, 5 μM [^{3}H]colchicine and 5 μM or 0.5 μM test compound.

Molecular modeling. All molecular docking studies were performed on a Viglen Genie Intel®Core™ i7-3770 vPro CPU@ 3.40 GHz x 8 running Ubuntu 14.04. Molecular Operating Environment (MOE) 2018.10[42] and Maestro (Schrödinger Release 2017-1)[41] were used as molecular modeling software. The tubulin structure was downloaded from the PDB data bank (http://www.rcsb.org/; PDB code 4O2B). The protein was pre-processed using the Schrödinger Protein Preparation Wizard by assigning bond orders, adding hydrogens and performing a restrained energy minimization of the added hydrogens using the OPLS_2005 force field. Ligand structures were built with MOE and then prepared using the Maestro LigPrep tool by energy minimizing the structures (OPLS_2005 force filed), generating possible ionization states at pH 7±2, generating tautomers and low-energy ring conformers. After isolating a tubulin dimer structure, a 12 Å docking grid (inner-box 10 Å and outer-box 22 Å) was prepared using as centroid the co-crystallized colchicine. Molecular docking studies were performed using Glide SP precision keeping the default parameters and setting 5 as number of output poses per input ligand to include in the solution. The output database was saved as mol2 file. The docking results were visually inspected for their ability to bind the active site.

5.6 References

1. Akhmanova, A.; Steinmetz, M. O. Control of microtubule organization and dynamics: two ends in the limelight. *Nat. Rev. Mol. Cell. Biol.* **2015,** 16, 711-726.
2. Brouhard, G. J.; Rice, L. M. The contribution of αβ-tubulin curvature to microtubule dynamics. *J. Cell Biol.* **2014**, *207*, 323-334.
3. Wade, R.H. On and around microtubules: an overview. *Mol. Biotechnol.* **2009**, *43*, 177-191.
4. Janke, C. The tubulin code: Molecular components, readout mechanisms, and functions. *J. Cell Biol.* **2014,** 206, 461-472.
5. Aylett, C. H. S.; Löwe, J.; Amos, L. A. New Insights into the Mechanisms of Cytomotive Actin and Tubulin Filaments. In *International Review of Cell and Molecular Biology*; Jeon, K. W., Ed.; Academic Press: Burlington, **2011**; Vol. 292, pp 1-71.
6. Manneville, E. S. From Signaling Pathways to Microtubule Dynamics: the Key Players. *Curr. Opin. Cell. Biol.* **2010**, *22*, 104-111.
7. Vindya, N. G.; Sharma, N.; Yadav, M.; Ethiraj, K. R. Tubulins-the target for anticancer therapy. *Curr. Top. Med. Chem.* **2015**, *15*, 73-82.
8. van Vuuren, R. J.; Visagie, M. H.; Theron, A. E.; Joubert, A.M. Antimitotic drugs in the treatment of cancer. *Cancer Chemother Pharmacol.* **2015**, *76*, 1101-1112.
9. Liu, Y. M.; Chen, H. L.; Lee, H. Y.; Liou, J. P. Tubulin inhibitors: a patent review. *Expert Opin. Ther. Pat.* **2014**, *24*, 69-88.
10. Porcù, E., Bortolozzi, R., Basso, G., Viola G. Recent advances on vascular disrupting agents *Future Med. Chem.* **2014**, *6*, 1485-1498.
11. Perez-Perez, M.J., Priego, E.M. ; Bueno, O.; Martins, M.S. ; Canela, M.D. ; Liekens, S. Blocking blood flow to solid tumours by destabilizing tubulin: an approach to targeting tumour growth, *J. Med. Chem.* **2016**, *59*, 8685-8711.
12. Greene, L. M.; Meegan, M. J.; Zisterer, D. M. Combretastatins: more than just vascular targeting agents? *J. Pharmacol. Exp. Ther.* **2015,** 355, 212-227.
13. Pettit, G. R.; Singh, S. B.; Hamel, E.; Lin, C. M.; Alberts, D. S.; Garcia-Kendall, D. Isolation and structure of the strong cell growth and tubulin inhibitor combretastatin A-4. *Experentia* **1989**, *45*, 209-211.
14. Lin, C. M.; Ho, H. H.; Pettit, G. R.; Hamel, E. Antimitotic natural products combretastatin A-4 and combretastatin A-2: studies on the mechanism of their inhibition of the binding of colchicine to tubulin. *Biochemistry* **1989**, *28*, 6984-6991.

15. Pinney, K. G.; Jelinek, C.; Edvardsen, K.; Chaplin, D. J.; Pettit, G. R. The Discovery and Development of the Combretastatins. In *Antitumour Agents from Natural Products*; Kingston, D., Newman, D., Cragg, G., Eds.; CRC Press: Boca Raton, FL, 2005; pp 23-46

16. Nathan, P.; Zweifel, M.; Padhani, A. R.; Koh, D.-M.; Ng, M.; Collins, D. J.; Harris, A.; Carden, C.; Smythe, J.; Fisher, N.; Taylor, N. J.; Stirling, J. J.; Lu, S.-P.; Leach, M. O.; Rustin, G. J. S.; Judson, I. Phase I trial of combretastatin A4 phosphate (CA4P) in combination with bevacizumab in patients with advanced cancer. *Clin. Cancer Res.* **2012**, *18*, 3428-3439.

17. Ng, Q.-S.; Mandeville, H.; Goh, V.; Alonzi, R.; Milner, J.; Carnell, D.; Meer, K.; Padhani, A. R.; Saunders, M. I.; Hoskin, P. J. Phase Ib trial of radiotherapy in combination with combretastatin-A4-phosphate in patients with non-small-cell lung cancer, prostate adenocarcinoma, and squamous cell carcinoma of the head and neck. *Ann. Oncol.* **2012**, *23*, 231-237.

18. Bahleda, R.; Sessa, C.; Del Conte, G.; Gianni, L.; Capri, G.; Varga, A.; Oprea, C.; Daglish, B.; Hospitel, M.; Soria, J.C. Phase I clinical and pharmacokinetic study of ombrabulin (AVE8062) combined with cisplatin/docetaxel or carboplatin/paclitaxel in patients with advanced solid tumours. *Invest. New Drugs* **2014**, *32*, 1188-1196.

19. Delmonte, A.; Sessa, C. AVE8062: a new combretastatin derivative vascular disrupting agents. *Exp. Opin. Invest. Drugs* **2009**, *18*, 1541-1548.

20. Greene, L. M.; Meegan, M. J.; Zisterer, D. M. Combretastatins: more than just vascular targeting agents? *J. Pharmacol. Exp. Ther.* **2015,** 355, 212-227.

21. Ji, Y. T.; Liu, Y. N.; Liu, Z. P. Tubulin colchicine binding site inhibitors as vascular disrupting agents in clinical developments. *Curr. Med. Chem.* **2015,** 22, 1348-1360.

22. Bukhari S.N.A., Kumar G.B., Revankar H.M., Qin H.L. Development of combretastatins as potent tubulin polymerization inhibitors. *Bioorg. Chem.* **2017**, *72*, 130-147.

23. Seddigi Z.S.; Malik M.S.; Saraswati A.P.; Ahmed S.A.; Babalghith A.O.; Lamfon H.A.; Kamal A. Recent advances in combretastatin based derivatives and prodrugs as antimitotic agents. *Med. Chem. Commun.* **2017**, *8*, 1592- 1603.

24. Kaur, R.; Kaur, G.; Gill, R. K.; Soni, R.; Bariwal, J. Recent developments in tubulin polymerization inhibitors: An overview. *Eur. J. Med. Chem.* **2014,** 87, 89-124.

25. Kamal, A.; Reddy, N. V. S.; Nayak, V. L.; Reddy, V. S.; Prasad, B.; Nimbarte, V. D.; Srinivasulu, V.; Vishunuvardhan, M. V. P. S.; Reddy, C. S. Synthesis and

biological evaluation of benzo[*b*]furans as inhibitors of tubulin polymerization and inducers of apoptosis. *ChemMedChem* **2014**, *9*, 117-128.

26. Tréguier, B.; Rasolofonjatovo, E.; Hamze, A.; Provot, O.; Wdzieczak-Bakala, J.; Dubois, J.; Brion, J.-D.; Alami, M. Synthesis of 2-(1-phenylvinyl)benzofurans and 2-(1-phenylvinyl)indoles as antimitotic agents by a tandem palladium-assisted coupling-cyclization reaction between 1-phenylvinyl iodides and *ortho*-substituted arylalkynes. *Eur. J. Org. Chem.* **2011**, *25*, 4868-4876.
27. Ping Quan, Y.; Ping Cheng, L.; Chi Wang, T.; Pang, W.; Hong Wu, F.; Wen Huang, J. Molecular modeling study, synthesis and biological evaluation of combretastatin A-4 analogues as anticancer agents and tubulin inhibitors. *Med. Chem. Commun.* **2018**, *9*, 316-327.
28. Romagnoli, R.; Baraldi, P. G.; Sarkar, T.; Carrion, M. D.; Cruz-Lopez, O.; Lopez-Cara, C.; Tolomeo, M.; Grimaudo, S.; Di Cristina, A.; Pipitone, M. R.; Balzarini, J.; Gambari, R.; Lampronti, I.; Saletti, R.; Brancale, A.; Hamel, E.. Synthesis and biological evaluation of 2-(3',4',5'-trimethoxybenzoyl)-3-*N*,*N*-dimethylamino benzo[*b*]furan derivatives as inhibitors of tubulin polymerization. *Bioorg. Med. Chem.* **2008**, *16*, 8419-8426.
29. Romagnoli, R., Baraldi, P.G.; Kimatrai Salvador, M; Prencipe, F.; Lopez-Cara, C.; Schiaffino Ortega, S.; Brancale, A.; Hamel, E.; Castagliuolo, I.; Mitola, S.; Ronca, R.; Bortolozzi, R.; Porcù, E.; Basso, G.; Viola, G: Design, Synthesis, in vitro and in vivo anticancer and antiangiogenic activity of novel 3-arylamino benzofuran derivatives targeting the colchicine site on tubulin. *J. Med. Chem.* **2015**, *58*, 3209-3222.
30. Flynn, B. L.; Hamel, E.; Jung, M. K. One-pot synthesis of benzo[*b*]furan and indole inhibitors of tubulin polymerization. *J. Med. Chem.* **2002**, *45*, 2670-2673.
31. Flynn, B. L.; Gill, G. S.; Grobelny, D. S.; Chaplin, J. H.; Paul, D.; Leske, A. F.; Lavranos, T. C.; Chalmers, D. K.; Charman, S. A.; Kostewicz, E.; Shackleford, D. M.; Morizzi, J.; Hamel, E.; Jung, M. K.; Kremmidiotis, G. Discovery of 7-hydroxy-6-methoxy-2-methyl-3 (3,4,5-trimethoxybenzoyl)benzo[*b*]furan (BNC 105), a tubulin polymerization inhibitor with potent antiproliferative and tumour vascular disrupting properties. *J. Med. Chem.* **2011**, *5*4, 6014-6027.
32. Kremmidiotis, G.; Leske, A. F.; Lavranos, T. C.; Beaumont, D.; Gasic, J.; Hall, A.; O'Callaghan, M.; Matthews, C. A.; Flynn, B. L. BNC105: a novel tubulin polymerization inhibitor that selectively disrupts tumour vasculature and displays single-agent antitumour efficacy. *Mol. Cancer Ther.* **2010**, *9*, 1562-1573.

33. Romagnoli, R.; Baraldi, P.G.; Carrion, M.D.; Lopez Cara, C.; Preti, D.; Fruttarolo, F:; Pavani, M.G.; Aghazadeh Tabrizi, M.; Tolomeo, M.; Grimaudo, S.; Di Antonella, C.; Balzarini, J.; Hadfield, J. A.; Brancale, A.; Hamel, E. Synthesis and biological evaluation of 2- and 3-aminobenzo[b]thiophene derivatives as antimitotic agents and inhibitors of tubulin polymerization. *J. Med. Chem.* **2007**, *50*, 2273-2277.

34. Borra, S.; Chandrasekhar,D.; Khound, S.; Maurya, R.A. Access to 1*a*,6*b*-dihydro-1*H*-benzofuro[2,3-*b*]azirines and benzofuran-2-amines via visible light triggered decomposition of α-azidochalcones. *Org. Lett.* **2017**, *19*, 5364−5367.

35. For the synthesis and characterization of 4-ethoxy-2-hydroxybenzaldehyde (**5f**) see: Binnemans, K.; Galyametdinov, Y.G.; Van Deun, R.; Bruce, D.W.; Collinson, S.R.; Polishchuk, A.P.; Bikchantaev, I.; Haase, W.; Prosvirin, A.V.; Tinchurina, L.; Litvinov, I.; Gubajdullin, A.; Rakhmatullin, A.; Uytterhoeven, K.; Van Meervelt, L. Rare-Earth-Containing Magnetic Liquid Crystals. *J. Am. Chem. Soc.* **2000,** *122,* 4335-4344.

36. For the synthesis and characterization of 4-*n*-propoxy-2-hydroxybenzaldehyde (**5g**) see: Kuo, H.-M.; Hsu, Y.-T.; Wang, Y.-W.; Lee, G.-H.; Lai, C.K. The π-π interactions enhanced in salicylaldimines and salicylaldazines. *Tetrahedron* **2015**, *71*, 7729-7738.

37. For the synthesis and characterization of 4-methoxy-2,3-dihydroxybenzaldehyde (**5n**) see: Han, S.; Zhang, F.-F.; Qian, H.-Y.; Chen, L.-L.; Pu, J.-B.; Xie, X.; Chen, J.-Z. Design, syntheses, structure-activity relationships and docking studies of coumarin derivatives as novel selective ligands for the CB2 receptor. *Eur. J. Med. Chem.* **2015**, *93*, 16-32.

38. 2-Azido-1-(3,4,5-trimethoxyphenyl)ethanone was synthesized from the corresponding 2-bromo-1-(3,4,5-trimethoxyphenyl)ethanone and sodium azide using the procedure reported in the following article: Prasad, B.; Reddy, V. G.; Krishna, N. H.; Reddy, N. V. S.; Nanubolu, J. B.; Alarifi, A.; Kamal, A. Annulation of 4-hydroxypyrones and α-keto vinyl azides; A regiospecific approach towards the synthesis of furo[3,2-*c*]pyrone scaffolds under catalyst free condition. *Chemistry Select* **2017**, *2*, 8122-8126.

39. Hamel, E. Evaluation of antimitotic agents by quantitative comparisons of their effects on the polymerization of purified tubulin. *Cell Biochem. Biophys.* **2003**, *38*, 1-21.

40. Verdier-Pinard, P.; Lai J.-Y.; Yoo, H.-D.; Yu, J.; Marquez, B.; Nagle, D. G.; Nambu, M.; White, J. D.; Falck, J. R.; Gerwick, W. H.; Day, B. W.; Hamel, E. Structure-

activity analysis of the interaction of curacin A, the potent colchicine site antimitotic agent, with tubulin and effects of analogs on the growth of MCF-7 breast cancer cells. *Mol. Pharmacol.* **1998**, *53*, 62-76.41. Schrödinger Release 2017-1: Maestro, Schrödinger, LLC, New York, NY, 2017.

41. Molecular Operating Environment (MOE 2015.10); Chemical Computing Group, Inc.: Montreal, Quebec, Canada; URL http://www.chemcomp.com 2018.

6. Conclusions

6.1 Summary

During the PhD program, my research interest aimed at the design, synthesis and optimization of novel potential anticancer agents with antiproliferative and antivascular activities which target microtubules, dynamic tubular protein that are assembled from α-tubulin/β-tubulin (αβ-tubulin) heterodimers.

Amongst diverse cancer small molecule drugs, those targeting **microtubules** represent one of the most effective classes of compounds available to date.[1] A large number of chemically distinct compounds, binding to soluble tubulin and/or directly to tubulin in microtubules, possess significant antimitotic properties, and are able to inhibit cell proliferation by interfering with microtubule polymerization dynamics.[2]

Moreover, tumour vasculature is an attractive new target for cancer therapy.[3] From an anatomical and functional points of view, the vascular system formed within cancerous tumours is abnormal, compared to normal vasculature.[4]

Recently, it has been observed that several drugs, especially microtubule-targeted drugs, can act as **vascular disrupting agents (VDAs)**, targeting the tumour vascular network thus causing an interruption of the supply of nutrients to the tumour, which leads to the death of the surrounding cells.[5] Of most relevance to the work of this thesis is Combretastatin A-4 (CA-4), a natural cis-stilbene isolated in 1989 from the South-African tree *Combretum Caffrum.*[6]

The isomerization of the *cis*-double bond of CA-4 to its t*rans*-form in solution is one of the major disadvantages of this molecule. When the *cis* double bond in CA-4 isomerizes to form thermally more stable *trans*-isomer, a result is a complete loss of biological activity.[7]

In order to address this issue, replacement of the *cis*-double bond by a rigid heterocyclic moiety to hinder the transformation to the *trans*-form has been shown as a viable strategy.[7]

Therefore, in the first research work two novel series of 2-methyl-4,5-disubstituted oxazole derivatives were synthesized with the aim to retain the bioactive configuration afforded by

the *cis*-double bond present in CA-4. All the synthesized compounds were evaluated for their *in vitro* antiproliferative activity, interactions with tubulin and cell cycle effects.
The most active agent, (4-(3,4,5-trimethoxyphenyl)-5-(4-ethoxyphenyl)-2-methyloxazole, **4i)**, was evaluated for antitumor activity *in vivo*. Experiments demonstrated that **4i** had excellent antitumor activity that was evident at lower doses than CA-4P, supporting its further development as an anticancer drug.

Carrying on my research work, a new class of simple synthetic inhibitors of tubulin polymerization based on the molecular skeleton of 2-alkoxycarbonyl-3-(3',4',5'-trimethoxyanilino) thiophene were synthesized. These derivatives were designed and synthesized based on modification of benzo[*b*]thiophene and thieno[2,3-*b*]pyridine analogues previously published.[8]
We explored SAR by examining various substitutions with EWGs and ERGs on the phenyl at the 5-position of the 2-alkoxycarbonyl-3-(3',4',5'-trimethoxyanilino) thiophene scaffold. The presence of ERGs such as methyl or methoxy was beneficial for antiproliferative activity, as these compounds proved to be more potent than the corresponding derivatives with the EWGs fluorine or chlorine.
It is clear that the substitution pattern on the phenyl at the 5-position of the 2-methoxycarbonyl-3-(3',4',5'-trimethoxyanilino) thiophene system plays an important role for anti-tubulin and antiproliferative activities, and this was supported by the molecular docking studies. SAR studies showed that the 2-methoxycarbonyl-3-(3',4',5'-trimethoxyanilino)-5-phenylthiophene derivative **4a**, its bio-isosteric thien-2'-yl analogue **4c** as well as the *para*-tolyl and *para*-methoxyphenyl analogues **4i** and **4k**, respectively, displayed high antiproliferative activities, with IC_{50} values ranging between 0.13-0.24, 0.16-0.25, 0.16-0.23 and 0.16-0.84 μM, respectively, against the L1210, FM3A, CEM and HeLa cell lines. Of all the tested compounds, derivative **4c** possessed the highest overall cytostatic potency with IC_{50} values ranging from 0.13 to 0.16 μM against the panel of four cancer cell lines. The results we obtained indicated that compound **4c** could induce tumour cell apoptosis through reducing the mitochondrial membrane potential and regulating the expression of apoptosis-related proteins in tumour cells.

An effective strategy to develop anticancer agents is the discovery of synergistic multi-targeting properties of new molecules.[9] Merging of two different bioactive molecules with different mechanism of action is one of the methods that are being adopted to treat cancer. Following this strategy, in another work we report the design and synthesis of a new series

4-(3',4',5'-trimethoxyanilino)-6-substituted thieno[3,2-*d*]pyrimidines, some of which possess both tubulin polymerization and EGFR kinase inhibitory properties. Optimal structure at the phenyl at the C-6 position of the 4-(3',4',5'-trimethoxyanilino)-thieno[3,2-*d*]pyrimidine system was explored by various substituents, with either electron-releasing or electron-withdrawing properties. The 4-(3',4',5'-trimethoxyanilino)-6-(*p*-tolyl) thieno[3,2-*d*]pyrimidine derivative **6g** was the most potent compound of the whole series, exhibiting an IC_{50} value of 19 nM against the NSCLC A549 cell line, which harbors $EGFR^{WT}$ and K-ras mutations.

Besides its potent antiproliferative activity and high competitive inhibitory activity on EGFR, compound **6g** also inhibited tubulin assembly through an interaction at the colchicine site, thereby combining EGFR inhibition with anti-tubulin activity.

Moreover, our results showed a high correlation between the *in vitro* antiproliferative activity against the cancer cell lines and inhibition of tubulin polymerization and EGFR kinase, which suggested that targeting both tubulin and EGFR kinase played major roles in the cancer cell growth inhibitory effects of these three molecules.

Finally, the last work has been focused on the development of 2-amino-3-(3',4',5'-trimethoxybenzoyl) benzo[*b*]furan derivatives, since it has been showed that the benzo[*b*]furan molecular skeleton is the core structure of many inhibitors of tubulin polymerization.[10–16]

The structure-activity relationship was investigated by the insertion of electron-withdrawing (F and Br) or electron releasing (alkoxy groups, OH, Me and NH_2) substituents on the benzene fused the furan ring of the benzo[*b*]furan molecular moiety.

Derivatives with a methoxy (**4d**), an ethoxy (**4f**), a bromine (**4k**) or a methyl (**4l**) at the C-6 position of the benzo[*b*]furan system exhibited potent antiproliferative activity, with IC_{50} values from single digit nanomolar to sub-nanomolar range. The C-6 ethoxy derivative **4f** and the C-6 methyl analogue **4l** resulted the two most potent compound of the series, exhibiting IC_{50} values of 0.005-2.8 and 0.3-3.5 nM, respectively, as compared with the range 0.8-3100 nM obtained with CA-4.

Biological results confirmed that tubulin is the intracellular target of these compounds, with the tested molecules (**3c**, **4d**, **4f**, **4g**. **4k** and **4l**) which resulted potent inhibitors of both tubulin-dependent reactions, with activities quantitatively similar to that of CA-4.

In conclusion, the antiproliferative activity of these compounds derives from an interaction with the colchicine site of tubulin and interference with microtubule assembly. This indicates

that the cellular actions of these agents result in mitotic arrest, caused by interference with mitosis-related processes, which is followed by apoptosis.

6.2 Related work

During my last year of PhD. I spent six months in Dr Jacobson's laboratory at National Institutes of Health (NIH), in Bethesda, Maryland, USA. During this period, I worked on three different but related projects that dealt with the purinergic pathway. I worked on developing and synthesizing novel compounds for targeting transmembrane receptors and membrane-bound enzyme that are involved in purinergic signaling (Figure 1).

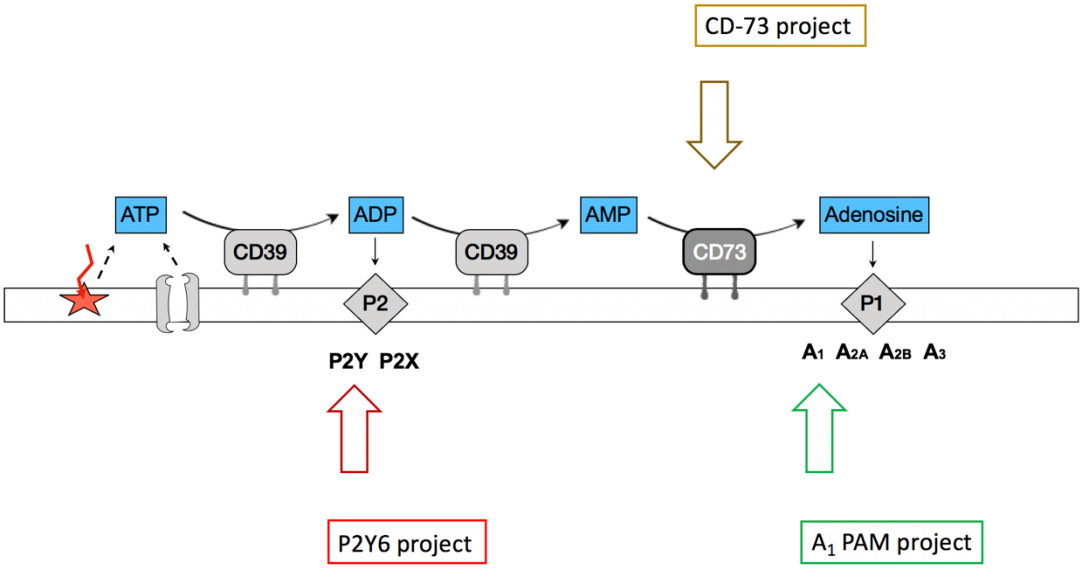

Figure 1. Targeting three purinergic pathways.

More specifically, in the first project, I synthesized positive allosteric modulators of A1 receptor that bind adenosine receptor.[17] In the second project worked on developing possible agonists of P2Y6 receptor, and in the third project I focused on the synthesis of inhibitors of CD-73 enzyme which is important for the conversation of AMP into adenosine.[18] I will provide a very rapid overview of the background and my synthetic method for each project. Intense efforts by medicinal chemists have focused on the development of both agonist and antagonist ligands for the adenosine receptors (ARs) and for the P2Y receptors (P2YRs) that interact with extracellular nucleotides.[19]

All of these receptors are G-protein-coupled receptors (GPCRs).[20,21]

These receptor families include 12 subtypes in total, also including the larger (P2Y) family that it is divided into two subgroups based on similarity of the receptor structure and second messenger coupling.[21]

In presence of injury or stress, intracellular sources – such as vesicles or transporters - release nucleotides that serve as signals of local challenge to tissues or cells.[22] The released nucleotides then interact with metabotropic GPCRs (P2YRs, adenosine or uridine 5′-triphosphates or 5′-diphosphates) or, in time can be converted metabolic enzymes. For example, the adenine nucleotides are converted by the action of ectonucleotidases (for example, CD39 that hydrolyzes ATP/ADP and CD73 that hydrolyzes AMP) to the nucleoside adenosine.[23]

Adenosine acts as a protective agent throughout the body by helping increase oxygen supply, mitigating inflammatory responses, or conditioning cells to withstand ischemic damage.[24]

Therefore, the development of potent and selective compounds able to bind adenosine receptors has been of great interest in medicinal chemistry research for more than three decades.[25] Moreover, the use of allosteric agonists in therapy could be more advantageous as compared to use non-allosteric agonists, since allosteric regulators could be used to selectively magnify the effects of endogenous adenosine.[26]

A_1 PAM project

In the first project, I worked on the synthesis of positive allosteric modulators of the A_1 receptor, the receptor that binds adenosine. PAMs (positive allosteric modulators) and NAMs (negative allosteric modulators) are relatively recently described classes of bioactive compounds that are of interest for their discrete mode of interaction with receptors, as compared to that of classical agonists and antagonists.[27] **Directly-acting compounds** bind the target receptor orthosterically — at the same site bound by the native agonist—or allosterically—at a distinct site.[28] On the other hand, **allosteric modulators** bind only to the topographically-distinct allosteric site and do not necessarily produce any effect on their own. Instead, they will indirectly enhance (PAM) or change (NAM) the binding affinity and/or efficacy of the natural ligand.[28]

Starting from works previously published by Prof. Romagnoli,[29,30] it was decided to optimize the 2-amino 3-aroyl thienyl core by introducing new substituents in 5 position using ethylene or acetylenic linkers. Following synthesis of the compounds, they were tested by the research group of Prof. Varani, at the University of Ferrara, in order to evaluate their capacity as positive allosteric modulators on CHO cells.

P2Y6 project

The goal of the second project was to development P2Y6 receptor agonists. P2Y6 is a receptor coupled to a Gq/11 protein following the activation of Cβ phospholipase. This enzyme hydrolyses phosphatidylinositol 4,5- bisphosphate (PIP2), producing the second messenger inositol 1,4,5-triphosphate (IP3) and diacylglycerol (DAG).[21] These products latter mediate the release of intracellular calcium ions with the activation of protein kinase C.[21]

Compounds that act as agonists of this receptor have high relevance in the therapeutic field because of the involved of P2Y6 in many physiological processes;[31] its endogenous agonist is UDP.[32]

The aim of this project was to synthesize modified nucleosides, the CDP analogues that were then tested by functional fluorescence in human cells expressing the P2Y6 receptor.

CD-73 project

The ATP released in the extracellular space is converted to AMP by phosphatases like CD-39.[33] The AMP thus produced is then converted into adenosine by a reaction catalysed by CD-73, an ectonucleotidase of 548 amino acids that presents a vast distribution in the human body: kidney, liver, lungs, brain and heart.[34] ATP and ADO (adenosine) has been considered as a checkpoint in purines pathway.[35] While ATP mediates pro-inflammatory processes, causing tumour cell death, excess of adenosine can cause immune suppression, promoting tumour growth and spread.[36] In the context of cancer, tumour cells can directly exploit ATP and adenosine receptors for survival, proliferation and motility.[36] Also, tumour cells have been found to express high levels of ectonucleotidases, such as CD73, that catabolize the formation of extracellular adenosine.[37]

As a consequence, extracellular adenosine can promote tumour angiogenesis, immune escape and metastasis.[36] Therefore, the ectonucleotidase CD73 may constitute a previously unrecognized target for cancer therapy; inhibitors of ectonucleotidases have a potential for use as novel drugs for cancer therapy.[36,38–40]

With the third project I then worked on the design and synthesis of new molecules capable of acting on CD-73, inhibiting its activity. These molecules are CDP analogous compounds, variously substituted and characterized by the presence of a methylene diphosphonate residue.

These compounds were then evaluated as inhibitors of ectonucleotidases by Muller's group, presenting very exciting results (a patent is being drafted in this regard).

6.3 References

1. Jordan, M. & Wilson, L. Microtubules as a target for anticancer drugs. *Nature Reviews Cancer* **4**, 253–265 (2004).
2. Stanton, R. A., Gernert, K. M., Nettles, J. H. & Aneja, R. Drugs that target dynamic microtubules: a new molecular perspective. *Medicinal research reviews* **31**, 443–481 (2011).
3. Keshet, E. & Ben-Sasson, S. A. Anticancer drug targets: approaching angiogenesis. *J Clin Invest* **104**, 1497–1501 (1999).
4. Pérez-Pérez, M.-J. *et al.* Blocking Blood Flow to Solid Tumors by Destabilizing Tubulin: An Approach to Targeting Tumor Growth. *J Med Chem* **59**, 8685–8711 (2016).
5. Gaya, A. & Rustin, G. Vascular disrupting agents: a new class of drug in cancer therapy. *Clinical oncology (Royal College of Radiologists (Great Britain))* **17**, 277–290 (2005).
6. Pettit, G., Singh, S., Niven, M., Hamel, E. & hmidt, J. Isolation, structure, and synthesis of combretastatins A-1 and B-1, potent new inhibitors of microtubule assembly, derived from Combretum caffrum. *Journal of natural products* **50**, 119–131 (1987).
7. Bukhari, S., Kumar, G., Revankar, H. & Qin, H.-L. Development of combretastatins as potent tubulin polymerization inhibitors. *Bioorg Chem* **72**, 130–147 (2017).
8. Romagnoli, R. *et al.* Synthesis and biological evaluation of 2-(alkoxycarbonyl)-3-anilinobenzo[b]thiophenes and thieno[2,3-b]pyridines as new potent anticancer agents. *J Med Chem* **56**, 2606–18 (2013).
9. Trusolino, L. & Bertotti, A. Compensatory Pathways in Oncogenic Kinase Signaling and Resistance to Targeted Therapies: Six Degrees of Separation. *Cancer Discov* **2**, 876–880 (2012).
10. Kamal, A. *et al.* Synthesis and Biological Evaluation of Benzo[b]furans as Inhibitors of Tubulin Polymerization and Inducers of Apoptosis. *Chemmedchem* **9**, 117–128 (2014).
11. Tréguier, B. *et al.* Synthesis of 2-(1-Phenylvinyl)benzofurans and 2-(1-Phenylvinyl)indoles as Antimitotic Agents by a Tandem Palladium-Assisted Coupling-Cyclization Reaction between 1-Phenylvinyl Iodides and ortho-Substituted Arylalkynes. *Eur J Org Chem* **2011**, 4868–4876 (2011).

12. Quan, Y. *et al.* Molecular modeling study, synthesis and biological evaluation of combretastatin A-4 analogues as anticancer agents and tubulin inhibitors. *Medchemcomm* **9**, 316–327 (2017).
13. Romagnoli, R. *et al.* Design, synthesis and structure–activity relationship of 2-(3′,4′,5′-trimethoxybenzoyl)-benzo[b]furan derivatives as a novel class of inhibitors of tubulin polymerization. *Bioorgan Med Chem* **17**, 6862–6871 (2009).
14. Romagnoli, R. *et al.* Design, synthesis, in vitro, and in vivo anticancer and antiangiogenic activity of novel 3-arylaminobenzofuran derivatives targeting the colchicine site on tubulin. *J Med Chem* **58**, 3209–22 (2015).
15. Flynn, B. L., Hamel, E. & Jung, K. M. One-Pot Synthesis of Benzo[b]furan and Indole Inhibitors of Tubulin Polymerization. *J Med Chem* **45**, 2670–2673 (2002).
16. Flynn, B. L. *et al.* Discovery of 7-hydroxy-6-methoxy-2-methyl-3-(3,4,5-trimethoxybenzoyl)benzo[b]furan (BNC105), a tubulin polymerization inhibitor with potent antiproliferative and tumor vascular disrupting properties. *J Med Chem* **54**, 6014–27 (2011).
17. Varani, K., Vincenzi, F., Merighi, S., Gessi, S. & Borea, P. Protein Reviews, Volume 19. *Adv Exp Med Biol* 193–232 (2017) doi:10.1007/5584_2017_61.
18. Robson, S. C., Sévigny, J. & Zimmermann, H. The E-NTPDase family of ectonucleotidases: Structure function relationships and pathophysiological significance. *Purinerg Signal* **2**, 409–430 (2006).
19. Carlsson, J. *et al.* Structure-Based Discovery of A2A Adenosine Receptor Ligands. *J Med Chem* **53**, 3748–3755 (2010).
20. Fredholm, B. B., IJzerman, A. P., Jacobson, K. A., Linden, J. & Müller, C. E. International Union of Basic and Clinical Pharmacology. LXXXI. Nomenclature and Classification of Adenosine Receptors—An Update. *Pharmacol Rev* **63**, 1–34 (2011).
21. Abbracchio, M. P. *et al.* International Union of Pharmacology LVIII: Update on the P2Y G Protein-Coupled Nucleotide Receptors: From Molecular Mechanisms and Pathophysiology to Therapy. *Pharmacol Rev* **58**, 281–341 (2006).
22. Dale, N. & Frenguelli, B. G. Release of Adenosine and ATP During Ischemia and Epilepsy. *Curr Neuropharmacol* **7**, 160–179 (2009).
23. Longhi, M., Robson, S. C., Bernstein, S. H., Serra, S. & Deaglio, S. Biological functions of ecto-enzymes in regulating extracellular adenosine levels in neoplastic and inflammatory disease states. *J Mol Med* **91**, 165–172 (2013).

24. Fredholm, B. Adenosine, an endogenous distress signal, modulates tissue damage and repair. *Cell Death Differ* **14**, 1315–1323 (2007).
25. Jacobson, K. A. & Gao, Z.-G. Adenosine receptors as therapeutic targets. *Nat Rev Drug Discov* **5**, 247–264 (2006).
26. Oh, E. Y. *et al.* A comprehensive comparative review of adenosine diphosphate receptor antagonists. *Expert Opin Pharmaco* **13**, 175–191 (2012).
27. Jacobson, K. A., Gao, Z.-G., Göblyös, A. & IJzerman, A. P. Chapter 7 Allosteric Modulation of Purine and Pyrimidine Receptors. *Adv Pharmacol* **61**, 187–220 (2011).
28. Milligan, G. & Smith, N. J. Allosteric modulation of heterodimeric G-protein-coupled receptors. *Trends Pharmacol Sci* **28**, 615–620 (2007).
29. Romagnoli, R. *et al.* Synthesis and biological evaluation of 2-amino-3-(4-chlorobenzoyl)-4-[N-(substituted) piperazin-1-yl]thiophenes as potent allosteric enhancers of the A1 adenosine receptor. *J Med Chem* **51**, 5875–9 (2008).
30. Romagnoli, R. *et al.* Synthesis and Biological Evaluation of Novel Allosteric Enhancers of the A1Adenosine Receptor Based on 2-Amino-3-(4′-Chlorobenzoyl)-4-Substituted-5-Arylethynyl Thiophene. *J Med Chem* **57**, 7673–7686 (2014).
31. Rafehi, M. & Müller, C. E. Tools and drugs for uracil nucleotide-activated P2Y receptors. *Pharmacol Therapeut* **190**, 24–80 (2018).
32. Communi, D., Parmentier, M. & Boeynaems, J.-M. Cloning, Functional Expression and Tissue Distribution of the Human P2Y6Receptor. *Biochem Bioph Res Co* **222**, 303–308 (1996).
33. Yegutkin, G. G. Enzymes involved in metabolism of extracellular nucleotides and nucleosides: Functional implications and measurement of activities. *Crit Rev Biochem Mol* **49**, 473–497 (2014).
34. Allard, D., Allard, B., Gaudreau, P.-O., Chrobak, P. & Stagg, J. CD73adenosine: a next-generation target in immuno-oncology. *Immunotherapy* **8**, 145–163 (2016).
35. Virgilio, D. F. & Adinolfi, E. Extracellular purines, purinergic receptors and tumor growth. *Oncogene* **36**, 293–303 (2017).
36. Yang, J., Liao, X., Yu, J. & Zhou, P. Role of CD73 in Disease: Promising Prognostic Indicator and Therapeutic Target. *Curr Med Chem* **25**, 2260–2271 (2018).
37. Bastid, J. *et al.* ENTPD1/CD39 is a promising therapeutic target in oncology. *Oncogene* **32**, 1743–1751 (2013).
38. Ghalamfarsa, G. *et al.* CD73 as a potential opportunity for cancer immunotherapy. *Expert Opin Ther Tar* **23**, 127–142 (2018).

39. RUIMIN, W. *et al.* Effects of CD73 on human colorectal cancer cell growth in vivo and in vitro. *Oncol Rep* **35**, 1750–1756 (2016).
40. Allard, D., Chrobak, P., Allard, B., Messaoudi, N. & Stagg, J. Targeting the CD73-adenosine axis in immuno-oncology. *Immunol Lett* **205**, 31–39 (2018).